Chlamydia trachomatis disrupts cytokinesis to accelerate nutrient acquisition from host cells

by

He Song Sun

A thesis submitted in conformity with the requirements
for the degree of Doctor of Philosophy

Department of Cell & Systems Biology
University of Toronto

Chlamydia trachomatis disrupts cytokinesis to accelerate nutrient acquisition from host cells

He Song Sun

Doctor of Philosophy

Department of Cell & Systems Biology
University of Toronto

2014

Abstract

Chlamydia trachomatis is the leading cause of bacterial sexually transmitted infections worldwide and it has been linked to increased risks of cervical cancer. Our study aims to understand the mechanisms by which chlamydia infection contributes to higher risks of tumorigenesis. We discovered in over 90% of infected human epithelial cells that chlamydia inclusions localized to the host cell centre during mitosis and prevented the completion of cleavage furrow ingression. Infected cells that failed to divide into two daughter cells re-entered interphase as tetraploid multinuclear cells, which are known initiators of tumorigenesis. In order to address whether chlamydia actively sought the host cell centre during mitosis, we created vacuoles using internalized latex beads and our findings indicated that chlamydia inclusions localized to the host cell centre much more frequently than similarly sized vacuoles. In addition, we demonstrated that metabolically inactive chlamydia inclusions localized to the cell centre less frequently than inclusions under normal conditions. Together, these results suggested that chlamydia actively localized to the host cell centre to efficiently block host cell mitosis. We took advantage of the microtubule-displacing capability of the *C. trachomatis* inclusions and demonstrated that astral microtubules could promote furrow initiation independent of the central spindle microtubules.

Microdomains on chlamydia inclusions play important roles in inclusion localization and chlamydia replication. We discovered that these structures were surprisingly resistant to bacterial protein synthesis and host Src family kinase inhibitors. Finally, we demonstrated that multinuclear cells that resulted from unsuccessful mitosis contained significantly higher Golgi content, an important nutrient source for chlamydia. Our results indicated that *C. trachomatis* in multinuclear cells intercepted Golgi-derived lipids faster than in mononuclear cells. Together, my results reveal that *C. trachomatis* inclusions robustly localize to the cell centre to block host cell mitosis in order to acquire host Golgi nutrients more quickly in multinucleated cells.

Acknowledgments

I am very thankful to my supervisor, Dr. Rene Harrison, for her guidance and support throughout my graduate study. Her leadership, enthusiasm and belief in my abilities have motivated me to overcome seemingly insurmountable challenges. Giving me just the right amount of guidance and independence has helped me to grow as an independent thinker. I would also like to thank my supervisory committee members, Dr. Mauricio Terebiznik and Dr. Andrew Wilde, for their guidance and insightful suggestions in my research work. Finally, I would like to thank the examiners, Dr. Albert Descoteaux and Dr. Andras Kapus, for their help with my defense.

I would also like to express my gratitude to my colleagues at UTSC. I would like to thank Edward Eng for very patiently teaching me how to culture and handle chlamydia when I first arrived at the lab. I am very thankful to Dr. Noushin Nabavi, Dr. Prerna Patel, Dr. Kristen Silver, Dr. Rosa da Silva and Dr. Sujeeve Jeganathan for basic lab training and being inspirational figures. I would like to thank all members of the Harrison, Terebiznik and Brown labs for being great friends both in and outside of the lab. I could not have done it without their help and friendship.

I would like to thank my Aunt Liu Dan and Uncles, Cui Hua Yang and Liu Chun for their love and support. I would like to thank great friends that I have made in Toronto, Zhu Shao Han and Liao Chang Jian for making this journey full of joy and laughter. Finally, I am very grateful to my parents, Liu Bing and Sun Guo Guang for making everything possible. This journey would not have been possible without their love and support and I hope this work makes them proud.

Table of Contents

List of Figures

List of Abbreviations

Abl	Abelson tyrosine-protein kinase 1
AHA	L-Azidohomoalanine
APC/C	Anaphase promoting complex/cyclosome
ATP	Adenosine triphosphate
Azi	Azithromycin
Bleb	Blebbistatin
BODIPY ceramide	*N*-(4,4-Difluoro-5,7-Dimethyl-4-Bora-3a,4a-Diaza-s-Indacene-3-Pentanoyl) Sphingosine
BrnQ	Branched-chain amino acid transport system carrier protein BrnQ
BUB3	Budding uninhibited by benzimidazole 3
BUBR1	Budding uninhibited by benzimidazole-related 1
CDK	Cyclin-dependent kinase
Cep170	Centrosomal protein 170kDa
CERT	Ceramide transfer protein
CPAF	Chlamydial protease-like activity factor
CPC	Chromosome passenger complex
Ctl	Control
CTP	Cytidine triphosphate

CytoD	Cytochalasin D
DIC	Differential interference contrast
DRAQ5	1,5-bis{[2-(di-methylamino) ethyl]amino}-4, 8-dihydroxyanthracene-9,10-dione
EB	Elementary body
Ect2	Epithelial cell transforming sequence 2 oncogene
Eps15	Epidermal growth factor receptor substrate 15
ER	Endoplasmic reticulum
ERK	Extracellular-signal-regulated kinase 1
ESCRT-III	Endosomal sorting complex required for transport-III
F-actin	Filamentous actin
GAG	Glycosaminoglycan
GAP	GTPase activating protein
GDP	Guanosine diphosphate
GEF	Guanine exchange factors
GM130	Golgi matrix protein of 130 kDa
GRASP	General receptor for phosphoinositides-associated scaffold protein
GTP	Guanosine triphosphate
Hc1	Histone H1-like protein Hc1
Hc2	Histone H1-like protein Hc2
Hpi	Hours post infection

Hpr	Hours post release
HPV	Human papillomavirus
IF	Immunofluorescence
Inc	Inclusion membrane protein
KIF4	Kinesin-like protein 4
LAMP1	Lysosome-associated membrane protein-1
LGV	Lymphogranuloma venereum
MAD2	Mitotic-arrest deficient
MEK1	Mitogen-activated protein kinase 1
Mklp	Mitotic kinesin-like protein
MOMP	Major outer membrane proteins
MT	Microtubule
MTOC	Microtubule organizing centre
Noc	Nocodazole
Npt1	Nucleoside phosphate transporter1
OmcA	Small cysteine-rich outer membrane protein OmcA
OmcB	Small cysteine-rich outer membrane protein OmcB
OmpA	Outer membrane protein A
PDGFR	Platelet-derived growth factor receptor
PDI	Protein disulfide isomerase

Plk	Polo-like kinase
Prc1	Protein regulator of cytokinesis 1
Rab	Ras-related protein
Rac1	Ras-related C3 botulinum toxin substrate 1
RacGAP1	Rac GTPase activating protein 1
RB	Reticulate body
RIPA	Radioimmunoprecipitation assay
ROCK	Rho-associated, coiled-coil containing protein kinase
SAC	Spindle assembly checkpoint
siRNA	Small interfering RNA
Sos1	Son of sevenless homolog 1
Src	Proto-oncogene tyrosine-protein kinase Src
TARP	Translocated actin recruiting protein
TTSS	Type III secretion system
UTP	Uracil triphosphate
Vav2	Guanine nucleotide exchange factor VAV2

List of Appendices

The research presented in this thesis has appeared or has been submitted as a series of original publications in refereed journals.

Chapter 3
Sun HS, Wilde A, Harrison RE (2012) *Chlamydia trachomatis* inclusions induce asymmetric cleavage furrow formation and ingression failure in host cells. Molecular and Cellular Biology 31(24):5011-22

Chapter 4
Sun HS, Harrison RE (Submitted) Chlamydia inclusions actively localize to the host cell centre during mitosis to co-opt replicated Golgi in multinuclear cells. Infection and Immunity

Appendix I
Sun HS, Eng EW, Jeganathan S, Sin AT, Patel PC, Gracey E, Inman RD, Terebiznik MR, Harrison RE (2013) *Chlamydia trachomatis* vacuole maturation in infected macrophages. Journal of Leukocyte Biology 92(4):815-27.

Chapter 1

Chlamydia trachomatis pathogenesis and host cell cycle

Literature review

1.1 Human pathogenic Chlamydia species and their epidemiology

Chlamydia trachomatis is the leading cause of bacterial sexually transmitted infections worldwide with over 90 million new cases of infection each year. It is estimated that more than 4 million new *C. trachomatis* infections occur each year in the United States alone (Farris and Morrison, 2011). *C. trachomatis* belongs to the *Chlamydia* genus of the *Chlamydiaceae* family, which also includes the genus *Chlamydophila* (Budai, 2007). There are two main pathogenic spices for humans within the *Chlamydiaceae* family: *C. trachomatis* and *Chlamydophila pneumoniae*. In addition, several other chlamydia species can occasionally jump from their natural animal hosts to humans (Bush and Everett, 2001). The *C. trachomatis* spices can be divided into two biovars: trachoma and lymphogranuloma venereum (LGV), based on their natural tissue tropism (Bush and Everett, 2001; Budai, 2007). Members of the trachoma biovar usually cause oculogenital infections in patients and primarily infect epithelial cells in the genital tract or the eye, while LGV biovar (L1-L3) infections show tropism towards lymphatic tissues (Abu el-Asrar et al., 1998; El-Asrar et al., 2000; Budai, 2007; Stary and Stary, 2008). *C. trachomatis* is thought to gain access to the lymphatic tissue through microtraumas that naturally occur in tissues (Stary and Stary, 2008). Epithelial and fibroblast cell lines are the most susceptible to *C. trachomatis* infection *in vitro* (Budai, 2007). *C. trachomatis* LGV can also infect mononuclear phagocytes and sometimes kill them (Yong et al., 1982; Schachter and Osoba, 1983); however, the replication rate of *C. trachomatis* is significantly slower in phagocytes than in epithelial cells or fibroblasts (Yong et al., 1982; Sun et al., 2012). *C. trachomatis* infections contribute to a wide range of human diseases, such as pelvic inflammatory disease, cervicitis and tubal infertility, which may persist even after infection clearance (Patton et al., 1994; Hafner et al., 2008). In addition, numerous epidemiological studies have identified *C. trachomatis* as both an independent factor and a cofactor with Human papillomavirus (HPV) to cause cervical cancer (Samoff et al., 2005; Silins et al., 2005; Koskela et al., 2000; Smith et al., 2004; Naucler et al., 2007; Wallin et al., 2002; Madeleine et al., 2007;

Al-Daraji and Smith, 2009). While the mechanism by which HPV causes cellular transformation is well established, how *C. trachomatis* infection contributes to cervical cancer is poorly understood (Simonetti et al., 2009). One of the challenges associated with *C. trachomatis* tumorigenesis studies is that mouse innate immunity can spontaneously clear C. *trachomatis* infection without prolonged inflammation (Farris and Morrison, 2011). Even though *Chlamydia muridarum* has been used in mouse models to mimic *C. trachomatis* infection, the two strains have marked life cycle and pathological differences (Morre et al., 2000). The other major human pathogen *C. pneumoniae* can cause community-acquired pneumonia, asthma, and chronic obstructive pulmonary disease (Hahn, 1995; Johnston and Martin, 2005; Blasi et al., 2002; Hahn, 1999). In addition, *C. pneumoniae* has also been linked to atherosclerosis, cardiovascular disease and Alzheimer's disease (Shima et al., 2010; Belland et al., 2004; Campbell et al.). Similar to *C. trachomatis*, *C. pneumoniae* has been identified by various epidemiological studies as a risk factor for lung cancer; however, the tumorigenic mechanism is currently unclear (Zhan et al., 2011; Littman et al., 2005, 2004). Work presented in this thesis describes a possible mechanism through which *C. trachomatis* infection can lead to polyploidy and possibly cancer.

1.2 *Chlamydia trachomatis* Life Cycle

Chlamydia trachomatis is an obligate intracellular bacterium that exists in two morphologically distinct forms: the spore-like elementary body (EB) and the replicative reticulate body (RB) (Abdelrahman and Belland, 2005). The infectious EB form is characterized by its electron-dense cytoplasm and it is well-adapted for extracellular survival and entry into susceptible host cells (Abdelrahman and Belland, 2005). The non-infectious, metabolically active RB form is well-suited for intracellular replication by binary fission (Abdelrahman and Belland, 2005; Shaw et al., 2000). Upon entry into a susceptible host cell, the EB resides in a host membrane-bound vacuole termed an inclusion, within which the EB differentiates into a RB and begins to replicate. *Chlamydia* inclusion grows substantially in size over time and intercepts essential nutrients such as amino acids, nucleotides and lipids to sustain bacterial replication (Hackstadt et al., 1996; Braun et al., 2008; Hackstadt et al., 1995a; Tipples and McClarty, 1993; Hatch, 1975a). In order to disseminate and spread the infection, *C. trachomatis* has evolved two distinct mechanisms: the lysis pathway, which kills the host cell in the process, and the extrusion pathway, which leaves a viable host cell behind (Hybiske and Stephens, 2007). The *C. trachomatis* life cycle is briefly summarized in in Figure 1.1.

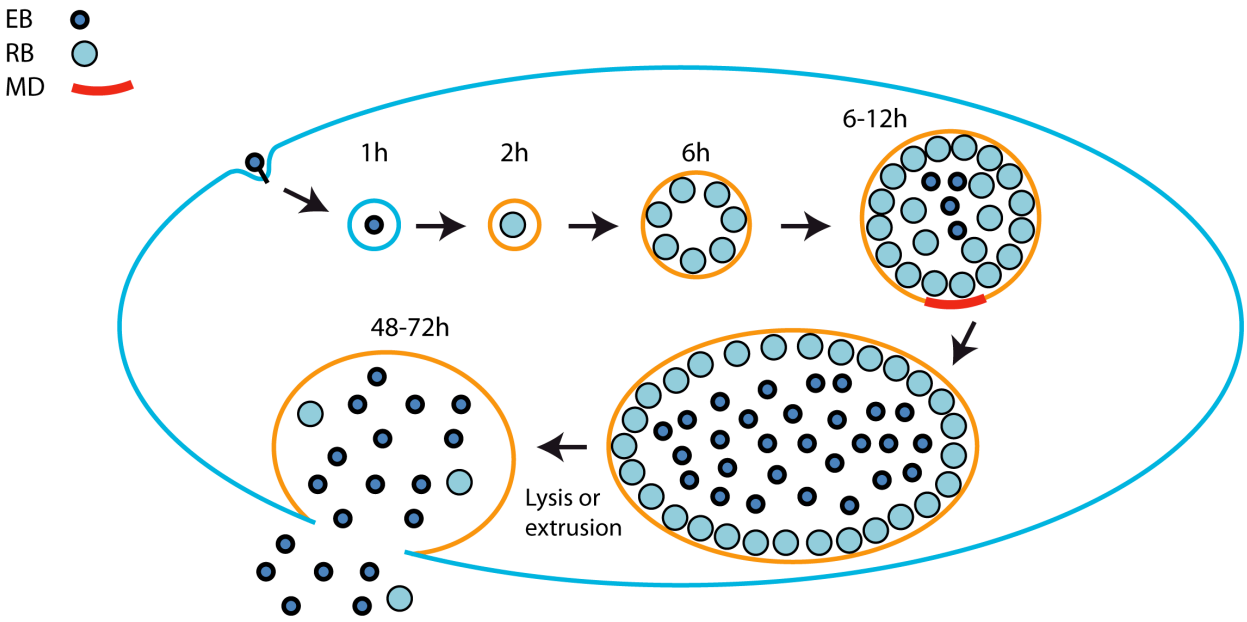

Figure 1.1 Life cycle of *C. trachomatis*. *C. trachomatis* elementary body (EB) binds to susceptible host cell surface and induces its own uptake into a membrane bound vacuole, called an inclusion. Upon entry into the host cell, EB reorganizes itself into the replicative reticulate body (RB) form within the inclusion and begins to divide. As infection progresses, the inclusion size increases substantially and RBs begin to differentiate back into EBs. Microdomains (red) that are enriched in several bacteria-derived Inclusion (Inc) proteins and cholesterol assemble on the inclusion membrane and play an essential role in *C. trachomatis* inclusion positioning during interphase. *C. trachomatis* can exit the host cell by either lysis, which kills the host cell in the process, or extrusion, which leaves a viable host cell behind.

1.2.1 Biphasic development cycle of *Chlamydia*

Chlamydia trachomatis was originally discovered in 1907 as the causative agent for trachoma, a devastating worldwide disease at the time. However, it was misclassified initially as a protozoan parasite and then as a virus until the 1960s, when it was finally recognized as a bacterium (Budai, 2007; Horn, 2008; Byrne, 2003). The *Chlamydia* development cycle is characterized by two distinct forms: the infectious but metabolically inactive EB, which is adapted for extracellular survival, and the non-infectious but metabolically-active RB, which is the replicative form responsible for bacterial growth inside a host cell. *C. trachomatis* EBs are approximately 0.3 μm in diameter and have highly cross-linked outer membrane protein complex, which provides stable structural rigidity for this spore-like form. A number of cysteine-rich chlamydial proteins, such as OmpA (Outer membrane protein A), OmcA and OmcB, are present in the EB's outer membrane and these proteins through disulfide interactions provide the strong structural support necessary for extracellular survival (Abdelrahman and Belland, 2005). A type III secretion system (TTSS), which plays important roles in chlamydia invasion, is also embedded in the EB outer membrane (Fields et al., 2003; Peters et al., 2007; Clifton et al., 2004). Within the confines of the bacterial plasma membrane, chlamydial DNA exists in a highly compacted format with the help of Hc1 (Histone H1-like protein Hc1) and Hc2, two chlamydial histone-like proteins (Brickman et al., 1993; Hackstadt et al., 1991; Barry et al., 1992). During the internalization process, the highly cross-linked disulfide bonds on the EB surface become reduced and the chlamydial DNA starts to decondense likely due to interaction with a small metabolite (Grieshaber et al., 2004; Hackstadt et al., 1985; Shaw et al., 2000; Cocchiaro and Valdivia, 2009). Following these structural changes, the resulting RBs are approximately 1 μm in diameter and contain decondensed DNA, which allow unimpeded bacterial transcription and replication (Abdelrahman and Belland, 2005). Large numbers of chlamydial genes involved in transcription, translation, protein modification and DNA replication are turned on within 2 hours of entering a susceptible host cell (Shaw et al., 2000). The RB contains higher density of TTSS than the EB and many of the TTSS in the RBs are concentrated at contact sites between the RB and the inclusion membrane based on electron microscopy studies, which may be important for efficient delivery of bacterial effector proteins into host cytoplasm (Matsumoto, 1982; Peters et al., 2007; Matsumoto, 1981; Fields et al., 2003). The RB divides by binary fission and begins to asynchronously differentiate back into EB 15 to 25 hours post infection (hpi). A number of late infection genes, such as Hc1 and

OmcB, are activated to suppress global transcription and increase cross-linking in the outer membrane, which allows the differentiation of RBs into the EB form (Moulder, 1991; Stirling and Richmond, 1977; Shaw et al., 2000).

1.2.2 Invasion, nutrient acquisition and growth of *Chlamydia*

***C. trachomatis* attachment and invasion**

The exact mechanisms by which *C. trachomatis* attaches and infects various cell types remain unclear; however, it is has been proposed that the attachment of chlamydia EB to the host cell surface involves two separate steps. The EB first reversibly binds to heparan sulphate-like glycosaminoglycans on the host cell surface through electrostatic interactions (Figure 1.2A). A number of seminal studies have shown that GAGs (glycosaminoglycans) and MOMPs (major outer membrane proteins) on the EB surface play important roles in host cell attachment likely at the reversible stage (Dautry-Varsat et al., 2005; Davis & Wyrick, 1997; Kuo, Lee, & Campbell, 2004; Su et al., 1996; Zhang & Stephens, 1992). It has been recently reported that, in addition to heparan sulfate, sulfation levels of host surface proteins are directly correlated with *C. trachomatis* EB attachment (Rosmarin et al., 2012). Following the weak reversible interaction, the EB irreversibly binds to specific host cell receptors and initiates internalization (Dautry-Varsat et al., 2005; Carabeo and Hackstadt, 2001; Fudyk et al., 2002). A number of host surface proteins, such as PDI (protein disulfide isomerase) and PDGFR (platelet-derived growth factor receptor), have been identified as receptors for the irreversible EB attachment to host cells (Figure 1.2B) (Elwell et al., 2008; Abromaitis and Stephens, 2009).

Since epithelial cells are the main natural host for *C. trachomatis*, this bacterium has evolved mechanisms to induce its efficient uptake by the non-phagocytic host. After the establishment of a stable interaction with the host cell surface, the EB is known to deliver its effector protein, TARP (Translocated Actin Recruiting Protein), into the host cytosol to facilitate its internalization (Clifton et al., 2004). TARP is injected into the host cytosol through the TTSS and it is rapidly tyrosine-phosphorylated by host cell kinases, such as Abl (Abelson tyrosine-protein kinase 1) and PDGFR (Elwell et al., 2008). Phosphorylated-TARP contributes to the EB uptake by recruiting actin and activating the Rho family GTPase, Rac, at the EB attachment sites (Figure 1.2) (Lane et al., 2008; Carabeo et al., 2004; Elwell et al., 2008; Clifton et al., 2004). Actin polymerization is required for EB invasion as this process is inhibited by actin-

depolymerization drug cytochalasin D (Boleti et al., 1999; Carabeo et al., 2002). Rac is also recruited to the sites of EB attachment and activated by two distinct guanine exchange factors (GEFs), Sos1 (Son of sevenless homolog 1) and Vav2 (Guanine nucleotide exchange factor VAV2), both of which bind to phosphorylated TARP (Lane et al., 2008). *C. trachomatis* can also invade host cells in a process resembling receptor-mediated endocytosis, where clathrin is recruited to EB internalization sites (Figure 1.2) (Majeed and Kihlström, 1991; Hodinka et al., 1988; Wyrick et al., 1989). Even though defective clathrin machinery generated from overexpression of dominant negative dynamin and Eps15 (Epidermal growth factor receptor substrate 15) did not significantly affect *C. trachomatis* entry into epithelial cells (Boleti et al., 1999), siRNA against clathrin heavy chain and other components of the clathrin-mediated endocytosis caused approximately 50% reduction in EB internalization (Hybiske and Stephens, 2007). Clathrin-coated pits and vesicles associate with EBs in polarized epithelial cells cultured on collagen-coated surface but not on glass (Wyrick et al., 1989). It is currently still unclear whether the TARP-induced uptake and clathrin-mediated endocytosis are independent or cooperate together to maximize EB invasion.

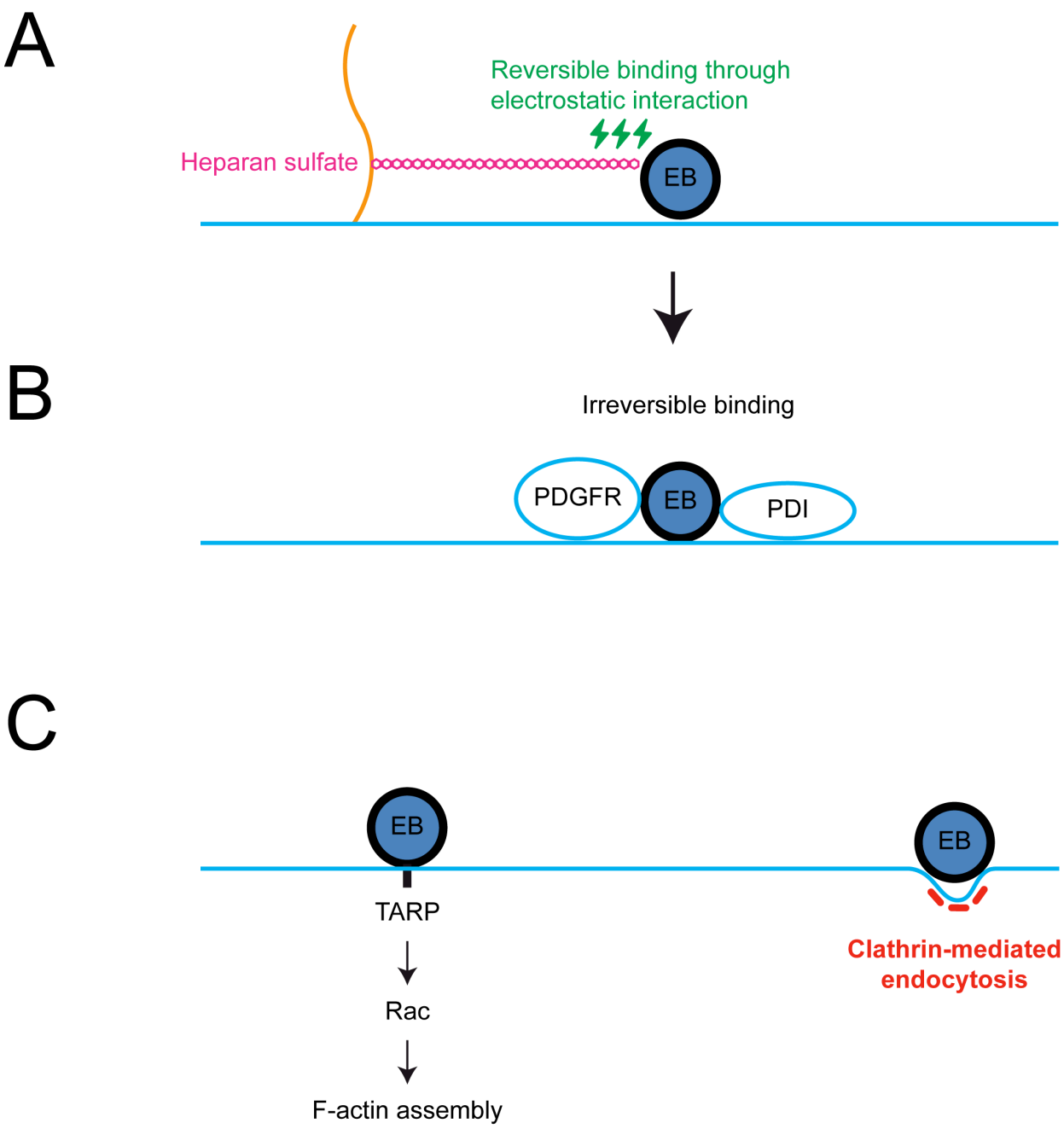

Figure 1.2 Attachment and infection of susceptible host cells by *C. trachomatis* EB. (A) The EB first reversibly binds to heparan sulphate and other proteoglycans on the host cell surface through electrostatic interactions. (B) The EB subsequently irreversibly binds to specific host protein receptors on the plasma membrane, such as PDI and PDGFR. (C) Internalization of EB can be achieved through two pathways. The chlamydial effector protein, TARP is injected into the host cytosol, where it recruits and activates the host Rac protein to promote F-actin assembly and plasma membrane protrusion. The second pathway occurs in a clathrin-dependent manner and resembles clathrin-mediated endocytosis.

Upon entry into a susceptible host cell, the EB rapidly differentiates into the metabolically active RB form inside the host membrane-bound inclusion. The inclusion membrane containing a newly internalized RB becomes very quickly modified and isolates itself from the endocytic pathway. Even though the exact mechanisms by which chlamydia inclusions avoid endocytic targeting remain enigmatic; it is clear that bacterial transcription and translation are essential for this evasion (Scidmore et al., 1996b, 2003). Inhibition of bacterial transcription or translation with antibiotics results in the lysosomal degradation of the internalized chlamydia (Scidmore et al., 1996b). The chlamydia inclusion is devoid of detectable levels of early and late endosome and lysosomal markers, such as Rab5 (Ras-related protein Rab5), Rab7 and LAMP1 (lysosome-associated membrane protein-1), in susceptible host cells (Scidmore et al., 2003; Heinzen et al., 1996). Interestingly, our laboratory has recently shown that *C. trachomatis* EBs are targeted extremely quickly to lysosomes within infected mouse macrophages, a resistant cell type that can suppress chlamydia growth (Sun et al., 2012). Even though nascent chlamydia inclusions do not associate with early and late endosomal markers in epithelial cells, they frequently recruit recycling endosomal markers, Rab1, Rab4, Rab6 and Rab11(Rzomp et al., 2003; Capmany et al., 2011; Rejman Lipinski et al., 2009).

C. trachomatis nutrient acquisition

C. trachomatis has a substantially reduced genome and lacks several *de novo* biosynthetic pathways due to its parasitic life style; and as a result has to import amino acid, nucleotides and lipids from the host cell for its growth (Kalman et al., 1999; Stephens et al., 1998; Cocchiaro and Valdivia, 2009; Saka and Valdivia, 2010). *C. trachomatis* intercepts host-derived sphingomyelin, cholesterol, and glucosylceramide through not yet fully understood processes involving Rab GTPases or CERT (ceramide transfer protein) (Carabeo et al., 2003; Scidmore et al., 1996a; Hackstadt et al., 1996; Su et al., 2004; Hackstadt et al., 1995b; Scidmore et al., 2003, 1996b; Derré et al., 2011). Studies in recent years have identified and highlighted the importance of a number of recycling and exocytic Rabs in chlamydia lipid acquisition and growth. siRNA knock down of Rab6 and Rab11 leads to significantly reduced sphingolipid acquisition and growth rate of *C. trachomatis* in infected epithelial cells (Rejman Lipinski et al., 2009). Similarly, disruption of Rab14 function by overexpression of dominant negative construct in infected epithelial cells also leads to a significant reduction in sphingolipid interception and *C. trachomatis* replication (Capmany et al., 2011; Capmany and Damiani,

2010). Moreover, ultrastructural analysis reveals a large number of aberrant *C. trachomatis* particles in cells with disrupted Rab14 function (Capmany and Damiani, 2010). *C. trachomatis* can exploit CERT, a host protein that is known to be involved in the non-vesicular transport of ceramide from ER to Golgi, and the inclusion acquires lipids through establishing direct contacts with the endoplasmic reticulum (ER) (Derré et al., 2011; Hanada et al., 2003). In order to increase lipid acquisition, *C. trachomatis* has evolved mechanisms to disrupt the normal Golgi structure, which will be discussed in detail in section 1.3.1. In addition to the Rab-mediated and CERT-mediated pathways, *C. trachomatis* can also target and import intact neutral lipid droplets from the host cytoplasm (Cocchiaro et al., 2008; Kumar et al., 2006).

Amino acids are another type of nutrient that *C. trachomatis* co-opts from the host cell, as its genome does not code for a complete amino acid *de novo* biosynthesis pathway. *C. trachomatis* imports host amino acids under normal growth conditions and its growth is greatly enhanced by eukaryotic protein synthesis inhibitor, such as cycloheximide, likely due to increased availability of free amino acids in the host cytosol (Hatch, 1975b; Ripa and Mårdh, 1977; Harper et al., 2000). Removal of all or single amino acids from the growth medium typically leads to attenuated *C. trachomatis* replication (Karayiannis and Hobson, 1981; Harper et al., 2000; Allan et al., 1985). Interestingly, several amino acids, such as leucine, isoleucine, methionine, or phenylalanine, when present in excess disrupts chlamydia growth (Al-Younes et al., 2006; Braun et al., 2008). This has been attributed to the competitive inhibitory effect on the chlamydia amino acid transporter BrnQ (Branched-chain amino acid transport system carrier protein BrnQ) by these excess amino acids, which prevents the import of another essential amino acid valine into the inclusion (Braun et al., 2008). Another potential source of amino acids and oligopeptides that can be exploited by *C. trachomatis* comes from recently degraded proteins in the host lysosome. Even though chlamydia inclusions do not colocalize with lysosomal markers (Heinzen et al., 1996; Scidmore et al., 2003), inclusions are in close proximity of the lysosomes throughout the infection (Ouellette et al., 2011). Degradation products of exogenous proteins containing taggable amino acid are incorporated into *C. trachomatis* inclusions and these degradation products promote chlamydia growth under nutrient-deprivation conditions (Ouellette et al., 2011).

Chlamydia does not have the biosynthetic machinery capable of carrying out *de novo* synthesis of purines and pyrimidines and has evolved at least two nucleotide transporters, Npt1

(nucleoside phosphate transporter1) and Npt2, to meet its DNA replication and energy transduction needs (Saka and Valdivia, 2010; Tjaden et al., 1999). Through these transporters, *C. trachomatis* imports three (ATP, GTP and UTP) nucleotides into the inclusion, while CTP can be imported from the host cytosol or converted from UTP by chlamydial enzymes (Tipples and McClarty, 1993). Even though *C. trachomatis* imports ATP from the host, it still contains sufficient glucose metabolic enzymes that are capable of replenishing its energy supply (Iliffe-Lee and McClarty, 1999). Lastly, *C. trachomatis* co-opts iron from the host cell for its growth and iron deficiency leads to aberrant chlamydia development and reduced replication (Raulston, 1997; Al-Younes et al., 2001). The chlamydia ribonucleotide reductase, an enzyme responsible for DNA replication, requires iron (III) as a cofactor for its normal function (Roshick et al., 2000; Jiang et al., 2007).

C. trachomatis growth

As the infection progresses, a large number of mid-cycle chlamydial genes become activated between 6 and 12 hpi. Many of these genes encode for proteins on the inclusion membrane or are involved in chlamydia metabolism and growth (Shaw et al., 2000). IncA (Inclusion membrane protein A) is one of the proteins that are expressed during the mid-cycle and it is important for mediating homotypic fusions between nascent *C. trachomatis* inclusions to form a single, large inclusion in the same host cell (Figure 1.3) (Hackstadt et al., 1999; Shaw et al., 2000). IncA mutants typically show drastically reduced replication rate based on reinfection and PCR-based assays. Instead of a single large inclusion, host cells infected with IncA mutants have many smaller inclusions in the cytoplasm (Suchland et al., 2008; Xia et al., 2005). The exact physiological benefits of fusion between smaller inclusion remains to be fully elucidated, because conventional gene-specific knockout tools currently do not exist for chlamydia and naturally occurring IncA mutant strains may carry additional mutations that will likely confound the results. Of particular interest to the research that will be presented in Chapter 4, mid-cycle Inc101, Inc222 and Inc850 along with the early-cycle IncB form small patches on the inclusion membrane surface called microdomains (Figure 1.3) (Mital et al., 2010). These microdomains can recruit active host Src family kinases, a group of tyrosine kinases that regulate a wide range of cellular functions, and are enriched in cholesterol (Figure 1.3) (Mital et al., 2010). Signaling pathways involving Src family kinases include adhesion and spreading, lamellipodia and migration, cell cycle progression and phospholipid metabolism (Thomas and Brugge, 1997). Src

kinase activities are significantly enhanced at 20 hpi and this enhancement depends on chlamydia protein synthesis (Mital and Hackstadt, 2011a). Active Fyn, a member of the Src family kinases, is recruited to the inclusion microdomains and plays an important role in sphingolipid acquisition by chlamydia (Mital and Hackstadt, 2011b). Moreover, these microdomains are essential for early trafficking of *C. trachomatis* inclusions to the microtubule organizing centre (MTOC) during interphase in the host cell (Figure 1.3) (Mital and Hackstadt, 2011a). *C. trachomatis* hijacks the retrograde MT-dependent dynein motor for its trafficking to the host MTOC and sequestration of dynein with blocking antibody microinjection abolishes this MTOC targeting of the inclusions (Grieshaber et al., 2003b). Interestingly, *C. trachomatis* inclusions in cells with attenuated Src family kinase activities also exhibit a dispersed distribution within the host cell similar to inclusions in cells microinjected with the dynein blocking antibody (Mital and Hackstadt, 2011a). These observations suggest that Src family kinases and dynein likely cooperate together to achieve the MTOC targeting of *C. trachomatis* inclusions. Consistent with this theory, inclusion microdomains, which colocalize with active Src kinases, overlap with dynein and spindle MTs during mitosis (Mital et al., 2010). Even though *C. trachomatis* growth is significantly reduced in cells with attenuated Src kinase activities where the inclusions are not trafficked to the host MTOC, the exact physiological impact of host MTOC targeting of *C. trachomatis* inclusion is still not fully understood due to the confounding effect of Src family kinases' involvement in *C. trachomatis* lipid acquisition (Mital and Hackstadt, 2011a; b). My work examining the role of microdomains in *C. trachomatis* inclusion positioning in mitosis, particularly after pharmacological inhibition, is presented in Chapter 4.

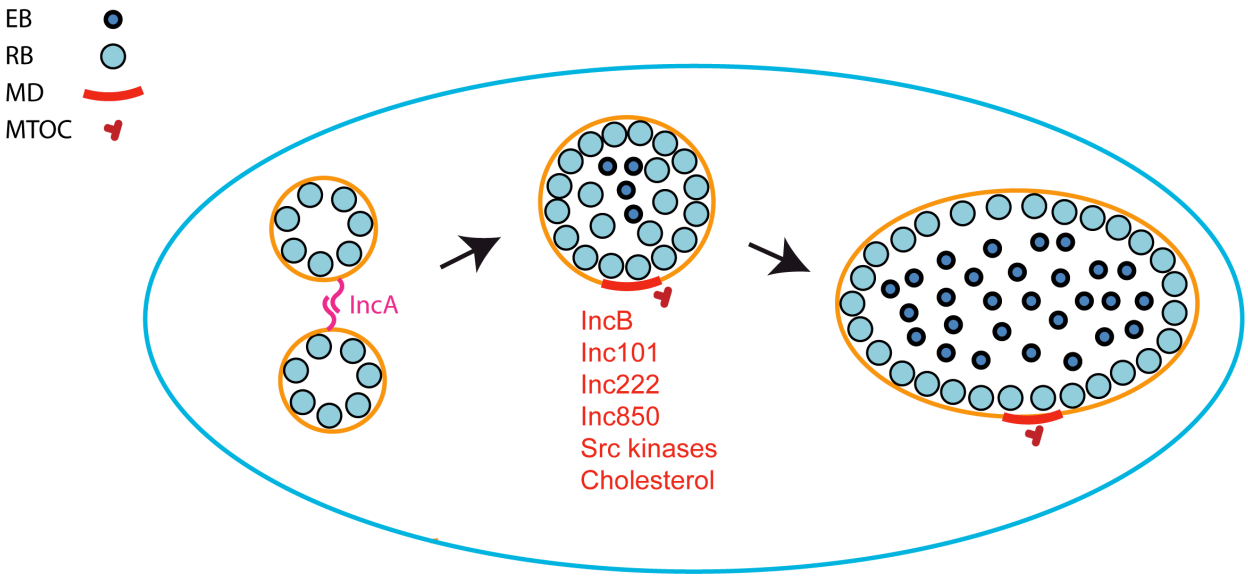

Figure 1.3 Inc proteins mediate inclusion fusion and microdomain formation. IncA is essential for the fusion of smaller inclusions into a single large inclusion. IncB, Inc101, Inc222 and Inc850 form small clusters on the inclusion surface termed microdomains. Microdomains can recruit active host Src family kinases and are enriched in cholesterol. Microdomains play important roles in lipid acquisition and association with the host cell MTOC.

As chlamydia RBs replicate by binary fission, the inclusion size also increases drastically over the course of the infection and by the end of the infection cycle the inclusion can occupy most of the host cytoplasm (Valdivia, 2008). Space constraint placed on the inclusion by densely packed host cytoskeletons is originally thought to be alleviated by the activities of the bacterial effector protein, chlamydial protease-like activity factor (CPAF) (Zhong, 2009; Kumar and Valdivia, 2008; Dong et al., 2004). Reorganization and recruitment of actin and intermediate filament around large chlamydia inclusions occurs after 26 hpi (Kumar and Valdivia, 2008). The presence of intact F-actin and intermediate filament networks are important for maintaining chlamydia inclusion integrity and disruption of these cytoskeletal networks with pharmacological agent or genetic knockout leads to deformed chlamydia inclusions (Kumar and Valdivia, 2008). This cytoskeletal rearrangement is initially attributed to CPAF, because this secreted chlamydial effector cleaves a number of host signaling and cytoskeletal proteins, including several members of the intermediate filament cytoskeleton (Kumar and Valdivia, 2008; Zhong, 2009; Dong et al., 2004). However, a preeminent study published in late 2012 shows that most of the reported cleavage or degradation of host proteins, including intermediate filament proteins, by CPAF are in fact artifacts of the cell lysate collection procedure (Chen et al., 2012). Chen et al. convincingly demonstrate that CPAF degradation of host proteins occurs only after the addition of radioimmunoprecipitation assay (RIPA) buffer, because brief treatment with a CPAF inhibitor immediately before lysate collection abolishes the cleavage of host proteins. Moreover, lysates collected with high concentration of urea, which leads to the instant denaturation of all proteins including CPAF, show no signs of degradation or cleavage of any of the tested host proteins that have been previously reported as substrate of CPAF. Nevertheless, the observation that F-actin and intermediate filaments are recruited to large *C. trachomatis* inclusions is still reproducible, indicating these cytoskeletal elements are modified, but through currently unknown mechanisms (Chen et al., 2012). The now disputed CPAF is still found to be autocatalytic and cleaves itself to become activated in infected cells with the new lysate collection procedure (Chen et al., 2012). A number of reported host and chlamydial proteins remain to be tested to confirm whether they are authentic substrates of CPAF in intact cells (Chen et al., 2012). Prolonged inhibition of CPAF activity with a membrane-permeable CPAF-specific inhibitory peptide leads to aberrant chlamydia inclusion and drastically reduced replication, indicating CPAF still plays an important role in maintaining normal *C. trachomatis* growth, albeit through yet to be determined mechanisms (Jorgensen et al., 2011).

1.2.3 Exit and dissemination strategies

As early as 18 hpi the RBs begin to asynchronously transition back into the EB form and loss of contact of RBs with the inclusion membrane may be the developmental cue that prompt the RBs to begin differentiating into the EB form (Peters et al., 2007; Wilson et al., 2006). Even though the exact differentiation steps are still mostly elusive, a number of late-cycle genes, which often encode EB-specific proteins, are activated around this time. OmcB, a cysteine-rich EB outer membrane protein that provides structural stability, is synthesized during the RB to EB transition (Clarke et al., 1988; Shaw et al., 2000). In addition to providing strong structural support, OmcB is also identified as a surface-exposed adhesin responsible for the initial attachment of EBs to the host cells (Fadel and Eley, 2007; Moelleken and Hegemann, 2008). Similarly, the histone-like protein Hc1, responsible for condensing the chlamydial DNA to meet the space constraint of an EB, is produced at the same time (Grieshaber et al., 2006a; Shaw et al., 2000). In addition, lipooligosaccharide plays an important role in the transition of *C. trachomatis* RB to EB. Disruption of lipooligosaccharide synthesis with pharmacological inhibitors prevents the production of infectious progenies without affecting the formation of large *C. trachomatis* inclusions, which are filled with RBs that are unable to transition back into the infectious EB form (Nguyen et al., 2011). Interestingly, *C. trachomatis* appears to have a lipooligosaccharide-sensing mechanism, because inhibition of lipooligosaccharide production causes substantially reduced OmcB, but not Hc1 synthesis (Nguyen et al., 2011).

Unlike the enigmatic transition from RB to EB, the release of *C. trachomatis* from host cells at the end of the infection cycle is relatively well documented. *C. trachomatis* can exit from the host cells in two distinct mechanisms: lysis or extrusion (Valdivia, 2008). The lysis pathway is characterized by the rapid ordered permeabilization of inclusion membrane, nuclear membrane and host plasma membrane (Hybiske and Stephens, 2007). This process requires cysteine proteases and pharmacological inhibition of these proteases prevents the initial lysis of the inclusion membrane (Hybiske and Stephens, 2007). The extrusion pathway is dependent on host F-actin, myosin II and RhoA (Ras homolog gene family member A) activities and it takes 2-3 hours to complete. At the beginning of extrusion, the inclusions protrude from the host cell and live imaging experiments show that these inclusions remain continuous with the host cell for some time before becoming fully released from the host (Hybiske and Stephens, 2007; Chin et al., 2012). Depolymerization of F-actin, or inhibition of myosin II or RhoA with pharmacological agents, leads to almost complete inhibition of extrusion events. Interestingly,

jasplakinolide, a drug that stabilizes F-actin and prevents F-actin depolymerization, increases the extrusion frequency to 100% of infected cells (Hybiske and Stephens, 2007). Consistent with this, *C. trachomatis* inclusions are surrounded by F-actin-rich coats, the disruption of which leads to significantly reduced extrusion events (Chin et al., 2012). Moreover, chlamydia protein synthesis and functional TTSS are both essential for maintaining these actin coats, indicating that *C. trachomatis* actively secretes effector proteins to sustain these structures. TARP has F-actin nucleating and bundling properties; however, its involvement in *C. trachomatis* extrusion remains to be tested (Jiwani et al., 2013; Jewett et al., 2006). Following chlamydia release, the fusion of lysosomes with host plasma membrane helps with wound repair to maintain host cell integrity (Beatty, 2007). This fusion event is serovar-specific and it requires calcium ions and actin-depolymerization. Depletion of calcium or inhibition of actin-depolymerization with pharmacological agents significantly reduces fusion events between lysosomes and host plasma membrane and host cell survival (Beatty, 2007).

1.3 *Chlamydia trachomatis*-induced cellular defects

C. trachomatis infections can induce numerous host cellular defects including Golgi fragmentation, supernumerary centrosomes, abnormal cell cycle and increased frequency of multinucleation (Johnson et al., 2009; Heuer et al., 2009; Knowlton et al., 2011; Balsara et al., 2006; Greene and Zhong, 2003). The exact mechanisms by which *C. trachomatis* causes these defects still remain fully elucidated; however, it is evident that many host proteins are exploited by *C. trachomatis* and contribute to these cellular defects. *C. trachomatis* induces Golgi fragmentation to enhance its lipid acquisition and accelerate its growth; however, it is still unclear what benefits *C. trachomatis* can gain from inducing supernumerary centrosomes, abnormal host cell cycle and multinucleation. The most glaring difficulty associated with studying these pathogenic mechanisms is the lack of specific genetic knockout tools for chlamydia (Heuer et al., 2007). Several recent advances in *Chlamydia* genetics attempt to address this problem which may accelerate our understanding of chlamydia pathogenesis (Nguyen and Valdivia, 2012; Kari et al., 2011). *C. trachomatis*-induced cellular defects discussed below are also diagrammatically summarized in Figure 1.4.

1.3.1 Golgi fragmentation

The Golgi apparatus is an organelle essential for the proper trafficking, processing and post-translational modification of eukaryotic proteins and lipids (Holthuis et al., 2001; Tang and

Wang, 2013). The mammalian Golgi apparatus consists of a number of flattened membranes (cisternae) stacked in parallel and is usually located in close proximity to the host MTOC (Shorter and Warren, 2002; Tang and Wang, 2013). Maintenance of the Golgi structure requires: an intact cytoskeletal network, such as MTs and F-actin; the continuous trafficking of membrane to and from other organelles; and members of the golgin and GRASP (general receptor for phosphoinositides-associated scaffold protein) protein families. Depolymerization of F-actin in mammalian cells causes the Golgi to collapse into a compact structure (Egea et al., 2006), while depolymerization of MTs leads to dispersion of the Golgi stacks away from the host MTOC (Tang and Wang, 2013). Inhibition of membrane trafficking from endoplasmic reticulum to Golgi with pharmacological agents such as Brefeldin A causes the loss of the stacked appearance of the Golgi, which can be reversed upon removal of Brefeldin A (Seemann et al., 2000a). The golgin family proteins are characterized by extensive coiled-coil domains, which may allow them to form stable tethering between cisternae or with transport vesicles. The golgin protein family have many members, such as Golgin84, GM130 (Golgi matrix protein of 130 kDa), p115, and giantin (Munro, 2011). Even though the exact mechanism remains unclear, Golgin84 is important for maintaining the integrity of the Golgi stacks and interestingly, overexpression or depletion of this protein causes Golgi stack fragmentation (Diao et al., 2003; Munro, 2011). The more well-studied member of the golgin family, GM130 interacts with p115 and giantin to mediate the tethering and fusion of ER-to-Golgi carriers with the Golgi (Seemann et al., 2000a; b; Marra et al., 2007). The depletion of GM130 leads to the shortening of the cisternae and fragmentation of the Golgi stacks (Marra et al., 2007). Due to its long coiled-coil domain, GM130 is likely involved in the tethering of adjacent cisternae within the Golgi stacks (Tang and Wang, 2013). Golgi reassembly stacking protein of 65 kD (GRASP65) and GRASP55 localize to the *cis*-Golgi and medial-to-*trans* Golgi respectively and cooperate together to maintain Golgi stack stability (Xiang and Wang, 2010). GRASP65 and GRASP55 first form stable homodimers on the same cisterna and subsequently these homodimers from adjacent cisternae can form oligomers that hold the cisternae in stacks (Tang and Wang, 2013). While depletion of GRASP65 or GRASP55 individually with siRNA reduces the number of cisternae in the Golgi stack, simultaneous depletion of both proteins with siRNA leads to the complete disassembly of the entire Golgi stack (Xiang and Wang, 2010). GRASP65 binds to and recruits GM130 to the *cis*-Golgi, which subsequently recruits p115 and giantin to the *cis*-Golgi network (Barr et al., 1998; Tang and Wang, 2013).

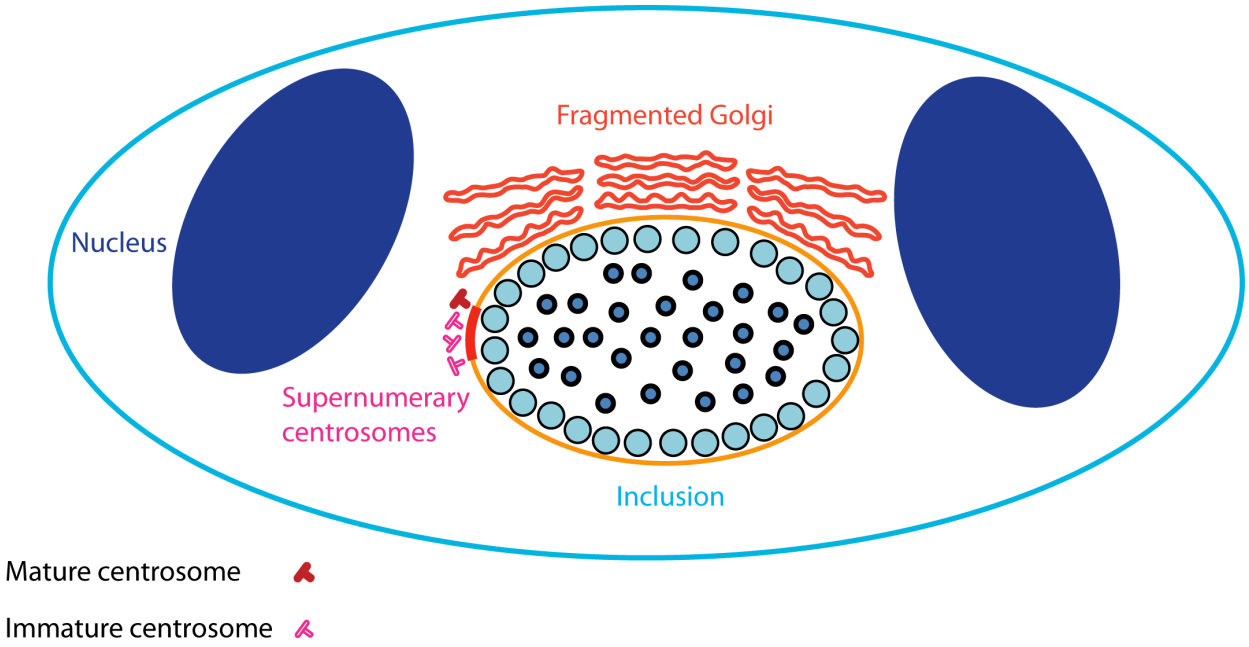

Figure 1.4 *C. trachomatis* infection leads to host Golgi fragmentation, centrosome amplification, mitotic entry delay and multinucleation. After *C. trachomatis* infection, the Golgi breaks down into mini-stacks and surrounds the inclusion, which is essential for efficient *C. trachomatis* lipid acquisition. Host centrosome numbers increase as *C. trachomatis* infection progresses and the majority of the amplified centrosomes lack mature centrosomal markers indicating they did not simply arise from failed cytokinesis. The number of multinucleated host cells increases over the course of the *C. trachomatis* infection and it has been postulated but not proven to be a result of cytokinesis failure.

In order to segregate into two daughter cells, the Golgi undergoes extensive fragmentation and vesiculation during early mitosis; as a result, proteins involved in maintaining normal Golgi integrity must be inactivated accordingly (Tang and Wang, 2013; Shorter and Warren, 2002; Wei and Seemann, 2010). A large number of G2 and mitotic kinases contribute to the fragmentation and vesiculation process by inactivating the maintenance factors (Persico et al., 2009). GRASP65 contains multiple phosphorylation sites for CDK1 (cyclin-dependent kinase 1)and Plk1 (polo-like kinase 1) and the phosphorylation of these sites can disrupt the oligomerization that holds the cisternae together, leading to the separation of the Golgi stacks (Tang and Wang, 2013; Wang et al., 2003). Similarly, GRASP55 can be phosphorylated and inactivated by mitogen-activated protein kinase 1 (MEK1) and extracellular-signal-regulated kinase 1 (ERK) during G2 to M transition (Corda et al., 2012; Xiang and Wang, 2010; Shorter and Warren, 2002; Tang and Wang, 2013). During early mitosis, Golgin84 also becomes phosphorylated, which may modify its activities to promote further Golgi fragmentation (Tang and Wang, 2013; Diao et al., 2003; Munro, 2011). Phosphorylation of GM130 by CDK1 at serine 25 during early mitosis prevents its interaction with p115, which contributes to the vesiculation of the Golgi (Lowe et al., 2000, 1998; Tang and Wang, 2013). Following the extensive vesiculation process, the Golgi mostly disintegrates into a Golgi haze consisting of thousands of sub-micron vesicles (Gaietta et al., 2006; Colanzi et al., 2003). A small number of Golgi membrane structures do not undergo vesiculation and carry GRASP and golgin proteins throughout mitosis, which may act as templates for Golgi reassembly during late mitosis. Interestingly, the Golgi membrane structures accumulate near each mitotic spindle pole, which may facilitate the Golgi inheritance into two daughter cells (Persico et al., 2009; Wei and Seemann, 2009; Shima et al., 1998).

During *C. trachomatis* infection, the Golgi stacks become progressively fragmented, which is important for normal chlamydia growth and development (Heuer et al., 2009; Rejman Lipinski et al., 2009; Christian et al., 2011). It is initially believed that *C. trachomatis* induces Golgi fragmentation by its secreted effector protein CPAF, as ectopic expression of this protein in host cells leads to Golgi fragmentation (Christian et al., 2011). By 36 hpi, intact Golgin84 protein is no longer detectable by western blotting (Heuer et al., 2009). Moreover, *C. trachomatis*-induced Golgi fragmentation can be prevented by treatment with CPAF inhibitors and siRNA knock down of Rab6 and Rab11 (Rejman Lipinski et al., 2009; Heuer et al., 2009; Christian et al.,

2011). Neither *C. trachomatis* infection, nor ectopic expression of CPAF in Rab6 and Rab11deficient cells leads to Golgi fragmentation, demonstrating the importance of these two Rab GTPases. When Golgi fragmentation is inhibited in *C. trachomatis*-infected cells with pharmacological agents or siRNA against Rab6 or Rab11, lipid acquisition and growth rate of *C. trachomatis* is significantly reduced (Rejman Lipinski et al., 2009; Heuer et al., 2009). Even though there is compelling evidence that CPAF cleaves Golgin84 resulting in the fragmentation of the Golgi stacks, the recent study by Chen et al. shows that CPAF does not actually cleave Golgin84 in intact host cells and the cleavage only occurs during the cell lysis procedure using RIPA buffer (Chen et al., 2012). When *C. trachomatis*-infected cells at 36 hpi are treated with CPAF inhibitor *clasto*-lactacystin 1 hour prior to lysis by RIPA, only intact Golgin84 protein is detected by western blot. Moreover, when cells are lysed with 8 M urea, which instantaneously denatures all enzymes including CPAF, only intact Golgin84 is detected. Nevertheless, Golgi still undergoes fragmentation following *C. trachomatis* infection and *C. trachomatis* in cells with non-fragmented Golgi grows substantially slower. These findings suggest that *C. trachomatis* induces Golgi fragmentation through a currently unknown mechanism to gain additional growth advantage by acquiring lipids more quickly (Chen et al., 2012). In this thesis, we present evidence that *C. trachomatis* may block host cell mitosis to gain access to additional Golgi lipids.

1.3.2 Centrosome amplification

The centrosome/ MTOC is the primary MT nucleating centre and it is essential for all MT-dependent processes, such as vesicle transport, organelle localization, and mitosis (Fukasawa, 2005). The centrosome consists of a pair of centrioles that are surrounded by a large number of pericentriolar material proteins (Andersen et al., 2003; Fukasawa, 2005; Bettencourt-Dias and Glover, 2007). Centrosome duplication is tightly regulated and only occurs once per cell cycle during S phase under normal conditions (Fukasawa, 2005). A large number of proteins contribute to the regulation of centrosome duplication and among these are the cell-cycle-specific kinases such as Plk4 and CDK2 (Strnad and Gönczy, 2008). Centrosome duplication is carried out through a semi-conservative mechanism where each existing centriole acts as the template for the formation of the new daughter centriole (Fukasawa, 2005; Bettencourt-Dias and Glover, 2007; Strnad and Gönczy, 2008; Kleylein-Sohn et al., 2007; Nigg, 2007). Following centrosome duplication in S phase, G2 cells contain two centrosomes that are tethered together to prevent premature separation (Bahe et al., 2005; Yang et al., 2006). Throughout the G2 phase,

the newly formed centrioles undergo a maturation process, which recruits additional centrosomal proteins, such as γ-tubulin and Cep170 (centrosomal protein 170kDa) (Kleylein-Sohn et al., 2007). As a result, age/maturity of the centrioles can be inferred based on the presence of these proteins. By late G2 phase, two fully matured centrosomes separate from each other and form the mitotic spindle poles. Following normal mitosis, each daughter cell inherits one spindle pole and re-enters interphase with one centrosome (Strnad and Gönczy, 2008; Fukasawa, 2005). Centrosome duplication is under tight regulation, because centrosome abnormalities can have severe consequences such as multiple mitotic spindle poles, missegregation of chromosomes, aneuploidy and cancer formation (Fukasawa, 2005; Nigg, 2007). Cellular defects such as loss of p53 function, uncoupling of centrosome duplication from cell cycle and cytokinesis failure can all lead to supernumerary centrosomes (Fukasawa et al., 1996; Duensing et al., 2000; Fukasawa, 2005; Meraldi et al., 2002). Experimental manipulation of proteins involved in the centrosome duplication process, such as Plk4 and CDK2, can also cause centrosome number fluctuations (Strnad and Gönczy, 2008).

C. trachomatis infection can lead to abnormal centrosome/MTOC positioning and supernumerary centrosomes in host cells and the number of centrosomes increases over time in infected cells (Grieshaber et al., 2006b). Instead of the usual perinuclear localization, centrosomes are frequently associated with *C. trachomatis* inclusions and become distanced from the nucleus (Grieshaber et al., 2006b). More than 50% of *C. trachomatis*-infected cells contain more than two γ-tubulin-positive centrosomes by 40 hpi, many of which develop multiple spindle poles and misaligned chromosomes after entering mitosis (Grieshaber et al., 2006b). The majority of the amplified centrosomes in *C. trachoamtis*-infected cells are immature centrosomes that lack mature centriole marker Cep170 (Johnson et al., 2009). Moreover, *C. trachomatis* may exploit host cell kinases that normally regulate centrosome duplication, such as Plk4 and CDK2, to cause centrosome amplification. Disruption of Plk4 and CDK2 activities in *C. trachomatis*-infected cells with dominant negative construct transfections can return the centrosome numbers to uninfected levels (Johnson et al., 2009). In addition, *C. trachomatis* also disrupts the centrosomal clustering mechanism, which can group multiple centrosomes into two spindle poles to prevent multipolarity during mitosis (Quintyne et al., 2005; Knowlton et al., 2011). Another recent study shows that centrosome mislocalization from the perinuclear region and genetic instability may occur in a chlamydia-infected mouse model (Knowlton et al., 2013). Even though there is clear evidence that *C. trachomatis* causes host cell

centrosome amplification and mitotic spindle pole multipolarity, the exact physiological benefits for *C. trachomatis* to cause these defects remains elusive.

1.3.3 Host cell cycle impediment and multinucleation caused by *Chlamydia*

Cell cycle of somatic mammalian cells

The somatic mammalian cell cycle is characterized by highly regulated duplication of DNA and organelles followed by division of the nucleus and cytoplasm into two daughter cells. Many proteins are involved in the progression through the four main phases of the cell cycle: G1 (preparation for DNA replication), S (DNA replication), G2 (preparation for mitosis) and M (cell division) (Teixeira and Reed, 2013). Cell-cycle-dependent kinases and cyclins are the central orchestrators of cell cycle signaling and they exert their regulatory activities by forming CDK-cyclin complexes, which can phosphorylate many target proteins that drive cell cycle progression (Teixeira and Reed, 2013; Malumbres and Barbacid, 2009). CDKs levels are relatively constant throughout the cell cycle and they are completely inactive in the absence of cyclin binding partners, while the levels of cyclins fluctuate greatly depending on the cell cycle stage. Cyclin levels are controlled through highly specific ubiquitin-mediated proteolysis. CDK activities are modulated by stimulatory or inhibitory phosphorylation and the presence of negative regulatory proteins (Teixeira and Reed, 2013). Major CDKs and their activating cyclins are summarized in Figure 1.5.

In normal somatic G1 cells, mitogenic signals are sensed by cyclinD, which then binds and activates CDK4 and 6. The activated CDK4/6 complexes turn on a number of genes that are essential for S phase (DNA replication) entry, such as cyclinE and DNA polymerase α (Teixeira and Reed, 2013; Malumbres and Barbacid, 2005). Following the expression of cyclinE, CDK2 becomes activated by forming complex with it to promote entry into S phase. Upon entry into S phase, cyclinE is degraded and cyclinA takes over its role by forming complexes with CDK2 (Malumbres and Barbacid, 2009; Sherr, 2000). In addition to activating CDK2, cyclinA also activates CDK1 and both CDK2-cyclinA and CDK1-cyclinA complexes are responsible for the completion of S phase and the transition to G2 (Malumbres and Barbacid, 2009). CyclinA levels decrease during G2 as they become degraded by ubiquitin-mediated proteolysis, while cyclinB levels begin to rise. Consequently, the cyclinA in CDK1-cyclinA complexes are replaced by cyclinBs such as cyclin B1 and B2. The CDK1-cyclinB1 complex has more than 70 known

substrates and regulates numerous events at the G2 to M transition including: centrosome separation, Golgi fragmentation, chromosome condensation and nuclear lamina breakdown (Malumbres and Barbacid, 2005). CDK1-cyclinB1 complex activities are essential for the entry into and proper progression through mitosis (Malumbres and Barbacid, 2005; Hochegger et al., 2008; Malumbres and Barbacid, 2009). Interphase cells with compromised CDK1-cyclinB complex activity by either pharmacological inhibition or genetic knock down of cyclinB accumulate in G2 and have difficulties entering mitosis (Vassilev et al., 2006; Yuan et al., 2004; Maurer et al., 2009; Brandeis et al., 1998). In addition, pharmacological inhibition of CDK1 activity in mitotic cells leads to premature anaphase onset and mitotic exit (Vassilev et al., 2006). During late mitosis, anaphase promoting complex/cyclosome (APC/C) facilitates the termination of CDK1 activity by targeting cyclinB for degradation (Malumbres and Barbacid, 2009). The reduced CDK1 activity leads to the reversal of cellular changes that occur during mitosis and allow cells to re-enter interphase (Malumbres and Barbacid, 2009; Teixeira and Reed, 2013).

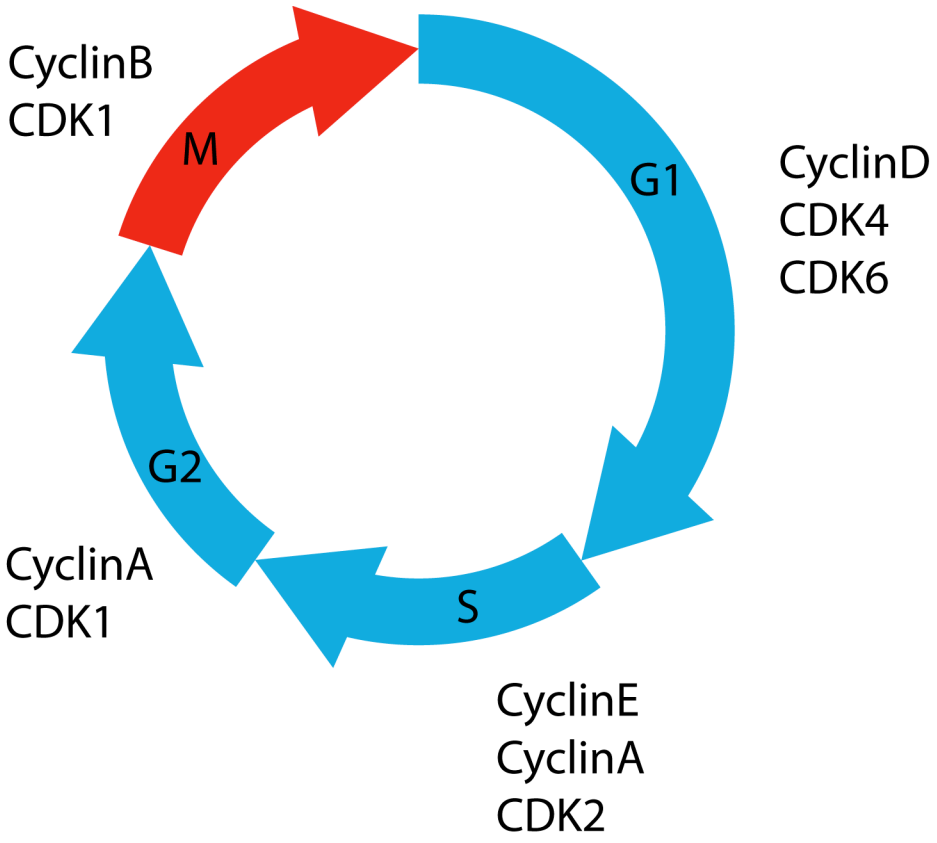

Figure 1.5 Major CDKs and cyclins responsible for mammalian cell cycle progression. In response to mitogenic signals, cyclinD activates CDK 4 and 6, which prepare the cell for entering S phase. CyclinE and cyclinA sequentially activate CDK2 to promote entry into and progression of S phase, during which DNA is replicated. In addition to CDK2, cyclinA also activates CDK1, which drives the completion of S phase and entry into G2. During G2, cyclinA is gradually replaced by cyclinB in forming complexes with CDK1, which is essential for promoting mitotic entry.

Several checkpoints exist in the cell cycle and coordinate with CDK complexes to ensure the accurate passage of complete genetic information to daughter cells (Elledge, 1996; Russell, 1998; Nigg, 2001). DNA damage or unreplicated DNA can trigger the DNA structure checkpoint and delay S phase or mitotic entry by preventing the activation of CDKs (Nigg, 2001; Karlsson-Rosenthal and Millar, 2006). Once cells enter mitosis, they are subject to the spindle assembly checkpoint (SAC), which prevents chromosome segregation and anaphase onset until all chromosomes have the correct bipolar attachment (Nigg, 2001). Both the DNA structure checkpoint and the SAC are essential in maintaining genome stability and loss of function in either checkpoint can lead to increased risks of cancer (Kops et al., 2005; Malumbres and Barbacid, 2009).

Cell cycle of *C. trachomatis*-infected mammalian cells

Cells infected by *C. trachomatis* can still undergo mitosis; however, the time required to complete the cell cycle is significantly longer than uninfected cells and increases with increasing bacterial load (Balsara et al., 2006; Greene et al., 2004; Horoschak and Moulder, 1978). *C. trachomatis* may also impede the host cell cycle by disrupting host mitotic entry or cytokinesis (Greene and Zhong, 2003; Balsara et al., 2006). It is originally discovered that cyclinB1, a major component of the CDK1-cyclinB complex essential for mitotic entry, is degraded following *C. trachomatis* infection (Balsara et al., 2006). In addition, the level of active CDK1 is significantly lower after *C. trachomatis* infection (Balsara et al., 2006). Subsequent studies suggest that the chlamydia effector CPAF is responsible for the degradation of cyclinB1, as ectopic expression of CPAF in uninfected cells is sufficient to cause similar cyclinB1 degradation as *C. trachomatis* infection (Paschen et al., 2008; Christian et al., 2011). The recent study by Chen et al. shows that cyclinB1 degradation is in fact an artifact of RIPA lysis and does not occur in intact cells; however, it is unclear whether the decrease in active CDK1 level is also a RIPA lysis artifact (Balsara et al., 2006; Chen et al., 2012). Nevertheless, *C. trachomatis*-infected cells still have a substantially longer cell cycle. A recent study using long term live cell imaging shows that the S and G2 phase of *C. trachomatis*-infected cells are more than 50% longer than that in uninfected cells (Brown et al., 2012). In addition to mitotic entry delay, studies have suggested that CPAF may act like APC/C and cause untimely degradation of securin, which may lead to the premature separation of sister chromatids and genome instability (Knowlton et al., 2011; Brown et al., 2012). However, it is still unclear whether securin is a true CPAF

substrate in intact cells, as these studies are not conducted under instant denaturation conditions that can prevent *in vitro* degradation artifacts (Knowlton et al., 2011; Brown et al., 2012). The current evidence indicates that *C. trachomatis* prolongs the host cell cycle through an unknown mechanism and may interfere with the host SAC.

1.4 Eukaryotic host cell mitosis and cytokinesis

The somatic cell cycle in eukaryotes is completed with the segregation of duplicated genetic material and the cytoplasm into two identical daughter cells through mitosis and cytokinesis. The CDK1-cyclinB complex is essential for mitotic entry by phosphorylating and activating many signaling proteins that mediate numerous cellular changes during mitosis, such as nuclear envelop breakdown, chromosome condensation, centrosome separation and mitotic spindle assembly (Hochegger et al., 2008; Enserink and Kolodner, 2010; Musacchio, 2011). Due to the high fidelity requirement in the cell division process, mitosis and cytokinesis are under strict regulation by a large number of proteins. The SAC is the best studied mitotic checkpoint that is responsible for safeguarding the faithful separation of chromosomes (Musacchio and Salmon, 2007). SAC prevents mitotic progression past metaphase until all of the chromosomes are correctly attached and oriented (Musacchio and Salmon, 2007). Cytokinesis, division of the cytoplasm, is achieved by the formation and constriction of a contractile ring and sealing of a narrow cytoplasmic canal between two daughter cells. The cytokinetic process is controlled by a large number of proteins that cooperate together to ensure successful cytoplasmic division. Failure in cytokinesis due to experimental manipulation or naturally occurring defects, such as chromosome bridges, can lead to the formation of tetraploid progeny cells.

1.4.1 Mitosis and mitotic SAC

Mitotic SAC in normal mammalian cells

The M (mitotic) phase is characterized by significant cellular changes that are mediated by CDK1-cyclinB complex substrates, such as nuclear envelop breakdown, chromosome condensation, centrosome separation and mitotic spindle assembly (Hochegger et al., 2008; Enserink and Kolodner, 2010). CDK1-cyclinB complexes receive input from several other signaling proteins, including cyclinA and Plk1, and phosphorylate structural lamins in the nuclear envelope and induce the nuclear envelop breakdown in early mitosis (Lindqvist et al., 2009; Enserink and Kolodner, 2010; Gong et al., 2007). CDK1-cyclinB complexes regulate

chromosome condensation by activating the condensin protein complex through phosphorylation, which allows further phosphorylation and full activation of the complex by Plk1 (Hirano, 2005; Abe et al., 2011). The separation of duplicated centrosomes during early prophase requires the kinesin-related protein, Eg5, which is phosphorylated by both CDK1-cyclinB and Plk1 (Blangy et al., 1995; Hochegger et al., 2008). Plk1 is essential for targeting Eg5 to the centrosomes and pharmacological inhibition of Plk1 leads to arrest of cells in early mitosis in a prometaphase-like state (Van Vugt et al., 2004; Santamaria et al., 2007; Lane and Nigg, 1996; Lenart et al., 2007). Sustained CDK1-cyclinB activity is essential for maintaining genome stability until the mitotic spindle assembly is completed, as pharmacological inhibition of CDK1 during early mitosis causes premature cytokinesis with significant chromosome missegregation (Vassilev et al., 2006). In order to protect against genome instability, cells have evolved the SAC to ensure that mitosis does not proceed forward until all chromosomes are correctly attached and oriented the metaphase plate (Musacchio and Salmon, 2007; Musacchio, 2011). This is achieved through inhibition of the APC/C activity in the presence of abnormal chromosome attachment or alignment (Musacchio and Salmon, 2007). Chromosome separation depends on the activity of separase, which cleaves cohesin that hold sister chromatids together. Separase is inactivated by its binding partner securin, which can be degraded by APC/C, until all the chromosomes are properly attached and aligned. APC/C must acquire an essential cofactor, Cdc20, in order to target and degrade securin and cyclinB. Cdc20 is inactivated by the mitotic checkpoint complex consisting of MAD2 (mitotic-arrest deficient), BUBR1 (budding uninhibited by benzimidazole-related 1) and BUB3 (budding uninhibited by benzimidazole) (Musacchio and Salmon, 2007). This mitotic checkpoint complex is only silenced when all chromosomes become attached and bi-oriented. In addition to the SAC, Aurora B, part of the chromosome passenger complex, may also play an important role in tension sensing between sister chromatids, the lack of which also results in APC/C activation delay (Musacchio and Salmon, 2007). Upon passing the SAC, the APC/C becomes activated and targets securin and cyclinB for proteolytic degradation. This will allow the onset of anaphase and subsequent exit from mitosis (Musacchio, 2011; Kops et al., 2005; Musacchio and Salmon, 2007). Together, these mechanisms ensure that all the chromosomes are attached by MTs from both poles and will segregate properly into two daughter cells. Mutation or abnormal expression of MAD2, BUBR1 or BUB3 are associated with various tumor and cancer cell lines (Kops et al., 2005).

SAC in *C. trachomatis*-infected cells

C. trachomatis infection has recently been proposed to interfere with the host SAC and allow cells with unaligned chromosomes to proceed through anaphase. Following *C. trachomatis* infection, CyclinB1 and securin are both degraded by CPAF, which may bypass SAC and promote anaphase onset (Knowlton et al., 2011; Musacchio and Salmon, 2007). Based on the recent study by Chen et al., we now know that cyclinB1 degradation by CPAF does not occur in intact cells; however, it is still currently unclear whether securin is degraded by CPAF (Chen et al., 2012). Nevertheless, M phase in *C. trachomatis*-infected cells is significantly shorter than uninfected cells based on live cell imaging. In addition, the frequency of chromosome bridges that are likely caused by unaligned chromosomes increases significantly after *C. trachomatis* infection (Brown et al., 2012). These findings suggest that *C. trachomatis* infection may lead to increased instances where the host SAC is bypassed through a currently unknown mechanism. The host SAC is not completely inactivated, because we have been successful in generating large numbers of *C. trachomatis*-infected mitotic cells using synchronization procedures involving low dose nocodazole treatment, which depends on functional SAC to sequester cells in metaphase (Enserink and Kolodner, 2010; Burke, 2000; Wang and Burke, 1995). In *C. trachomatis*-infected mitotic cells, inclusions appear to associate with the host mitotic spindle poles through microdomains, which are enriched in IncB, Inc101, Inc222 and Inc850 (Figure 1.3) (Mital et al., 2010). Ectopically expressed Inc850-mCherry accumulates at the host centrosome in uninfected cells; however, the exact molecular mechanism by which inclusion domains associate with host mitotic spindles is still unclear (Mital et al., 2010). My work examining the possible contribution of microdomains to inclusion positioning during mitosis after treatments with various inhibitors is presented in Chapter 4.

1.4.2 Cytokinesis and signaling proteins

Cytokinesis in normal mammalian cells

Following the activation of APC/C, sister chromatids separate, the central spindle forms and a cleavage furrow ingresses between the segregating chromosomes (Green et al., 2012; Barr and Gruneberg, 2007; Fededa and Gerlich, 2012). A number of proteins essential for proper cytokinesis ingression are summarized in Figure 1.6. The central spindle consists of bundles of overlapping antiparallel MTs at the equatorial region of the cell in between the segregating chromosomes (Fededa and Gerlich, 2012). CDK1-cyclinB complexes are inactivated by the APC/C-mediated degradation of cyclinB; as a result, many CDK1 substrates start to become

dephosphorylated and activated by various phosphatases (Wurzenberger and Gerlich, 2011; Green et al., 2012).

Prc1 (protein regulator of cytokinesis 1) and the centralspindlin complex are essential in the formation of the central spindle and are both activated following CDK1 inactivation (Zhu et al., 2006; Bieling et al., 2010; Subramanian et al., 2010; Mishima et al., 2002; Pavicic-Kaltenbrunner et al., 2007; Hutterer et al., 2009). Once activated following CDK1 inactivation, Prc1 selectively cross-links antiparallel MTs and recruits KIF4 (kinesin-like protein 4), which facilitates the MT bundling process and regulates length of the central spindle (Figure 1.6) (Hu et al., 2011; Kurasawa et al., 2004; Zhu and Jiang, 2005). KIF4 knockdown leads to abnormally long and misaligned central spindles likely due to the inability of Prc1 to localize to the plus ends of the central spindle MTs (Zhu et al., 2006; Hu et al., 2011; Kurasawa et al., 2004; Zhu and Jiang, 2005). The tetrameric centralspindlin complex consists of 2 subunits of Mklp1 (mitotic kinesin-like protein) and RacGAP1 (Rac GTPase activating protein 1, also known as HsCyk4 or MgcRacGAP) (Pavicic-Kaltenbrunner et al., 2007). Similar to Prc1, the Mklp1, the subunit responsible for MT bundling, becomes dephosphorylated and activated following CDK1 inactivation (Mishima et al., 2004). The MT bundling capability of the centralspindlin complex is further enhanced by its phosphorylation by the chromosome passenger complex (CPC) (Glotzer, 2009). The CPC, through activity of its AuroraB kinase subunit, significantly elevates the MT bundling activity of the centralspindlin complex by liberating it from its inhibitory binding protein 14-3-3 (Guse et al., 2005; Douglas et al., 2010). The RacGAP1 subunit of the centralspindlin complex can be phosphorylated by Plk1, which is targeted to the central spindle through binding to Prc1 and Mklp2 (Neef et al., 2007, 2003). Depletion of RacGAP1 using siRNA prevents normal central spindle localization of Ect2 (Epithelial cell transforming sequence 2 oncogene) and equatorial accumulation of RhoA (Yuce et al., 2005; Chalamalasetty et al., 2006). Even though Plk1 is not directly involved in the assembly of the central spindle, it is essential for cleavage furrow formation by promoting the recruitment of Ect2 to the central spindle through phosphorylation of RacGAP1 (Petronczki et al., 2007; Green et al., 2012; Fededa and Gerlich, 2012). Ect2 is initially targeted to the central spindle by binding to the RacGAP1 subunit of the centralspindlin complex and then loaded onto the plasma membrane at the cleavage site (Su, Takaki, and Petronczki 2011). Ect2 is an indispensable GEF (guanine nucleotide exchange factor) that activates RhoA by converting the GDP bound RhoA into the active GTP bound form at the division plane (Yuce et al., 2005; Nishimura and Yonemura,

2006). Depletion of Ect2 leads to the lack of RhoA activation and subsequent cytokinesis failure (Chalamalasetty et al., 2006; Yuce et al., 2005). In addition, GEF-H1 may also contribute to localized RhoA activation at the cleavage furrow (Birkenfeld et al., 2007).

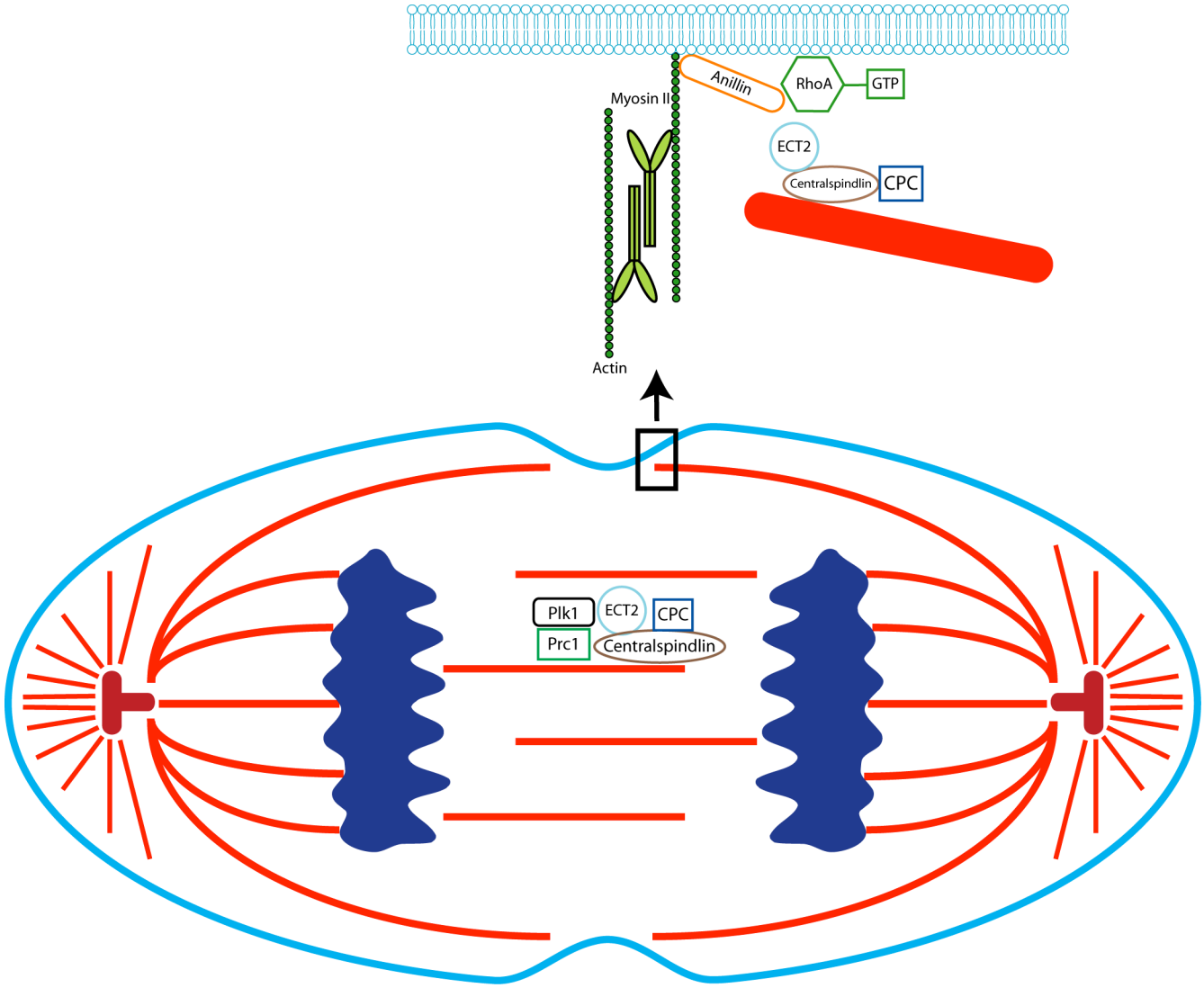

Figure 1.6 Signaling proteins essential for cytokinesis. Actomyosin filaments consisting of F-actin and myosin II are assembled at the cleavage furrow during telophase to provide the force necessary to drive furrow ingression. Activated RhoA promotes both the assembly and stabilization of actomyosin filament through recruitment and activation of downstream proteins, such as Rho-kinase and anillin. RhoA is activated by Ect2, which is recruited to the cleavage plane by the centralspindlin complex. Plk1 phosphorylates the centralspindlin complex to create the bindings sites to promote equatorial Ect2 targeting. Plk1 localizes to the cleavage site by binding to Prc1 and Mklp2.

Active RhoA through its effector proteins promote the assembly of the contractile ring, which consists of actomyosin filament and generates the force that drives furrow ingression (Fededa and Gerlich, 2012). RhoA promotes the assembly of actomyosin filament through two types of effector proteins: formins, which stimulate the assembly of actin filaments, and Rho kinases, such as ROCK (Rho-associated, coiled-coil containing protein kinase), which activate myosin II through phosphorylation of its regulatory light chain (Matsumura et al., 2011; Severson et al., 2002; Watanabe et al., 2008; Matsumura, 2005). Disruption of normal RhoA level or activity leads to the lack of furrow formation and cytokinesis failure (Drechsel et al., 1997; Kamijo et al., 2006; Kimura et al., 2000; Yoshida et al., 2009). Interestingly, cytokinesis failure naturally occurs in postnatal hepatocytes leading to the formation of binuclear cells in both mouse and human livers (Guidotti et al., 2003; Margall-Ducos et al., 2007). In hepatocytes that fail cytokinesis, RhoA does not accumulate strongly at the cleavage plane and no furrow is formed (Margall-Ducos et al., 2007). Anillin, an important cleavage furrow scaffold protein, is also recruited to the equatorial plasma membrane by RhoA (Liu et al., 2012; Brill et al., 2011; Hickson and O'Farrell, 2008b; D'Avino et al., 2008). In addition to RhoA, anillin can also bind to many proteins and cellular structures at the cleavage furrow, including F-actin, myosin II, RacGAP1 and plasma membrane lipids (Liu et al., 2012; Piekny and Maddox, 2010; Fededa and Gerlich, 2012; Green et al., 2012). Due to its ability to bind to such a diverse range of proteins and structures, anillin has been proposed to be the linker between the actomyosin machinery and the plasma membrane (Piekny and Maddox, 2010). Even though anillin is not required for cleavage furrow initiation, its function is essential for contractile ring stabilization and completion of cytokinesis (Piekny and Glotzer, 2008; Piekny and Maddox, 2010). Anillin also helps stabilize RhoA accumulation at the ingressing cleavage furrows (Piekny and Glotzer, 2008; Zhao and Fang, 2005b). Anillin depletion with siRNA leads to drastically reduced RhoA levels at the cell equator and unstable furrow ingression (Zhao and Fang, 2005b; Piekny and Glotzer, 2008). Many postnatal cardiomyocytes naturally fail cytokinesis and this failure has been proposed to be caused by insufficient anillin accumulation at the cleavage furrow (Engel et al., 2006). The exact mechanism by which RhoA is restricted to a narrow band at the cell equator is not fully understood; however, RacGAP1 of the centralspindlin complex appears to contribute to restricting RhoA distribution (Miller and Bement, 2009; Green et al., 2012). Point mutation in the GAP domain of RacGAP1 leads to widening of the RhoA band, while deletion of the GAP domain leads to unstable oscillation of the RhoA band along the plasma membrane

(Miller and Bement, 2009). RhoA zone restriction may be achieved through constant flux between GTP and GDP bound forms of RhoA by the actions of Ect2 and RacGAP1 (Miller and Bement, 2009). Central spindle MTs may also deliver stimulatory Rho GEFs, such as Ect2 and possibly GEF-H1, to the equatorial plasma membrane to promote local RhoA activation, while dynamic astral MTs inhibit contractile activity globally (astral relaxation model). Contrary to the astral relaxation model, results presented in this thesis suggest that the lack of astral MTs caused by the presence of a *C. trachomatis* inclusion, does not lead to RhoA activation or increased contractility (see Chapter 3).

By the end of the cleavage furrow ingression, two prospective daughter cells are connected through the midbody, a narrow cytoplasmic canal, which will become sealed in a process called abscission. The actomyosin contractile ring constricts to 1-2 μm in diameter before switching to an actin-independent process of membrane closure (Guizetti and Gerlich, 2010; Steigemann and Gerlich, 2009). It is essential for cleavage furrow proteins such as F-actin and RhoA to leave the midbody prior to abscission (Guizetti and Gerlich, 2010). Prolonged activation of RhoA or Ect2 leads to abscission failure (Chalamalasetty et al., 2006). The midbody is filled with dense MT bundle derived from the central spindle and contains more than 100 proteins including KIF4, anillin and GM130 (Kechad et al., 2012; Skop et al., 2004). Anillin plays essential roles in anchoring the midbody to the overlaying plasma membrane and preventing the plasma membrane from regressing (Guizetti and Gerlich, 2010). Golgi-derived vesicles and endosomes accumulate at both ends of the midbody and fuse with the midbody plasma membrane (Gromley et al., 2005; Goss and Toomre, 2008; Schiel et al., 2011). ESCRT-III (Endosomal sorting complex required for transport-III) is essential for successful abscission by mediating further membrane constriction and fission, which are known functions of this protein complex in other biological processes, to complete abscission (Hurley and Hanson, 2010; Fededa and Gerlich, 2012). Depletion of ESCRT components with siRNA leads to abscission failure and plasma membrane regression (Guizetti et al., 2011; Carlton et al., 2008; Morita et al., 2007). Abscission is inhibited by AuroraB at the midbody, which is recruited by unsegregated chromatins, to protect against potential cytokinesis failure or aneuploidy (Mendoza et al., 2009; Steigemann et al., 2009). Upon clearance of any lagging chromatins from the midbody, abscission can finally complete and the residual midbody structure is inherited by one of the two daughter cells (Green et al., 2012; Fededa and Gerlich, 2012). The residual midbody can be expelled into the extracellular space, degraded by autophagy or allowed to persist (Fededa and Gerlich, 2012).

Interestingly, a recent study suggests that accumulation of undegraded midbody residuals can contribute to cellular transformation and tumorigenesis (Kuo et al., 2011).

Disruption of cytokinesis

A non-genetic cause of cytokinesis failure attributed to entosis has been described by Krajcovic et al. (Krajcovic et al., 2011). Entosis is a process where a host cell engulfs a neighboring cell resulting in the formation of a large vacuole in the host cell. The vacuole can disrupt formation of the cleavage furrow within the host cell and cause cytokinesis failure. The side of the host cell containing the entosis vacuole frequently does not have furrow ingression, while a furrow forms and ingresses from the side further away from the vacuole. This unique unilateral cleavage furrow formation in the presence of the entosis vacuole may be attributed to the eccentric positioning of the mitotic spindle, which has been proposed to cause asymmetrical cleavage furrow formation in invertebrate systems (Rappaport 1961; Rappaport and Conrad 1963; Rappaport and Rappaport 1983). Green urchin and Hydractinia eggs naturally have unilateral cleavage furrows and have eccentrically located mitotic spindles (Rappaport and Conrad, 1963; Bement et al., 2005). Experimental manipulations such as oil droplet injection, glass bead insertion or glass needle perforation can induce similar unilateral furrow ingressions, likely due to an eccentric shift of the mitotic spindle caused by these manipulations (Rappaport and Rappaport, 1983; Bement et al., 2005; Rappaport, 1961; Rappaport and Conrad, 1963). Regardless of how the unilateral cleavage furrows originate, the ingressing furrows always occur on the side of the cell closer to the mitotic spindle.

Microbial infections can also induce cytokinesis failure. Toxin B and exoenzyme C3, secreted by *Clostridium difficile* and *Clostridium limosum* respectively, can both inactivate RhoA in the host cytosol and cause cytokinesis failure (Huelsenbeck et al., 2009). *Pseudomonas aeruginosa* through its type III-secreted exotoxin T disrupts cytokinesis, likely through inactivation of RhoA (Shafikhani and Engel, 2006). Exotoxin T also interferes with abscission by preventing recruitment of syntaxin2, an essential component of the membrane fusion machinery, to the midbody (Low et al., 2003; Shafikhani and Engel, 2006). Interestingly, protozoan parasite *Theileria annulata* binds to Plk1 and localizes itself to the central spindle and midbody between the two dividing daughter cells (Von Schubert et al., 2010). Surprisingly, such an obtrusive localization by *T. annulata* does not lead to cytokinesis or abscission failure and this equatorial

positioning may facilitate the parasite's distribute to both daughter cells (Von Schubert et al., 2010).

Thesis introduction

C. trachomatis infection leads to significant host cell multinucleation, a hallmark defect linked to tumorigenesis (Ganem et al., 2007); however, the mechanism by which *C. trachomatis* leads to host cell multinucleation is poorly understood. Furthermore, it is unclear whether *C. trachomatis* gains any physiological benefits from disrupting host cytokinesis. The main focus of my work is to understand how *C. trachomatis* infection leads to host multinucleation and whether this confers any advantage to the bacterium. We propose that *C. trachomatis* actively localizes to the host cell centre during mitosis and blocks host cell cytokinesis. As a result, *C. trachomatis* can acquire lipid nutrients faster from the resulting multinucleated cell, which retains Golgi apparatus meant for two daughter cells. Work presented in this thesis is conducted using *C. trachomatis* L2 strain, which has been used extensively in multinucleation, centrosome amplification and Golgi fragmentation studies, in an epithelial tissue culture model. In order to identify the mitotic stages affected by *C. trachomatis* leading to multinucleation, we first developed a synchronization procedure to generate large numbers of infected mitotic cells. Following observation of the unique unilateral cleavage furrow defect during telophase, we examined signaling proteins essential for furrow initiation, stabilization and ingression to understand why only one furrow formed. Next, we created similarly sized vacuoles as *C. trachomatis* inclusions using internalized latex beads to determine whether the cytokinesis defect was purely due to steric hindrance. In addition, we created metabolically inactive *C. trachomatis* inclusions with antibiotics to determine whether they actively localized to the host cell centre. We attempted to identify the exact mechanisms by which *C. trachomatis* inclusions localized to the host cell centre using a number of pharmacological inhibitors. Finally, we confirmed that blocking host cytokinesis indeed provided additional advantage to *C. trachomatis*. These results are presented in two data chapters that are briefly summarized below.

Chapter 3 describes the precise mitotic defect causing cytokinesis failure through immunofluorescence (IF) and fluorescent live cell imaging of synchronized human epithelial cells. The presence of *C. trachomatis* inclusion at the host cell equator led to the formation of a unique unilateral cleavage furrow which eventually became blocked by the inclusion. The contractile and signaling proteins necessary for cleavage furrow formation were consistently mislocalized on the side of the cell closer to the *C. trachomatis* inclusion. Similarly sized inert vacuole formed by internalized large latex beads could cause similar cleavage furrow defects if

they localized to the cell equator during telophase. Interestingly, the inert bead vacuoles only localized to the host cell equator 50% of the time while the *C. trachomatis* inclusions localized to the cell equator in over 95% of infected cells. Inhibition of *C. trachomatis* protein synthesis caused more inclusions to move away from the cell equator during telophase. Together, these results suggested that *C. trachomatis* actively localized to the host cell equator to block host cell cytokinesis.

Chapter 4 presents results demonstrating that the *C. trachomatis*-induced unilateral cleavage furrow defect also occurs in asynchronous cells. We attempted to determine the mechanism of central localization of the inclusion during mitosis. Our findings suggested that *C. trachomatis* inclusions positioned themselves to the host cell equator as early as metaphase and this localization likely depended on inclusion microdomains. Even though antibiotic inhibition of *C. trachomatis* protein synthesis reduced the number of inclusions localizing to the host cell equator, the majority of the inclusions still positioned themselves at the cell centre during mitosis. This was likely due to the high stability of the inclusion microdomains, which appeared to remain intact after 7 hours of *C. trachomatis* protein synthesis inhibition. Finally, we examined if there was a bacteria benefit to blocking host cell cytokinesis. Our fluorescent live cell imaging showed that *C. trachomatis* inclusions intercept fluorescent lipid markers more rapidly in multinuclear cells than in single nuclear cells. This lipid nutrient advantage by inclusions within multinucleated cells suggested that blocking host cell cytokinesis could indeed confer additional growth advantage to *C. trachomatis*.

Chapter 2

Materials and Methods

2.1 Cell culture, transfection, reagents and *C. trachomatis* infection

HeLa CCL-2, NIH3T3 and HEK293 cells (ATCC) and previously described CHO-IIA cells (Vieira et al., 2004) were grown in Dulbecco's Modified Eagle Medium (DMEM; Wisent) supplemented with 10% heat-inactivated fetal bovine serum (Wisent). MCF10A cells were cultured as described previously (Debnath et al., 2003). All cell cultures were maintained at 37 °C in 5% CO2 atmosphere. For the generation of a stable H2B cell line, HeLa cells were transfected with mCherry-H2B (Steigemann et al., 2009) using Fugene HD (Roche) for 3 days, followed by 600 ng/ml puromycin (Invivogen) selection for 2 weeks. For fluorescent live cell imaging, Cerulean-Lifeact (Riedl et al., 2008; Munsie et al., 2009) was transiently transfected into the above mentioned stable HeLa cell line using Fugene HD. Azithromycin, thymidine, nocodazole, aphidicolin, blebbistatin, cytochalasin D, PP2 and poly-L-lysine were purchased from Sigma and monastrol was purchased from Santa Cruz Biotechnology.

Chlamydia trachomatis L2 was propagated and purified from HeLa cells and stored at -80 °C as previously described (Caldwell et al., 1981). *C. trachomatis* was added to HeLa cells and centrifuged at 300g for 20 minutes to synchronize the infection.

2.2 Cell cycle synchronization

For the initial mitotic defect screening, an aphidicolin and nocodazole double synchronization protocol was adapted from Sauer et. al (Sauer et al., 2005). HeLa cells were treated with 1.6 µg/ml aphidicolin for 16 hours to synchronize the cells at S phase without affecting bacterial replication (McClarty and Tipples, 1991). Following aphidicolin wash-out, cells were incubated with 40 ng/ml nocodazole for 14 hours to arrest cells in mitosis. Cells were infected at such a time point that it would be 24 hpi by the time of mitotic cell collection. Mitotic cells were tapped off and washed twice. Released cells were plated onto poly-L-lysine coated coverslips. Progression through mitosis was monitored by fixing cells with 4% paraformaldehyde (PFA) at indicated time points. Mitotic stages were quantified using previously described phenotypes

(Barr and Gruneberg, 2007; Birkenfeld et al., 2007; Steigemann et al., 2009; Walczak et al., 2010).

In order to avoid potential artifacts caused by nocodazole, monastrol was used to synchronize HeLa cells for the study of signaling protein localization, DIC and fluorescent live cell imaging. HeLa cells were incubated with 100 μM monastrol for 8 hours before they were released for 55 minutes to obtain telophase cells (Burkard et al., 2009). In order to obtain bead-containing telophase CHOIIA cells, the cells were allowed to phagocytose IgG-opsonized 15μm beads overnight before they were treated with monastrol as described above. For cytokinesis completion experiments, monastrol synchronized cells were released for 3 hours with or without azithromycin treatment. To generate mitotic cells for inclusion positioning quantification after treatment with various inhibitors, HeLa cells were synchronized at 28 hpi with 40 ng/ml nocodazole for 8 hours to induce mitotic checkpoint. Following the mitotic release, HeLa cells were treated immediately with 2 μM cytochalasin D or 100 μM blebbistatin (Sigma Aldrich) for 55 minutes before fixation. For MT depolymerization experiments, mitotic cells were released from low dose nocodazole block for 30 minutes to allow some cells to progress past the mitotic checkpoint. Then the cells were treated with 1 μM nocodazole for 25 minutes to completely depolymerize their MT network. For Src family kinase inhibition, 25 μM PP2 was added together with 40 ng/ml nocodazole at 28 hpi for 8 hours. PP2 was always present in the culture media even after the mitotic release, until the cells were fixed. For antibiotic treatment, 20 μg/ml azithromycin was added together with monastrol or 40 ng/ml nocodazole at 28 hpi for 8 hours and azithromycin was always present in the media until fixation.

To generate large numbers of multinuclear cells for Golgi content quantification, HeLa cells were synchronized with 2 mM thymidine for 24 hours into S-phase. Following thymidine washout, cells were synchronized with 40 ng/ml nocodazole for 14 hours to obtain large numbers of mitotic cells. By the end of the nocodazole treatment, mitotic cells were tapped off from the culture flask, collected and washed twice. These mitotic cells were seeded onto 25 mm glass coverslips pre-treated with poly-L-lysine to assist cell adhesion. Cells were released in drug-free media for 30 minutes before 100 μM blebbistatin, 2 μM cytochalasin D or 10 μM wiscostatin was added to block furrow ingression. These inhibitors were kept in the media for 3 hours and then removed with 5 thorough washes. Cells were released for another 5 hours to allow recovery from the treatment before fixation.

2.3 Immunofluorescence and antibodies

To stain acetylated-α-tubulin, α-tubulin, actin, myosin II and GM130, HeLa cells grown on coverslips were fixed with 4% PFA in phosphate buffered saline (PBS) for 15 minutes. To visualize RhoA and anillin, HeLa cells were fixed by ice-cold 10% trichloroacetic acid (TCA; BioShop) for 10 minutes. Cells fixed by PFA or TCA were permeabilized for 20 minutes using 0.1% Triton X-100 in PBS with 100mM glycine. For Ect2, Mklp1, Plk1, Prc1, γ-tubulin and Inc101 staining, cells were fixed and permeabilized using ice-cold 100% methanol for 10 minutes. Cells were blocked in 5% FBS overnight, followed by primary and fluorescent secondary antibody incubation for 1 hour each. Actin and DNA were visualized by Alexa Fluor 488 phalloidin and DAPI respectively.

Primary antibodies against acetylated-α-tubulin (T6793; 1:5000), α-tubulin (T9026; 1:1000) γ-tubulin (1:200) and myosin IIB heavy chain (M7939; 1:200) were purchased from Sigma Aldrich. RhoA (26c4; 1:100), Mklp1 (N19; 1:100), Plk1 (F8; 1:100), Prc1 (H70; 1:100), and chlamydia (Chlam III; 1:100) antibodies were purchased from Santa Cruz Technology. GM130 (610822; 1:200) was purchased from BD. Ect2 antibody was a generous gift from Dr. Michael Glotzer. Anillin antibody was a gracious gift from Dr. William Trimble. Rabbit anti-chlamydia and anti-Inc101 antibodies were kindly donated by Dr. David Hackstadt. Alexa Fluor488 phalloidin (1:500) and DAPI (1:10,000) were obtained from Invitrogen. Donkey anti-mouse or donkey anti-rabbit Dylight secondary antibodies were purchased from Jackson ImmunoResearch Laboratories and were used at recommended dilutions.

2.4 Phagocytosis

Polystyrene beads (PolySciences) with a mean diameter of 15μm were opsonized with 2mg/ml human IgG (Sigma Aldrich) for 1 hour and unbound IgG was removed by washing once with PBS. The IgG-opsonized beads were then added to CHO-IIA cells overnight to allow internalization by phagocytosis. External beads were washed away before live cell DIC imaging.

2.5 Nascent protein synthesis labelling

Nascent *C. trachomatis* protein synthesis was detected with Click-iT AHA protein synthesis labelling kit (Invitrogen). Azithromycin was added to *C. trachomatis*-infected cells at 28 hpi and incubated for 7 hours at a final concentration of 20 μg/ml. Methionine-free media (Invitrogen)

was supplemented with 1mM sodium pyruvate, 4mM L-glutamine, and 0.2mM L-cystine-2HCl and was added to infected cells for 1 hour to deplete pre-existing free methionine. Serum was not included in this media to prevent serum contribution of free methionine, while azithromycin was always present at 20 µg/ml until cells were fixed. Methionine-free media containing 50 µM AHA was added to cells for 3 hours before fixation with 4% PFA. After permeabilization with 0.25% Triton X-100 in PBS for 20 minutes, AHA incorporation was visualized using 50 µM Alexa Fluor 555 alkyne, triethylammonium (A20013, Invitrogen) in manufacturer-recommended reaction buffer (C10269, Invitrogen). Incubation time and washes were performed exactly as described in manufacturer's protocol.

For experiments involving cycloheximide, following 1 hour methionine starvation, cycloheximide (Sigma Aldrich) was added alone or together with azithromycin, with final concentrations of 100 µM and 20 µg/ml respectively, to *C. trachomatis*-infected cells at 30 hpi. AHA was added at the same time as cycloheximide and cells were incubated for 2 hours before fixation.

2.6 Microscopy

Epifluorescence images were acquired with EC Plan-Neofluoar 40x/ 1.3 oil objective and AxioCam MRm camera mounted on either an AxioVert 200M or Axio Observer Z1 microscope (Carl Zeiss). Structured illumination images were taken with the above mentioned objective and the images were captured using AxioCam HRm camera with ApoTome module on AxioVert 200M microscope (Carl Zeiss). Spinning disk confocal images were taken with a Plan-Apochromat 40x/ 1.3 Oil objective and CSU-X1 (Yokogawa). Images were captured with Cascade 1K EMCCD (Photometrics) on Axio Observer Z1 (Carl Zeiss).

For long term live cell DIC imaging, asynchronous HeLa cells were seeded onto 35 mm glass-bottom dishes (MatTek) in DMEM and infected with *C. trachomatis* for 28-36 hours before imaging. Live cell DIC imaging was conducted using Carl Zeiss AxioObserver Z1 epifluorescent microscope with a 20x/ 0.8 Plan Apochromat air objective. The culturing environment was maintained at 37 °C with 5% CO_2 using an Incubator XL-S1 with TempModule S1, CO_2 module S1, and heating device humidity S1 (Carl Zeiss). Images were acquired using AxioCam MRm camera through 20x/ 0.8 Plan Apochromat air objective. The

time-lapse imaging was carried out once every 3 minutes for 24 hours and field of views with mitotic events were selected and a representative field was shown.

For live fluorescent ceramide trafficking experiments, infected HeLa cells were stained with DRAQ5 (Cell Signaling) for 10 minutes to label both the host and *C. trachomatis* DNA. Following the DNA stain, 35 mm culture dish containing *C. trachomatis*-infected HeLa cells was screened using a spinning disk confocal microscope with temperature and CO_2 control. Fields with both mononuclear and multinuclear cells were chosen and the imaging began as soon as BSA-complexed BODIPY FL C5-ceramide (Life Technologies) was added to the cells. The uptake of fluorescent ceramide into *C. trachomatis* inclusions was recorded once every 30 seconds for 30 minutes.

2.7 Flow cytometry

Mononuclear or blebbistatin-treated multinuclear cells were fixed by ice cold 80% ethanol for 30 minutes on ice and washed twice in PBS containing 1% FBS. Cells were blocked with 5% FBS for 1 hour before incubating with GM130 primary and Cy2 secondary antibodies for 1 hour each with gentle shaking in the dark. Following secondary staining, cells were incubated with 50 µg/ml propidium iodide (PI) solution containing 1 mg/ml RNAse A (Sigma Aldrich) in the dark at room temperature with gentle shaking for 30 minutes. Diploid and tetraploid cell populations were gated using PI histograms and their respective GM130 signals were recorded. The fold changes of GM130 signal in multinuclear cells after blebbistatin treatment was normalized against mononuclear G1 cells under control condition. At least 10,000 cells were measured per experiment and two independent experiments were performed.

2.8 Quantifications

For mitotic progression quantification, epifluorescence images of more than 100 control and 100 infected cells were quantified per time point per trial. Size and position of *C. trachomatis* inclusions during telophase were quantified based on epifluorescence images of 165 telophase cells at 1.5 hpr (hours post release) and 94 telophase cells at 3 and 4 hpr from three independent experiments. *C. trachomatis* inclusions were quantified as equatorial if they touched the chromosome band at the cell centre in metaphase. Inclusions were quantified as equatorial if they were located between the segregating chromosomes during telophase. Inclusions that did not meet these criteria were quantified as polar. Localization of actin, myosin II, anillin, RhoA,

Ect2, Mklp1, Plk1 and Prc1 were quantified based on structured illumination images of more than 100 control and 100 infected telophase cells. Equal accumulation of actin, myosin, anillin and RhoA was scored when the fluorescence intensity of the protein on both sides of the equatorial cortex were within 80% of each other. Normal localization of Ect2, Mklp1, Plk1 and Prc1 was defined as a clear band of protein across the entire equatorial width of telophase cells, defined by DIC imaging.

Golgi content in mononuclear and multinuclear HeLa cells was quantified based on GM130 signal intensity. Epifluorescent images of mononuclear and multinuclear HeLa cells were acquired at identical exposure and excitation intensity. GM130 fluorescence intensity in mononuclear and multinuclear cells was analyzed using ImageJ. The fold change in GM130 signal intensity was normalized against control cells, which went through the same synchronization procedure but did not receive the blebbistatin treatment.

The quantification of fluorescent ceramide acquisition in live infected HeLa cells was carried out using Volocity. The total fluorescent intensity in *C. trachomatis* inclusions by the end of the live spinning disk confocal imaging was measured. Threshold for the quantification was defined such that only bacterial particles that have clearly-defined shape were included, which eliminated most of the background signal. The ceramide signal intensity in multinuclear cells was normalized against intensities in mononuclear cells to generate the fold changes.

All statistical tests were performed using the Student's t-test and $p < 0.05$ was used as the significance cut-off.

Chapter 3

Chlamydia trachomatis inclusions induce asymmetric cleavage furrow formation and ingression failure in host cells

A modified version of this chapter was previously published as:

Sun, H.S., Wilde, A., and Harrison, R.E. (2011). *Chlamydia trachomatis* inclusions induce asymmetric cleavage furrow formation and ingression failure in host cells. Molecular and Cellular Biology 31 (24), 5011-22. ***Featured on cover of 32 (20) issue, 2012.**

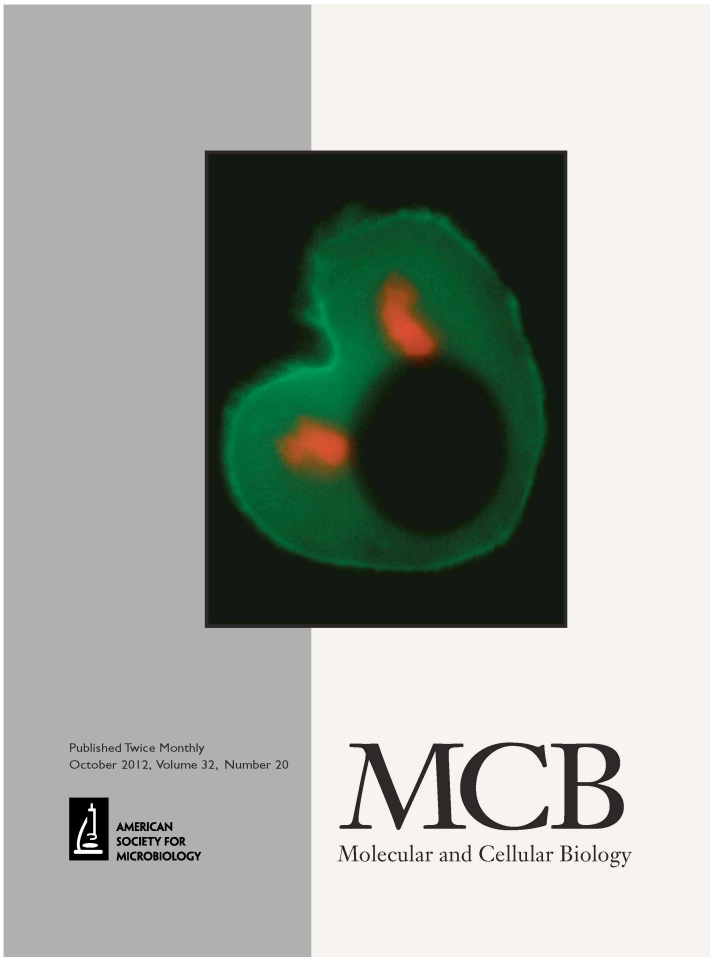

Chapter 3
Chlamydia trachomatis inclusions induce asymmetric cleavage furrow formation and ingression failure in host cells

3.1 Introduction

Chlamydia trachomatis is an obligate intracellular bacterium that is the leading cause of bacterial sexually transmitted diseases worldwide (Ying et al., 2007). Recent epidemiological studies have linked *C. trachomatis* infection to increased risk of cervical cancer (Madeleine et al., 2007; Samoff et al., 2005). In various human and other mammalian cell lines, *C. trachomatis* infection can lead to significant increases in host cell multinucleation (Greene and Zhong, 2003), a phenotype well linked to tumorigenesis (Fujiwara et al., 2005; Ganem et al., 2007; Olaharski et al., 2006; Storchova and Pellman, 2004). A defect in cytokinesis was theorized, but not proven, in causing multinucleation in *C. trachomatis*-infected cells (Greene and Zhong, 2003). As a result, the mechanism by which *C. trachomatis* causes multinucleation has remained unclear.

Numerous quality control mechanisms exist in eukaryotic cells to ensure the proper segregation of genetic material into two daughter cells during mitosis. In mammalian cells, cytoplasmic division at the end of mitosis is mediated by the formation of a bilateral cleavage furrow, which is under heavy spatiotemporal regulation (Barr and Gruneberg, 2007). Cleavage furrow ingression is driven by force generated by the actomyosin filaments, consisting of actin and non-muscle myosin II (Barr and Gruneberg, 2007). The assembly of actomyosin filament is tightly controlled through phosphorylation of myosin II regulatory light chain (RLC), which in turn is regulated by RhoA through its effector proteins Rho kinase and citron kinase (Matsumura, 2005). In order to have continuous force generation throughout furrow ingression, Rho kinase and citron kinase localization is stabilized by anillin, a scaffolding protein recruited by RhoA (Hickson and O'Farrell, 2008a). Ect2, a Rho guanine exchange factor, plays a critical role in defining the cleavage plane by recruiting and activating RhoA at the precise time and location (Yuce et al., 2005). Following degradation of the CDK1-cyclinB1 complex, centralspindlin complex assumes critical roles not only in the bundling of midzone microtubules (MTs), but also in the recruitment of Ect2 to the cell equator (Piekny et al., 2005). Plk1 also plays an

essential role in the recruitment of Ect2 to the cleavage plane by phosphorylating the RacGAP1 subunit of the centralspindlin complex allowing Ect2 binding to this complex (Petronczki et al., 2007; Green et al., 2012; Fededa and Gerlich, 2012).

The *C. trachomatis* inclusion is a vacuolar structure in which the bacteria reside and replicate within the host cell and it can continue to grow until it occupies most of the cell volume (Valdivia, 2008). *C. trachomatis* can exit the host cells by two distinct mechanisms: cell lysis and extrusion. The lysis pathway involves the activation of cysteine protease which kills the host cell in the process (Hybiske and Stephens, 2007). In the extrusion pathway, the *C. trachomatis* inclusion pinches off as a vacuole, taking some or all of the bacteria from the current host, leaving the host cell intact (Beatty, 2007; Hybiske and Stephens, 2007). In our study, we observed a unique asymmetry in cleavage furrow formation in human cells after *C. trachomatis* infection, which often led to the formation of multinucleated cells. Signaling proteins essential for cleavage furrow initiation, ingression and stabilization were displaced from regions of the cell cortex lacking the cleavage furrow. This unique unilateral cleavage furrow defect was dependent on the equatorial positioning of the *C. trachomatis* inclusion, which were present at the host cell equator in over 95% of infected cells. Similarly-sized inert vacuoles generated from internalized large latex beads only localized to the equator in approximately 50% of the cells. Antibiotic inhibition of chlamydia protein synthesis for 8 hours decreased the number of inclusions that localized to the host cell equator during telophase. Together, these observations provide evidence that *C. trachomatis* contributes to host genome duplication by disrupting host cell cleavage furrow formation and ingression.

3.2 Results

3.2.1 *C. trachomatis* infection induces host cell multinucleation and prolongs host telophase during mitosis

To confirm that *C. trachomatis* infection can lead to increased host cell multinucleation, we infected HeLa cells with *C. trachomatis* L2 at MOI of approximately 1. Cells were fixed at 12, 24, and 36 hpi and stained for α-tubulin (red), chlamydia (cyan) and DNA (blue). As expected, the inclusion sizes increased substantially over the course of infection (Figure 3.1A). Our quantification at various time points showed that the number of multinucleated cells increased significantly as early as 24 hpi and continued to rise at 36 hpi (Figure 3.1B). During the quantification process, we noticed an interesting phenotype resembling blocked cytokinesis in

host cells. In uninfected cells, the two daughter cells were connected through the narrow cytoplasmic bridge, termed the midbody, during late cytokinesis (Figure 3.1C, arrow). At 36 hpi, *C. trachomatis*-infected cells appeared to have a midbody within a single cell body instead of between two distinct daughter cells (Figure 3.1C, top arrow). The *C. trachomatis* inclusion (Figure 3.1C, arrowhead) appeared to be indented at the midbody (Figure 3.1C, bottom arrow), suggesting the inclusion might be under mechanical stress.

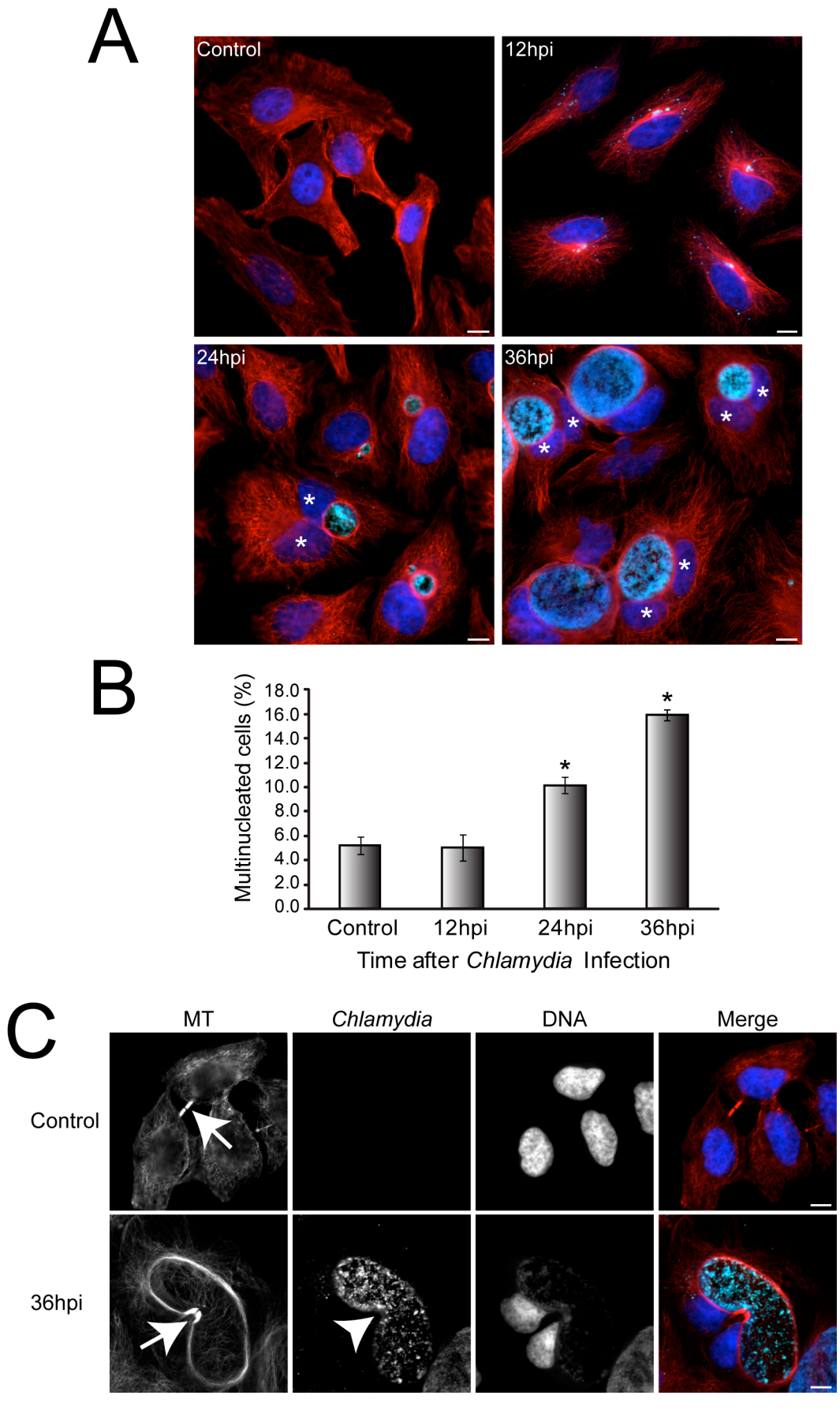
A
Control
12hpi
24hpi
36hpi
B
Multinucleated cells (%)
18.0
16.0
14.0
12.0
10.0
8.0
6.0
4.0
2.0
0.0
Control
12hpi
24hpi
36hpi
Time after Chlamydia Infection
C
MT
Chlamydia
DNA
Merge
Control
36hpi

Figure 3.1 *C. trachomatis* infection induces multinucleation in cultured human cells. (A) HeLa cells were infected with *C. trachomatis* L2 at MOI of 1 for indicated time periods before fixation. Cells were immunostained with anti-α-tubulin (red), anti-chlamydia (cyan) antibodies and DNA were visualized using DAPI (blue). Multiple nuclei in infected cells are marked by asterisks. Scale bars = 10 μm. (B) A significant increase of multinucleated cells was first observed at 24 hpi ($p < 0.05$) and the number of multinucleated cells increased significantly by 36 hpi ($p < 0.005$). Error bars represent SEM from three independent experiments. (C) Uninfected control and *C. trachomatis*-infected cells containing midbodies were examined for potential defects that could lead to multinucleation. Midbodies are indicated by arrows.

Due to the relative rare occurrence of mitotic cells after *C. trachomatis* infection, we developed a synchronization protocol to obtain large numbers of infected mitotic cells in order to identify the exact stage that was affected by *C. trachomatis*. *C. trachomatis* infection was carried out at such a time point that it would be 24 hpi by the time of mitotic cell collection (Figure 3.2A). Following the tap-off procedure, a population of mitotic cells was obtained and released from nocodazole for indicated time periods before fixation (Figure 3.2A). Cells at each mitotic stage were quantified based on previously established phenotypes (Figure 3.2B) (Barr and Gruneberg, 2007; Birkenfeld et al., 2007; Steigemann et al., 2009; Walczak et al., 2010) and the mitotic stage composition was shown for each time point (Figure 3.2C-I). At 0.5 hour post release (hpr), over 96% of the collected cells were in prophase or metaphase, suggesting that the tap-off procedure produced a relatively pure population of mitotic cells (Figure 3.2C and D). Very low numbers of anaphase and telophase cells were observed initially after synchronous release (Figure 3.2E and F). Cells in cytokinesis increased dramatically as time passed (Figure 3.2G). Cells in abscission and interphase were largely absent at early time points as expected, and began to appear at 2 and 3 hpr (Figure 3.2H and I). No significant change was detected in prophase, metaphase and anaphase progression between uninfected and *C. trachomatis*-infected cells when they were collected at 24 hpi (Figure 3.2C-E). Interestingly, there was a significant increase of *C. trachomatis*-infected telophase cells at 1.5 hpr, compared to control cells (Figure 3.2 F). There was also a significant decrease in *C. trachomatis*-infected cells in cytokinesis at 1.5 hpr, compared to control cells (Figure 3.2G). Together, these results suggested that telophase was prolonged after *C. trachomatis* infection.

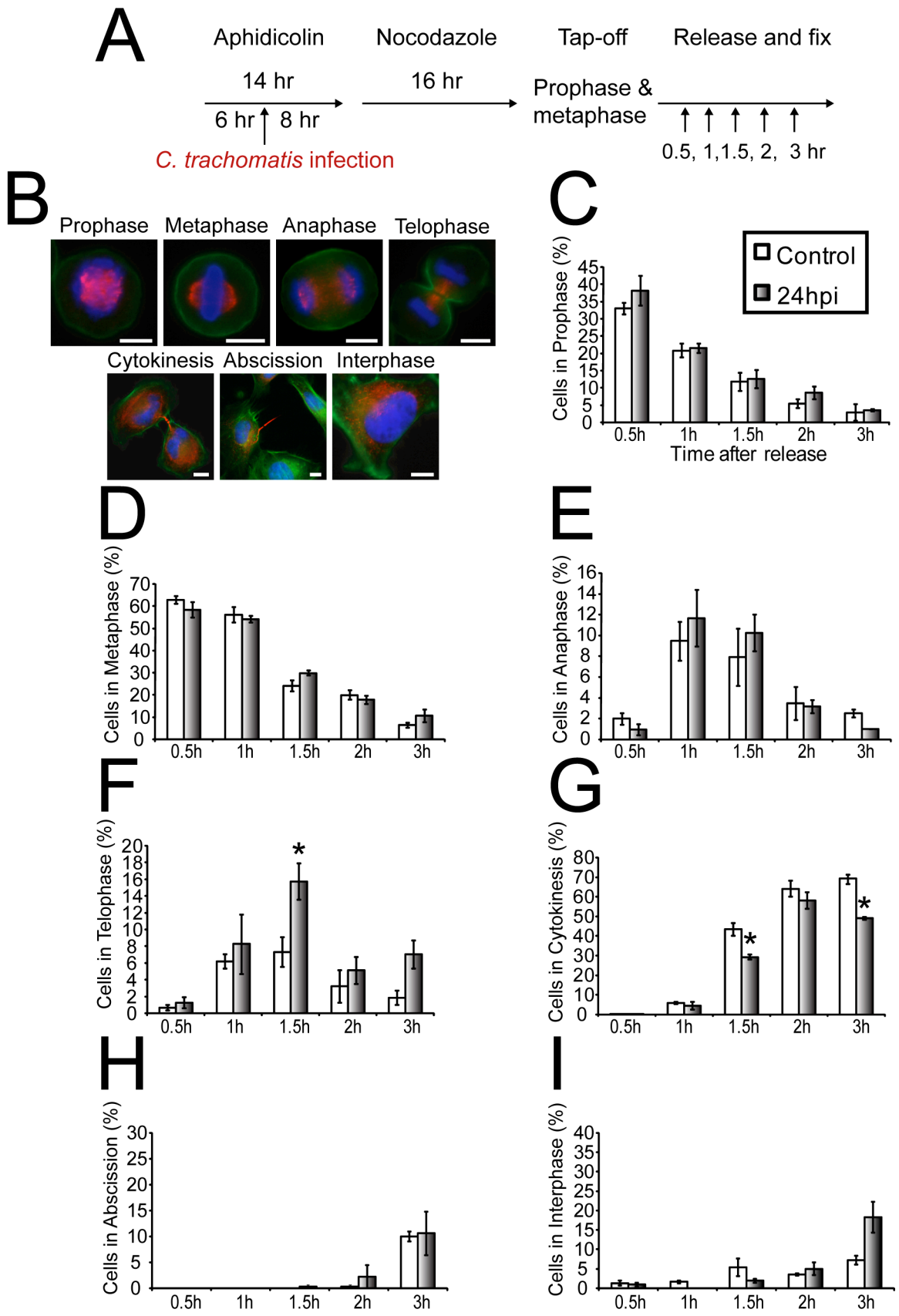
A
Aphidicolin
14 hr
6 hr
8 hr
C. trachomatis infection
Nocodazole
16 hr
Tap-off
Prophase & metaphase
Release and fix
0.5, 1,1.5, 2, 3 hr
B
Prophase
Metaphase
Anaphase
Telophase
Cytokinesis
Abscission
Interphase
C
Control
24hpi
Cells in Prophase (%)
Time after release
D
Cells in Metaphase (%)
E
Cells in Anaphase (%)
F
Cells in Telophase (%)
G
Cells in Cytokinesis (%)
H
Cells in Abscission (%)
I
Cells in Interphase (%)
0.5h
1h
1.5h
2h
3h

Figure 3.2 An accumulation of host cells in telophase occurs after *C. trachomatis* infection. (A) Aphidicolin and nocodazole double-synchronized cells were collected at 24 hpi and released for indicated time periods before fixation. Mitotic apparatus was stained with anti-acetylated α-tubulin (red) antibody. F-actin and DNA were visualized using Alexa Fluor 488 phalloidin (green) and DAPI (blue) respectively. (B) Representative phenotypes used in quantification for each mitotic stage. Scale bars = 10 μm. (C-I) At least 100 cells were quantified at each time point per trial. (C) The progression of prophase cells did not change significantly after *C. trachomatis* infection. (D) The progression of metaphase cells did not become significantly altered by *C. trachomatis* infection. (E) Anaphase cells started to appear at 1 hour post release (hpr). No significant change in anaphase progression was detected. (F) Following *C. trachomatis* infection, there was a significant increase of telophase cells at 1.5 hpr. (G) A corresponding significant decrease was observed for cells in cytokinesis, the stage after telophase, at 1.5 hpr. (H and I) No significant changes for these stages could be detected after *C. trachomatis* infection. Error bars represent SEM from three independent experiments. Asterisks indicate statistical significance between control and *C. trachomatis*-infected cells ($p < 0.05$).

3.2.2 Telophase defect caused by *C. trachomatis* infection depends on the size and location of the inclusion

We subsequently examined telophase cells more closely at different time points after release to identify any possible defects that could be attributed to *C. trachomatis* infection. Interestingly, many infected telophase cells at 3 and 4 hpr, which had been held in telophase for an extend period of time, lacked an ingressing furrow on one side (Figure 3.3A). Accumulation of F-actin occurred at both ingressing furrows in most telophase cells at 1.5 hpr, while F-actin only accumulated at a single cleavage furrow in infected cells at 3 and 4 hpr (Figure 3.3A). Inclusion size analysis revealed that the average size of *C. trachomatis* inclusions was 20% of the total cell area for telophase cells at 1.5 hpr (Figure 3.3B). The inclusion size was 40% in telophase cells at 3 and 4 hpr (Figure 3.3B), indicating a strong correlation between large inclusions and severely prolonged telophase. This significant increase in inclusion size is likely due to difference in the number of bacteria that initially infected the cells. We also observed that 44% of telophase cells contained centrally located *C. trachomatis* inclusions at 1.5 hpr, and this number increased to 88% in telophase cells at 3 and 4 hpr (Figure 3.3C). In order to consistently obtain large *C. trachomatis* inclusions, we increased the infection time to 36 hours. Significantly more *C. trachomatis* inclusions localized to the host cell center during telophase at 36 hpi than at 24 hpi (Figure 3.3D).

We monitored mitotic events with fluorescent live cell imaging to confirm the cleavage furrow defect after *C. trachomatis* infection. *C. trachomatis* infection was carried out for 36 hours to obtain large inclusions that produced prominent telophase defects (Figure 3.3A and B). Cerulean-Lifeact (Riedl et al., 2008; Munsie et al., 2009) was transiently transfected into HeLa cells stably expressing mCherry-H2B to dual label F-actin and chromosomes. Uninfected cells formed normal cleavage furrows on both sides of the cell during telophase (n= 29 out of 29; Figure 3.3E). In contrast, infected cells often formed a single, F-actin-rich, cleavage furrow on the equatorial cortex away from the inclusion (n=13 out of 14; Figure 3.3F). The ingressing furrow was blocked by *C. trachomatis* when it reached and pressed against the inclusion (Figure 3.3F). Our fluorescent and DIC analysis showed that that host cells with unilateral cleavage furrows typically exited mitosis without dividing into two daughter cells, forming multinucleated interphase cells (n=27 out of 33; Figure 3.3F).

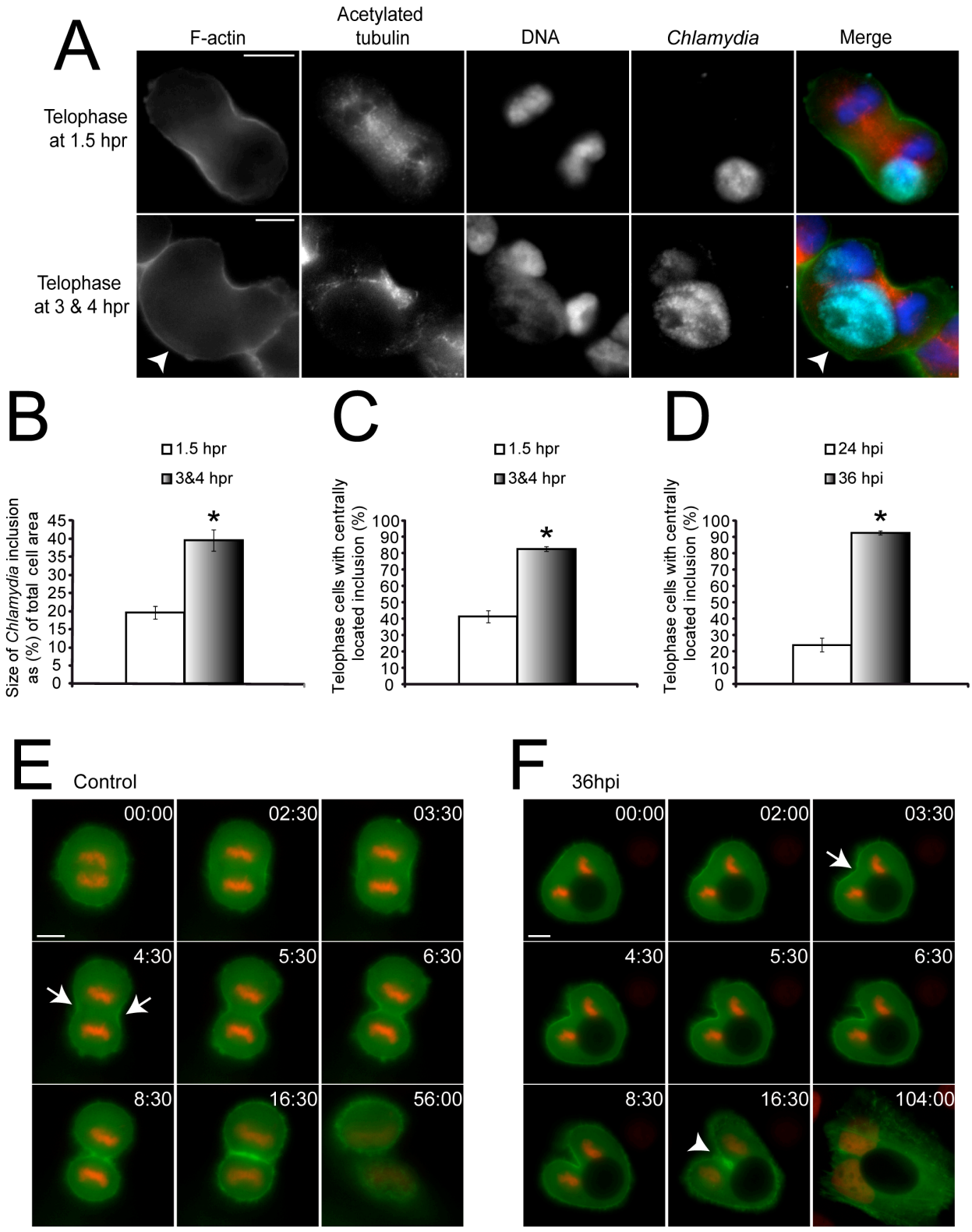
A
F-actin
Acetylated tubulin
DNA
Chlamydia
Merge
Telophase at 1.5 hpr
Telophase at 3 & 4 hpr
B
1.5 hpr
3&4 hpr
Size of Chlamydia inclusion as (%) of total cell area
C
1.5 hpr
3&4 hpr
Telophase cells with centrally located inclusion (%)
D
24 hpi
36 hpi
Telophase cells with centrally located inclusion (%)
E
Control
00:00
02:30
03:30
4:30
5:30
6:30
8:30
16:30
56:00
F
36hpi
00:00
02:00
03:30
4:30
5:30
6:30
8:30
16:30
104:00

Figure 3.3 *C. trachomatis* infection causes unilateral cleavage furrow formation and leads to host cell multinucleation. (A) *C. trachomatis*-infected telophase cells were obtained using aphidicolin and nocodazole. Mitotic apparatus (red), *C. trachomatis* (cyan), F-actin (green) and DNA (blue) were visualized as described in Methods. A representative telophase cells at 1.5 hpr showed normal cleavage furrow formation (top), while telophase cells at 3&4 hpr often exhibited a single unilateral cleavage furrow (arrowhead). (B) Telophase cells at 3&4 hpr contained significantly larger *C. trachomatis* inclusions than those at 1.5 hpr ($p < 0.01$). (C) Telophase cells at 3&4 hpr had significantly more centrally located *C. trachomatis* inclusions than those at 1.5 hpr ($p < 0.005$). (D) Infected telophase cells at 36 hpi had significantly more centrally located inclusions than cells at 24 hpi ($p<0.005$). (E and F) Cerulean-Lifeact (green) was transiently transfected into HeLa cells stably expressing mCherry-H2B (red). Numbers indicate minutes:seconds. (E) Uninfected cells always showed bilateral actin accumulation and furrow ingression at the cell equator during telophase as indicated by arrows (n= 29 out of 29). (F) *C. trachomatis*-infected cells containing centrally located inclusions often exhibited a unilateral cleavage furrow as marked by arrow (n= 13 out of 14). The unilaterally ingressing furrow eventually became blocked by the inclusion and could not ingress further (arrowhead). Error bars represent SEM from three independent experiments. Scale bars = 10 μm.

Live cell imaging provided great insights into the dynamics of this unilateral cleavage furrow defect and confirmed that this furrowing defect could indeed lead to host cell multinucleation. We subsequently examined this defect more closely using IF, which allowed us to visualize additional host proteins such as MTs (Figure 3.4A-E, red). HeLa cells infected with *C. trachomatis* were synchronized with low dose nocodazole for 8 hours and released for 4-5 hours before fixation. Similar to the live cell imaging results, early telophase phase cells could only form a single F-actin-rich furrow on the side of the cell further away from the *C. trachomatis* inclusion (Figure 3.4A). As the single furrow ingressed, it eventually pressed against the central spindle MT bundle and the *C. trachomatis* inclusion (Figure 3.4B). As the furrow ingressed further, the force driving the ingression was strong enough that it created a large indentation in the *C. trachomatis* inclusion (Figure 3.4C). The unilateral furrow pressed against the *C. trachomatis* inclusion for some time before the furrow began to slowly regress, likely as a result of reduce actomyosin filament activity (Figure 3.4D). The cleavage furrow eventually regressed completely forming a multinucleated interphase cell containing the midbody (Figure 3.4E). Consistent with these results, we determined that the central positioning of *C. trachomatis* inclusions was highly correlated with host cell multinucleation. If *C. trachomatis* infection could induce multinucleation independent of its equatorial localization, then we would expect approximately 50% of multinucleated cells contained equatorial inclusions, while the other 50% contained polar inclusions (Figure 3.5A). However, our quantification of *C. trachomatis*-infected multinuclear cells showed that over 98% of these cells contained equatorial inclusions (Figure 3.5B), indicating a strong correlation between inclusion positioning and host cell multinucleation. Together, these results showed that the *C. trachomatis*-induced unilateral cleavage furrow defect could indeed induce host cell multinucleation and this defect was likely dependent on the equatorial localization of the inclusion.

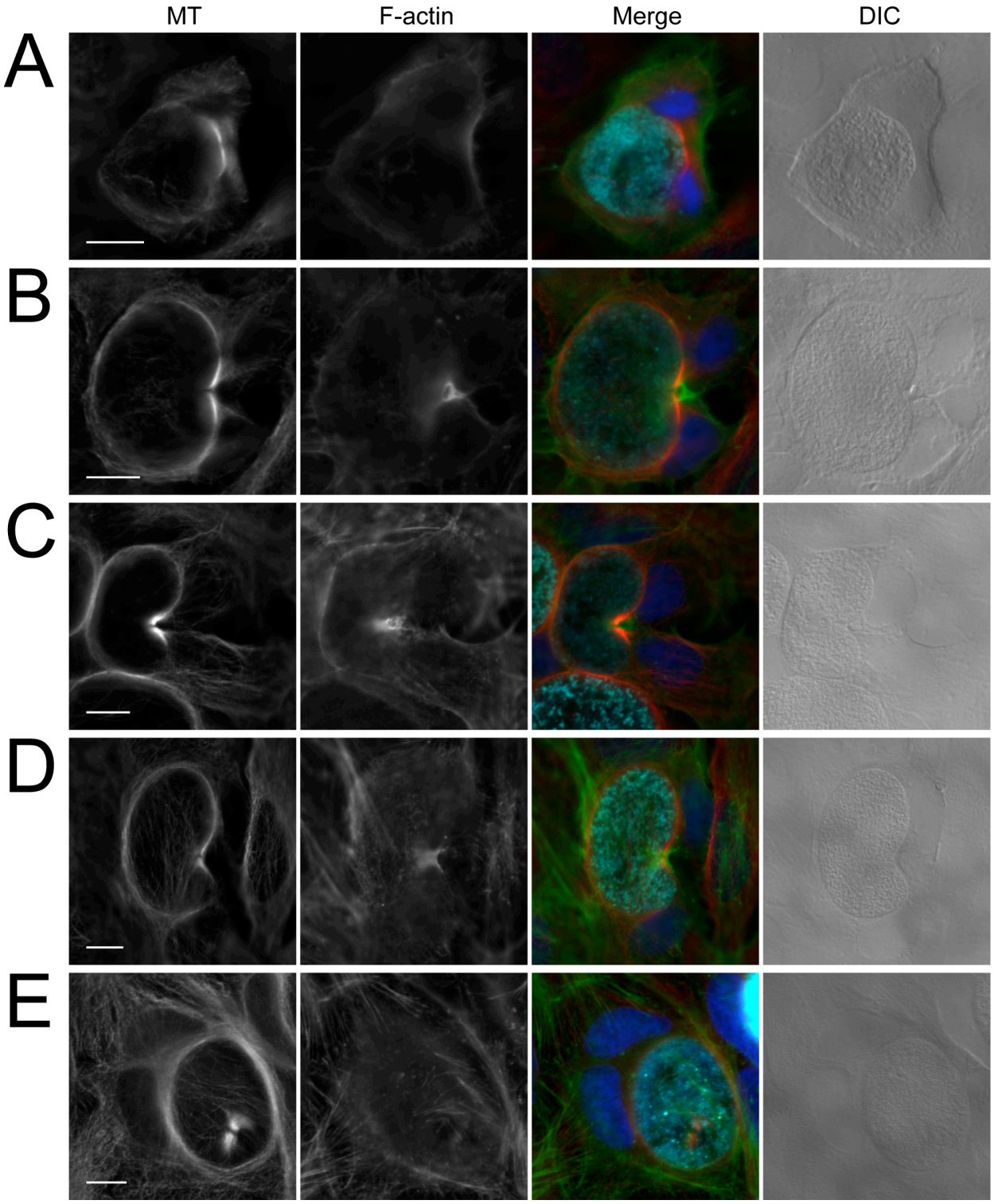
MT
F-actin
Merge
DIC
A
B
C
D
E

Figure 3.4 The unilateral cleavage furrows can deform equatorial *C. trachomatis* inclusions but cannot complete ingression. HeLa cells infected with *C. trachomatis* were synchronized with low dose nocodazole for 8 hours and released for 4-5 hours before fixation. Cells were stained with anti-α-tubulin (red) and anti-chlamydia antibodies (cyan). (A) A representative early telophase cell with a unilateral cleavage furrow is shown. The ingressing furrow has not reached the *C. trachomatis* inclusion at this point. (B) The unilateral furrow which has ingressed deep enough to begin pressing against the inclusion. Intense F-actin accumulation was observed at the unilateral furrow. (C) The ingressing furrow created a sizable indentation within the *C. trachomatis* inclusion and pushed the midbody against the inclusion. (D) The midbody MT bundle began to depolymerize and the ingressed unilateral furrow started to regress. (E) The host cell eventually re-entered interphase without dividing into two daughter cells. The recent cytokinesis failure is marked by an internal midbody and two nuclei. Scale bars = 10 μm.

A

If multinucleation is independent of *C. trachomatis* inclusion positioning

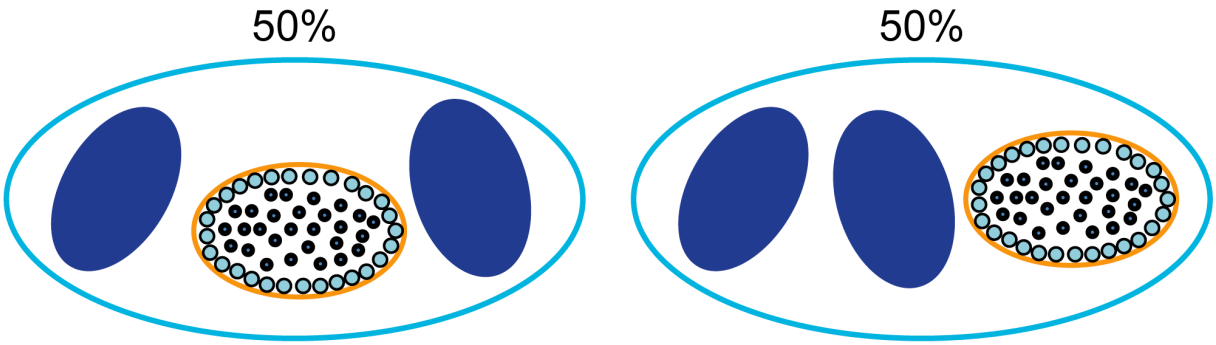

B

Quantification of inclusion positioning relative to host nuceli in multinuclear cells

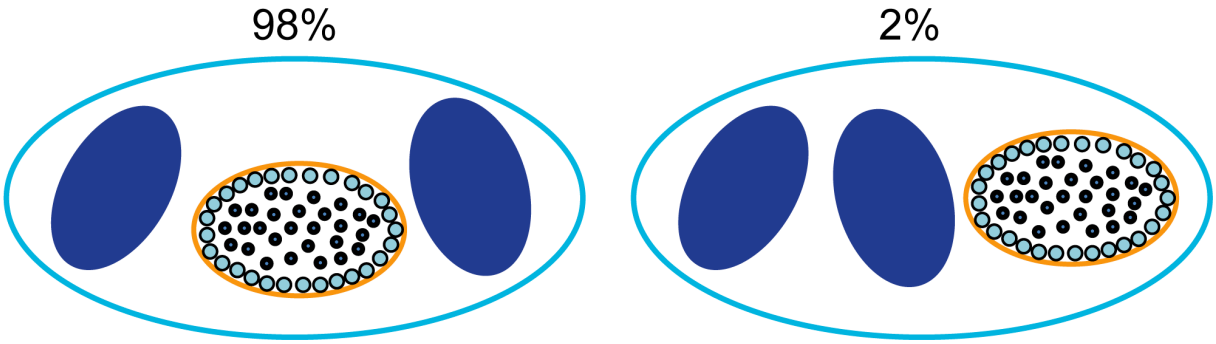

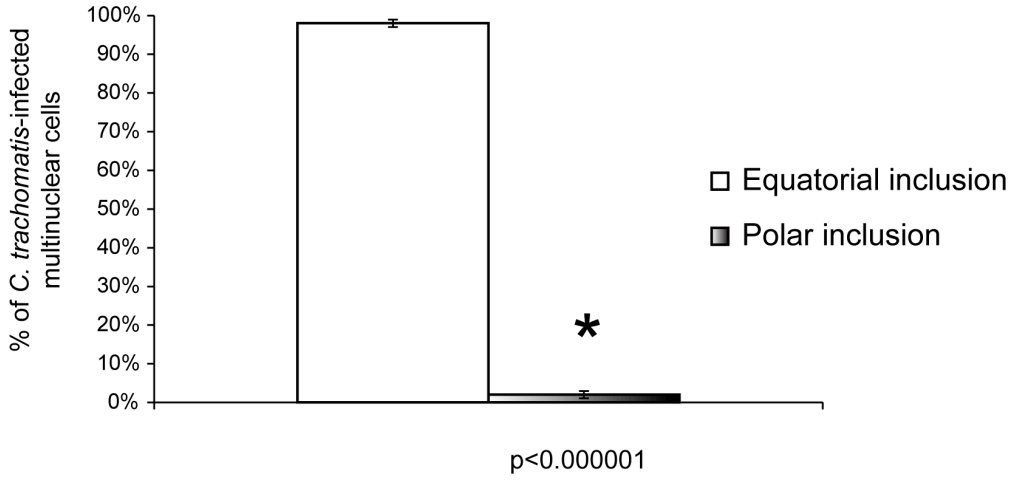

Figure 3.5 Equatorial localization of *C. trachomatis* inclusions is important for causing host cell multinucleation defects. (A) If host cell multinucleation was independent of *C. trachomatis* inclusion positioning, approximately 50% of multinucleated cells should contain polar inclusions, while the other 50% contain equatorial inclusions. (B) Quantification of inclusion positioning in multinuclear host cells revealed that 98% of multinuclear cells contained equatorial inclusions between the two nuclei. At least 50 multinuclear cells were quantified per trial. Error bars represent SEM from three independent experiments.

3.2.3 *C. trachomatis* inclusion disrupts RhoA and downstream signaling events necessary for cleavage furrow formation

Since unilateral cleavage furrows were routinely induced in *C. trachomatis*-infected telophase cells, we next monitored the recruitment of relevant cleavage furrow cytoskeletal and signaling proteins. Monastrol was used to synchronize HeLa cells to avoid potential disruption of signaling events caused by MT-depolymerizing agents (Nishimura and Yonemura, 2006). *C. trachomatis* infection was carried out for 36 hours to obtain large inclusions, and phalloidin staining revealed that 73% of uninfected versus 13% of infected telophase cells had equal accumulation of F-actin at the equatorial cortices (Figure 3.6A). We next examined the localization of the F-actin motor, myosin II, and observed that 79% of uninfected but only 4% of infected telophase cells had equal myosin II accumulation at the equatorial cortices (Figure 3.6B). These results indicated a strong contractile defect at the cell cortex near *C. trachomatis* inclusion during furrow ingression.

Due to the lack of actomyosin filament assembly at one side of the cell, we looked at upstream signaling proteins that are responsible for the stabilization and activation of the contractile machinery. We first examined anillin, a scaffold protein responsible for stabilizing actomyosin filaments and localized RhoA distribution (Hickson and O'Farrell, 2008a; Piekny and Glotzer, 2008), and observed equal accumulation at the cell equator in 100% of uninfected but only 4% of infected telophase cells (Figure 3.6C). We next examined the accumulation of RhoA, the activator of actomyosin filament assembly and recruiter of anillin (D'Avino, 2009). RhoA was equally accumulated on both equatorial cortices in 99% of uninfected but just 1% of *C. trachomatis*-infected telophase cells (Figure 3.6D). Attenuated F-actin, myosin II, anillin and RhoA accumulation always occurred on the side of telophase cells closer to the inclusion (Figure 3.6A-D). Notably, the displacement of myosin II, anillin, and RhoA in *C. trachomatis*-infected cells was already prominent during anaphase (Figure 3.7B-D). It is also worth noting that the localization of F-actin, myosin II, anillin and RhoA appeared to be normal when the *C. trachomatis* inclusions were located in the polar region of the host cells (Figure 3.8A-D).

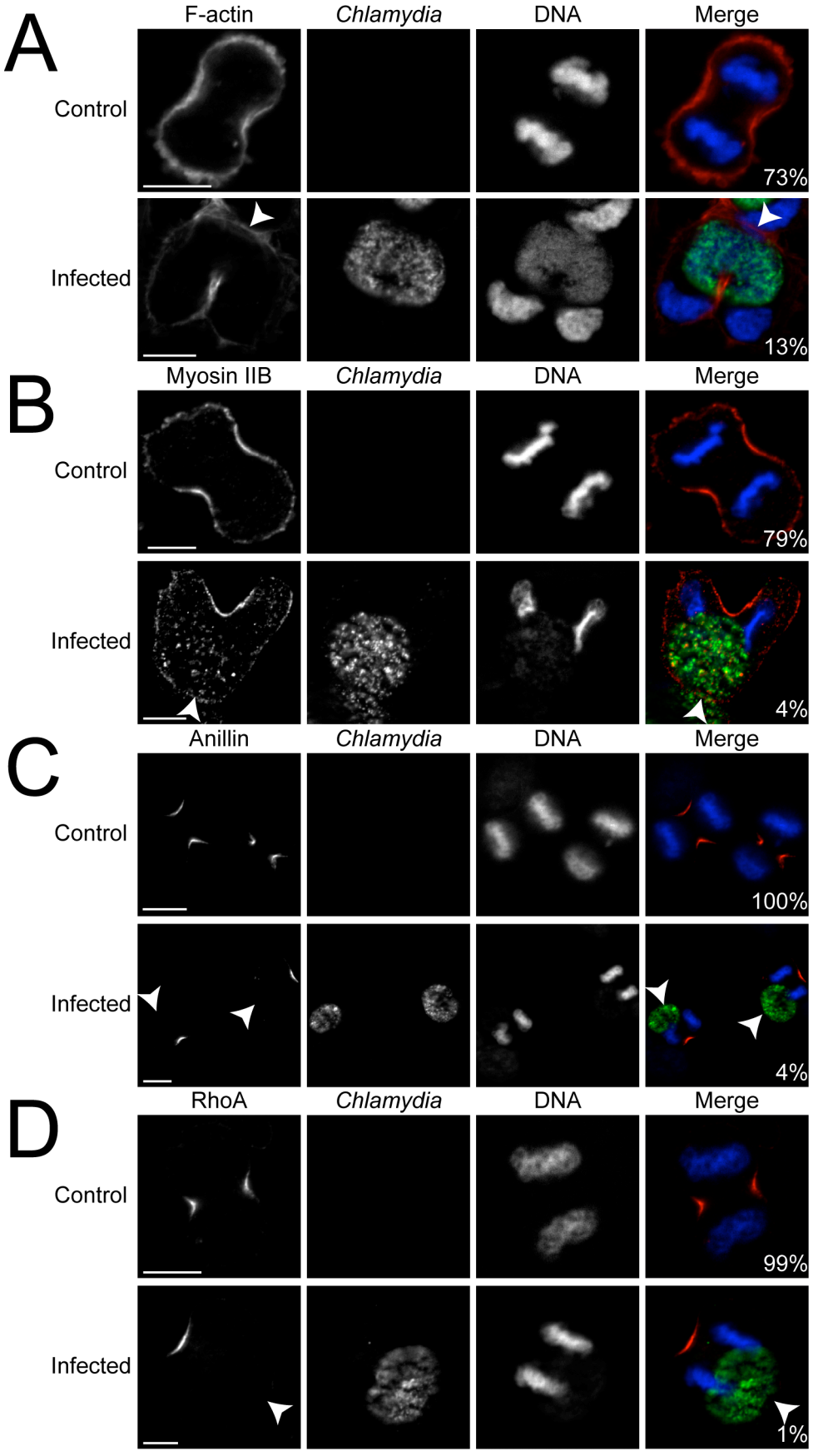
A
F-actin
Chlamydia
DNA
Merge
Control
73%
Infected
13%
B
Myosin IIB
Chlamydia
DNA
Merge
Control
79%
Infected
4%
C
Anillin
Chlamydia
DNA
Merge
Control
100%
Infected
4%
D
RhoA
Chlamydia
DNA
Merge
Control
99%
Infected
1%

Figure 3.6 *C. trachomatis* infection disrupts the accumulation of actin, myosin II, anillin and RhoA during telophase. (A-D) *Chlamydia* (green) and DNA (blue) were stained as described in Methods. Arrowheads indicated prospective furrowing plasma membrane lacking normal cytoskeletal or signaling protein accumulation. Numbers indicate percentages of cells with normal bilateral accumulation for each protein (red). Scale bars = 10 μm.

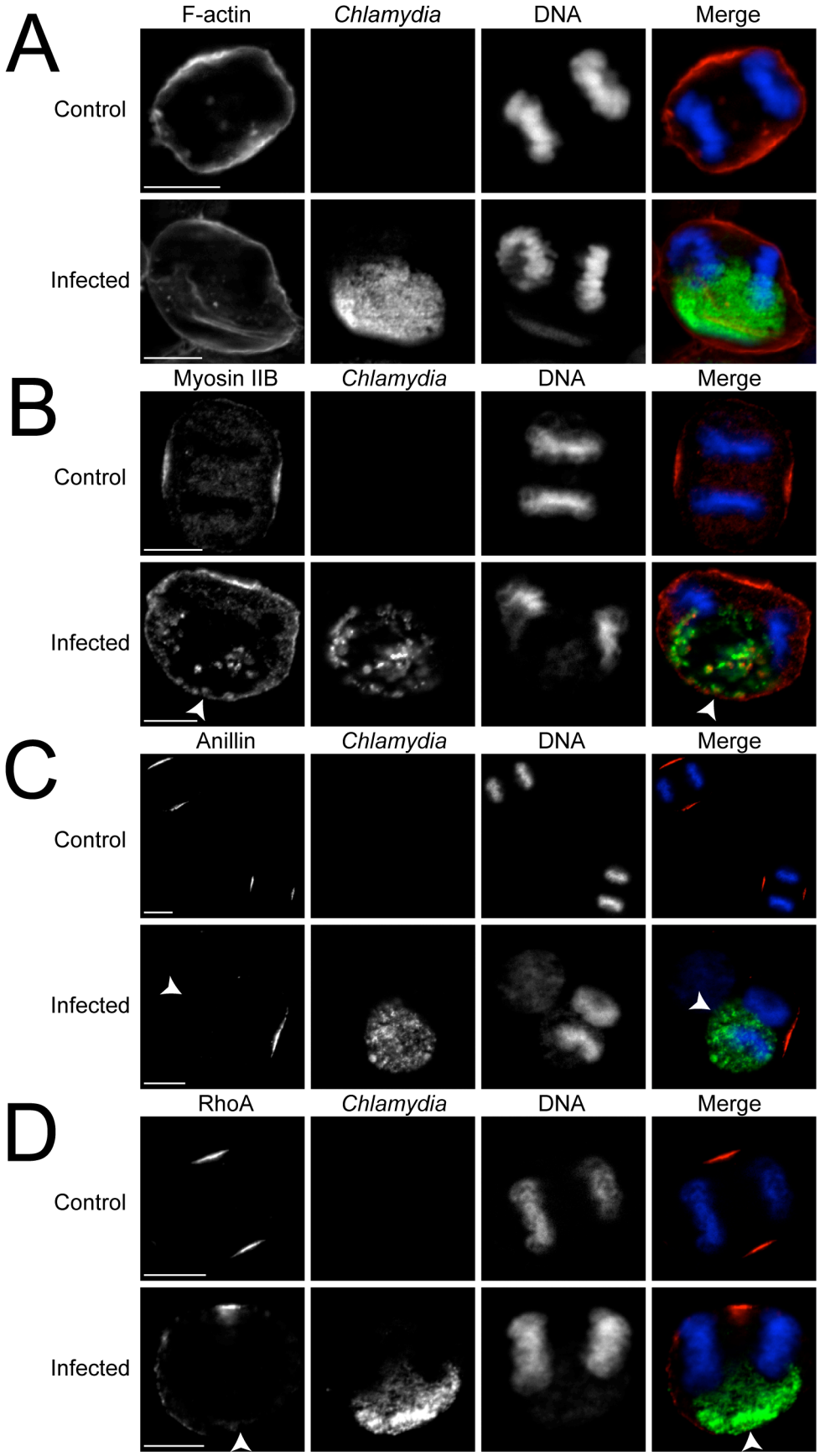
A
F-actin
Chlamydia
DNA
Merge
Control
Infected
B
Myosin IIB
Chlamydia
DNA
Merge
Control
Infected
C
Anillin
Chlamydia
DNA
Merge
Control
Infected
D
RhoA
Chlamydia
DNA
Merge
Control
Infected

Figure 3.7 *C. trachomatis* infection disrupts the accumulation of myosin II, anillin and RhoA during anaphase. (A-D) *Chlamydia* (green) and DNA (blue) were stained as described in Methods. Arrowheads indicated regions of the cell cortex lacking normal signaling protein accumulation. (A) The mislocalization of actin was not clear at anaphase. (B-D) The mislocalization of myosin II (B, red), anillin (C, red) and RhoA (D, red) was already prominent during anaphase. Scale bars = 10 μm.

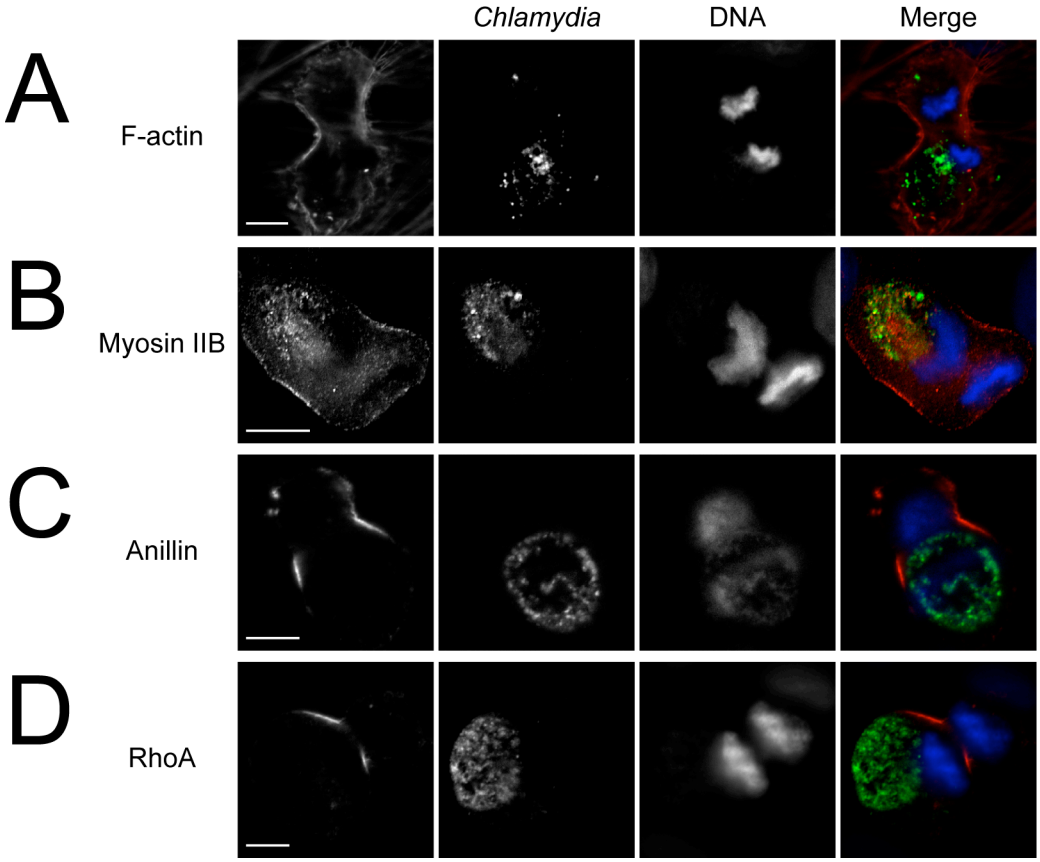

Figure 3.8 Host cell cleavage furrow formation is unaffected by *C. trachomatis* inclusions in the polar region. (A-D) *C. trachomatis* (green) and DNA (blue) were stained as described in Methods. Actin (A, red), myosin II (B, red), anillin (C, red), and RhoA (D, red) accumulated at both equatorial cortices in the presence of polar inclusions.

3.2.4 Ect2 and Plk1 localization is disrupted in the presence of *C. trachomatis* inclusions

To understand how RhoA became mislocalized on only one side of the cell, we investigated the localization of Ect2, a RhoGEF known to activate and promote RhoA localization (Nishimura and Yonemura, 2006; Somers and Saint, 2003; Yuce et al., 2005). The typical Ect2 localization, showing a linear distribution across the equatorial plane (Nishimura and Yonemura, 2006; Petronczki et al., 2007; Yuce et al., 2005), was only observed in 2% of *C. trachomatis*-infected telophase cells versus 99% of uninfected cells (Figure 3.9A). Instead, infected cells showed a linear, truncated staining pattern that rarely extended to cell cortices adjacent to the inclusions (Figure 3.9A). Similarly, the distribution of Mklp1, which is part of the centralspindlin complex that recruits Ect2 to the spindle midzone (Nishimura and Yonemura, 2006; Yuce et al., 2005; Zhao and Fang, 2005a), was normal in 97% of control telophase cells, while only 2% of infected telophase cells showed Mklp1 staining that spanned the entire equatorial plane (Figure 3.9B).

Plk1 is known to play very important roles in recruiting Ect2 to the centralspindlin complex and to the cell equator (Petronczki et al., 2007; Wolfe et al., 2009). Upon studying the localization of Plk1, we observed that 97% of uninfected versus 9% of *C. trachomatis*-infected telophase cells had normal Plk1 distribution, which spanned the equatorial width (Figure 3.9C). We subsequently examined the distribution of Prc1, a protein that recruits Plk1 to the cell equator (Von Schubert et al., 2010; D'Avino et al., 2007; Neef et al., 2007). Whereas, Prc1 showed normal distribution in 99% of uninfected cells, only 3% infected telophase cells showed typical Prc1 staining that traversed the equatorial plane (Figure 3.9D). Analysis of anaphase cells, showed similar patterns of disruption for Ect2, Mklp1, Plk1 and Prc1 in *C. trachomatis*-infected cells (Figure 3.10A-D). Notably, when *C. trachomatis* inclusions were in the polar region of the dividing host cells, Ect2, Mklp1, Plk1 and Prc1 all exhibited the normal linear distribution across the equatorial width of the host cells (Figure 3.11 A-D).

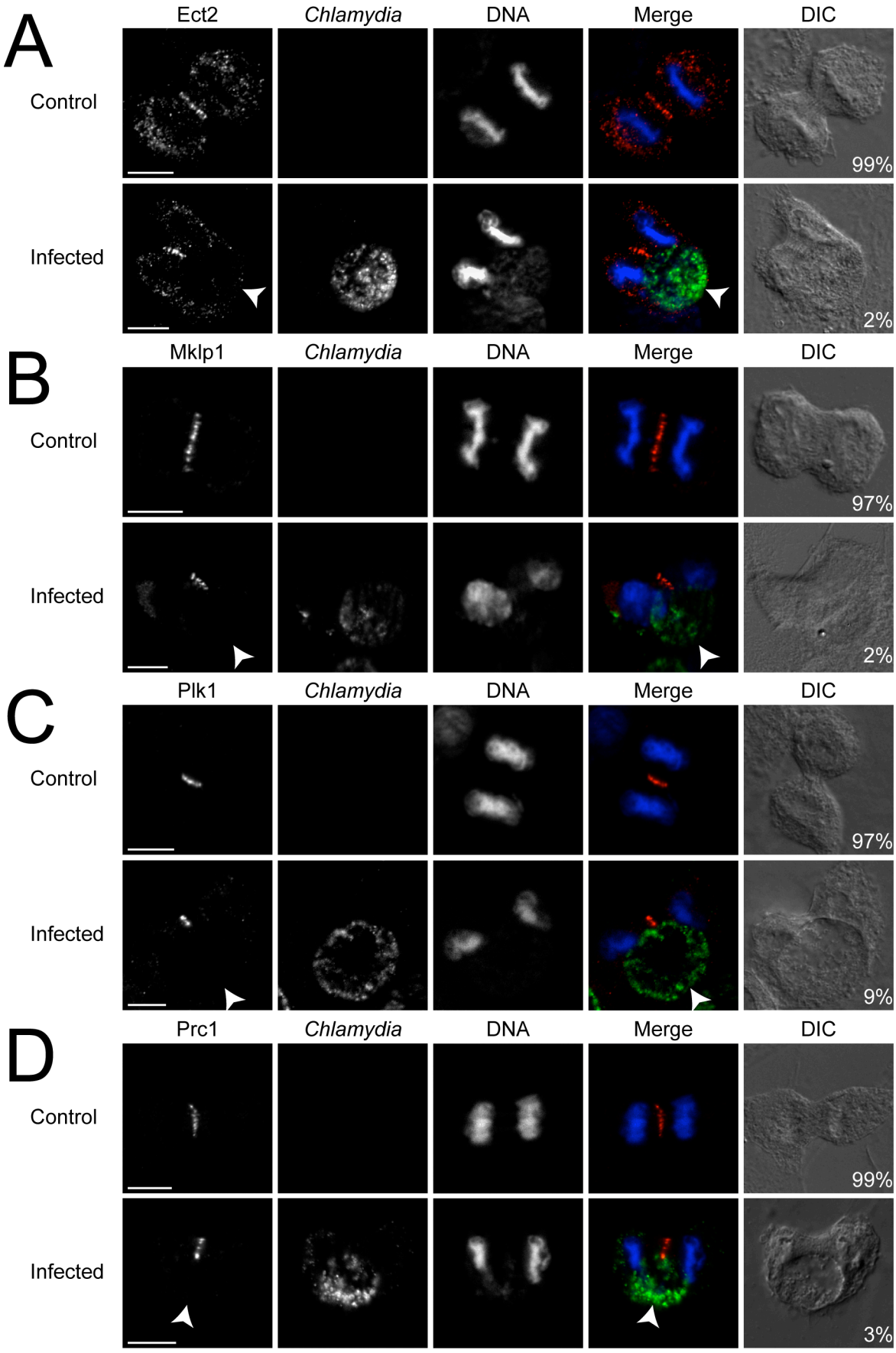
A
Ect2
Chlamydia
DNA
Merge
DIC
Control
99%
Infected
2%
B
Mklp1
Chlamydia
DNA
Merge
DIC
Control
97%
Infected
2%
C
Plk1
Chlamydia
DNA
Merge
DIC
Control
97%
Infected
9%
D
Prc1
Chlamydia
DNA
Merge
DIC
Control
99%
Infected
3%

Figure 3.9 *C. trachomatis* infection disrupts the equatorial localization of Ect2, Mklp1, Plk1 and Prc1 during telophase. (A-D) *Chlamydia* (green) and DNA (blue) were stained as described in Methods. Arrowheads marked equatorial cell cortex lacking normal signaling protein targeting. Numbers indicate percentages of cells with normal equatorial accumulation for each protein, which spanned the equatorial width (red). Scale bars = 10 μm.

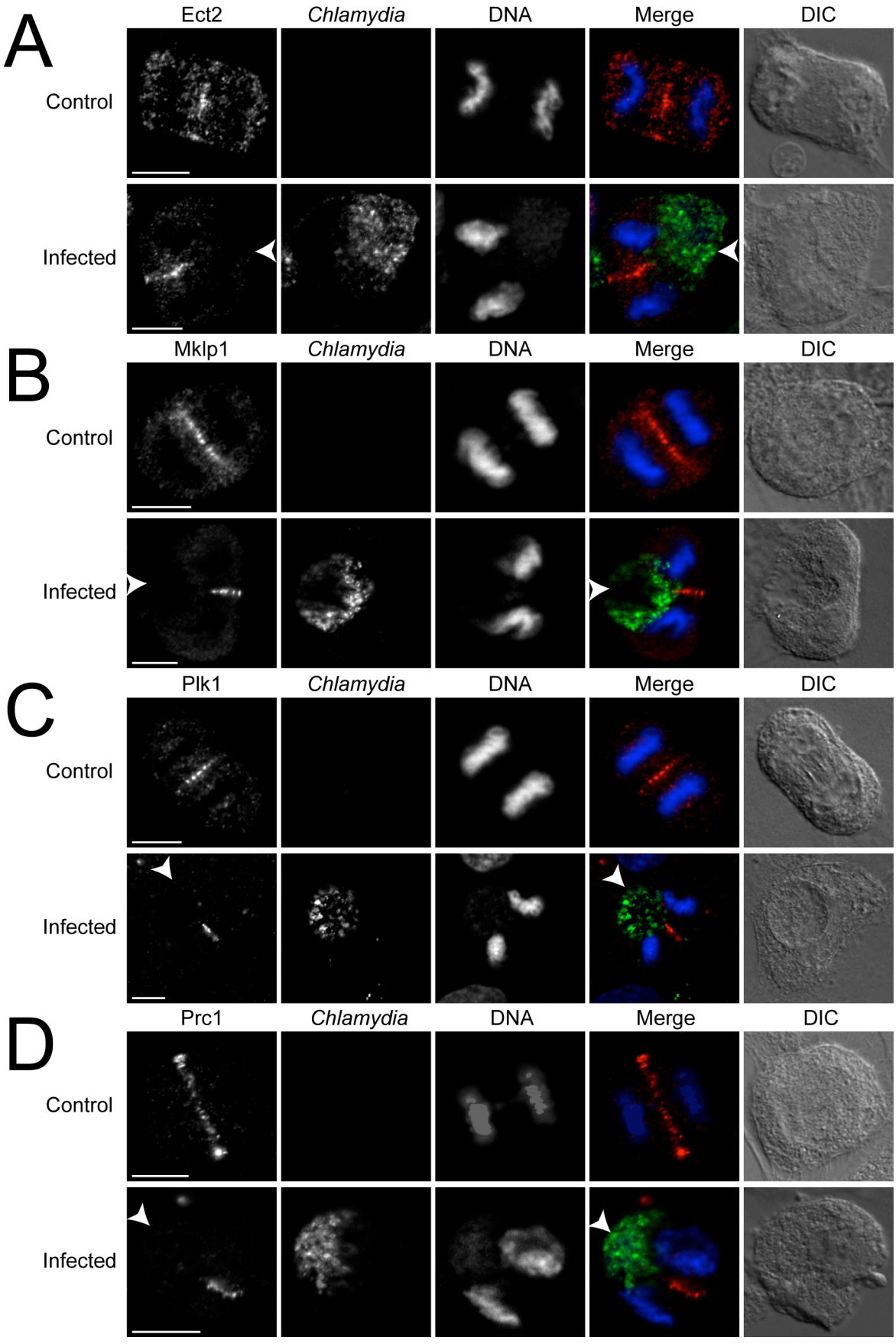
A
Ect2
Chlamydia
DNA
Merge
DIC
Control
Infected
B
Mklp1
Chlamydia
DNA
Merge
DIC
Control
Infected
C
Plk1
Chlamydia
DNA
Merge
DIC
Control
Infected
D
Prc1
Chlamydia
DNA
Merge
DIC
Control
Infected

Figure 3.10 *C. trachomatis* infection disrupts the localization of Ect2, Mklp1, Plk1 and Prc1 during anaphase. (A-D) *C. trachomatis* (green) and DNA (blue) were visualized as described in Methods. Arrowheads indicated equatorial cell cortex lacking normal signaling protein accumulation. The disruption of Ect2 (A, red), Mklp1 (B, red), Plk1 (C, red), and Prc1 (D, red) localization was already prominent during anaphase. Scale bars = 10 μm.

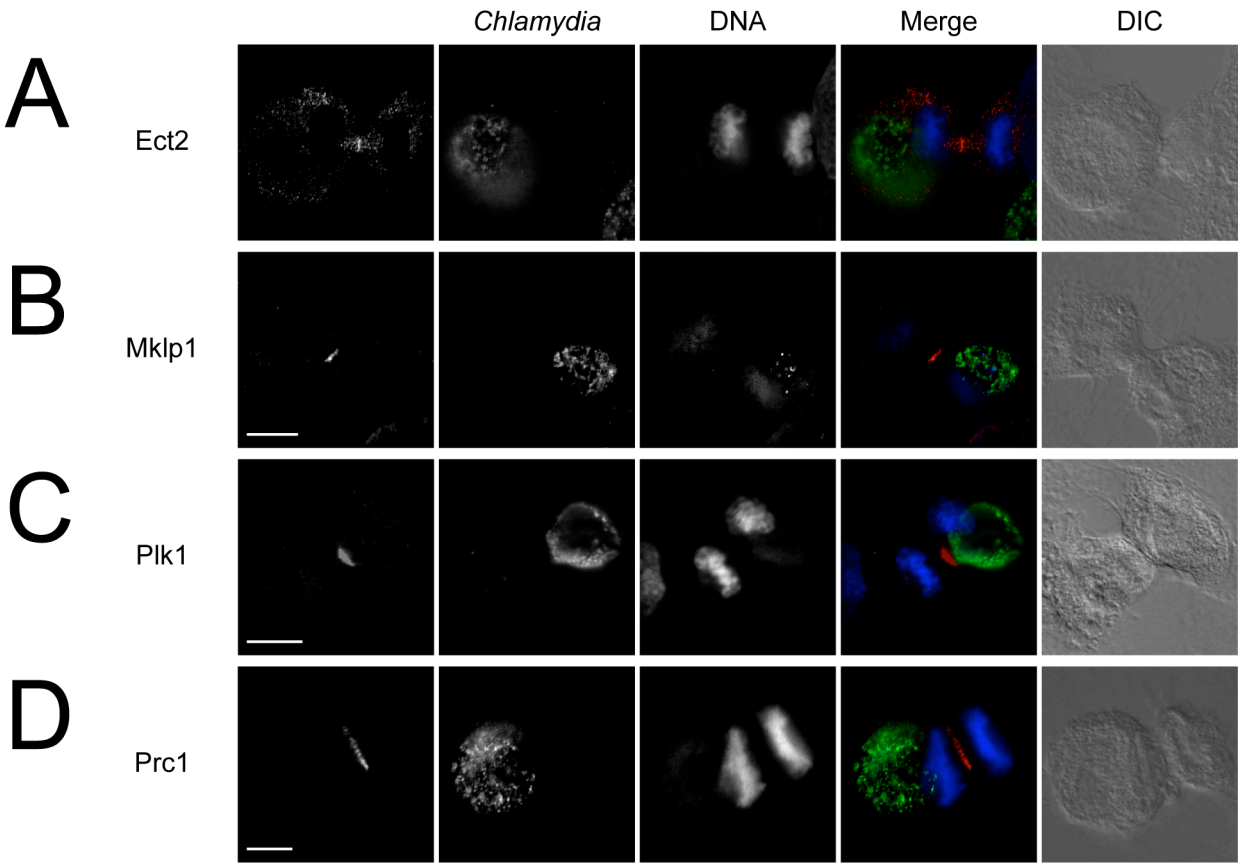

Figure 3.11 Host cell signaling protein localization is unaffected by polar *C. trachomatis* inclusions. (A-D) *C. trachomatis* (green) and DNA (blue) were stained as described in Methods. Ect2 (A, red), Mklp1 (B, red), Plk1 (C, red), and Prc1 (D, red) crossed the entire equatorial width when the inclusions were in the polar region.

3.2.5 Mislocalization of signaling proteins occurs in concert with displaced astral and central spindle MTs

A consistent defect was observed in Ect2, Mklp1, Plk1, Prc1 (Figure 3.9A-D) and Aurora B (data not shown) localization after *C. trachomatis* infection in mitotic cells. We hypothesized that delivery of these molecules was impaired due to MT organization disruption in *C. trachomatis*-infected cells. Control cells showed normal MT targeting to the furrowing cell cortices that were enriched for myosin II (Figure 3.12A). In contrast, only the cell cortex further away from *C. trachomatis* inclusions in infected cells showed robust MT targeting and myosin II accumulation (Figure 3.12A). The inclusion side had negligible or very sparse MT penetration with corresponding attenuated myosin II signal (Figure 3.12A). F-actin, anillin and RhoA showed identical localization as myosin II in relation to MT density (data not shown). We next investigated the distribution of central spindle MTs and Ect2 in *C. trachomatis*-infected cells. Ect2 was recruited as a perpendicular line across the mitotic midzone in uninfected telophase cells as expected (Figure 3.12B). Ect2 in *C. trachomatis*-infected cells similarly decorated the central spindle MTs, but both Ect2 and central spindle MTs were severely displaced away from the cell cortex adjacent to the inclusion (Figure 3.12B). Mklp1, Plk1 and Prc1 showed identical localization pattern as Ect2 in relation to MT distribution (data not shown).

We quantified the fluorescence intensity of MTs at each cleavage furrow and found that 89% of uninfected and only 9% of infected telophase cells had equal density of MTs at both equatorial cortices (Figure 3.12C). Fine step Z-stacks taken using spinning disk confocal revealed that MTs were equally distributed on both sides of uninfected telophase cells, while both central spindle and astral MTs were severely displaced to one side of the cell and rarely extended to the cell cortex adjacent to the *C. trachomatis* inclusion in infected cells (Figure 3.12D). Since *C. trachomatis* inclusions could induce very robust MT displacement in some regions of the cell cortex, we took advantage of this unique property to examine the role of astral MTs in promoting furrow formation. In the few instances where *C. trachomatis* inclusions were located at a polar region, no anillin accumulation was observed at cortical areas receiving dramatically lower astral MTs (Figure 3.13A). Small, centrally located *C. trachomatis* inclusions often blocked midzone MT from reaching the cortex yet allowed some astral MTs to reach the overlying cell cortex. Telophase cells with such inclusions showed modest equatorial anillin accumulation (Figure 3.13B). These results suggested that astral MTs had a positive, stimulatory

effect on cleavage furrow formation and the lack of astral MTs alone was insufficient to promote contractility.

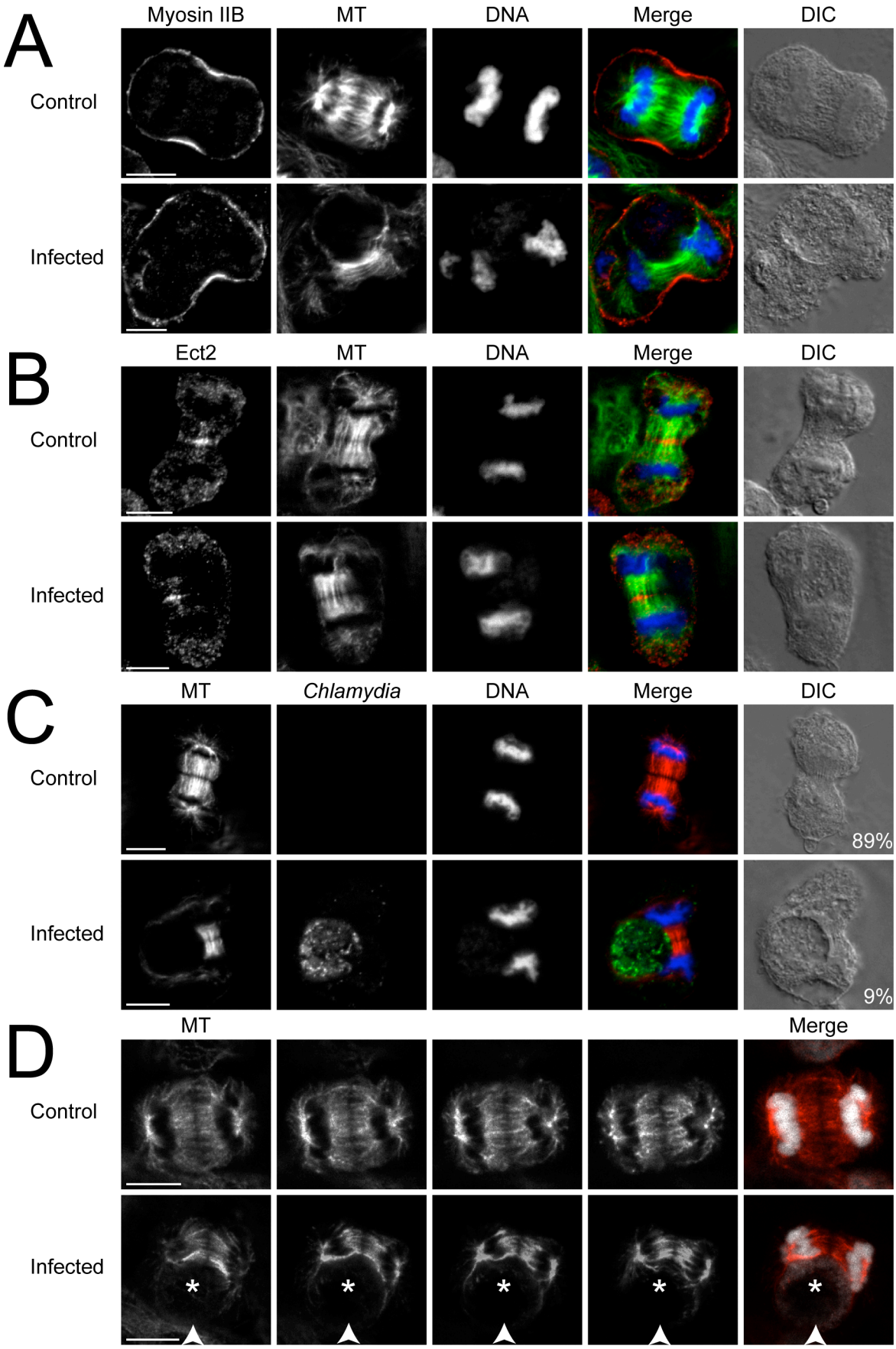
A
Myosin IIB
MT
DNA
Merge
DIC
Control
Infected
B
Ect2
MT
DNA
Merge
DIC
Control
Infected
C
MT
Chlamydia
DNA
Merge
DIC
Control
89%
Infected
9%
D
MT
Merge
Control
Infected
*
*
*
*
*

Figure 3.12 The mislocalization of myosin II and Ect2 coincides with MT displacement. (A-E) MT, *C. trachomatis* and DNA were stained as described in Methods. (A) Similar density of MTs (green) reached both equatorial cortices and myosin II (red) accumulated equally on both sides in uninfected cells. In *C. trachomatis*-infected cells, the lack of myosin II accumulation always coincided with the lack of MTs. (B) Ect2 (red) decorated the midzone MTs (green) across the equatorial width in uninfected telophase cells. After *C. trachomatis* infection, the midzone and astral MTs were severely shifted to one side of the telophase cell and Ect2 only accumulated where the MTs were present. (C) Both equatorial cortices received equal amounts of MTs (red) in 89% of uninfected but only 9% of infected telophase cells. (D) A series of spinning disk confocal images at different Z-planes showed that MTs (red) were distributed equally towards the cortex on both sides of the control cell; while both midzone and astral MTs were severely displaced from the side containing *C. trachomatis* inclusion (asterisks). Arrowheads indicate sites of reduced MT density at the cell cortex near the inclusion. DNA was shown in white. Scale bars = 10 μm.

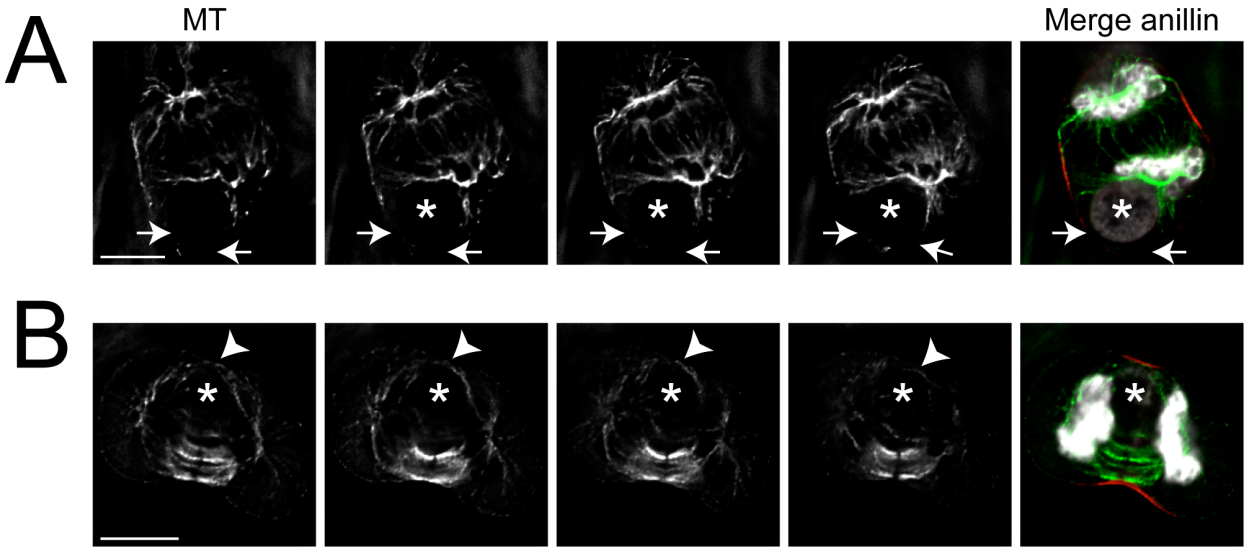

Figure 3.13 Astral MTs deliver positive furrow-inducing signals to the equatorial cell cortex (A) Astral MTs (green) could no longer reach some regions of the cell cortex due to the presence of a *C. trachomatis* inclusion (asterisks). No accumulation of the contractile element anillin (red) was observed in parts of the cell cortex with diminished astral MTs (arrows). At least 100 cells were screened for ectopic anillin accumulation. (B) Small, centrally located inclusion (asterisks) could displace central spindle MTs (green) while allowing astral MTs to reach the prospective furrowing cell cortex. Modest accumulation of anillin (red) was promoted by the presence of a few astral MTs (arrowheads). At least 30 cells with small, centrally located inclusions were examined. Scale bars = 10 μm.

3.2.6 Ingested latex beads mimic the *C. trachomatis* inclusion as a physical barrier and can induce unilateral cleavage furrow defect

We asked the question whether the *C. trachomatis* inclusion caused the displacement of cytoskeletal and signaling proteins by simply acting as a physical barrier. To mimic such an intracellular physical obstacle, Chinese Hamster Ovary (CHO) cells stably expressing Fcγ receptors (CHO-IIA cells) were used to internalize IgG-opsonized 15-micron polystyrene beads. While the phagocytic uptake of these large beads was extremely low (data not shown), we were able to obtain sufficient numbers of cells with internalized beads to compare their progression through cell division with the more reliably generated *C. trachomatis* inclusion-containing cells. Using DIC live cell imaging, we observed two phenotypes in dividing cells. CHO-IIA cells that contained a bead in the polar region successfully divided into two daughter cells (Figure 3.14A). When beads were centrally located in CHO-IIA cells, a unilateral cleavage furrow formed (Figure 3.14B), similar to *C. trachomatis*-infected cells. These cells were often prevented from dividing into two daughter cells (Figure 3.14B). Cells with internalized beads that failed to divide eventually formed multinucleated interphase cells (n=18 out of 18, Figure 3.14B). We confirmed that signaling proteins such as RhoA were unable to accumulate at the cell cortex near the equatorially located latex bead, which closely resembled the defect caused by *C. trachomatis* inclusion (Figure 3.14C, left). Conversely, RhoA accumulated at both equatorial cortices in the presence of a polar latex bead (Figure 3.14C, right). The success rate of division for cells with centrally located beads was significantly lower than that of cells with beads in the polar region (Figure 3.14D). This result suggested that the mechanical hindrance due to the presence of a large vacuole at the cell equator is sufficient to disrupt cytokinesis.

The polystyrene beads were chosen to have a size comparable to that of *C. trachomatis* inclusions at 36 hpi (Figure 3.14E). Despite having identical relative sizes, over 95% of *C. trachomatis* inclusions at 36 hpi localized to the cell equator, whereas less than 54% of the beads were present in the cell equator during telophase (Figure 3.14F). These results showed that *C. trachomatis* inclusions localized to the cell equator much more efficiently than inert particles of similar size, suggesting that *C. trachomatis* might be actively localizing to the cell equator.

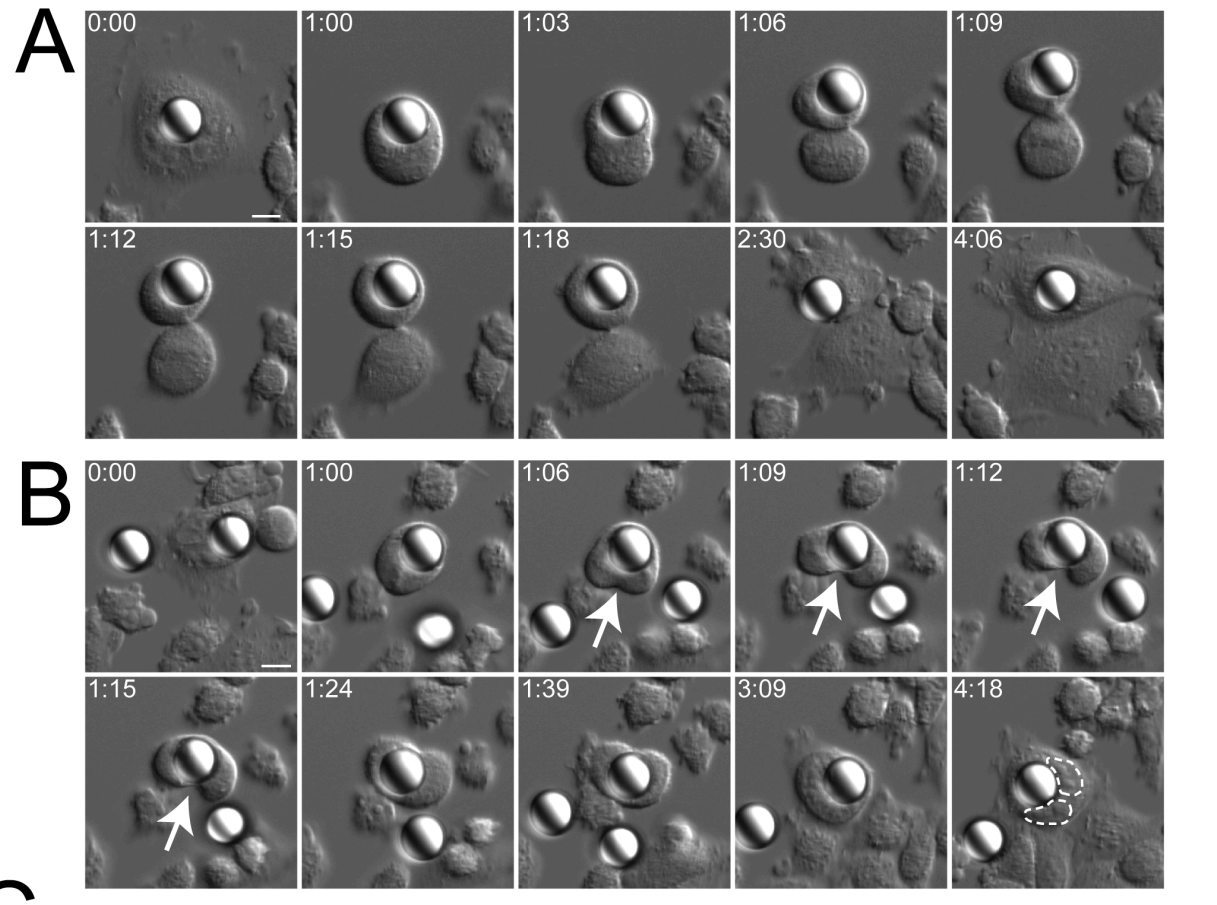
A
0:00
1:00
1:03
1:06
1:09
1:12
1:15
1:18
2:30
4:06
B
0:00
1:00
1:06
1:09
1:12
1:15
1:24
1:39
3:09
4:18

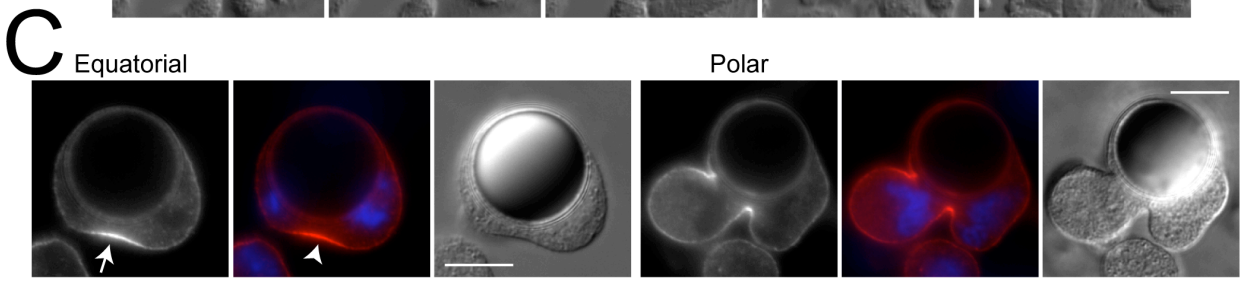
C
Equatorial
Polar

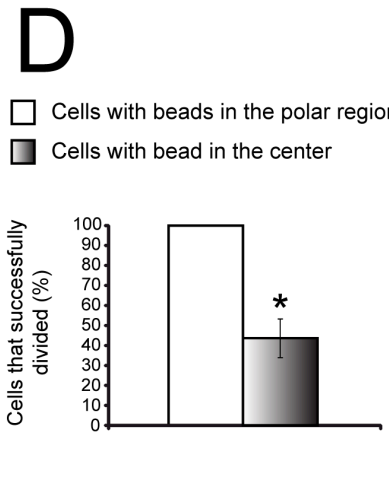
D
Cells with beads in the polar region
Cells with bead in the center
Cells that successfully divided (%)
100
90
80
70
60
50
40
30
20
10
0
*

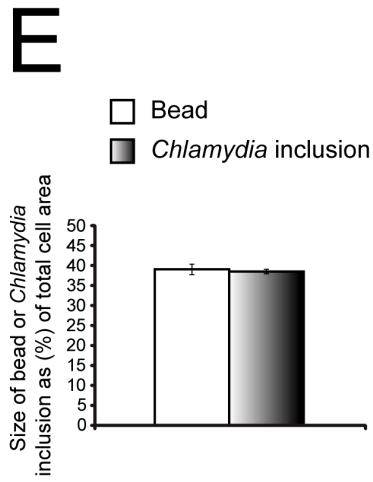
E
Bead
Chlamydia inclusion
Size of bead or Chlamydia inclusion as (%) of total cell area
50
45
40
35
30
25
20
15
10
5
0

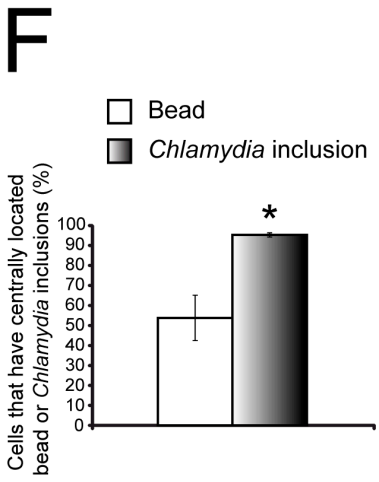
F
Bead
Chlamydia inclusion
Cells that have centrally located bead or Chlamydia inclusions (%)
100
90
80
70
60
50
40
30
20
10
0
*

Figure 3.14 Centrally located large polystyrene beads can recapitulate the unilateral cleavage furrow defect. (A and B) CHO-IIA cells that internalized a bead were subject to DIC imaging. Numbers indicate hours:minutes. Scale bars = 10 μm. (A) Cells with beads in the polar region were able to form bilateral cleavage furrows and successfully divide into two discrete daughter cells (n= 16 out of 16). (B) When the bead was in the cell center, a unilateral cleavage furrow (arrows) could be induced. Cytoplasmic division frequently failed in cells with centrally positioned beads (n=18 out of 27). Two nuclei were outlined with dashed lines. (C) RhoA (red) only accumulated at the equatorial cell cortex away from the centrally located latex bead in CHO IIA cells. RhoA accumulated bilaterally when the latex bead was not in the cell centre. DNA was stained with DAPI (blue) (n= 10 out of 10). (D) Cells containing centrally located beads had a significantly lower success rate of division than cells containing beads in the polar region ($p < 0.005$). (E) The relative size of 15 μm beads compared to host cells was indistinguishable from that of the *C. trachomatis* inclusions at 36 hpi ($p > 0.74$). (F) *C. trachomatis* inclusions localized to the cell equator significantly more often than similarly sized beads during telophase ($p < 0.005$). (C-E) Error bars represent SEM from at least three independent experiments.

3.2.7 Active bacterial protein synthesis contributes to the equatorial localization of *C. trachomatis* inclusions

Despite recent development, gene-specific genetic knockout tools are not available for chlamydia (Kari et al., 2011; Nguyen and Valdivia, 2012). In order to address whether *C. trachomatis* was actively localizing to the center of dividing cells, we created metabolically inactive *C. trachomatis* inclusions using azithromycin, one of the most commonly prescribed antibiotics for treating *C. trachomatis* infection (Kimberly A. Workowski, 2006). To block *C. trachomatis* protein synthesis, azithromycin was added to cells at 28 hpi to allow initial growth of the inclusion to an intrusive size. We assessed bacterial protein synthesis with a non-radioactive nascent protein synthesis labelling technique using L-azidohomoalanine (AHA). *C. trachomatis* particles in untreated cells were brightly labelled with AHA and appeared as distinct puncta within the inclusion (Figure 3.15A), while no bacteria showed visible incorporation of AHA 7 hours after azithromycin treatment (Figure 3.15B). AHA incorporation by *C. trachomatis* inclusion was unaffected by cycloheximide, a host protein synthesis inhibitor (Figure 3.15C). In addition, simultaneous cycloheximide and azithromycin treatment knocked out both host and bacterial AHA incorporation (Figure 3.15D). Together, these results validated the use of AHA for detecting chlamydial protein synthesis.

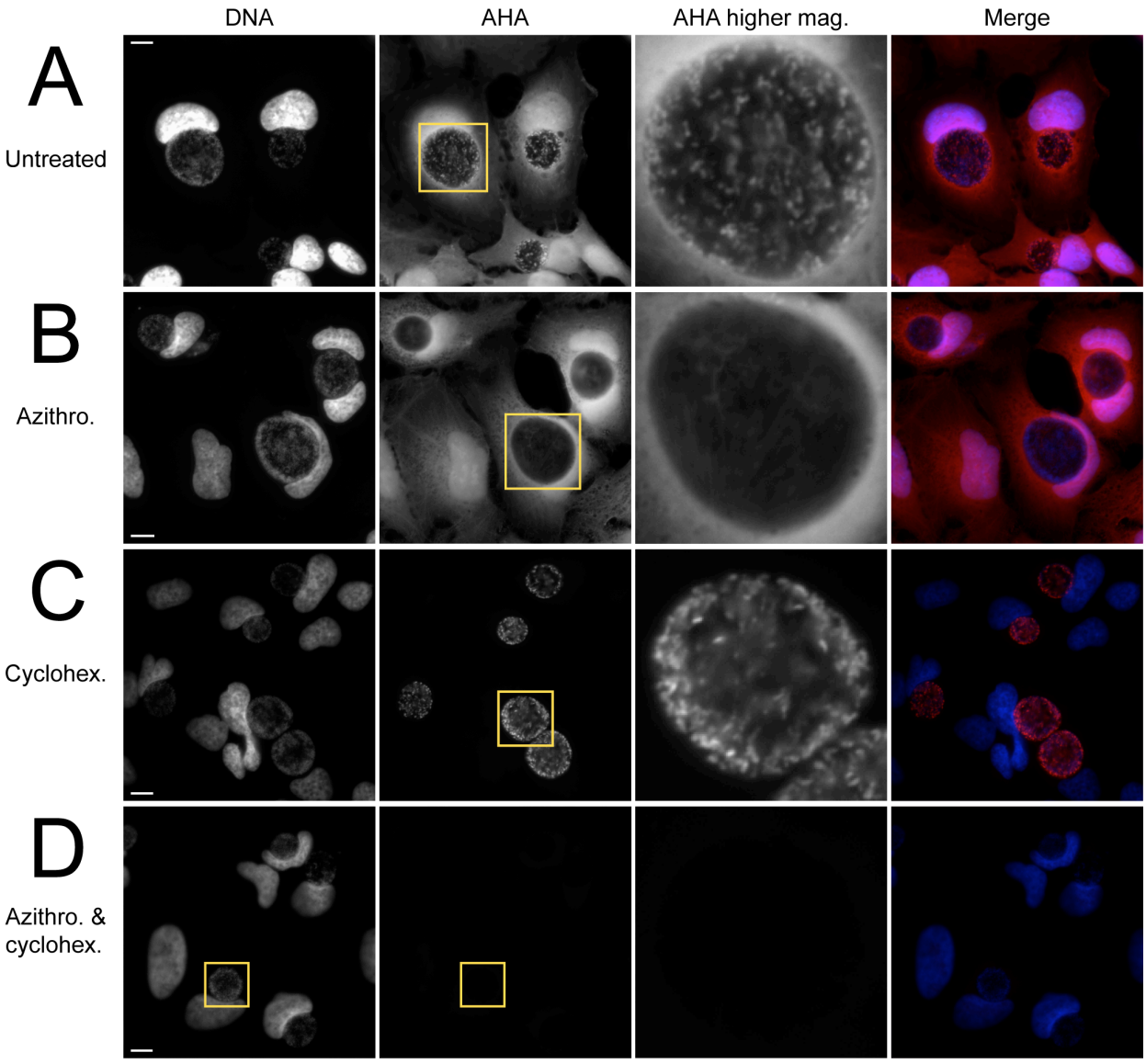
DNA
AHA
AHA higher mag.
Merge
A
Untreated
B
Azithro.
C
Cyclohex.
D
Azithro. &
cyclohex.

Figure 3.15 Azithromycin prevents *C. trachomatis* protein synthesis. Cells were untreated, treated with cycloheximide (cyclohex) and azithromycin (azithro) alone or in combination for 1 hour before labelling with AHA to detect nascent protein synthesis. (A) Untreated cells showed uniform distribution of AHA (red) in the cytosol and punctate staining in the *C. trachomatis* inclusions. (B) Inclusions in azithromycin-treated cells lacked detectable accumulation of AHA. (C) Cycloheximide-treated cells had low levels of host protein synthesis, while *C. trachomatis* protein synthesis was unaffected. (D) Azithromycin and cycloheximide treatment largely inhibited both host and *C. trachomatis* protein synthesis as shown by diminished AHA signal.

To monitor cleavage furrow formation, we examined the localization of RhoA in these azithromycin-treated cells. Following antibiotic treatment, we observed that RhoA was still severely mislocalized in the presence of centrally positioned inclusions (Figure 3.16A and C). Cells with identical inclusion sizes were chosen for comparison to ensure that any difference we detected was not solely due to the difference in inclusion size (Figure 3.16B). Interestingly, analysis of antibiotic-treated cells revealed a significant increase of *C. trachomatis* inclusions in the polar region of cells compared to untreated cells (Figure 3.16D). After azithromycin treatment, cells with inclusions in the polar region were able to form normal bilateral cleavage furrows (Figure 3.17A), similar to CHO-IIA cells with beads in the polar region (Figure 3.14A and C). Over 98% of cells with inclusions in the polar region successfully completed furrow ingression, while less than 20% of cells with equatorial inclusions were able to complete furrow ingression (Figure 3.17B and C). Following antibiotic treatment, there was a significant increase in the percentage of cells that successfully completed furrow ingression (Figure 3.17D). Thus, protein synthesis of *C. trachomatis* influenced the spatial distribution of this bacterial compartment in dividing cells, which largely determined the efficiency of cleavage furrow disruption.

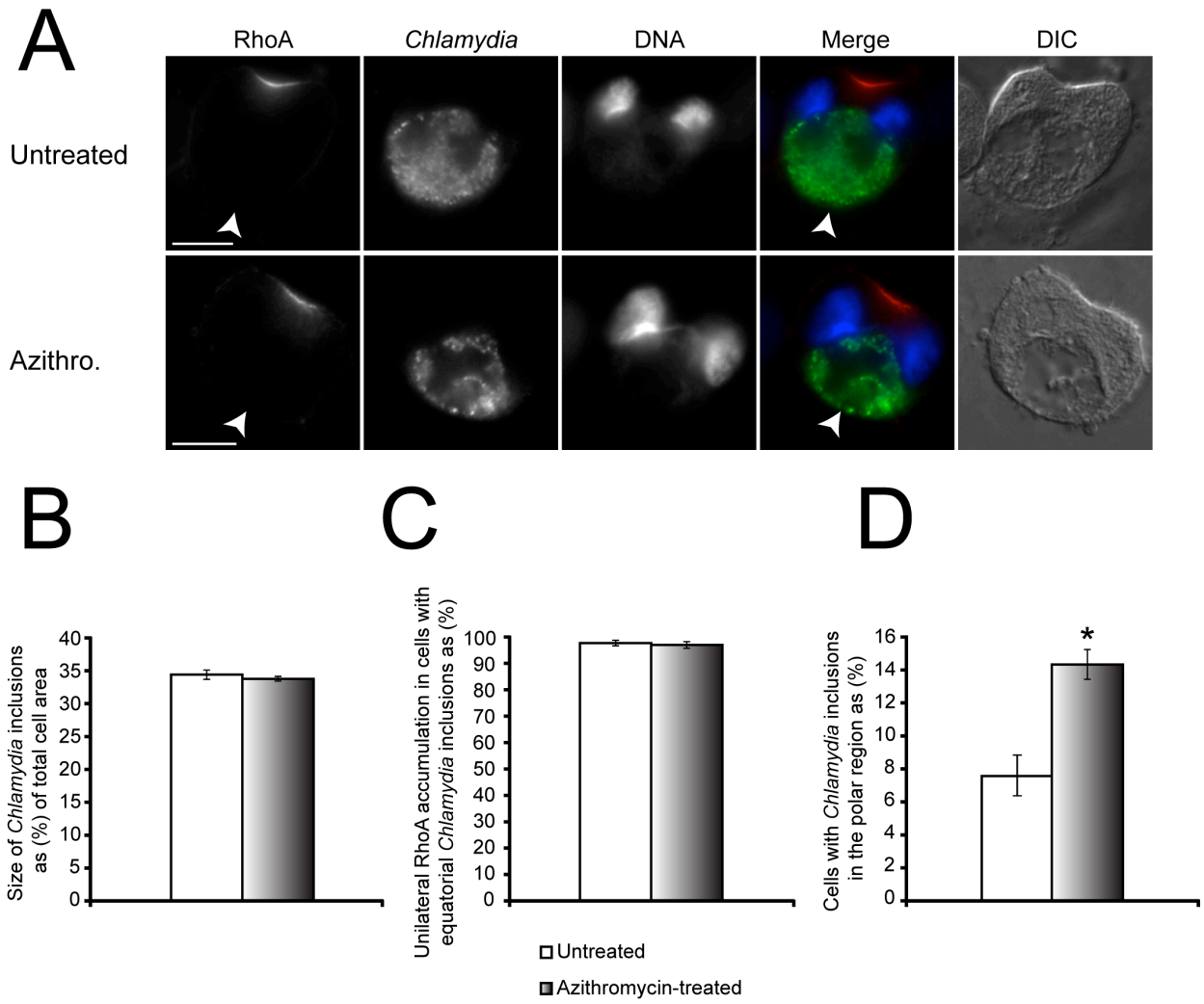

Figure 3.16 Azithromycin treatment increases the number of polar inclusions. (A) Similar to untreated cells, after azithromycin treatment, centrally located *C. trachomatis* inclusions still caused RhoA mislocalization during telophase (arrowheads). (B) Telophase cells with similarly sized *C. trachomatis* inclusions ($p > 0.56$) were chosen, with and without azithromycin treatment, for subsequent RhoA distribution and inclusion positioning analysis. (C) Azithromycin treatment did not rescue the RhoA mislocalization defect when the *C. trachomatis* inclusion was centrally located ($p > 0.72$). (D) A significant increase of cells containing *C. trachomatis* inclusions in the polar region was detected after azithromycin treatment ($p < 0.05$). Error bars represent SEM from three independent experiments.

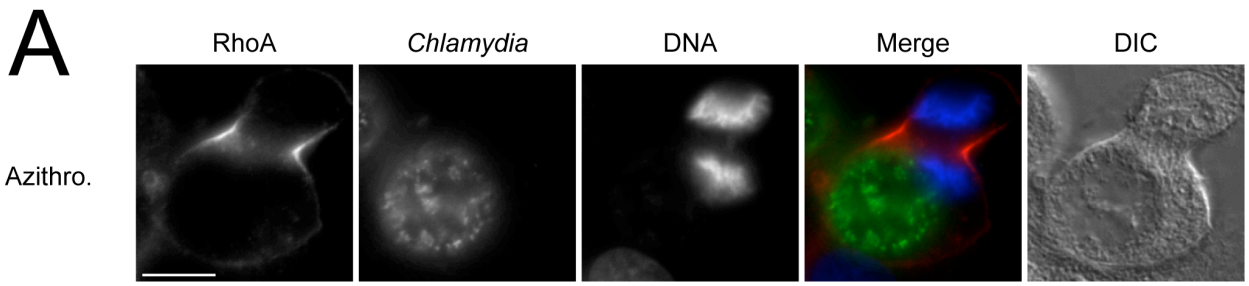
A
RhoA
Chlamydia
DNA
Merge
DIC
Azithro.

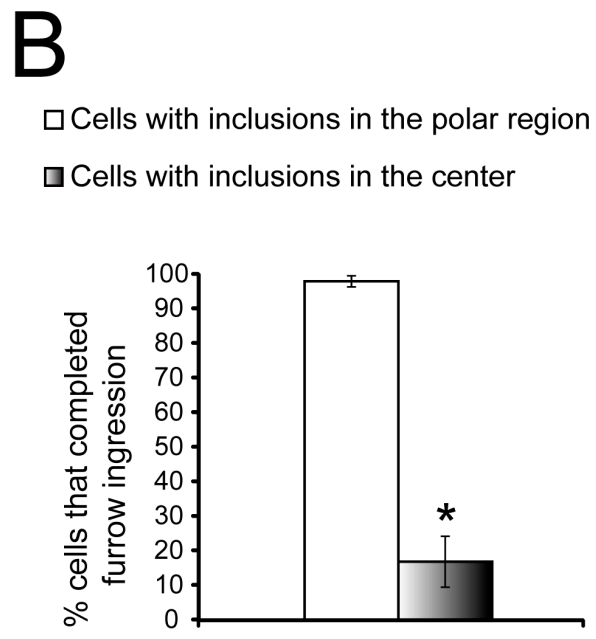
B
Cells with inclusions in the polar region
Cells with inclusions in the center
% cells that completed furrow ingression
100
90
80
70
60
50
40
30
20
10
0
*

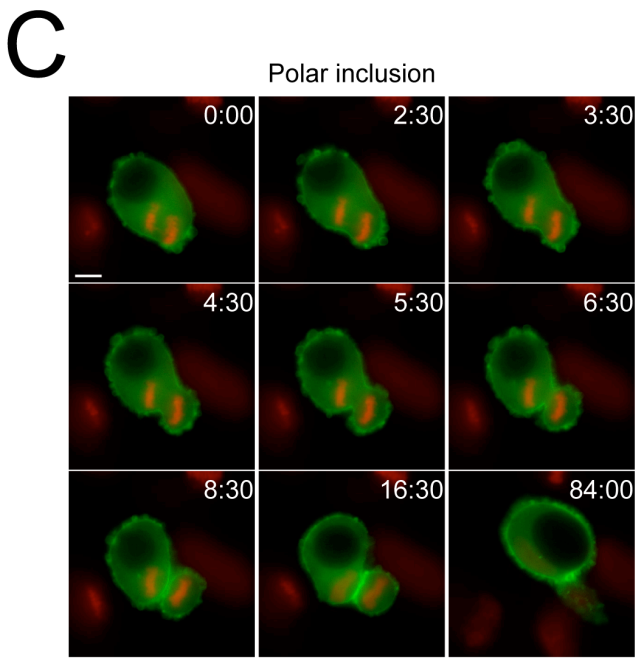
C
Polar inclusion
0:00
2:30
3:30
4:30
5:30
6:30
8:30
16:30
84:00

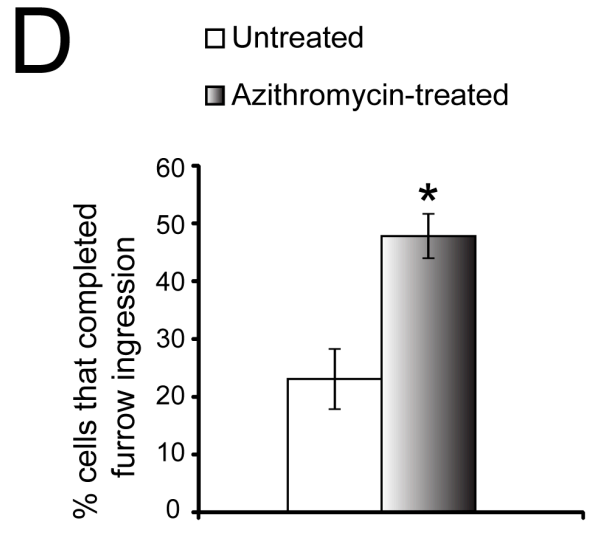
D
Untreated
Azithromycin-treated
% cells that completed furrow ingression
60
50
40
30
20
10
0
*

Figure 3.17 Cells containing polar *C. trachomatis* inclusions can successfully divide. (A) Cells containing polar inclusions after azithromycin treatment had normal bilateral RhoA accumulation and furrow ingression. (B) Cells containing *C. trachomatis* inclusions in the polar region did not cause observable cleavage furrow defects (n= 48 out of 49), while cells with equatorially located inclusions rarely completed cleavage furrow ingression (n= 6 out of 33) ($p< 0.01$). (C) Fluorescent live cell imaging (F-actin, green; DNA, red) confirmed that cells with polar *C. trachomatis* inclusions divided normally into two daughter cells. Numbers indicate minutes:seconds. Scale bars = 10 μm (D) Azithromycin treatment for 7 hours significantly increased the percentage of infected cells that completed furrow ingression ($p< 0.05$). More than 70 cells were quantified per experiment. Error bars represent SEM from three independent experiments.

3.3 Discussion

This study shows that *C. trachomatis* inclusions at later stages of infection can disrupt cleavage furrow formation on one side of the host cell, thus leading to a unique unilateral furrow ingression that often failed to complete. Numerous epidemiological studies have identified *C. trachomatis* as both an independent risk factor and a co-factor with human papillomavirus to cause cervical cancer (Madeleine et al., 2007; Samoff et al., 2005). In addition, *Chlamydia pneumonia*, whose life cycle is similar to *C. trachomatis*, has also been shown to increase the risks of lung cancer (Jackson et al., 2000; Littman et al., 2004). The tumorigenic effects of *C. pneumonia* may be caused by chronic inflammation (Chaturvedi et al., 2010) and *C. trachomatis* infection has been shown to lead to supernumerary centrosome formation, another possible contributing factor to tumorigenesis (Grieshaber et al., 2006b; Johnson et al., 2009; Knowlton et al., 2011). Our study provides a mechanism by which *C. trachomatis* causes host cytokinesis failure and multinucleation with very high efficiency. We demonstrated the mechanism by which *C. trachomatis* inclusions efficiently disrupted host cleavage furrow formation. Starting as far upstream as Plk1 and Prc1, we observed a consistent and sharp reduction of all the major downstream signaling elements, including the actomyosin machinery, at the inclusion side. Our live cell imaging showed no indication of partially formed or regressed furrows on the inclusion side, suggesting that cleavage furrow initiation was impaired.

C. trachomatis inclusions reproducibly mimicked the elegant oil droplet studies performed by Rappaport in echinoderm eggs (Rappaport and Rappaport, 1983), where unilateral cleavage formation was also induced. In Rappaport's study, a vacuole was generated by injecting an oil droplet into the dividing cell (Rappaport and Rappaport, 1983). The oil droplet likely displaced the mitotic spindle apparatus to an eccentric position and prevented the spindle MTs from delivering the necessary signaling proteins to the equatorial cortex adjacent to the oil droplet. In the current study, we were able to recapitulate the unilateral cleavage furrow using centrally located, large latex beads in CHO-IIA cells, suggesting the asymmetric cleavage formation was caused by the physical presence of a large vacuole. Green urchin and Hydractinia embryo cells spontaneously form unilateral cleavage furrows, which have been attributed to naturally occurring eccentric mitotic spindles (Rappaport and Conrad, 1963; Bement et al., 2005). Due to the high consistency by which *C. trachomatis* causes the unilateral cleavage furrow defect, we

were able to confirm that the mitotic spindle also became eccentrically positioned, due to the presence of a large inclusion with high resolution IF.

Our study is the first to systematically assess the localization of key signaling elements during unilateral cleavage formation. Previous studies that observed unilateral cleavage furrows lacked large scale IF quantifications due to the transiency of furrow ingression (Campbell et al., 1989). In our study, we consistently obtained large numbers of telophase cells exhibiting unilateral furrows with monastrol synchronization and *C. trachomatis* infection. Also unique about this system was that endogenous proteins were not experimentally knocked down and were functional based on their recruitment and ability to promote at least one cleavage furrow. It is important to note that normal bilateral cleavage furrows formed and ingressed, when the *C. trachomatis* inclusion was located in the polar region. Together, these observations suggested that *C. trachomatis*-induced cleavage furrow defect was the result of physical displacement instead of degradation of host signaling proteins essential for furrow initiation. Ect2 is recruited to the midzone MTs to promote RhoA activation at the overlying cell cortex (Petronczki et al., 2007; Yuce et al., 2005). In the presence of *C. trachomatis* inclusions, Ect2 was physically blocked from reaching some of the prospective furrowing regions, and the absence of RhoA at these regions suggested that Ect2 could only activate RhoA locally. This provided direct evidence that Ect2 was responsible for the spatial control of RhoA activation during mitosis, without using global protein knock down techniques such as siRNA (Piekny et al., 2005). Similarly, activated RhoA could only exert its function locally in the cell, as we only observed recruitment of anillin and actomyosin filament assembly on the same side where RhoA accumulated. In addition, we observed that active RhoA did not diffuse laterally towards the inclusion side along the equatorial cortex as the unilateral furrow ingressed. This suggests that RhoA may not require a negative regulator to switch RhoA to the inactive form in order to prevent it from diffusing from the equatorial region, as it appeared that RhoA might become immobilized once it was activated. This is in contrast to the theory that RhoA must be deactivated by GAPs in order to restrict the active Rho zone at the equatorial cortex (Miller and Bement, 2009).

We also took advantage of the unique protein displacing property of the *C. trachomatis* inclusion to provide novel insights regarding the controversial role of MTs in cleavage plane specification. Numerous studies have suggested that dynamic astral MTs inhibit global

contractility and the furrow occurs at the cell equator because it has the lowest density of astral MTs (Canman et al., 2003; Motegi, Velarde, Piano, & Sugimoto, 2006; Werner, Munro, & Glotzer, 2007; Foe & von Dassow, 2008; Murthy & Wadsworth, 2008; von Dassow, 2009). Most of these studies used either MT poisons such as nocodazole or genetic tools to destabilize dynamic MTs, which would inadvertently remove dynamic MTs in the central spindle as well, leading to confounding results. In our system, MTs were physically displaced from certain regions of the cell cortex and we were able to directly observe the effect of different MT populations on furrow induction without globally altering MT stability. Large *C. trachomatis* inclusions prevented targeting of MTs to the neighbouring cell cortex and generated regions on the cell cortex that received no detectable levels of MTs and yet no contractile activity was observed. Our live cell imaging showed no indication of partially formed or regressed furrows on the inclusion side, suggesting that cleavage furrow initiation was impaired. Additionally, these experiments demonstrated that there were neither ectopic furrows nor actin waves on the cell cortex receiving non-detectable levels of astral MTs. It has been proposed that dynamic astral MTs exist in the highest concentration at the poles, which inhibits polar contractile activity in general (Foe and Von Dassow, 2008; Odell and Foe, 2008; Fededa and Gerlich, 2012). Smaller *C. trachomatis* inclusions created regions on the polar cell cortex that lacked detectable levels of astral MTs and yet no furrow-inducing elements or furrows were observed at these regions. This suggests that dynamic astral MTs are not necessary to inhibit ectopic polar contractility. Moreover, we observed that smaller, centrally located *C. trachomatis* inclusions selectively displaced midzone MTs, yet permitted low levels of astral MTs to reach the prospective furrowing cell cortex. Cells containing such inclusions exhibited partial recruitment of key furrow elements to the equatorial cell cortex. Based on our experiments, we could not definitively determine whether the central spindle MTs are essential for full anillin accumulation, because the reduced anillin accumulation on the inclusion side could have resulted from reduced levels of astral MT targeting to the equatorial cortex due to the presence of the small inclusion. Collectively, these results support the paradigm that astral MTs deliver positive furrow-inducing signals to the prospective furrowing plasma membrane (Glotzer, 2004).

We showed that *C. trachomatis* inclusions could localize to the cell equator more efficiently than similarly sized vacuoles generated by internalized beads, indicating the bacteria are actively localizing to the cell center. A recent study on *Theileria* showed that the parasite can

recruit host Plk1 and localize to the host central spindle (Von Schubert et al., 2010). Unlike *Theileria*, none of the host signaling proteins that we examined were noticeably recruited to the *C. trachomatis* inclusion membrane. Due to the lack of gene-specific *C. trachomatis* genetic manipulation tools, we had to generate metabolically inactive *C. trachomatis* inclusions to address whether *C. trachomatis* proteins contributed to the central localization of the inclusions during telophase. The significant increase of inclusions in the host polar region during telophase after antibiotic treatment suggested that *C. trachomatis* protein synthesis played a role in positioning this bacterial compartment. It is likely that the antibiotic treatment reduced the expression of some *C. trachomatis* proteins on the inclusion surface that were important for its positioning. Interestingly, the majority of *C. trachomatis* inclusions devoid of detectable levels of protein synthesis for at least 7 hours still localized to the host cell center, suggesting factors essential for *C. trachomatis* positioning might have been expressed or recruited before antibiotic treatment at 28hpi.

The *C. trachomatis*-induced cleavage furrow and cytokinesis defect is highly dependent on the inclusion location. Cells with large inclusions in the polar region were able to form normal cleavage furrows and have normal signaling protein localization; moreover, almost 100% of *C. trachomatis*-infected cells that contained inclusions in the polar region successfully divided into two daughter cells. Therefore, it was unlikely that the cleavage furrow formation defect was caused by generic host protein degradation. Our results demonstrated that conventional antibiotic treatment such as azithromycin was effective in blocking *C. trachomatis* protein synthesis; however, it could not fully rescue the unilateral cleavage furrow defect that frequently resulted in the formation of multinucleated host cells. It has been previously shown that *C. trachomatis* could exit by extrusion in more than 50% of infected host cells, which could remain viable afterwards (Beatty, 2007; Hybiske and Stephens, 2007). Therefore, it is reasonable to speculate that *C. trachomatis* may contribute to tumorigenesis by causing host genome duplication and leaving behind viable tetraploid host cells following extrusion exit. It has been recently demonstrated that 3T3 cells that have been cured of *C. trachomatis* infection can become anchorage-independent, a hallmark for tumorigenic cells (Knowlton et al., 2013). In addition, *C. muridarum* can infect actively dividing cells and cause premalignant lesions in the cervix of mouse models (Knowlton et al., 2013). Our results suggest that *C. trachomatis* patients should be screened carefully for premalignant lesions even after the clearance of bacteria, as antibiotics cannot rescue the cleavage furrow defect in majority of the infected cells.

In conclusion, our results demonstrate that *C. trachomatis*-induced host cell multinucleation is primarily caused by a cleavage furrow ingression defect due to the presence of a large equatorial *C. trachomatis* inclusion during mitosis. This is the first time that a bacterium has been documented to physically block the host cell mitosis. Our findings also suggest that *C. trachomatis* is actively localizing to the host cell equator during telophase, because it localizes to the host cell centre much more frequently than similarly-sized inert vacuole and inhibition of bacterial protein synthesis reduces the equatorial localization of *C. trachomatis* inclusions.

Chapter 4

Chlamydia inclusions actively localize to the host cell centre during mitosis to co-opt replicated Golgi in multinuclear cells

A modified version of this chapter was submitted to Infection and Immunity

Chapter 4
Chlamydia inclusions actively localize to the host cell centre during mitosis to co-opt replicated Golgi in multinuclear cells

4.1 Introduction

The obligate intracellular pathogen, *Chlamydia trachomatis*, is the leading cause of bacterial sexually transmitted infections worldwide and epidemiological studies have suggested a link between *C. trachomatis* infection and higher risks of cervical cancer (Madeleine et al., 2007; W.H.O., 2001). Chlamydiae exist in two distinct forms: the infectious elementary body, which is well-suited for extracellular survival, and the non-infectious reticulate body, which is the intracellular replicative form (Beatty et al., 1994). Once chlamydiae enters a susceptible host cell, it resides in a host membrane-bound vacuole termed an inclusion, where the EBs differentiate into the RBs and begin to replicate (Hatch et al., 1984). The size of the inclusion increases drastically over the course of the infection and the inclusion can occupy almost the entire host cytoplasm toward the end of the infection (Neeper et al., 1990; Hybiske and Stephens, 2007). During later stages of the infection, the RBs differentiate into the EBs prior to exiting the host cell by lysis or extrusion (Hackstadt et al., 1997; Hybiske and Stephens, 2007). The cysteine protease-mediated lytic pathway involves the rapid sequential permeabilization of inclusion, nuclear and plasma membranes, which ultimately kills the host cell (Hybiske and Stephens, 2007). Unlike lysis, the chlamydial inclusion can also extrude leaving behind a viable host cell in a process termed extrusion (Beatty, 2007; Hybiske and Stephens, 2007). Actin and myosin have been shown to play essential roles in the extrusion pathway and a recent study has shown that the *C. trachomatis* inclusion can recruit an actin-coat around itself (Chin et al., 2012; Hybiske and Stephens, 2007).

The *C. trachomatis* inclusion is known to recruit the microtubule (MT)-dependent motor, dynein, for its trafficking to the host microtubule organizing centre (MTOC) during early stages of the infection in interphase cells (Grieshaber et al., 2003a; Clausen et al., 1997). Recent studies have identified microdomains on the inclusion membrane that are enriched in several inclusion proteins, including Inc101, Inc222, Inc850 and IncB. These microdomains can recruit active Src family kinases, which have been shown to also play important roles in inclusion

localization to the host MTOC during early infection (Mital et al., 2010). Lack of Src family kinase activities is shown to negatively impact *C. trachomatis* replication (Mital and Hackstadt, 2011a). In addition, microdomains have been observed in close proximity to the host MTOCs in both interphase and mitotic cells during later stages of infection (Mital et al., 2010).

Chlamydiae are known to exploit host amino acids, lipids and nucleotides to ensure its replication (Hackstadt et al., 1995b, 1996; Kumar et al., 2006; Braun et al., 2008; Hatch, 1975a). *C. trachomatis* disrupts the normal Golgi structure and recruits the fragmented Golgi stacks around the inclusion to gain increased access to host Golgi-derived lipids, which can significantly improve *C. trachomatis* replication rate in interphase cells (Heuer et al., 2009). During mitosis, the Golgi undergoes a fragmentation process and becomes thousands of sub-micron vesicles that form the Golgi haze during mitosis (Shima et al., 1998; Gaietta et al., 2006). These Golgi vesicles are then partitioned into two daughter cells with guidance from the mitotic spindle (Shima et al., 1998; Wei and Seemann, 2009). After the completion of cell division, two distinct Golgi stacks that are formed during cytokinesis fuse together to reform an intact Golgi in each daughter cell (Gaietta et al., 2006). However, the fate and Golgi content within multinucleated cells has not been examined to date. This is particularly germane with respect to chlamydial infection, which can induce significant host cell multinucleation by blocking cleavage furrow ingression or abscission (Greene and Zhong, 2003; Brown et al., 2012; Sun et al., 2011). Our work described in Chapter 3 has shown that *C. trachomatis* inclusions can localize to the cell equator, where cleavage furrows usually form and ingress, at a much higher frequency than similarly sized vacuole generated by internalized latex beads (Sun et al., 2011). Moreover, chlamydial protein synthesis contributes to the equatorial positioning of the inclusion during furrow ingression (Sun et al., 2011).

Here we examine the role of the host cell cytoskeleton and interphase inclusion-positioning elements on inclusion positioning during mitosis. We also assessed whether centralized inclusions in mitosis confers a benefit to this bacterium. Using IF and live cell imaging, we show that multinuclear cells that fail to divide contain higher Golgi content than mononuclear cells. Moreover, *C. trachomatis* can intercept Golgi-derived lipids more rapidly in multinuclear cells than in single nuclear cells. Our work strongly suggests that *C. trachomatis* actively seeks to block host cell division to gain additional growth advantage in multinucleated cells.

4.2 Results

4.2.1 Effects of inhibiting host proteins and bacterial protein synthesis on *C. trachomatis* inclusion positioning

We have previously demonstrated in synchronized HeLa cells that *C. trachomatis* inclusions localize to the cell equator and block furrow ingression during telophase using fluorescent live cell imaging (Sun et al., 2011). Synchronized cells had to be used for fluorescent live cell imaging due to significant phototoxicity and cell death associated with long-term imaging of asynchronous cultures. To confirm that central localization of inclusions during mitosis also occurred in asynchronous cells, we conducted long-term live DIC imaging experiments on *C. trachomatis*-infected HeLa cells. Multi-day DIC imaging of HeLa cells had no detectable adverse effect on cell viability or division (data not shown). In asynchronous, naturally dividing cells, *C. trachomatis* inclusions still very frequently localized to the cell equator and disrupted the normal cleavage furrow formation (Figure 4.1A, arrows).

In an attempt to identify the mechanism by which *C. trachomatis* inclusions localized to the cell centre during telophase, we tested the effects of various inhibitors against key cytoskeletal components and signaling molecules on inclusion positioning during telophase. The positioning of *C. trachomatis* inclusion was revealed using IF. Since F-actin and myosin accumulate at the cell equator during telophase (Glotzer, 2004), we inhibited F-actin polymerization and myosin activity with cytochalasin D and blebbistatin, respectively, and examined the effect on inclusion localization. *C. trachomatis*-infected HeLa cells were synchronized with low dose nocodazole (40 ng/ml) for 8 hours before they were released from mitotic block and treated with cytochalasin D (2 μM) or blebbistatin (100 μM) for 55 minutes until fixation. The number of cells with polar inclusions did not change significantly after these treatments (Figure 4.1B and C). We also used nocodazole to disrupt MTs as *C. trachomatis* inclusions use MTs to travel to the host MTOC (Grieshaber et al., 2003a); and we were interested whether this would cause the inclusions to move away from the cell equator. Since nocodazole induces mitotic checkpoint in cells at metaphase (Lanni and Jacks, 1998), we could only add it once the cells have progressed past metaphase. As a result, *C. trachomatis*-infected cells were synchronized for 8 hours and released for 30 minutes to allow cells progress past metaphase before they were treated with 1 μM nocodazole for 25 minutes until fixation. Nocodazole treatment for 25 minutes did not cause significant changes in inclusion localization (Figure 4.1B and C). It has been reported recently

that Src-family kinases play important roles in the trafficking of *C. trachomatis* (Mital et al., 2010; Mital and Hackstadt, 2011a); so we inhibited Src kinase activity with a Src family kinase inhibitor, PP2 (25 μM), for 8 hours. Src kinase inhibition did not significantly impact *C. trachomatis* inclusion positioning during telophase after controlling for inclusion size (Figure 4.1B and C). Interestingly, azithromycin still had a profound impact on inclusion positioning as previously reported (Sun et al., 2011). In the current study, *C. trachomatis*-infected HeLa cells were synchronized with low dose nocodazole and treated with azithromycin for 8 hours and azithromycin treatment increased the number of cells with polar inclusions to more than 30%, while approximately 5% of untreated cells had polar inclusions (Figure 4.1D).

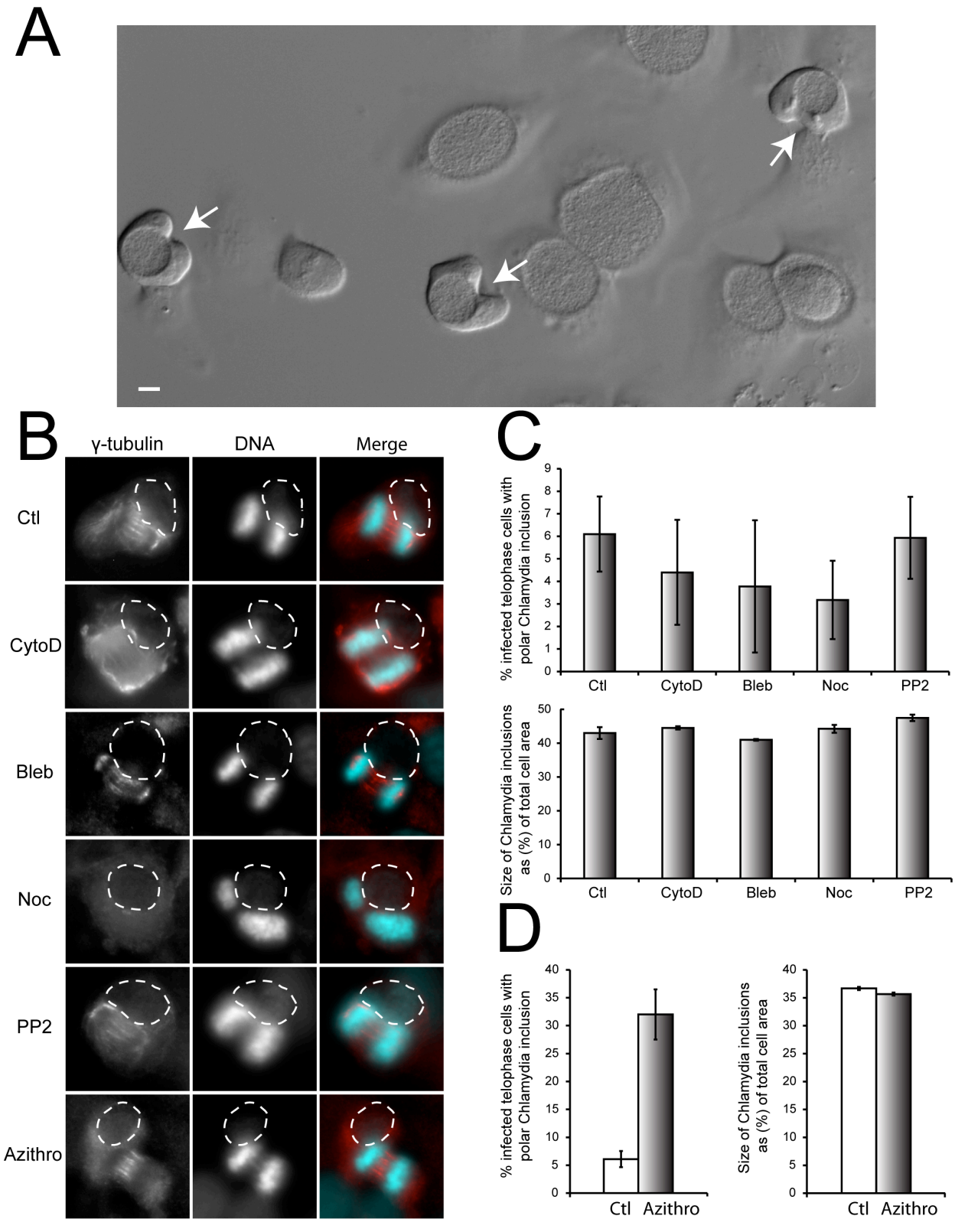
A
B
γ-tubulin
DNA
Merge
Ctl
CytoD
Bleb
Noc
PP2
Azithro
C
% infected telophase cells with polar Chlamydia inclusion
Ctl
CytoD
Bleb
Noc
PP2
Size of Chlamydia inclusions as (%) of total cell area
D
% infected telophase cells with polar Chlamydia inclusion
Ctl
Azithro
Size of Chlamydia inclusions as (%) of total cell area
Ctl
Azithro

Figure 4.1 *C. trachomatis* inclusions localize to the cell centre very efficiently and this process is resistant to disruption of F-actin, myosin and Src family kinase activities. (A) Naturally dividing HeLa cells infected by *C. trachomatis* were imaged using long-term live DIC imaging. Arrows indicate cells containing centrally located inclusions during telophase. (B) *C. trachomatis*-infected cells were synchronized with low dose nocodazole and treated with various inhibitors. Inclusion positioning was determined using γ-tubulin (red) and DAPI staining (cyan). Inclusions were outlined by dotted lines. (C) Inclusion localization in cells with identical inclusion sizes was quantified in at least 50 cells per experiment. (D) Inclusion localization in cells with identical inclusion sizes treated with azithromycin. At least 30 cells per experiment were quantified. Error bars represent SEM from three independent experiments.

4.2.2 *C. trachomatis* inclusions localize to the cell centre as early as metaphase during cell division

Since inhibition of various host proteins involved in telophase progression did not impact *C. trachomatis* positioning, we examined whether the inclusions localized to the cell equator at earlier stages of cell division, which would make the inclusions less susceptible to these drugs. Based on our live DIC imaging of naturally dividing infected cells, *C. trachomatis* inclusions appeared to localize to the cell equator, marked by the condensed chromosome band (Figure 4.2A, arrows), as early as metaphase. Since DIC imaging does not provide conclusive evidence of the relative positioning of the chromosome band and inclusion, we confirmed this observation with IF of synchronized cells in metaphase and telophase (Figure 4.2B). Quantification of inclusion positioning in the two mitotic phases revealed that *C. trachomatis* inclusions localized to the cell equator in over 90% of the cells during both phases, suggesting that the inclusions already localized to the host cell equator as early as metaphase (Figure 4.2C). Together, these results indicate that *C. trachomatis* inclusion central positioning in mitosis is achieved before telophase.

A

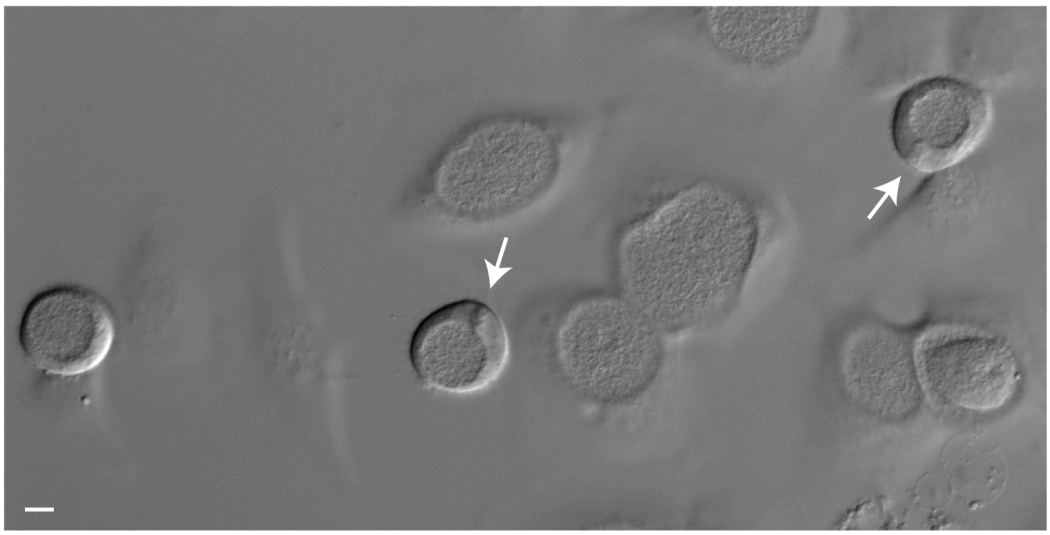

B

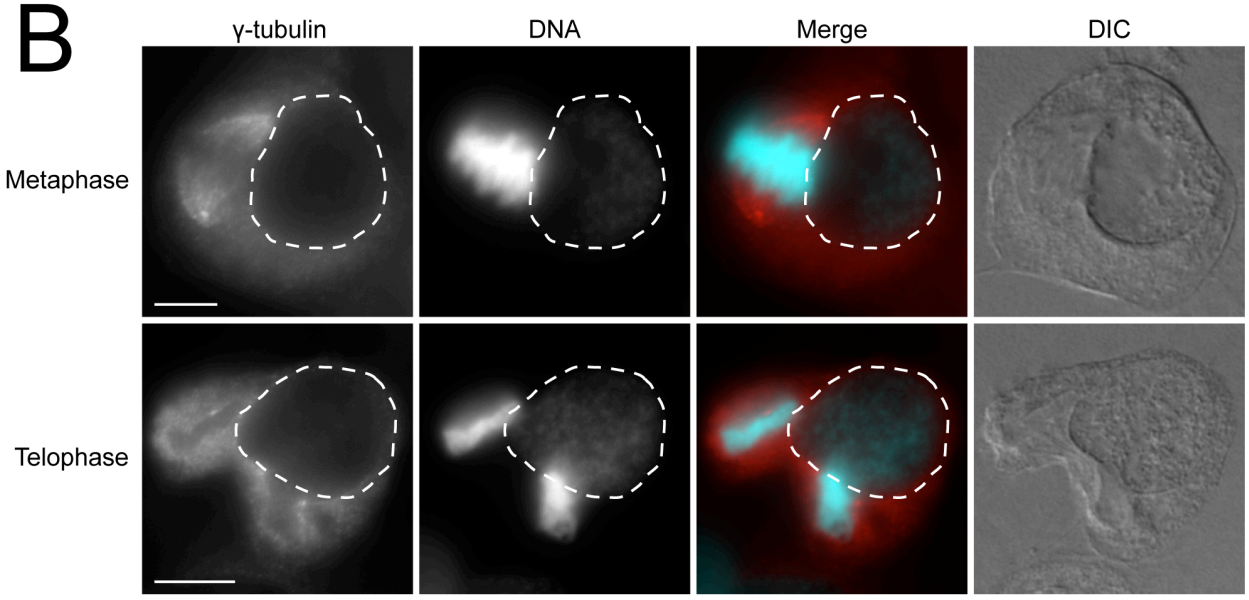
γ-tubulin
DNA
Merge
DIC
Metaphase
Telophase

C

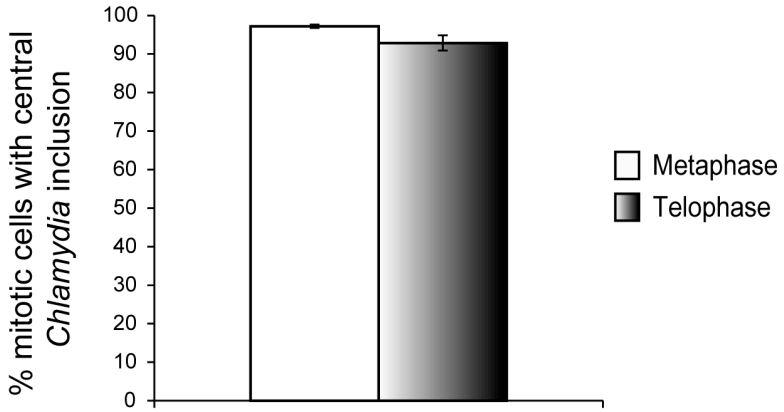
% mitotic cells with central Chlamydia inclusion
100
90
80
70
60
50
40
30
20
10
0
Metaphase
Telophase

Figure 4.2 *C. trachomatis* inclusions are at the cell centre by metaphase. (A) *C. trachomatis* inclusions in asynchronous cells localized to the cell centre during metaphase as marked by the equatorial chromosome band (arrows). (B) *C. trachomatis*-infected HeLa cells were synchronized with low dose nocodazole for 8 hours at 28 hpi and released for either 30 (metaphase) or 55 minutes (telophase) before fixation. Inclusion positioning was visualized with γ-tubulin (red) and DAPI (cyan) staining. Inclusions were outlined by dotted lines. (C) *C. trachomatis* inclusion positioning was quantified in both metaphase and telophase cells. Approximately 97% of metaphase and 93% of telophase cells contained centrally located inclusions at 36 hpi ($p > 0.2$). At least 50 cells were quantified for each mitotic phase per experiment. Error bars represent SEM from three independent experiments.

4.2.3 *C. trachomatis* inclusion microdomains are in close proximity to host MTOCs in mitosis

Several *C. trachomatis* inclusion proteins cluster on the inclusion membrane and form microdomains, which play important roles in early inclusion trafficking to the MTOC during interphase (Mital et al., 2010; Mital and Hackstadt, 2011a). We speculated that inclusion microdomains would persist through cell division and contribute to the central localization. We first examined the localization of these microdomains and host MTOCs during metaphase and telophase in cells infected with *C. trachomatis* for 36 hours. Microdomains and host MTOCs were labeled using Inc101 and γ-tubulin antibodies as previously described (Mital et al., 2010; Mital and Hackstadt, 2011a). We examined inclusion microdomain integrity and positioning relative to the host MTOCs in the presence of various inhibitors to candidate cytoskeletal and signaling proteins to determine whether these inhibitors had any effect. In untreated and cells treated with cytochalasin D or blebbistatin, microdomains on inclusions were still intact and in close proximity to the host MTOC during metaphase (Figure 4.3). Since nocodazole caused mitotic arrest, we only added it to cells once they progressed past metaphase. In cells treated with nocodazole for 25 minutes, microdomains were still present but they appeared to be further away from the host MTOCs during telophase (Figure 4.3). Microdomains are known to interact with host Src family kinases, which play an essential role in early inclusion positioning (Mital and Hackstadt, 2011a). Surprisingly, treatment with PP2, a Src family kinase inhibitor, for 8 hours did not disrupt the integrity or the positioning of microdomains relative to host MTOCs during metaphase (Figure 4.3). This suggests that Src kinase function is not essential for maintaining inclusion positioning during later stages of infection. Interestingly, even treatment with azithromycin for 8 hours also did not affect the integrity or positioning of the microdomains, indicating that these microdomains were likely very stable once they were formed (Figure 4.3). We also examined the relative positioning of microdomains and host MTOC in telophase cells, with and without inhibitors. Similar to metaphase, microdomains in telophase did not become significantly disrupted by any of the inhibitors tested (Figure 4.4). Together, these findings suggest that microdomains are highly stable once they are formed and are resistant to various cytoskeletal and signaling protein inhibitions.

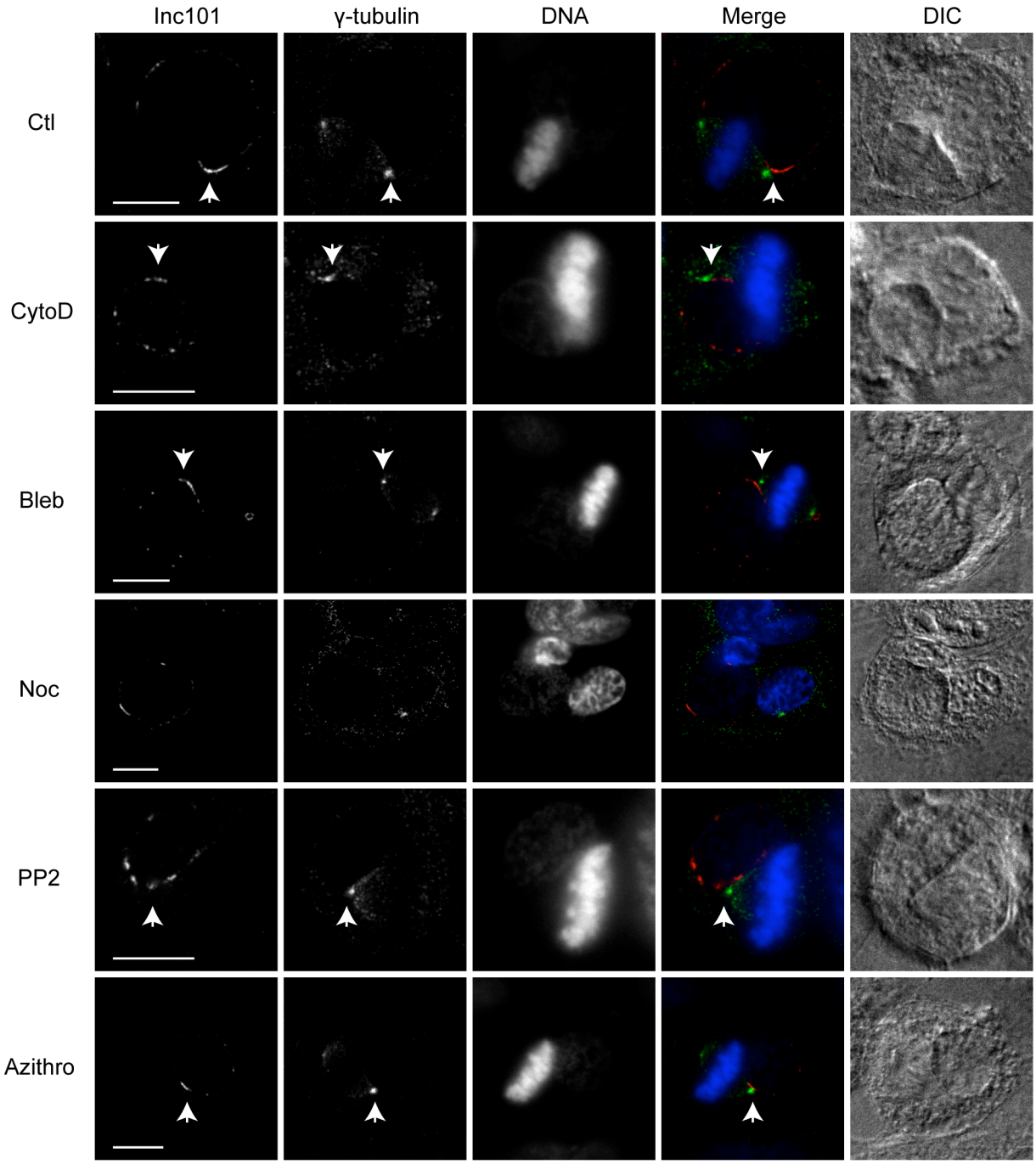
Inc101
γ-tubulin
DNA
Merge
DIC
Ctl
CytoD
Bleb
Noc
PP2
Azithro

Figure 4.3. *C. trachomatis* inclusion microdomains are in close proximity to host MTOCs during metaphase. *C. trachomatis*-infected HeLa cells were synchronized with low dose nocodazole for 8 hours at 28 hpi and released from mitotic block before being treated with various inhibitors. Microdomain and host MTOC were visualized using Inc101 (red) and γ-tubulin (green) antibodies respectively. Arrows indicate close proximity of the microdomains to host MTOC, even after treatment with various inhibitors. Images were taken using spinning disk confocal microscope and a single optical slice is shown. Scale bars = 10 μm.

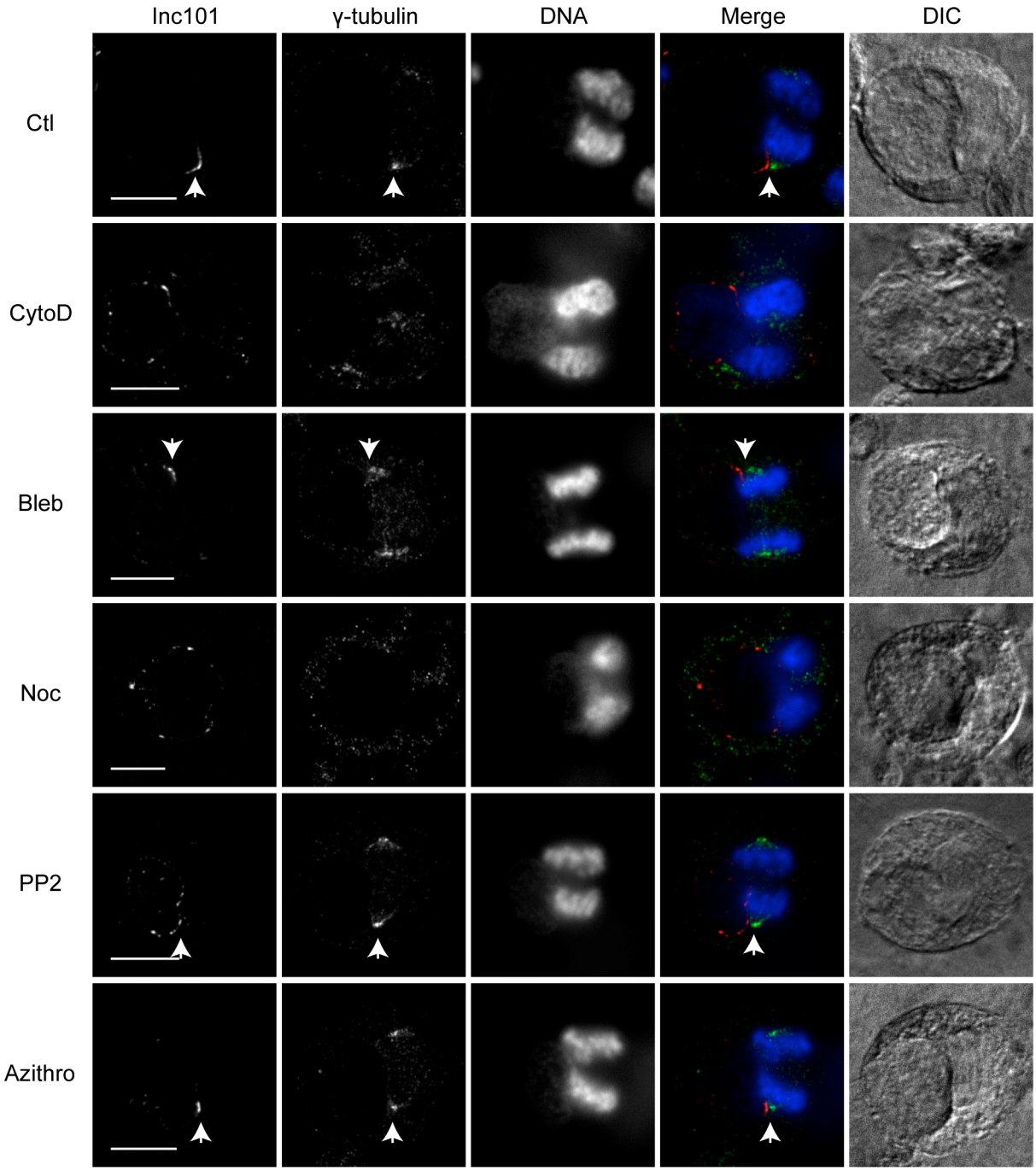
Inc101
γ-tubulin
DNA
Merge
DIC
Ctl
CytoD
Bleb
Noc
PP2
Azithro

Figure 4.4. *C. trachomatis* microdomains are in close proximity to host MTOCs during telophase. *C. trachomatis*-infected HeLa cells were synchronized with low dose nocodazole for 8 hours at 28 hpi and released from mitotic block before being treated with various inhibitors. Microdomain and host MTOC were visualized using Inc101 (red) and γ-tubulin (green) antibodies respectively. Arrows indicate close proximity of the microdomains to host MTOCs, even after treatment with various inhibitors. Images were taken using spinning disk confocal microscope and a single optical slice is shown. Scale bars = 10 μm.

4.2.4 *C. trachomatis* inclusion microdomains associate with mitotic spindle MTs

Since spindle MT strands emanate from the host MTOC during mitosis, we next examined the mitotic spindle to determine whether the inclusion microdomains interacted with the spindle MTs. In metaphase cells, inclusion microdomains associated with spindle MTs and none of the inhibitors tested affected this association except nocodazole, which caused a complete depolymerization and disappearance of MT strands (Figure 4.5). These results suggest that microdomains may contribute to the inclusion positioning through interacting with spindle MTs. Interestingly, even though azithromycin increased the number of cells with polar inclusions, it did not disrupt the association between microdomains and host mitotic spindle MTs (Figure 4.5). In addition, we also examined the relative positioning of microdomain and spindle MTs during telophase. In telophase cells, microdomains were observed to associate with both astral and midzone MTs, suggesting that once host cells entered telophase, *C. trachomatis* inclusions could exploit both MT populations to maintain their equatorial localization (Figure 4.6). Interestingly, in azithromycin-treated cells that had polar inclusions, the inclusions still contained prominent microdomains; however, they did not appear to associate with the central spindle MTs. Together, these results suggest that the increase in the number of cells with polar inclusions after azithromycin treatment is not caused by disintegration of the microdomains, which persisted after the 8 hour antibiotic treatment.

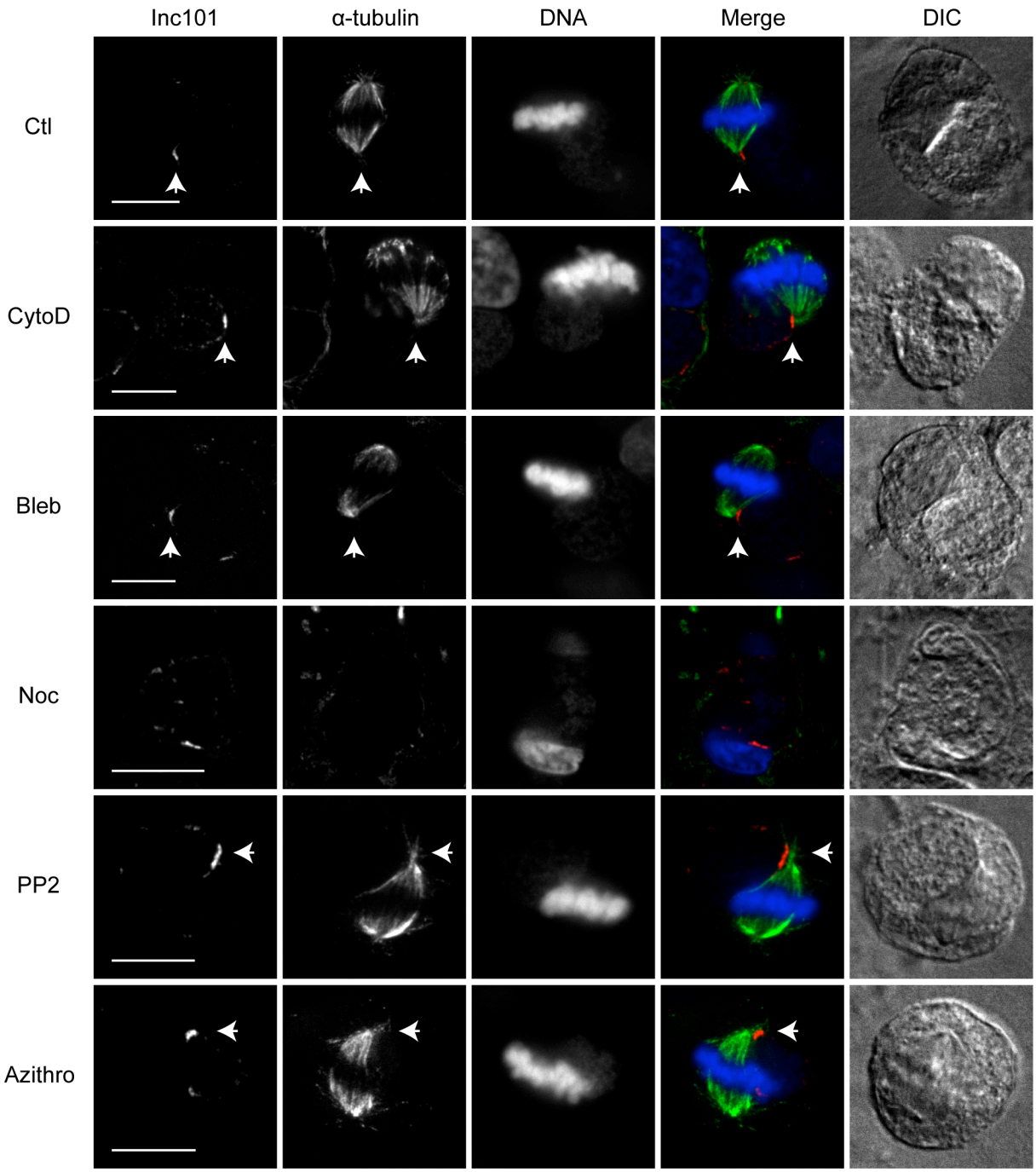
Inc101
α-tubulin
DNA
Merge
DIC
Ctl
CytoD
Bleb
Noc
PP2
Azithro

Figure 4.5 *C. trachomatis* microdomains directly overlap with host mitotic spindle MTs in metaphase. *C. trachomatis*-infected HeLa cells were synchronized with low dose nocodazole for 8 hours at 28 hpi and released from mitotic block before being treated with various inhibitors. Microdomain and spindle MTs were visualized using Inc101 (red) and α-tubulin (green) antibodies respectively. Images were taken using spinning disk confocal microscope and a single optical slice is shown. Arrows indicate overlap between microdomains and spindle MTs. Scale bars = 10 μm.

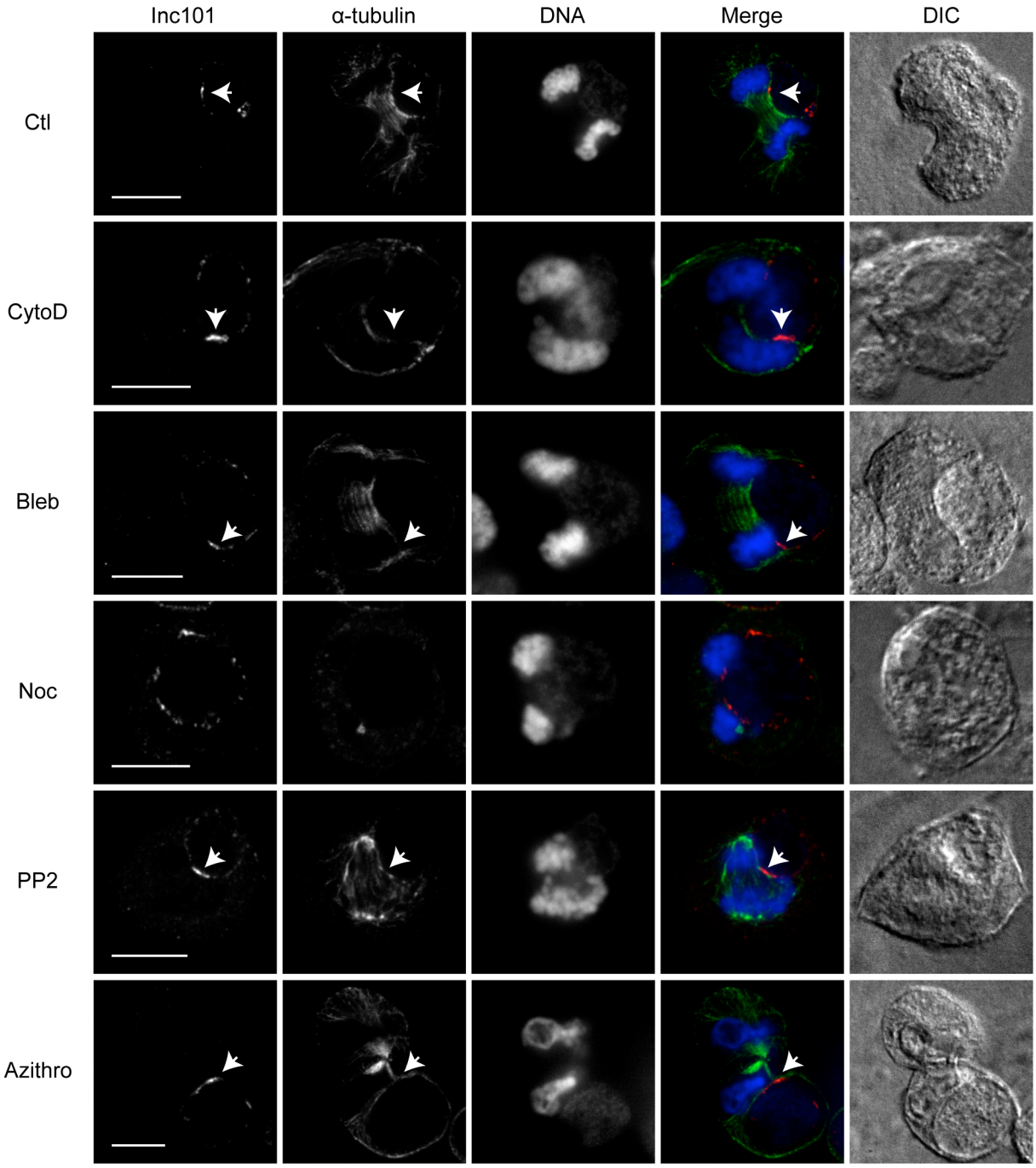

Figure 4.6. *C. trachomatis* microdomains overlap with mitotic spindle MTs during telophase. *C. trachomatis*-infected HeLa cells were synchronized with low dose nocodazole for 8 hours and released from mitotic block before being treated with various inhibitors. Microdomain and spindle MTs were visualized using Inc101 (red) and α-tubulin (green) antibodies respectively. Images were taken using spinning disk confocal microscope and a single optical slice is shown. Arrows indicate overlap between microdomains and spindle MTs. Scale bars = 10 μm.

4.2.5 Golgi content increases in cells that fail to divide

Based on our observation that chlamydial protein synthesis played an important role in localizing the inclusion to the cell centre to block host cell division (Figure 4.1D), we next explored whether blocking host cell division conferred any physiological benefits to *C. trachomatis*. It has been well documented that the replicative success of *C. trachomatis* is highly dependent on access to host Golgi lipids (Heuer et al., 2009). We first examined Golgi distribution in infected cells after successful or blocked mitosis using IF. As previously reported, under normal conditions each daughter cell would inherit approximately half of the Golgi content from the mother cell after cell division (Figure 4.7A) (Shima et al., 1998; Gaietta et al., 2006). In the rare instances when host cell mitosis was not blocked by the inclusion, approximately half of the total Golgi content was inherited by each daughter cell similar to un-infected cells (Figure 4.7A). Consequently, the *C. trachomatis* inclusion would no longer have access to Golgi lipids in the other daughter cell upon successful completion of host cell division, unless the *C. trachomatis* inclusion also separates into two daughter cells. Based on our live cell imaging experiments, *C. trachomatis* inclusions rarely divided into two daughter cells, suggesting *C. trachomatis* would indeed very often lose Golgi content to the uninfected daughter cell. In cells where *C. trachomatis* inclusions blocked the separation of the two daughter cells, the Golgi began to reform regardless of whether cleavage furrow ingression was completed (Figure 4.7B). In addition, the blocked furrow eventually regressed and the Golgi content that was meant for two daughter cells was retained in a single infected multinucleated cell. The presence of an internal midbody indicated that the cell recently failed to divide into two daughter cells. Golgi in cells that failed to divide surrounded the *C. trachomatis* inclusion similar to Golgi in mononuclear cells, suggesting the entire reformed Golgi apparatus in multinuclear cells was exploited (Figure 4.7B). To ensure this was not a cell line-specific phenomenon, we confirmed this observation in several human (MCF10A and HEK293) and mouse (NIH3T3) cell lines (Figure 4.8). In all the cell lines examined, the Golgi apparatus in infected multinuclear cells always surrounded the inclusion as observed in mononuclear cells, indicating *C. trachomatis* could exploit the additional Golgi content in multinuclear cells (Figure 4.8).

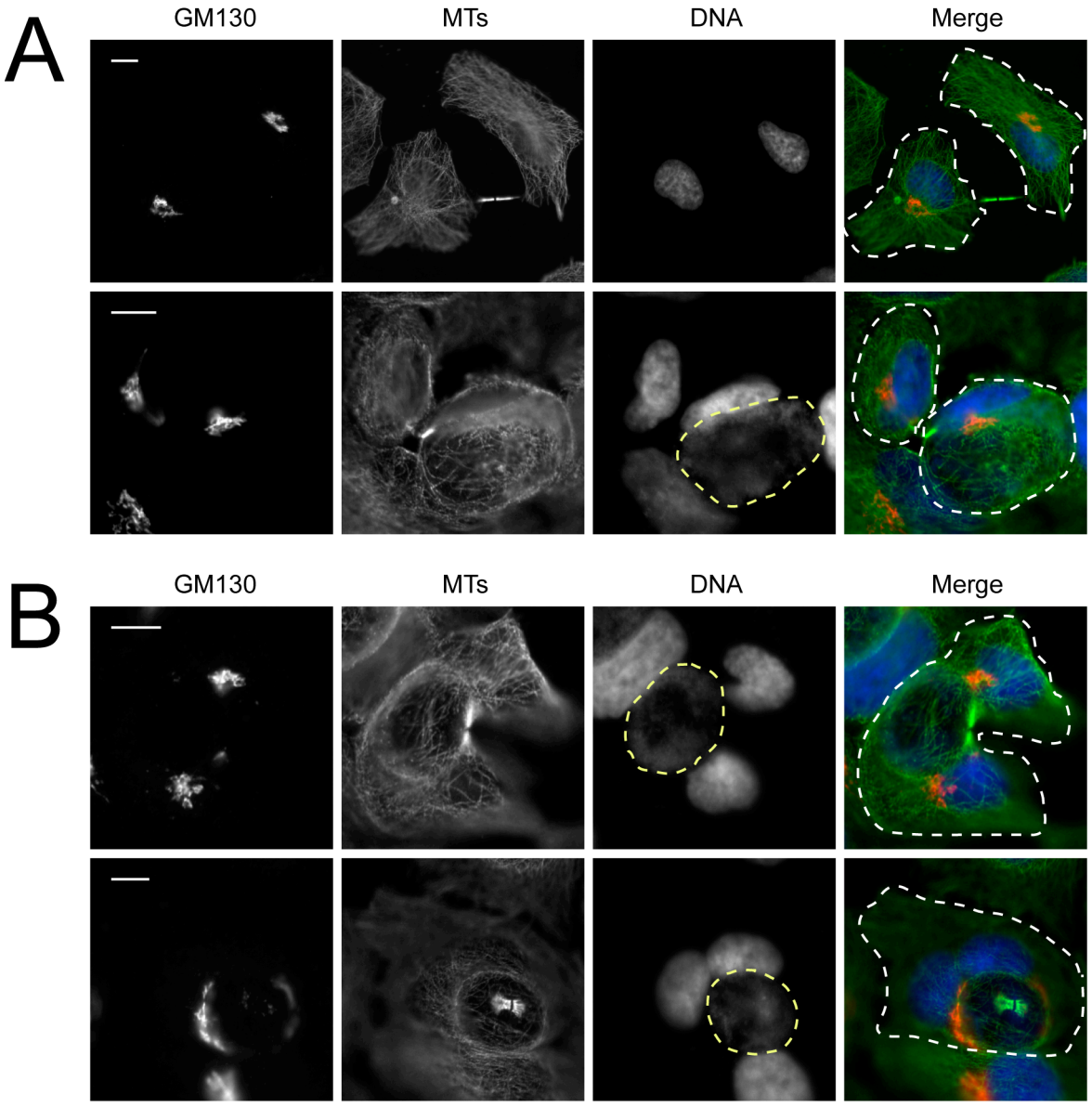
A
GM130
MTs
DNA
Merge
B
GM130
MTs
DNA
Merge

Figure 4.7. *C. trachomatis* inclusions co-opt the entire Golgi apparatus when host mitosis is blocked. (A) After a recent division event, marked by intense midbody α-tubulin (green) staining, each daughter cell inherited part of the Golgi indicated by GM130 staining (red). In the rare instances where *C. trachomatis* inclusion did not block furrow ingression, the uninfected daughter cell inherited part of the Golgi apparatus. *C. trachomatis* inclusion is marked by the dotted line as revealed by DAPI staining (blue). (B) In most *C. trachomatis*-infected telophase cells, the Golgi stacks began to reform even though furrow ingression was blocked by the inclusion. The prominent internal midbody indicated a multinuclear cell that recently failed to divide into two daughter cells. This multinuclear cell also contained fragmented Golgi stacks that surrounded the *C. trachomatis* inclusion. Scale bars = 10 μm.

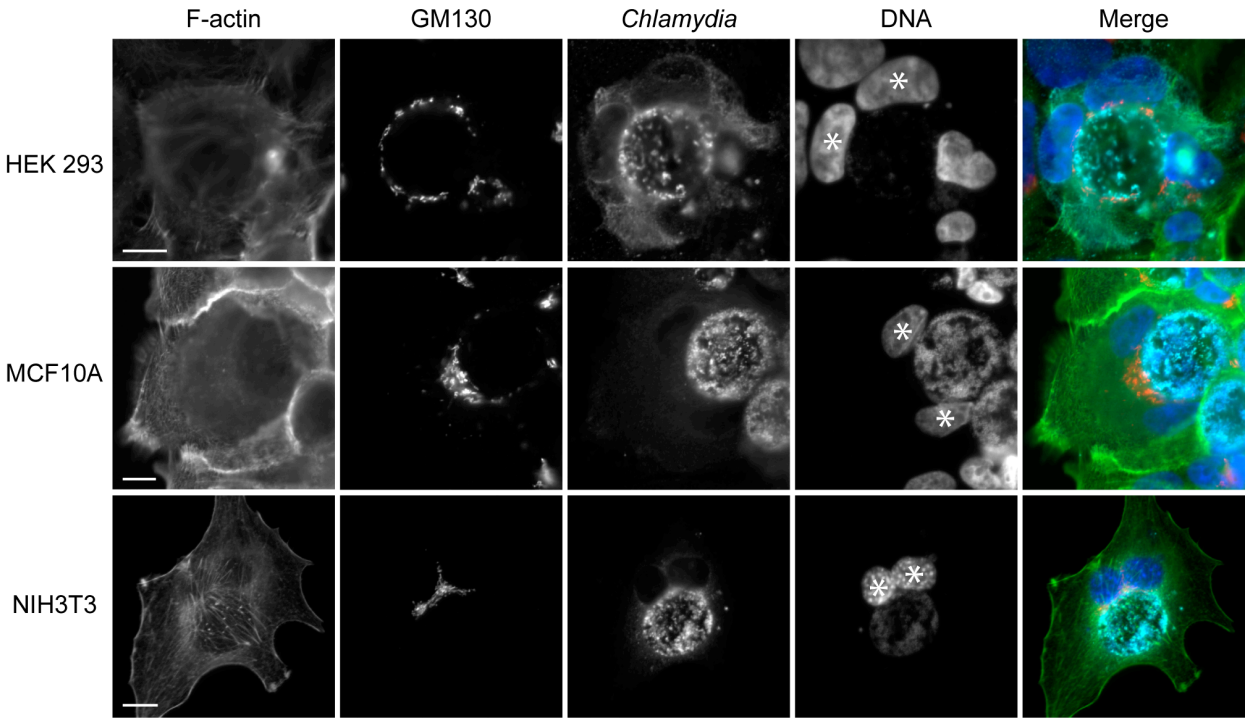

Figure 4.8 Golgi in multinuclear cells surrounds *C. trachomatis* inclusions in several cell lines. The Golgi apparatus (red) in multinuclear HEK293 (human fibroblast), MCF10A (human epithelial) and NIH3T3 (mouse fibroblast) cells (green, F-actin) was observed to surround the *C. trachomatis* inclusions (cyan). Scale bars = 10 µm.

In order to quantitatively measure the degree to which Golgi content was increased in cells that failed to divide, we artificially created cells that failed to divide. In this analysis, we did not use *C. trachomatis* to generate multinuclear cells, because *C. trachomatis* is known to modify Golgi structure and intercept Golgi content, which could interfere with our total Golgi content measurements. Instead, we used a previously described synchronization procedure (Whitfield et al., 2002) and the resulting mitotic cells were either untreated or treated with blebbistatin to block furrow ingression. After a recovery period of 5 hours from blebbistatin treatment, cells were fixed and stained for GM130 to label the Golgi. Both mononuclear and multinuclear cells were generated under both untreated and blebbistatin-treated conditions (Figure 4.9A). In order to ensure that what we observed was not a blebbistatin-specific phenotype, we also used cytochalasin D or wiscostatin in place of blebbistatin to induce multinucleation (Figure 4.9A). Epifluorescent images revealed that the multinuclear cells had physically larger Golgi apparatus than mononuclear cells regardless of how they were generated (Figure 4.9A). Quantification of GM130 signal intensity using IF images revealed that multinuclear cells contained approximately twice the amount of Golgi compared to mononuclear cells (Figure 4.9B). In addition, we also repeated the Golgi protein intensity measurement with flow cytometry, which measures the total protein intensity in the entire cell. The 4N population under control conditions mostly consisted of mononuclear cells that had progressed past S phase. Based on our IF analysis, approximately 96% of the cells were multinuclear after blebbistatin treatment; therefore, the 4N population in the treatment group were mostly multinuclear cells. Our flow cytometry data showed that multinuclear cells contained approximately 70% more Golgi content than mononuclear cells. Together, these results suggest that on average, cells that fail to divide into two daughter cells indeed contain significantly higher Golgi content than mononuclear cells.

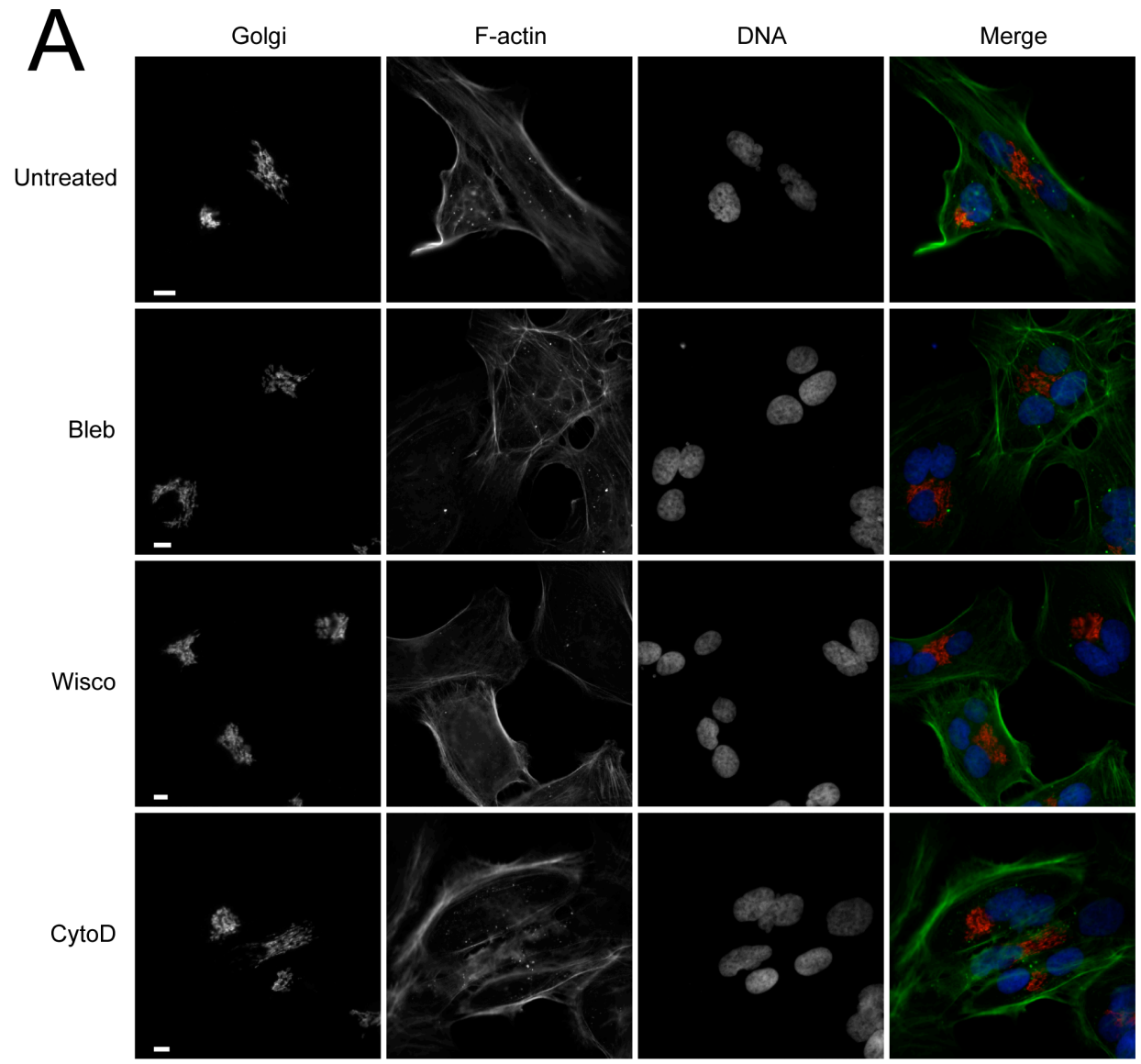
A
Golgi
F-actin
DNA
Merge
Untreated
Bleb
Wisco
CytoD

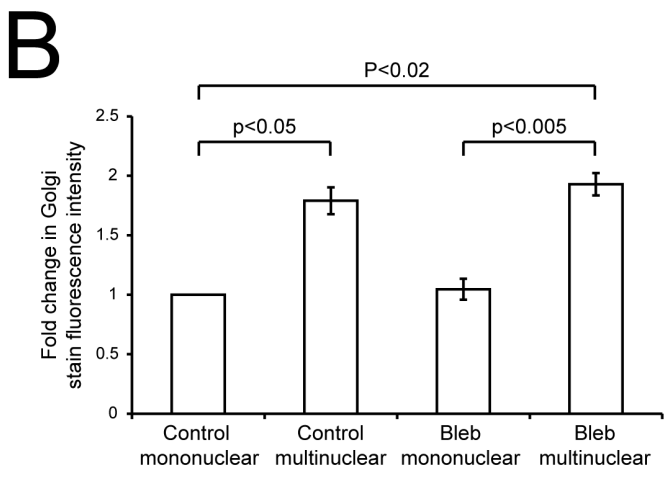
B
P<0.02
p<0.05
p<0.005
Fold change in Golgi stain fluorescence intensity
2.5
2
1.5
1
0.5
0
Control mononuclear
Control multinuclear
Bleb mononuclear
Bleb multinuclear

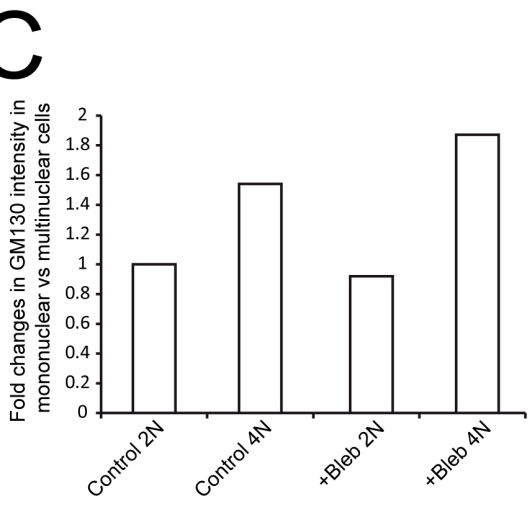
C
Fold changes in GM130 intensity in mononuclear vs multinuclear cells
2
1.8
1.6
1.4
1.2
1
0.8
0.6
0.4
0.2
0
Control 2N
Control 4N
+Bleb 2N
+Bleb 4N

Figure 4.9 The Golgi content increases in multinuclear cells that fail to divide. (A) Cells were synchronized into mitosis and then treated with blebbistatin (Bleb), wiscostatin (Wisco) or cytochalasin D (CytoD) to inhibit furrow ingression to generate large numbers of multinuclear cells. The resulting cells were fixed and stained for F-actin (green), Golgi (GM130, red) and DNA (blue). Scale bars = 10 μm. (B) Quantification of GM130 signal intensity in IF images of mononuclear and multinuclear cells revealed that multinuclear cells contained significantly more Golgi protein than mononuclear cells. (C) Flow cytometry analysis of cells stained with GM130 revealed that multinuclear cells contained significantly higher Golgi content than mononuclear cells.

4.2.6 *C. trachomatis* intercepts Golgi-derived lipids more rapidly in multinuclear cells compared to mononuclear

Since our results suggested that multinuclear cells that failed to divide contained higher Golgi content, we next examined whether *C. trachomatis* can acquire Golgi-derived nutrients more rapidly in these multinuclear cells. To answer this question, we conducted spinning disk confocal live cell imaging to monitor fluorescent BODIPY-ceramide trafficking to the inclusion (Heuer et al., 2009). HeLa cells seeded on glass-bottom dishes were infected with *C. trachomatis* for 36 hours and fields containing both multinuclear and mononuclear cells were chosen. Imaging was started as soon as the fluorescent ceramide was added to the cells and the trafficking to *C. trachomatis* particles inside the inclusions were monitored in mononuclear and multinuclear cells. In order to label individual *C. trachomatis* particles, we pre-incubated infected cells with DRAQ5 for 10 minutes (Sun et al., 2012). Through these live imaging experiments, we consistently observed that individual bacterial particles in multinuclear cells (Figure 4.10A, arrow) obtained fluorescent ceramide signals more rapidly than those in mononuclear cells (Figure 4.10A, arrowheads) within the same imaging field. The number of brightly-labeled *C. trachomatis* particles appeared to be much higher in multinuclear cells compared to mononuclear cells, even though the inclusion sizes were comparable. Quantification of the total ceramide fluorescence intensity in *C. trachomatis* inclusions revealed that inclusions acquired ceramide much more rapidly in multinuclear cells than in mononuclear cells (Figure 4.10B). This again suggests that generation of multinuclear cells through blocking host cell division could indeed enhance nutrient acquisition by *C. trachomatis*, which could in turn confer growth advantage to the bacteria.

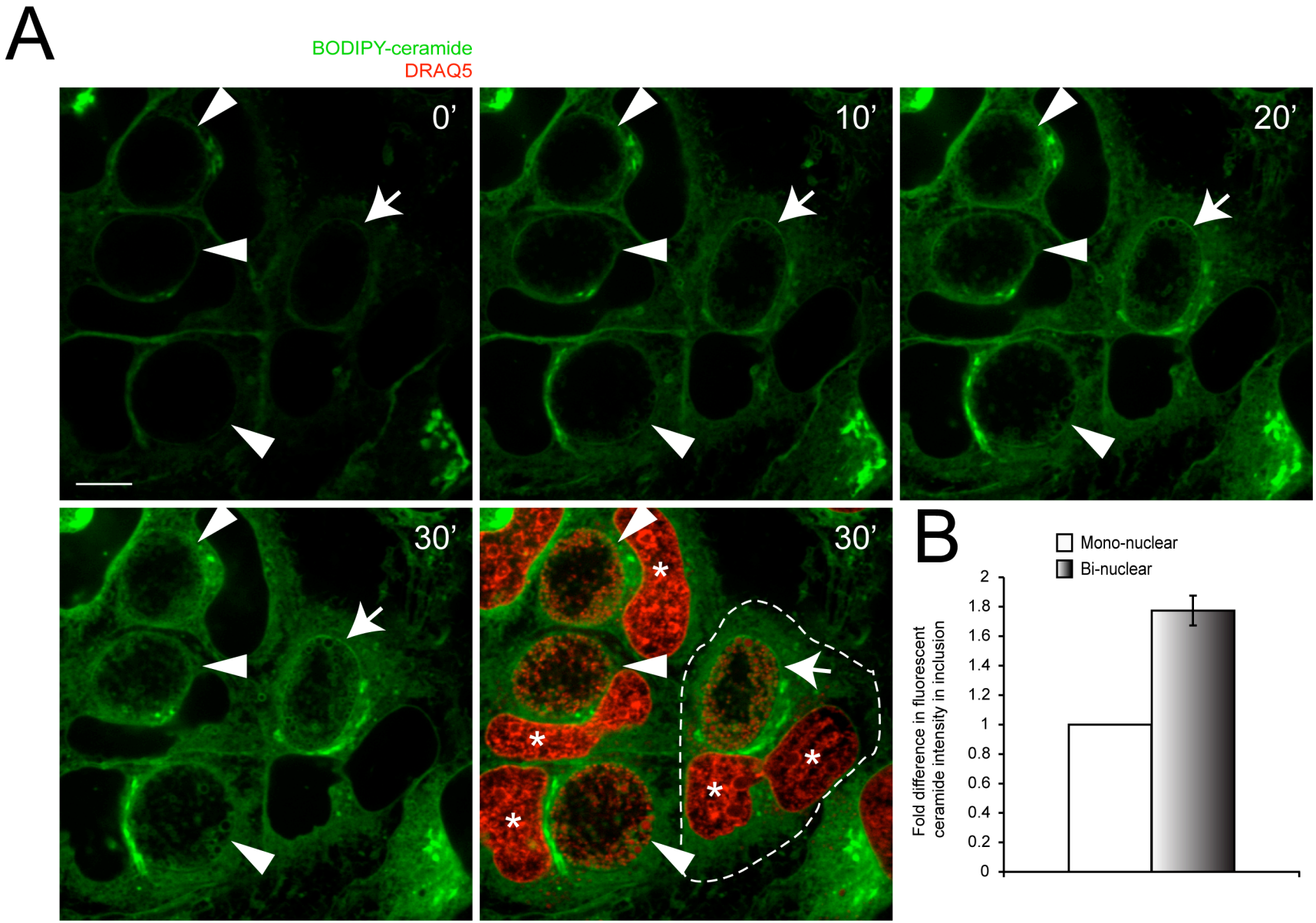
A
BODIPY-ceramide
DRAQ5
0’
10’
20’
30’
30’
B
Mono-nuclear
Bi-nuclear
Fold difference in fluorescent ceramide intensity in inclusion
2
1.8
1.6
1.4
1.2
1
0.8
0.6
0.4
0.2
0

Figure 4.10 *C. trachomatis* inclusions can acquire fluorescent Golgi-derived lipid markers more rapidly in multinuclear cells than in mononuclear cells. (A) *C. trachomatis*-infected cells were imaged immediately after the addition of fluorescent ceramide (green) to determine the rate of lipid acquisition by inclusions. *C. trachomatis* inclusions and host nuclei were revealed by DNA stain (DRAQ5, red). Outline of the multinuclear cell is indicated by dotted line. Arrowheads mark the inclusions in single nuclear cells, while arrow indicates inclusion in multinuclear cell. Numbers indicate minutes after addition of ceramide. Scale bars = 10 μm. (B) Quantification of fluorescence intensity inside *C. trachomatis* inclusions showed that *C. trachomatis* particles can intercept Golgi-derived lipids significantly faster in multinuclear cells than in mononuclear cells.

4.3 Discussion

We have previously demonstrated that *C. trachomatis* inclusions localize very efficiently to the host cell centre during telophase using fluorescent live imaging and IF in synchronized cells (Sun et al., 2011). In the current study, we confirmed these observations with long term live cell DIC imaging in asynchronous cells. Consistent with our previous report, *C. trachomatis* inclusions in asynchronous cells also localized to the cell centre very frequently, blocked furrow ingression and induced the formation of multinuclear host cells. The long term DIC imaging did not involve the use of any synchronization agents and it did not cause detectable levels of phototoxicity-associated cell death; therefore, these results are the most accurate description of mitotic defects caused by *C. trachomatis*.

Another microorganism, *Theileria*, can bind to host mitotic signaling protein, Plk1, and localize to the host cell centre (Von Schubert et al., 2010). In the current study, we attempted to identify the mechanism by which *C. trachomatis* localized to the cell centre using various cytoskeletal and signaling protein inhibitors. Quantification of inclusion positioning, after controlling for inclusion size, revealed that cytochalasin D, blebbistatin, nocodazole and PP2 did not cause significant changes in inclusion localization. It has been reported that *C. trachomatis* inclusions can recruit F-actin for the maintenance of their integrity and for extrusion in a myosin II-dependent manner (Chin et al., 2012; Kumar and Valdivia, 2008). In our study, it is not surprising that cytochalasin D and blebbistatin, targeting F-actin and myosin II respectively, did not change the inclusion positioning during mitosis, since neither F-actin nor myosin II were recruited to the inclusion surface during mitosis. However, it is unexpected that nocodazole and PP2, which target MTs and Src family kinases respectively, did not cause significant changes in inclusion positioning. We and others have demonstrated that *C. trachomatis* inclusions appeared to associate with host MTs at microdomains and depend on MTs for their localization especially during early stages of the infection (Grieshaber et al., 2003b; Mital et al., 2010). It has been documented that dynein is in close proximity to inclusion microdomains during mitosis and *C. trachomatis* depends on this MT-based motor for its trafficking during early stages of the infection (Mital et al., 2010; Grieshaber et al., 2003b). Nocodazole did not have a significant impact on inclusion positioning in our experiment likely because of timing of the treatment. Nocodazole induces mitotic arrest in metaphase cells (Lanni and Jacks, 1998); as a result, we could only add it after cells have progressed past metaphase to quantify inclusion positioning

during telophase. Due to the transient nature of anaphase and telophase, nocodazole treatment could only be carried out for 25 minutes. It is interesting to note that 97% of metaphase cells contain centrally located *C. trachomatis* inclusions indicating that the central positioning is likely completed as early as metaphase. This could explain the lack of change in inclusion positioning after nocodazole treatment of anaphase and telophase cells. These results suggested that MTs were dispensable for maintaining central inclusion positioning after metaphase. Src family kinases have been implicated to play essential roles in inclusion trafficking to the host MTOC during early stages of infection (Mital and Hackstadt, 2011a). Unlike nocodazole, infected cells were treated with PP2 for 8 hours to inhibit Src kinase functions and yet this did not significantly alter inclusion positioning during mitosis at 36 hours post infection. This suggests that while Src kinases play important roles in inclusion localization during early stages of infection, they are dispensable for maintaining inclusion positioning during later stages of the infection. This observation should be further confirmed by examining the impact of PP2 treatment on known targets of Src family kinase in order to assess the effectiveness of the inhibitor itself (Kong et al., 2011).

During mitosis, *C. trachomatis* inclusion microdomains were in close proximity to host MTOCs and they likely interacted through spindle MTs, which appeared to associate with microdomains in both metaphase and telophase cells. Interestingly, inclusion microdomains can associate with both astral and midzone MTs in telophase cells, which may serve as the landmark structures that *C. trachomatis* inclusions use to localize to the cell equator. In addition, our study is the first to discover that apparent integrity of the inclusion microdomains, based on Inc101 staining, is resistant to azithromycin or PP2 treatment for 8 hours. We have previously demonstrated that azithromycin can reduce *C. trachomatis* protein synthesis to an undetectable level within 1 hour (Sun et al., 2011). This suggests that the microdomains are very stable once formed and Inc101 does not have a high protein turnover rate, as bacterial protein synthesis is blocked for at least 7 hours. Chloramphenicol, an antibiotic that inhibits bacterial protein synthesis, has been demonstrated to be highly effective in disrupting inclusion localization to the host MTOC during early stages of infection (Mital and Hackstadt, 2011a). However, during later stages of infection after the microdomains have formed, inclusion positioning became more resistant to antibiotic treatment targeting bacterial protein synthesis, such as azithromycin. Even though the number of cells with polar inclusions increased to approximately 30% after azithromycin, 70% of infected cells still contained central *C. trachomatis* inclusions in the absence of detectable

levels of bacterial protein synthesis for at least 7 hours. It is interesting to note that polar inclusions in azithromycin-treated cells still contained prominent microdomains revealed by Inc101 staining. The persistence of microdomain structures, which have been implicated in inclusion positioning (Mital and Hackstadt, 2011a), after azithromycin treatment during later stages of infection could explain why this drug was unable to rescue the mitotic defect in majority of the infected cells. Similarly, while Src family kinases play important roles in early inclusion trafficking (Mital and Hackstadt, 2011a), they do not appear to affect inclusion microdomain integrity during later stages of the infection, which could explain the lack of changes in inclusion positioning after PP2 treatment.

Our study is the first to demonstrate that there is a physiological benefit for *C. trachomatis* to block host mitosis. Golgi content, measured by GM130 staining, was increased by approximately 70-90% in cells that failed to divide compared to mononuclear cells that went through the same synchronization protocol and successfully divided. To our knowledge, this is the first study comparing Golgi content in multinuclear and mononuclear cells. Previous studies have demonstrated that Golgi is partitioned into two daughter cells during mitosis under normal conditions (Gaietta et al., 2006; Wei and Seemann, 2009; Altan-Bonnet et al., 2006). Following mitosis, Golgi is reformed by the fusion of two distinct Golgi stacks into a common stack in each daughter cell (Gaietta et al., 2006). Similar to uninfected cells, *C. trachomatis*-infected cells that successfully divided into two daughter cells distributed Golgi into each daughter cell. Consequently, *C. trachomatis* lost access to approximately half of the Golgi after completion of cytokinesis. In a cell whose cytokinesis was blocked, Golgi was retained in a single multinuclear cell and the reformed Golgi surrounded the *C. trachomatis* inclusion as it would in a mononuclear cell (Heuer et al., 2009). Since *C. trachomatis* can be spontaneously cleared by the mouse immune system, *C. muridarum* has been used in a recent study to demonstrate that this bacterium can infect mitotically active cells *in vivo* (Knowlton et al., 2013). This suggests that *C. trachomatis* will very likely encounter naturally dividing cells in human patients as well. *C. trachomatis* infection induces the formation of multinuclear host cells and the efficiency by which *C. trachomatis* causes this defect is enhanced by the presence of bacterial protein synthesis (Sun et al., 2011; Greene and Zhong, 2003; Brown et al., 2012). Our current study showed that inclusions in multinuclear cells acquired fluorescent ceramide, a marker for Golgi-derived lipids, much more rapidly than those in mononuclear cells. This indicates that inclusions

can acquire lipids, an essential nutrient that can directly affect *C. trachomatis* replication, faster in multinuclear cells that have failed to divide.

Our results demonstrate that *C. trachomatis* inclusions have a lipid acquisition advantage when they block host cell division. In addition, this blockage, while resistant to cytochalasin D, blebbistatin, nocodazole and PP2 treatment, is affected by bacterial protein synthesis. These findings strongly suggest that *C. trachomatis* is actively seeking the host cell centre during host cell division to gain additional growth advantage. With the exciting emergency of novel genetic manipulation techniques for *C. trachomatis* (Kari et al., 2011; Wang et al., 2011), it will be interesting to systematically assess single-protein knock-out mutants to determine which *C. trachomatis* proteins are important for inclusion positioning and blocking host cell mitosis.

Chapter 5
Summary and Future Directions

Epidemiological studies have established *C. trachomatis* infection as an independent risk factor for increased risks of cervical cancer. The major focus of my work has been to understand the mechanism by which *C. trachomatis* infection leads to host cell multinucleation a well-established cellular defect that can lead to aneuploidy and tumorigenesis. We demonstrated that *C. trachomatis* inclusions actively localized to the host cell centre and disrupted the normal bilateral cleavage furrow formation. The side of the cell proximal to the inclusion typically lacked an ingressing furrow resulting in a unique unilateral cleavage furrow defect, which often ingressed and became blocked by the *C. trachomatis* inclusion. The lack of an ingressing furrow was due to the disruption of signaling protein accumulation on the equatorial cellular cortex proximal to the *C. trachomatis* inclusion, which was caused by the displacement of mitotic spindle MTs from these regions. *C. trachomatis* inclusions localized much more frequently to the host cell equator than inert vacuoles. Inhibition of bacterial protein synthesis resulted in a decrease in the equatorial localization of *C. trachomatis* inclusions. Microdomains on the inclusion surface likely played an important role in inclusion positioning during mitosis and they were resistant not only to treatment with various host cytoskeletal and signaling protein inhibitors but also to bacterial protein synthesis inhibitor. Finally, we confirmed that blocking host cell cytokinesis could indeed confer additional nutrient acquisition advantage to *C. trachomatis*, as inclusions intercepted Golgi-derived lipid markers much faster in multinuclear cells than in mononuclear cells.

C. trachomatis **as a model to study cleavage furrow signaling**

MTs play a critical role in establishing the cleavage furrow, although the precise MT subsets involved in this are still under intense debate. It has been postulated that dynamic astral MTs inhibits global contractility and a cleavage furrow forms at the cell equator due to the lowest density of these MTs (Glotzer, 2004). Moreover, removal of dynamic MTs through pharmacological or genetic means from the polar cell cortex leads to ectopic contractile activities (Canman et al., 2000; Kurz et al., 2002; Fededa and Gerlich, 2012; Foe and von Dassow, 2008; Bement et al., 2005) . In our experiments, we took advantage of the MT-

displacing capability of astral MTs and examined cells with small *C. trachomatis* inclusions where astral MTs were physically prevented from reaching the polar cell cortex (Figure 5.1A). Neither ectopic furrowing nor accumulation of contractile elements was observed at these regions on the plasma membrane, indicating elimination of dynamic astral MTs from the cellular cortex alone is insufficient to induce contractility. Many of the furrow-inducing signaling proteins depend on MTs for their equatorial localization during late mitosis and cytokinesis (Glotzer, 2009). Pharmacological or genetic alteration of MT stability inevitably causes non-specific depolymerization of non-astral MTs, such as MTs in the central spindle. Since central spindle MTs contain high densities of furrow-inducing elements, any disruption of these MTs could result in the release of these complexes into the cytosol and cause ectopic furrowing (D'Avino et al., 2006). In our studies, MT stability was not artificially altered and furrow-inducing proteins were still present and functional, since cells containing polar inclusions could form bilateral cleavage furrows that ingressed normally.

Moreover, astral MTs appeared to promote modest accumulation of furrow-inducing proteins at the cell equator independent of the central spindle (Figure 5.1B). Previous studies examining the roles of different MT populations were unable to physically displace a specific population of MTs and relied on genetic knock down of proteins important for central spindle formation (Glotzer, 2004). However, knock down of proteins important for central spindle formation, such as Prc1or Mklp1, disrupts localization of signaling proteins such as Plk1 and Ect2 to astral MTs as well (Neef et al., 2007; Yuce et al., 2005; Nishimura and Yonemura, 2006). This creates an insurmountable hurdle for examining the exact role of astral and central spindle MTs. In our experiments, since the central spindle MTs are held together, they can be displaced from the equatorial cell cortex as a large bundle by a small centrally located *C. trachomatis* inclusion. The result of this displacement was that only astral MTs were able to reach certain regions of the equatorial cell cortex and this was achieved without artificially knocking down any proteins. In these instances where only astral MTs were able to reach the equatorial cell cortex, modest accumulation of furrow-inducing proteins was observed at the equatorial cortex (Figure 5.1B). This is consistent with the theory that astral MTs deliver positive, furrow-inducing signals to the equatorial plasma membrane (Glotzer, 2009). Future experiments aimed to addressing the controversy regarding the roles of different MT populations should take advantage of this MT-displacing capability of *C. trachomatis* inclusions to rigorously examine the contribution of different MT populations to cleavage furrow formation.

In addition, the induction of unilateral cleavage furrow by *C. trachomatis* inclusion will be confirmed in different cell lines from various species, such as NIH3T3, HEK293 and MCF10A cells, in order to ensure that this defect is not a cell-type specific artifact. Similarly, contribution of astral and midzone MTs to furrow formation should also be confirmed in these established cell lines.

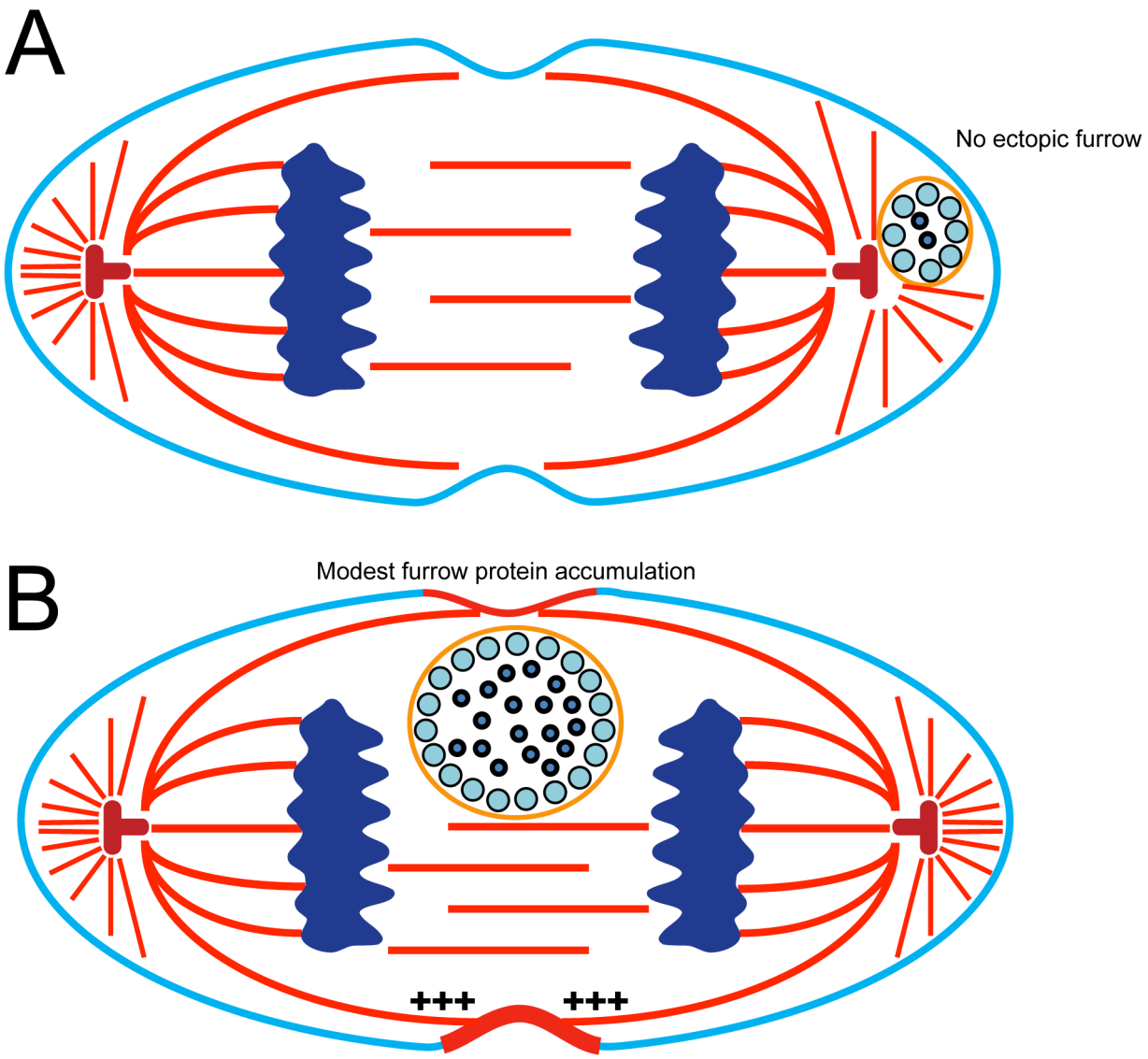

Figure 5.1 Astral MTs deliver positive, stimulatory signals to the equatorial cell cortex. (A) Small polar *C. trachomatis* inclusions can displace astral MTs and create regions on the polar cell cortex that receive no MT targeting. In these regions, neither ectopic furrows nor contractile activities were observed. (B) Small equatorial inclusions can displace the central spindle MTs as a bundle while allow some astral MTs to reach the equatorial cell cortex. Modest accumulation of furrow-inducing proteins at the equatorial cortex can be induced by astral MTs alone.

Growth advantage for microbes that disrupt host cytokinesis

We demonstrated that *C. trachomatis* can intercept Golgi-derived lipid markers much faster in multinuclear cells than in mononuclear cells, indicating blockage of host cell cytokinesis could confer additional growth advantage to *C. trachomatis* (Figure 5.2). In addition to lipids, *C. trachomatis* also import host nucleic acids and amino acids from the host. Polyploid cells, like the multinuclear cells induced by *C. trachomatis* infection do not initiate a second round of DNA synthesis in the presence of functional p53 (Doherty et al., 2003; Andreassen et al., 2001; Kaufmann et al., 1997, 2001). As a result, it is reasonable to speculate that the level of free nucleic acids in host cells that are meant for host DNA synthesis will rise, which can allow faster *C. trachomatis* acquisition of these important DNA precursors for bacterial growth. It will be interesting to compare the rate of *C. trachomatis* DNA synthesis in mononuclear and multinuclear cells. Naturally occurring polyploid cells, such as hepatocytes, are hypothesized to have elevated protein synthesis by diverting energy from cell division and membrane synthesis (Davoli and De Lange, 2011). However, it is unclear whether a similar host protein synthesis enhancement, which will very likely reduce the levels of free amino acids for *C. trachomatis* to import, is observed in multinuclear cells induced by *C. trachomatis*. It will be interesting to compare the rates of *C. trachomatis* protein synthesis in mononuclear and multinuclear host cells using AHA. In addition to *C. trachomatis*, *Clostridium difficile*, *Clostridium limosum* and *Pseudomonas aeruginosa* can also disrupt host cytokinesis by inactivating RhoA through toxin secretions into host cells (Huelsenbeck et al., 2009; Shafikhani and Engel, 2006). However, unlike *C. trachomatis*, these bacteria are not intracellular and it is unlikely that they can gain direct growth advantage from inducing host multinucleation (Madan and Jr, 2012). Host cytokinesis disruption by *C. difficile*, *C. limosum* and *P. aeruginosa* may slow down the epithelial wound repair process to allow additional spreading of the infection (Madan and Jr, 2012), which may also occur during *C. trachomatis* infection.

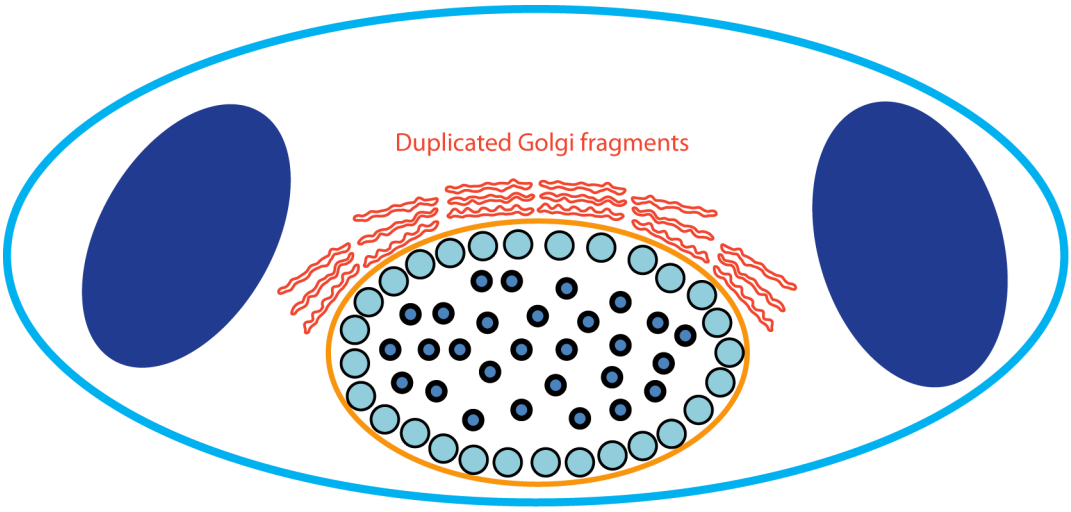

Figure 5.2 Increased Golgi content in multinuclear cells allows faster lipid acquisition by *C. trachomatis*. Golgi content is increased in multinuclear cells and this allows faster lipid acquisition by *C. trachomatis*.

Tumorigenic potential of *C. trachomatis*-infected cells

Our studies have demonstrated that *C. trachomatis* induces significant host cell multinucleation by disrupting host cell furrow ingression (Figure 5.3). A similar unilateral cleavage furrow defect can be induced by entosis, a process where one cell engulfs another living cell in high-grade tumors (Krajcovic et al., 2011). The host cell can still undergo mitosis after engulfing another living cell, which resides in a vacuole within the host cell (Krajcovic et al., 2011; Overholtzer et al., 2007). However, when the vacuole happens to be at the cell equator, a unilateral cleavage furrow similar to the ones induced by *C. trachomatis* inclusion is frequently observed (Krajcovic et al., 2011). Very similar to the *C. trachomatis* inclusion, the cell-in-cell vacuole often prevents the accumulation of actomyosin filament and MT targeting to the equatorial cortex nearby (Figure 5.3) (Krajcovic et al., 2011). In addition, when the cell-in-cell vacuole is in the polar region of the cell, a bilateral furrow forms normally and cell division successfully completes, while unilateral furrow ingression is often prevented from completing in the presence of an equatorial vacuole very similar to what we see in *C. trachomatis*-infected cells (Krajcovic et al., 2011). The frequency of the cell-in-cell vacuole has also been correlated with tumor grades, with higher tumor grades (the more aggressive tumors) containing more cell-in-cell vacuoles. Within the highest tumor grade (grade 3) included in the study, there are on average approximately 5 cell-in-cell structures per 10 fields of view under 20x objective (Krajcovic et al., 2011), which translates to a frequency of less than 2.5%. However, in the case of *C. trachomatis*-infected cells, the frequency of equatorial inclusion that can cause the unilateral cleavage furrow defect is approximately 95%. This suggests that *C. trachomatis* inclusions have much higher potential to cause cytokinesis defects and subsequent aneuploidy than entosis. Cells cured of *C. trachomatis* infection by antibiotics have been recently shown to develop anchorage independent growth on soft agar, suggesting *in vitro* tumorigenic potential of these cells (Knowlton et al., 2013).

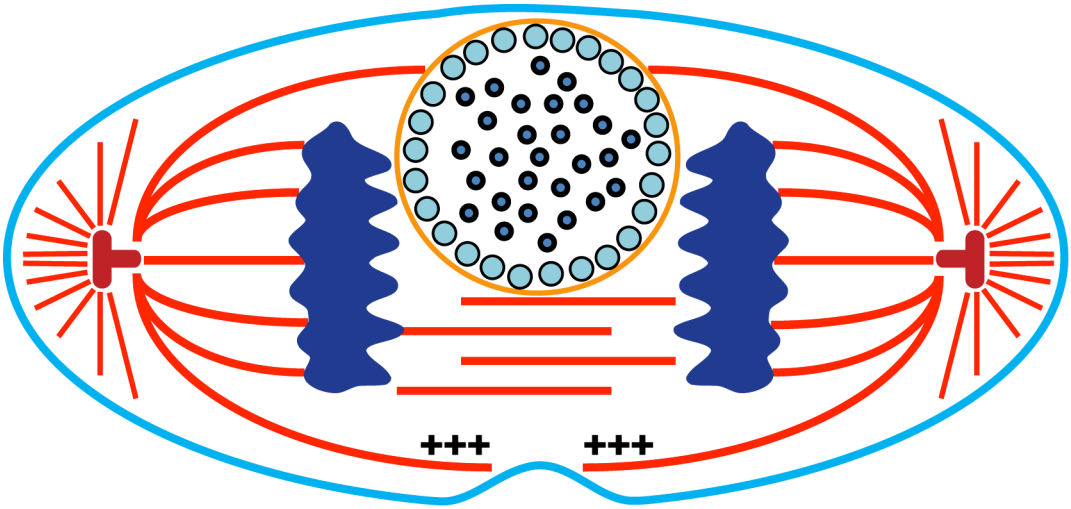

Figure 5.3 *C. trachomatis* inclusions disrupt bilateral furrow formation by preventing MT targeting to the cell cortex. Both astral and central spindle MTs are prevented from reaching equatorial cell cortex resulting in the lack of accumulation of furrow-inducing proteins on one side of the cell.

To confirm the tumorigenic effects due to cytokinesis failure, future studies should first confirm that the infected multinuclear cells can survive *C. trachomatis* infection either through extrusion of the inclusion or through antibiotic clearance, as many chlamydia patients are eventually treated for their infection. Cells cured of *C. trachomatis* infection can be subjected to growth rate and colony formation assays to confirm their *in vitro* tumorigenic potential. If cells cleared of *C. trachomatis* infection show faster growth rate and form colonies *in vitro*, *in vivo* tumorigenicity of these cells should be tested by xenografting them into nude mice and monitoring tumor formation.

Our work has demonstrated that the obligate intracellular bacterium *C. trachomatis* actively disrupts host cell cytokinesis to gain additional nutrient acquisition advantage. It will be important to assess whether other intracellular bacteria have evolved parallel mechanisms to disrupt host cell division in order to gain additional growth advantage. Moreover, it is crucial to confirm the *in vivo* oncogenic effects of *C. trachomatis* infection to assist the medical community make informed policy decisions on additional screening for re-malignant lesions in chlamydia patients.

References

Abdelrahman, Y.M., and R.J. Belland. 2005. The chlamydial developmental cycle. *FEMS microbiology reviews*. 29:949–59. doi:10.1016/j.femsre.2005.03.002.

Abe, S., K. Nagasaka, Y. Hirayama, H. Kozuka-Hata, M. Oyama, Y. Aoyagi, C. Obuse, and T. Hirota. 2011. The initial phase of chromosome condensation requires Cdk1-mediated phosphorylation of the CAP-D3 subunit of condensin II. *Genes & development*. 25:863–74. doi:10.1101/gad.2016411.

Abromaitis, S., and R.S. Stephens. 2009. Attachment and entry of Chlamydia have distinct requirements for host protein disulfide isomerase. *PLoS pathogens*. 5:e1000357. doi:10.1371/journal.ppat.1000357.

Abu el-Asrar, A.M., K. Geboes, K.F. Tabbara, S.A. al-Kharashi, L. Missotten, and V. Desmet. 1998. Immunopathogenesis of conjunctival scarring in trachoma. *Eye (London, England)*. 12 (Pt 3a:453–60. doi:10.1038/eye.1998.104.

Al-Daraji, W.I., and J.H. Smith. 2009. Infection and cervical neoplasia: facts and fiction. *International journal of clinical and experimental pathology*. 2:48–64.

Allan, I., T.P. Hatch, and J.H. Pearce. 1985. Influence of cysteine deprivation on chlamydial differentiation from reproductive to infective life-cycle forms. *Journal of general microbiology*. 131:3171–7.

Altan-Bonnet, N., R. Sougrat, W. Liu, E.L. Snapp, T. Ward, and J. Lippincott-Schwartz. 2006. Golgi inheritance in mammalian cells is mediated through endoplasmic reticulum export activities. *Molecular biology of the cell*. 17:990–1005. doi:10.1091/mbc.E05-02-0155.

Al-Younes, H.M., J. Gussmann, P.R. Braun, V. Brinkmann, and T.F. Meyer. 2006. Naturally occurring amino acids differentially influence the development of Chlamydia trachomatis and Chlamydia (Chlamydophila) pneumoniae. *Journal of medical microbiology*. 55:879–86. doi:10.1099/jmm.0.46445-0.

Al-Younes, H.M., T. Rudel, V. Brinkmann, A.J. Szczepek, and T.F. Meyer. 2001. Low iron availability modulates the course of Chlamydia pneumoniae infection. *Cellular microbiology*. 3:427–37.

Andersen, J.S., C.J. Wilkinson, T. Mayor, P. Mortensen, E.A. Nigg, and M. Mann. 2003. Proteomic characterization of the human centrosome by protein correlation profiling. *Nature*. 426:570–4. doi:10.1038/nature02166.

Andreassen, P.R., O.D. Lohez, F.B. Lacroix, and R.L. Margolis. 2001. Tetraploid state induces p53-dependent arrest of nontransformed mammalian cells in G1. *Molecular biology of the cell*. 12:1315–28.

Bahe, S., Y.-D. Stierhof, C.J. Wilkinson, F. Leiss, and E.A. Nigg. 2005. Rootletin forms centriole-associated filaments and functions in centrosome cohesion. *The Journal of cell biology*. 171:27–33. doi:10.1083/jcb.200504107.

Balsara, Z.R., S. Misaghi, J.N. Lafave, and M.N. Starnbach. 2006. Chlamydia trachomatis infection induces cleavage of the mitotic cyclin B1. *Infection and immunity*. 74:5602–8. doi:10.1128/IAI.00266-06.

Barr, F.A., and U. Gruneberg. 2007. Cytokinesis: placing and making the final cut. *Cell*. 131:847–60. doi:10.1016/j.cell.2007.11.011.

Barr, F.A., N. Nakamura, and G. Warren. 1998. Mapping the interaction between GRASP65 and GM130, components of a protein complex involved in the stacking of Golgi cisternae. *The EMBO journal*. 17:3258–68. doi:10.1093/emboj/17.12.3258.

Barry, C.E., S.F. Hayes, and T. Hackstadt. 1992. Nucleoid condensation in Escherichia coli that express a chlamydial histone homolog. *Science (New York, N.Y.)*. 256:377–9.

Beatty, W.L. 2007. Lysosome repair enables host cell survival and bacterial persistence following Chlamydia trachomatis infection. *Cell Microbiol*. 9:2141–2152. doi:CMI945 [pii] 10.1111/j.1462-5822.2007.00945.x.

Beatty, W.L., R.P. Morrison, and G.I. Byrne. 1994. Persistent chlamydiae: from cell culture to a paradigm for chlamydial pathogenesis. *Microbiol Rev*. 58:686–699.

Belland, R.J., S.P. Ouellette, J. Gieffers, and G.I. Byrne. 2004. Chlamydia pneumoniae and atherosclerosis. *Cellular microbiology*. 6:117–27.

Bement, W.M., H.A. Benink, and G. von Dassow. 2005. A microtubule-dependent zone of active RhoA during cleavage plane specification. *The Journal of cell biology*. 170:91–101. doi:10.1083/jcb.200501131.

Bettencourt-Dias, M., and D.M. Glover. 2007. Centrosome biogenesis and function: centrosomics brings new understanding. *Nature reviews. Molecular cell biology*. 8:451–63. doi:10.1038/nrm2180.

Bieling, P., I.A. Telley, and T. Surrey. 2010. A minimal midzone protein module controls formation and length of antiparallel microtubule overlaps. *Cell*. 142:420–32. doi:10.1016/j.cell.2010.06.033.

Birkenfeld, J., P. Nalbant, B.P. Bohl, O. Pertz, K.M. Hahn, and G.M. Bokoch. 2007. GEF-H1 modulates localized RhoA activation during cytokinesis under the control of mitotic kinases. *Dev Cell*. 12:699–712. doi:S1534-5807(07)00114-1 [pii] 10.1016/j.devcel.2007.03.014.

Blangy, A., H.A. Lane, P. d'Hérin, M. Harper, M. Kress, and E.A. Nigg. 1995. Phosphorylation by p34cdc2 regulates spindle association of human Eg5, a kinesin-related motor essential for bipolar spindle formation in vivo. *Cell*. 83:1159–69.

Blasi, F., S. Damato, R. Cosentini, P. Tarsia, R. Raccanelli, S. Centanni, and L. Allegra. 2002. Chlamydia pneumoniae and chronic bronchitis: association with severity and bacterial clearance following treatment. *Thorax*. 57:672–6.

Boleti, H., A. Benmerah, D.M. Ojcius, N. Cerf-Bensussan, and A. Dautry-Varsat. 1999. Chlamydia infection of epithelial cells expressing dynamin and Eps15 mutants: clathrin-independent entry into cells and dynamin-dependent productive growth. *Journal of cell science*. 112 (Pt 1:1487–96.

Brandeis, M., I. Rosewell, M. Carrington, T. Crompton, M.A. Jacobs, J. Kirk, J. Gannon, and T. Hunt. 1998. Cyclin B2-null mice develop normally and are fertile whereas cyclin B1-null mice die in utero. *Proceedings of the National Academy of Sciences of the United States of America*. 95:4344–9.

Braun, P.R., H. Al-Younes, J. Gussmann, J. Klein, E. Schneider, and T.F. Meyer. 2008. Competitive inhibition of amino acid uptake suppresses chlamydial growth: involvement of the chlamydial amino acid transporter BrnQ. *Journal of bacteriology*. 190:1822–30. doi:10.1128/JB.01240-07.

Brickman, T.J., C.E. Barry, and T. Hackstadt. 1993. Molecular cloning and expression of hctB encoding a strain-variant chlamydial histone-like protein with DNA-binding activity. *Journal of bacteriology*. 175:4274–81.

Brill, J.A., R. Wong, and A. Wilde. 2011. Phosphoinositide function in cytokinesis. *Current biology : CB*. 21:R930–4. doi:10.1016/j.cub.2011.10.001.

Brown, H.M., A.E. Knowlton, and S.S. Grieshaber. 2012. Chlamydial infection induces host cytokinesis failure at abscission. *Cell Microbiol*. 14:1554–1567. doi:10.1111/j.1462-5822.2012.01820.x.

Budai, I. 2007. Chlamydia trachomatis: milestones in clinical and microbiological diagnostics in the last hundred years: a review. *Acta microbiologica et immunologica Hungarica*. 54:5–22. doi:10.1556/AMicr.54.2007.1.2.

Burkard, M.E., J. Maciejowski, V. Rodriguez-Bravo, M. Repka, D.M. Lowery, K.R. Clauser, C. Zhang, K.M. Shokat, S.A. Carr, M.B. Yaffe, and P. V Jallepalli. 2009. Plk1 self-organization and priming phosphorylation of HsCYK-4 at the spindle midzone regulate the onset of division in human cells. *PLoS Biol*. 7:e1000111.

Burke, D.J. 2000. Complexity in the spindle checkpoint. *Current Opinion in Genetics & Development*. 10:26–31. doi:10.1016/S0959-437X(99)00040-4.

Bush, R.M., and K.D. Everett. 2001. Molecular evolution of the Chlamydiaceae. *International journal of systematic and evolutionary microbiology*. 51:203–20.

Byrne, G.I. 2003. Chlamydia uncloaked. *Proceedings of the National Academy of Sciences of the United States of America*. 100:8040–2. doi:10.1073/pnas.1533181100.

Caldwell, H.D., J. Kromhout, and J. Schachter. 1981. Purification and partial characterization of the major outer membrane protein of Chlamydia trachomatis. *Infection and immunity*. 31:1161–76.

Campbell, L.A., C.C. Kuo, and J.T. Grayston. Chlamydia pneumoniae and cardiovascular disease. *Emerging infectious diseases*. 4:571–9. doi:10.3201/eid0404.980407.

Campbell, S., S.J. Richmond, and P. Yates. 1989. The development of Chlamydia trachomatis inclusions within the host eukaryotic cell during interphase and mitosis. *Journal of general microbiology*. 135:1153–65.

Canman, J.C., L.A. Cameron, P.S. Maddox, A. Straight, J.S. Tirnauer, T.J. Mitchison, G. Fang, T.M. Kapoor, and E.D. Salmon. 2003. Determining the position of the cell division plane. *Nature*. 424:1074–8. doi:10.1038/nature01860.

Canman, J.C., D.B. Hoffman, and E.D. Salmon. 2000. The role of pre- and post-anaphase microtubules in the cytokinesis phase of the cell cycle. *Curr Biol*. 10:611–614. doi:S0960-9822(00)00490-5 [pii].

Capmany, A., and M.T. Damiani. 2010. Chlamydia trachomatis intercepts Golgi-derived sphingolipids through a Rab14-mediated transport required for bacterial development and replication. *PloS one*. 5:e14084. doi:10.1371/journal.pone.0014084.

Capmany, A., N. Leiva, and M.T. Damiani. 2011. Golgi-associated Rab14, a new regulator for Chlamydia trachomatis infection outcome. *Communicative & integrative biology*. 4:590–3. doi:10.4161/cib.4.5.16594.

Carabeo, R.A., S.S. Grieshaber, E. Fischer, and T. Hackstadt. 2002. Chlamydia trachomatis induces remodeling of the actin cytoskeleton during attachment and entry into HeLa cells. *Infection and immunity*. 70:3793–803.

Carabeo, R.A., S.S. Grieshaber, A. Hasenkrug, C. Dooley, and T. Hackstadt. 2004. Requirement for the Rac GTPase in Chlamydia trachomatis invasion of non-phagocytic cells. *Traffic (Copenhagen, Denmark)*. 5:418–25. doi:10.1111/j.1398-9219.2004.00184.x.

Carabeo, R.A., and T. Hackstadt. 2001. Isolation and characterization of a mutant Chinese hamster ovary cell line that is resistant to Chlamydia trachomatis infection at a novel step in the attachment process. *Infection and immunity*. 69:5899–904.

Carabeo, R.A., D.J. Mead, and T. Hackstadt. 2003. Golgi-dependent transport of cholesterol to the Chlamydia trachomatis inclusion. *Proceedings of the National Academy of Sciences of the United States of America*. 100:6771–6. doi:10.1073/pnas.1131289100.

Carlton, J.G., M. Agromayor, and J. Martin-Serrano. 2008. Differential requirements for Alix and ESCRT-III in cytokinesis and HIV-1 release. *Proceedings of the National Academy of Sciences of the United States of America*. 105:10541–6. doi:10.1073/pnas.0802008105.

Chalamalasetty, R.B., S. Hümmer, E.A. Nigg, and H.H.W. Silljé. 2006. Influence of human Ect2 depletion and overexpression on cleavage furrow formation and abscission. *Journal of cell science*. 119:3008–19. doi:10.1242/jcs.03032.

Chaturvedi, A.K., C.A. Gaydos, P. Agreda, J.P. Holden, N. Chatterjee, J.J. Goedert, N.E. Caporaso, and E.A. Engels. 2010. Chlamydia pneumoniae infection and risk for lung cancer. *Cancer Epidemiol Biomarkers Prev*. 19:1498–1505. doi:1055-9965.EPI-09-1261 [pii] 10.1158/1055-9965.EPI-09-1261.

Chen, A.L., K.A. Johnson, J.K. Lee, C. Sütterlin, and M. Tan. 2012. CPAF: a Chlamydial protease in search of an authentic substrate. *PLoS pathogens*. 8:e1002842. doi:10.1371/journal.ppat.1002842.

Chin, E., K. Kirker, M. Zuck, G. James, and K. Hybiske. 2012. Actin recruitment to the Chlamydia inclusion is spatiotemporally regulated by a mechanism that requires host and bacterial factors. *PloS one*. 7:e46949. doi:10.1371/journal.pone.0046949.

Christian, J.G., J. Heymann, S.A. Paschen, J. Vier, L. Schauenburg, J. Rupp, T.F. Meyer, G. Häcker, and D. Heuer. 2011. Targeting of a chlamydial protease impedes intracellular bacterial growth. *PLoS pathogens*. 7:e1002283. doi:10.1371/journal.ppat.1002283.

Clarke, I.N., M.E. Ward, and P.R. Lambden. 1988. Molecular cloning and sequence analysis of a developmentally regulated cysteine-rich outer membrane protein from Chlamydia trachomatis. *Gene*. 71:307–14.

Clausen, J.D., G. Christiansen, H.U. Holst, and S. Birkelund. 1997. Chlamydia trachomatis utilizes the host cell microtubule network during early events of infection. *Molecular microbiology*. 25:441–9.

Clifton, D.R., K.A. Fields, S.S. Grieshaber, C.A. Dooley, E.R. Fischer, D.J. Mead, R.A. Carabeo, and T. Hackstadt. 2004. A chlamydial type III translocated protein is tyrosine-phosphorylated at the site of entry and associated with recruitment of actin. *Proceedings of the National Academy of Sciences of the United States of America*. 101:10166–71. doi:10.1073/pnas.0402829101.

Cocchiaro, J.L., Y. Kumar, E.R. Fischer, T. Hackstadt, and R.H. Valdivia. 2008. Cytoplasmic lipid droplets are translocated into the lumen of the Chlamydia trachomatis parasitophorous vacuole. *Proceedings of the National Academy of Sciences of the United States of America*. 105:9379–84. doi:10.1073/pnas.0712241105.

Cocchiaro, J.L., and R.H. Valdivia. 2009. New insights into Chlamydia intracellular survival mechanisms. *Cellular microbiology*. 11:1571–8. doi:10.1111/j.1462-5822.2009.01364.x.

Colanzi, A., C. Suetterlin, and V. Malhotra. 2003. Cell-cycle-specific Golgi fragmentation: how and why? *Current opinion in cell biology*. 15:462–7.

Corda, D., M.L. Barretta, R.I. Cervigni, and A. Colanzi. 2012. Golgi complex fragmentation in G2/M transition: An organelle-based cell-cycle checkpoint. *IUBMB life*. 64:661–70. doi:10.1002/iub.1054.

D'Avino, P.P. 2009. How to scaffold the contractile ring for a safe cytokinesis - lessons from Anillin-related proteins. *J Cell Sci*. 122:1071–1079.

D'Avino, P.P., V. Archambault, M.R. Przewloka, W. Zhang, K.S. Lilley, E. Laue, and D.M. Glover. 2007. Recruitment of Polo kinase to the spindle midzone during cytokinesis requires the Feo/Klp3A complex. *PLoS One*. 2:e572. doi:10.1371/journal.pone.0000572.

D'Avino, P.P., M.S. Savoian, L. Capalbo, and D.M. Glover. 2006. RacGAP50C is sufficient to signal cleavage furrow formation during cytokinesis. *Journal of cell science*. 119:4402–8. doi:10.1242/jcs.03210.

D'Avino, P.P., T. Takeda, L. Capalbo, W. Zhang, K.S. Lilley, E.D. Laue, and D.M. Glover. 2008. Interaction between Anillin and RacGAP50C connects the actomyosin contractile ring with spindle microtubules at the cell division site. *Journal of cell science*. 121:1151–8. doi:10.1242/jcs.026716.

Von Dassow, G. 2009. Concurrent cues for cytokinetic furrow induction in animal cells. *Trends in cell biology*. 19:165–73. doi:10.1016/j.tcb.2009.01.008.

Dautry-Varsat, A., A. Subtil, and T. Hackstadt. 2005. Recent insights into the mechanisms of Chlamydia entry. *Cellular microbiology*. 7:1714–22. doi:10.1111/j.1462-5822.2005.00627.x.

Davis, C.H., and P.B. Wyrick. 1997. Differences in the association of Chlamydia trachomatis serovar E and serovar L2 with epithelial cells in vitro may reflect biological differences in vivo. *Infection and immunity*. 65:2914–24.

Davoli, T., and T. de Lange. 2011. The causes and consequences of polyploidy in normal development and cancer. *Annual review of cell and developmental biology*. 27:585–610. doi:10.1146/annurev-cellbio-092910-154234.

Debnath, J., S.K. Muthuswamy, and J.S. Brugge. 2003. Morphogenesis and oncogenesis of MCF-10A mammary epithelial acini grown in three-dimensional basement membrane cultures. *Methods (San Diego, Calif.)*. 30:256–68.

Derré, I., R. Swiss, and H. Agaisse. 2011. The lipid transfer protein CERT interacts with the Chlamydia inclusion protein IncD and participates to ER-Chlamydia inclusion membrane contact sites. *PLoS pathogens*. 7:e1002092. doi:10.1371/journal.ppat.1002092.

Diao, A., D. Rahman, D.J.C. Pappin, J. Lucocq, and M. Lowe. 2003. The coiled-coil membrane protein golgin-84 is a novel rab effector required for Golgi ribbon formation. *The Journal of cell biology*. 160:201–12. doi:10.1083/jcb.200207045.

Doherty, S.C., S.R. McKeown, V. McKelvey-Martin, C.S. Downes, A. Atala, J.J. Yoo, D.A. Simpson, and W.K. Kaufmann. 2003. Cell cycle checkpoint function in bladder cancer. *Journal of the National Cancer Institute*. 95:1859–68.

Dong, F., H. Su, Y. Huang, Y. Zhong, and G. Zhong. 2004. Cleavage of host keratin 8 by a Chlamydia-secreted protease. *Infection and immunity*. 72:3863–8. doi:10.1128/IAI.72.7.3863-3868.2004.

Douglas, M.E., T. Davies, N. Joseph, and M. Mishima. 2010. Aurora B and 14-3-3 coordinately regulate clustering of centralspindlin during cytokinesis. *Current biology : CB*. 20:927–33. doi:10.1016/j.cub.2010.03.055.

Drechsel, D.N., A.A. Hyman, A. Hall, and M. Glotzer. 1997. A requirement for Rho and Cdc42 during cytokinesis in Xenopus embryos. *Current Biology*. 7:12–23. doi:10.1016/S0960-9822(06)00023-6.

Duensing, S., L.Y. Lee, A. Duensing, J. Basile, S. Piboonniyom, S. Gonzalez, C.P. Crum, and K. Munger. 2000. The human papillomavirus type 16 E6 and E7 oncoproteins cooperate to induce mitotic defects and genomic instability by uncoupling centrosome duplication from the cell division cycle. *Proceedings of the National Academy of Sciences of the United States of America*. 97:10002–7. doi:10.1073/pnas.170093297.

Egea, G., F. Lázaro-Diéguez, and M. Vilella. 2006. Actin dynamics at the Golgi complex in mammalian cells. *Current opinion in cell biology*. 18:168–78. doi:10.1016/j.ceb.2006.02.007.

El-Asrar, A.M., K. Geboes, S.A. Al-Kharashi, A.A. Al-Mosallam, L. Missotten, L. Paemen, and G. Opdenakker. 2000. Expression of gelatinase B in trachomatous conjunctivitis. *The British journal of ophthalmology*. 84:85–91.

Elledge, S.J. 1996. Cell cycle checkpoints: preventing an identity crisis. *Science (New York, N.Y.)*. 274:1664–72.

Elwell, C.A., A. Ceesay, J.H. Kim, D. Kalman, and J.N. Engel. 2008. RNA interference screen identifies Abl kinase and PDGFR signaling in Chlamydia trachomatis entry. *PLoS pathogens*. 4:e1000021. doi:10.1371/journal.ppat.1000021.

Engel, F.B., M. Schebesta, and M.T. Keating. 2006. Anillin localization defect in cardiomyocyte binucleation. *Journal of molecular and cellular cardiology*. 41:601–12. doi:10.1016/j.yjmcc.2006.06.012.

Enserink, J.M., and R.D. Kolodner. 2010. An overview of Cdk1-controlled targets and processes. *Cell division*. 5:11. doi:10.1186/1747-1028-5-11.

Fadel, S., and A. Eley. 2007. Chlamydia trachomatis OmcB protein is a surface-exposed glycosaminoglycan-dependent adhesin. *Journal of medical microbiology*. 56:15–22. doi:10.1099/jmm.0.46801-0.

Farris, C.M., and R.P. Morrison. 2011. Vaccination against Chlamydia genital infection utilizing the murine C. muridarum model. *Infection and immunity*. 79:986–96. doi:10.1128/IAI.00881-10.

Fededa, J.P., and D.W. Gerlich. 2012. Molecular control of animal cell cytokinesis. *Nature cell biology*. 14:440–7. doi:10.1038/ncb2482.

Fields, K.A., D.J. Mead, C.A. Dooley, and T. Hackstadt. 2003. Chlamydia trachomatis type III secretion: evidence for a functional apparatus during early-cycle development. *Molecular microbiology*. 48:671–83.

Foe, V.E., and G. von Dassow. 2008. Stable and dynamic microtubules coordinately shape the myosin activation zone during cytokinetic furrow formation. *J Cell Biol*. 183:457–470. doi:jcb.200807128 [pii] 10.1083/jcb.200807128.

Fudyk, T., L. Olinger, and R.S. Stephens. 2002. Selection of mutant cell lines resistant to infection by Chlamydia spp [corrected]. *Infection and immunity*. 70:6444–7.

Fujiwara, T., M. Bandi, M. Nitta, E. V Ivanova, R.T. Bronson, and D. Pellman. 2005. Cytokinesis failure generating tetraploids promotes tumorigenesis in p53-null cells. *Nature*. 437:1043–7. doi:10.1038/nature04217.

Fukasawa, K. 2005. Centrosome amplification, chromosome instability and cancer development. *Cancer letters*. 230:6–19. doi:10.1016/j.canlet.2004.12.028.

Fukasawa, K., T. Choi, R. Kuriyama, S. Rulong, and G.F. Vande Woude. 1996. Abnormal centrosome amplification in the absence of p53. *Science (New York, N.Y.)*. 271:1744–7.

Gaietta, G.M., B.N.G. Giepmans, T.J. Deerinck, W.B. Smith, L. Ngan, J. Llopis, S.R. Adams, R.Y. Tsien, and M.H. Ellisman. 2006. Golgi twins in late mitosis revealed by genetically

encoded tags for live cell imaging and correlated electron microscopy. *Proceedings of the National Academy of Sciences of the United States of America*. 103:17777–82. doi:10.1073/pnas.0608509103.

Ganem, N.J., Z. Storchova, and D. Pellman. 2007. Tetraploidy, aneuploidy and cancer. *Curr Opin Genet Dev*. 17:157–162. doi:S0959-437X(07)00037-8 [pii] 10.1016/j.gde.2007.02.011.

Glotzer, M. 2004. Cleavage furrow positioning. *J Cell Biol*. 164:347–351. doi:10.1083/jcb.200310112 jcb.200310112 [pii].

Glotzer, M. 2009. The 3Ms of central spindle assembly: microtubules, motors and MAPs. *Nature reviews. Molecular cell biology*. 10:9–20. doi:10.1038/nrm2609.

Gong, D., J.R. Pomerening, J.W. Myers, C. Gustavsson, J.T. Jones, A.T. Hahn, T. Meyer, and J.E. Ferrell. 2007. Cyclin A2 regulates nuclear-envelope breakdown and the nuclear accumulation of cyclin B1. *Current biology : CB*. 17:85–91. doi:10.1016/j.cub.2006.11.066.

Goss, J.W., and D.K. Toomre. 2008. Both daughter cells traffic and exocytose membrane at the cleavage furrow during mammalian cytokinesis. *The Journal of cell biology*. 181:1047–54. doi:10.1083/jcb.200712137.

Green, R.A., E. Paluch, and K. Oegema. 2012. Cytokinesis in animal cells. *Annual review of cell and developmental biology*. 28:29–58. doi:10.1146/annurev-cellbio-101011-155718.

Greene, W., Y. Xiao, Y. Huang, G. McClarty, and G. Zhong. 2004. Chlamydia-infected cells continue to undergo mitosis and resist induction of apoptosis. *Infection and immunity*. 72:451–60.

Greene, W., and G. Zhong. 2003. Inhibition of host cell cytokinesis by Chlamydia trachomatis infection. *The Journal of infection*. 47:45–51.

Grieshaber, N.A., E.R. Fischer, D.J. Mead, C.A. Dooley, and T. Hackstadt. 2004. Chlamydial histone-DNA interactions are disrupted by a metabolite in the methylerythritol phosphate pathway of isoprenoid biosynthesis. *Proceedings of the National Academy of Sciences of the United States of America*. 101:7451–6. doi:10.1073/pnas.0400754101.

Grieshaber, N.A., J.B. Sager, C.A. Dooley, S.F. Hayes, and T. Hackstadt. 2006a. Regulation of the Chlamydia trachomatis histone H1-like protein Hc2 is IspE dependent and IhtA independent. *Journal of bacteriology*. 188:5289–92. doi:10.1128/JB.00526-06.

Grieshaber, S.S., N.A. Grieshaber, and T. Hackstadt. 2003a. Chlamydia trachomatis uses host cell dynein to traffic to the microtubule-organizing center in a p50 dynamitin-independent process. *J Cell Sci*. 116:3793–3802. doi:10.1242/jcs.00695 jcs.00695 [pii].

Grieshaber, S.S., N.A. Grieshaber, and T. Hackstadt. 2003b. Chlamydia trachomatis uses host cell dynein to traffic to the microtubule-organizing center in a p50 dynamitin-independent process. *Journal of Cell Science*. 116:3793–802. doi:10.1242/jcs.00695.

Grieshaber, S.S., N.A. Grieshaber, N. Miller, and T. Hackstadt. 2006b. Chlamydia trachomatis causes centrosomal defects resulting in chromosomal segregation abnormalities. *Traffic*. 7:940–949. doi:TRA439 [pii] 10.1111/j.1600-0854.2006.00439.x.

Gromley, A., C. Yeaman, J. Rosa, S. Redick, C.-T. Chen, S. Mirabelle, M. Guha, J. Sillibourne, and S.J. Doxsey. 2005. Centriolin anchoring of exocyst and SNARE complexes at the midbody is required for secretory-vesicle-mediated abscission. *Cell*. 123:75–87. doi:10.1016/j.cell.2005.07.027.

Guidotti, J.-E., O. Brégerie, A. Robert, P. Debey, C. Brechot, and C. Desdouets. 2003. Liver cell polyploidization: a pivotal role for binuclear hepatocytes. *The Journal of biological chemistry*. 278:19095–101. doi:10.1074/jbc.M300982200.

Guizetti, J., and D.W. Gerlich. 2010. Cytokinetic abscission in animal cells. *Seminars in cell & developmental biology*. 21:909–16. doi:10.1016/j.semcdb.2010.08.001.

Guizetti, J., L. Schermelleh, J. Mäntler, S. Maar, I. Poser, H. Leonhardt, T. Müller-Reichert, and D.W. Gerlich. 2011. Cortical constriction during abscission involves helices of ESCRT-III-dependent filaments. *Science (New York, N.Y.)*. 331:1616–20. doi:10.1126/science.1201847.

Guse, A., M. Mishima, and M. Glotzer. 2005. Phosphorylation of ZEN-4/MKLP1 by aurora B regulates completion of cytokinesis. *Current biology : CB*. 15:778–86. doi:10.1016/j.cub.2005.03.041.

Hackstadt, T., W. Baehr, and Y. Ying. 1991. Chlamydia trachomatis developmentally regulated protein is homologous to eukaryotic histone H1. *Proceedings of the National Academy of Sciences of the United States of America*. 88:3937–41.

Hackstadt, T., E.R. Fischer, M.A. Scidmore, D.D. Rockey, and R.A. Heinzen. 1997. Origins and functions of the chlamydial inclusion. *Trends Microbiol*. 5:288–293. doi:S0966-842X(97)01061-5 [pii] 10.1016/S0966-842X(97)01061-5.

Hackstadt, T., D.D. Rockey, R.A. Heinzen, and M.A. Scidmore. 1996. Chlamydia trachomatis interrupts an exocytic pathway to acquire endogenously synthesized sphingomyelin in transit from the Golgi apparatus to the plasma membrane. *The EMBO journal*. 15:964–77.

Hackstadt, T., M.A. Scidmore, and D.D. Rockey. 1995a. Lipid metabolism in Chlamydia trachomatis-infected cells: directed trafficking of Golgi-derived sphingolipids to the chlamydial inclusion. *Proc Natl Acad Sci U S A*. 92:4877–4881.

Hackstadt, T., M.A. Scidmore, and D.D. Rockey. 1995b. Lipid metabolism in Chlamydia trachomatis-infected cells: directed trafficking of Golgi-derived sphingolipids to the chlamydial inclusion. *Proc Natl Acad Sci U S A*. 92:4877–4881.

Hackstadt, T., M.A. Scidmore-Carlson, E.I. Shaw, and E.R. Fischer. 1999. The Chlamydia trachomatis IncA protein is required for homotypic vesicle fusion. *Cellular microbiology*. 1:119–30.

Hackstadt, T., W.J. Todd, and H.D. Caldwell. 1985. Disulfide-mediated interactions of the chlamydial major outer membrane protein: role in the differentiation of chlamydiae? *Journal of bacteriology*. 161:25–31.

Hafner, L., K. Beagley, and P. Timms. 2008. Chlamydia trachomatis infection: host immune responses and potential vaccines. *Mucosal immunology*. 1:116–30. doi:10.1038/mi.2007.19.

Hahn, D.L. 1995. Treatment of Chlamydia pneumoniae infection in adult asthma: a before-after trial. *The Journal of family practice*. 41:345–51.

Hahn, D.L. 1999. Chlamydia pneumoniae, asthma, and COPD: what is the evidence? *Annals of allergy, asthma & immunology : official publication of the American College of Allergy, Asthma, & Immunology*. 83:271–88, 291; quiz 291–2. doi:10.1016/S1081-1206(10)62666-X.

Hanada, K., K. Kumagai, S. Yasuda, Y. Miura, M. Kawano, M. Fukasawa, and M. Nishijima. 2003. Molecular machinery for non-vesicular trafficking of ceramide. *Nature*. 426:803–9. doi:10.1038/nature02188.

Harper, A., C.I. Pogson, M.L. Jones, and J.H. Pearce. 2000. Chlamydial development is adversely affected by minor changes in amino acid supply, blood plasma amino acid levels, and glucose deprivation. *Infection and immunity*. 68:1457–64.

Hatch, T.P. 1975a. Utilization of L-cell nucleoside triphosphates by Chlamydia psittaci for ribonucleic acid synthesis. *J Bacteriol*. 122:393–400.

Hatch, T.P. 1975b. Competition between Chlamydia psittaci and L cells for host isoleucine pools: a limiting factor in chlamydial multiplication. *Infection and immunity*. 12:211–20.

Hatch, T.P., I. Allan, and J.H. Pearce. 1984. Structural and polypeptide differences between envelopes of infective and reproductive life cycle forms of Chlamydia spp. *J Bacteriol*. 157:13–20.

Heinzen, R.A., M.A. Scidmore, D.D. Rockey, and T. Hackstadt. 1996. Differential interaction with endocytic and exocytic pathways distinguish parasitophorous vacuoles of Coxiella burnetii and Chlamydia trachomatis. *Infection and immunity*. 64:796–809.

Heuer, D., C. Kneip, A.P. Mäurer, and T.F. Meyer. 2007. Tackling the intractable - approaching the genetics of Chlamydiales. *International journal of medical microbiology : IJMM*. 297:569–76. doi:10.1016/j.ijmm.2007.03.011.

Heuer, D., A. Rejman Lipinski, N. Machuy, A. Karlas, A. Wehrens, F. Siedler, V. Brinkmann, and T.F. Meyer. 2009. Chlamydia causes fragmentation of the Golgi compartment to ensure reproduction. *Nature*. 457:731–5. doi:10.1038/nature07578.

Hickson, G.R., and P.H. O'Farrell. 2008a. Anillin: a pivotal organizer of the cytokinetic machinery. *Biochem Soc Trans*. 36:439–441.

Hickson, G.R.X., and P.H. O'Farrell. 2008b. Rho-dependent control of anillin behavior during cytokinesis. *The Journal of cell biology*. 180:285–94. doi:10.1083/jcb.200709005.

Hirano, T. 2005. Condensins: organizing and segregating the genome. *Current biology : CB*. 15:R265–75. doi:10.1016/j.cub.2005.03.037.

Hochegger, H., S. Takeda, T. Hunt, S.W. Oncogenic, R. Bernardo, S.J. Clin, and E. Metab. 2008. Cyclin-dependent kinases and cell-cycle transitions: does one fit all? *Nature reviews. Molecular cell biology*. 9:910–6. doi:10.1038/nrm2510.

Hodinka, R.L., C.H. Davis, J. Choong, and P.B. Wyrick. 1988. Ultrastructural study of endocytosis of Chlamydia trachomatis by McCoy cells. *Infection and immunity*. 56:1456–63.

Holthuis, J.C., T. Pomorski, R.J. Raggers, H. Sprong, and G. Van Meer. 2001. The organizing potential of sphingolipids in intracellular membrane transport. *Physiological reviews*. 81:1689–723.

Horn, M. 2008. Chlamydiae as symbionts in eukaryotes. *Annual review of microbiology*. 62:113–31. doi:10.1146/annurev.micro.62.081307.162818.

Horoschak, K.D., and J.W. Moulder. 1978. Division of single host cells after infection with chlamydiae. *Infection and immunity*. 19:281–6.

Hu, C.-K., M. Coughlin, C.M. Field, and T.J. Mitchison. 2011. KIF4 regulates midzone length during cytokinesis. *Current biology : CB*. 21:815–24. doi:10.1016/j.cub.2011.04.019.

Huelsenbeck, S.C., M. May, G. Schmidt, and H. Genth. 2009. Inhibition of cytokinesis by Clostridium difficile toxin B and cytotoxic necrotizing factors--reinforcing the critical role of RhoA in cytokinesis. *Cell motility and the cytoskeleton*. 66:967–75. doi:10.1002/cm.20390.

Hurley, J.H., and P.I. Hanson. 2010. Membrane budding and scission by the ESCRT machinery: it's all in the neck. *Nature reviews. Molecular cell biology*. 11:556–66. doi:10.1038/nrm2937.

Hutterer, A., M. Glotzer, and M. Mishima. 2009. Clustering of centralspindlin is essential for its accumulation to the central spindle and the midbody. *Current biology : CB*. 19:2043–9. doi:10.1016/j.cub.2009.10.050.

Hybiske, K., and R.S. Stephens. 2007. Mechanisms of host cell exit by the intracellular bacterium Chlamydia. *Proc Natl Acad Sci U S A*. 104:11430–11435. doi:0703218104 [pii] 10.1073/pnas.0703218104.

Hybiske, K., and R.S. Stephens. 2007b. Mechanisms of Chlamydia trachomatis entry into nonphagocytic cells. Infect Immun. 75:3925-3934.

Iliffe-Lee, E.R., and G. McClarty. 1999. Glucose metabolism in Chlamydia trachomatis: the "energy parasite" hypothesis revisited. *Molecular microbiology*. 33:177–87.

Jackson, L.A., S.P. Wang, V. Nazar-Stewart, J.T. Grayston, and T.L. Vaughan. 2000. Association of Chlamydia pneumoniae immunoglobulin A seropositivity and risk of lung cancer. *Cancer Epidemiol Biomarkers Prev*. 9:1263–1266.

Jewett, T.J., E.R. Fischer, D.J. Mead, and T. Hackstadt. 2006. Chlamydial TARP is a bacterial nucleator of actin. *Proceedings of the National Academy of Sciences of the United States of America*. 103:15599–604. doi:10.1073/pnas.0603044103.

Jiang, W., D. Yun, L. Saleh, E.W. Barr, G. Xing, L.M. Hoffart, M.-A. Maslak, C. Krebs, and J.M. Bollinger. 2007. A manganese(IV)/iron(III) cofactor in Chlamydia trachomatis ribonucleotide reductase. *Science (New York, N.Y.)*. 316:1188–91. doi:10.1126/science.1141179.

Jiwani, S., S. Alvarado, R.J. Ohr, A. Romero, B. Nguyen, and T.J. Jewett. 2013. Chlamydia trachomatis Tarp harbors distinct G and F actin binding domains that bundle actin filaments. *Journal of bacteriology*. 195:708–16. doi:10.1128/JB.01768-12.

Johnson, K.A., M. Tan, and C. Sütterlin. 2009. Centrosome abnormalities during a Chlamydia trachomatis infection are caused by dysregulation of the normal duplication pathway. *Cellular microbiology*. 11:1064–73. doi:10.1111/j.1462-5822.2009.01307.x.

Johnston, S.L., and R.J. Martin. 2005. Chlamydophila pneumoniae and Mycoplasma pneumoniae: a role in asthma pathogenesis? *American journal of respiratory and critical care medicine*. 172:1078–89. doi:10.1164/rccm.200412-1743PP.

Jorgensen, I., M.M. Bednar, V. Amin, B.K. Davis, J.P.Y. Ting, D.G. McCafferty, and R.H. Valdivia. 2011. The Chlamydia protease CPAF regulates host and bacterial proteins to maintain

pathogen vacuole integrity and promote virulence. *Cell host & microbe*. 10:21–32. doi:10.1016/j.chom.2011.06.008.

Kalman, S., W. Mitchell, R. Marathe, C. Lammel, J. Fan, R.W. Hyman, L. Olinger, J. Grimwood, R.W. Davis, and R.S. Stephens. 1999. Comparative genomes of Chlamydia pneumoniae and C. trachomatis. *Nature genetics*. 21:385–9. doi:10.1038/7716.

Kamijo, K., N. Ohara, M. Abe, T. Uchimura, H. Hosoya, J.-S. Lee, and T. Miki. 2006. Dissecting the role of Rho-mediated signaling in contractile ring formation. *Molecular biology of the cell*. 17:43–55. doi:10.1091/mbc.E05-06-0569.

Karayiannis, P., and D. Hobson. 1981. Amino acid requirements of a Chlamydia trachomatis genital strain in McCoy cell cultures. *Journal of clinical microbiology*. 13:427–32.

Kari, L., M.M. Goheen, L.B. Randall, L.D. Taylor, J.H. Carlson, W.M. Whitmire, D. Virok, K. Rajaram, V. Endresz, G. McClarty, D.E. Nelson, and H.D. Caldwell. 2011. Generation of targeted Chlamydia trachomatis null mutants. *Proceedings of the National Academy of Sciences of the United States of America*. 108:7189–93. doi:10.1073/pnas.1102229108.

Karlsson-Rosenthal, C., and J.B.A. Millar. 2006. Cdc25: mechanisms of checkpoint inhibition and recovery. *Trends in cell biology*. 16:285–92. doi:10.1016/j.tcb.2006.04.002.

Kaufmann, W.K., C.I. Behe, V.M. Golubovskaya, L.L. Byrd, C.D. Albright, K.M. Borchet, S.C. Presnell, W.B. Coleman, J.W. Grisham, and G.J. Smith. 2001. Aberrant cell cycle checkpoint function in transformed hepatocytes and WB-F344 hepatic epithelial stem-like cells. *Carcinogenesis*. 22:1257–69.

Kaufmann, W.K., J.L. Schwartz, J.C. Hurt, L.L. Byrd, D.A. Galloway, E. Levedakou, and R.S. Paules. 1997. Inactivation of G2 checkpoint function and chromosomal destabilization are linked in human fibroblasts expressing human papillomavirus type 16 E6. *Cell growth & differentiation : the molecular biology journal of the American Association for Cancer Research*. 8:1105–14.

Kechad, A., S. Jananji, Y. Ruella, and G.R.X. Hickson. 2012. Anillin acts as a bifunctional linker coordinating midbody ring biogenesis during cytokinesis. *Current biology : CB*. 22:197–203. doi:10.1016/j.cub.2011.11.062.

Kimberly A. Workowski, S.M.B. 2006. Sexually Transmitted Diseases Treatment Guidelines, 2006. 55:RR–11.

Kimura, K., T. Tsuji, Y. Takada, T. Miki, and S. Narumiya. 2000. Accumulation of GTP-bound RhoA during cytokinesis and a critical role of ECT2 in this accumulation. *The Journal of biological chemistry*. 275:17233–6. doi:10.1074/jbc.C000212200.

Kleylein-Sohn, J., J. Westendorf, M. Le Clech, R. Habedanck, Y.-D. Stierhof, and E.A. Nigg. 2007. Plk4-induced centriole biogenesis in human cells. *Developmental cell*. 13:190–202. doi:10.1016/j.devcel.2007.07.002.

Knowlton, A.E., H.M. Brown, T.S. Richards, L.A. Andreolas, R.K. Patel, and S.S. Grieshaber. 2011. Chlamydia trachomatis infection causes mitotic spindle pole defects independently from its effects on centrosome amplification. *Traffic (Copenhagen, Denmark)*. 12:854–66. doi:10.1111/j.1600-0854.2011.01204.x.

Knowlton, A.E., L.J. Fowler, R.K. Patel, S.M. Wallet, and S.S. Grieshaber. 2013. Chlamydia induces anchorage independence in 3T3 cells and detrimental cytological defects in an infection model. *PloS one*. 8:e54022. doi:10.1371/journal.pone.0054022.

Kong, L., Z. Deng, H. Shen, and Y. Zhang. 2011. Src family kinase inhibitor PP2 efficiently inhibits cervical cancer cell proliferation through down-regulating phospho-Src-Y416 and phospho-EGFR-Y1173. Mol Cell Biochem. 348:11-19.

Kops, G.J.P.L., B.A.A. Weaver, and D.W. Cleveland. 2005. On the road to cancer: aneuploidy and the mitotic checkpoint. *Nature reviews. Cancer*. 5:773–85. doi:10.1038/nrc1714.

Koskela, P., T. Anttila, T. Bjorge, A. Brunsvig, J. Dillner, M. Hakama, T. Hakulinen, E. Jellum, M. Lehtinen, P. Lenner, T. Luostarinen, E. Pukkala, P. Saikku, S. Thoresen, L. Youngman, and J. Paavonen. 2000. Chlamydia trachomatis infection as a risk factor for invasive cervical cancer. *Int J Cancer*. 85:35–39. doi:10.1002/(SICI)1097-0215(20000101)85:1<35::AID-IJC6>3.0.CO;2-A [pii].

Krajcovic, M., N.B. Johnson, Q. Sun, G. Normand, N. Hoover, E. Yao, A.L. Richardson, R.W. King, E.S. Cibas, S.J. Schnitt, J.S. Brugge, and M. Overholtzer. 2011. A non-genetic route to aneuploidy in human cancers. *Nature cell biology*. 13:324–30. doi:10.1038/ncb2174.

Kumar, Y., J. Cocchiaro, and R.H. Valdivia. 2006. The obligate intracellular pathogen Chlamydia trachomatis targets host lipid droplets. *Current biology : CB*. 16:1646–51. doi:10.1016/j.cub.2006.06.060.

Kumar, Y., and R.H. Valdivia. 2008. Actin and intermediate filaments stabilize the Chlamydia trachomatis vacuole by forming dynamic structural scaffolds. *Cell host & microbe*. 4:159–69. doi:10.1016/j.chom.2008.05.018.

Kuo, C., A. Lee, and L.A. Campbell. 2004. Cleavage of the N-linked oligosaccharide from the surfaces of Chlamydia species affects attachment and infectivity of the organisms in human epithelial and endothelial cells. *Infection and immunity*. 72:6699–701. doi:10.1128/IAI.72.11.6699-6701.2004.

Kuo, T.-C., C.-T. Chen, D. Baron, T.T. Onder, S. Loewer, S. Almeida, C.M. Weismann, P. Xu, J.-M. Houghton, F.-B. Gao, G.Q. Daley, and S. Doxsey. 2011. Midbody accumulation through evasion of autophagy contributes to cellular reprogramming and tumorigenicity. *Nature cell biology*. 13:1214–23. doi:10.1038/ncb2332.

Kurasawa, Y., W.C. Earnshaw, Y. Mochizuki, N. Dohmae, and K. Todokoro. 2004. Essential roles of KIF4 and its binding partner PRC1 in organized central spindle midzone formation. *The EMBO journal*. 23:3237–48. doi:10.1038/sj.emboj.7600347.

Kurz, T., L. Pintard, J.H. Willis, D.R. Hamill, P. Gonczy, M. Peter, and B. Bowerman. 2002. Cytoskeletal regulation by the Nedd8 ubiquitin-like protein modification pathway. *Science*. 295:1294–1298. doi:10.1126/science.1067765 295/5558/1294 [pii].

Lane, B.J., C. Mutchler, S. Al Khodor, S.S. Grieshaber, and R.A. Carabeo. 2008. Chlamydial Entry Involves TARP Binding of Guanine Nucleotide Exchange Factors. *PLoS Pathogens*. 4:e1000014. doi:10.1371/journal.ppat.1000014.

Lane, H.A., and E.A. Nigg. 1996. Antibody microinjection reveals an essential role for human polo-like kinase 1 (Plk1) in the functional maturation of mitotic centrosomes. *The Journal of cell biology*. 135:1701–13.

Lanni, J.S., and T. Jacks. 1998. Characterization of the p53-dependent postmitotic checkpoint following spindle disruption. *Molecular and cellular biology*. 18:1055–64.

Lenart, P., M. Petronczki, M. Steegmaier, B. Di Fiore, J.J. Lipp, M. Hoffmann, W.J. Rettig, N. Kraut, and J.M. Peters. 2007. The small-molecule inhibitor BI 2536 reveals novel insights into mitotic roles of polo-like kinase 1. *Curr Biol*. 17:304–315. doi:S0960-9822(07)00831-7 [pii] 10.1016/j.cub.2006.12.046.

Lindqvist, A., V. Rodríguez-Bravo, and R.H. Medema. 2009. The decision to enter mitosis: feedback and redundancy in the mitotic entry network. *The Journal of cell biology*. 185:193–202. doi:10.1083/jcb.200812045.

Littman, A.J., L.A. Jackson, and T.L. Vaughan. 2005. Chlamydia pneumoniae and lung cancer: epidemiologic evidence. *Cancer epidemiology, biomarkers & prevention : a publication of the American Association for Cancer Research, cosponsored by the American Society of Preventive Oncology*. 14:773–8. doi:10.1158/1055-9965.EPI-04-0599.

Littman, A.J., E. White, L.A. Jackson, M.D. Thornquist, C.A. Gaydos, G.E. Goodman, and T.L. Vaughan. 2004. Chlamydia pneumoniae infection and risk of lung cancer. *Cancer Epidemiol Biomarkers Prev*. 13:1624–1630. doi:13/10/1624 [pii].

Liu, J., G.D. Fairn, D.F. Ceccarelli, F. Sicheri, and A. Wilde. 2012. Cleavage furrow organization requires PIP(2)-mediated recruitment of anillin. *Current biology : CB*. 22:64–9. doi:10.1016/j.cub.2011.11.040.

Low, S.H., X. Li, M. Miura, N. Kudo, B. Quiñones, and T. Weimbs. 2003. Syntaxin 2 and endobrevin are required for the terminal step of cytokinesis in mammalian cells. *Developmental cell*. 4:753–9.

Lowe, M., N.K. Gonatas, and G. Warren. 2000. The mitotic phosphorylation cycle of the cis-Golgi matrix protein GM130. *The Journal of cell biology*. 149:341–56.

Lowe, M., C. Rabouille, N. Nakamura, R. Watson, M. Jackman, E. Jämsä, D. Rahman, D.J. Pappin, and G. Warren. 1998. Cdc2 kinase directly phosphorylates the cis-Golgi matrix protein GM130 and is required for Golgi fragmentation in mitosis. *Cell*. 94:783–93.

Madan, R., and W.A.P. Jr. 2012. Immune responses to Clostridium difficile infection. *Trends in molecular medicine*. 18:658–66. doi:10.1016/j.molmed.2012.09.005.

Madeleine, M.M., T. Anttila, S.M. Schwartz, P. Saikku, M. Leinonen, J.J. Carter, M. Wurscher, L.G. Johnson, D.A. Galloway, and J.R. Daling. 2007. Risk of cervical cancer associated with Chlamydia trachomatis antibodies by histology, HPV type and HPV cofactors. *Int J Cancer*. 120:650–655.

Majeed, M., and E. Kihlström. 1991. Mobilization of F-actin and clathrin during redistribution of Chlamydia trachomatis to an intracellular site in eucaryotic cells. *Infection and immunity*. 59:4465–72.

Malumbres, M., and M. Barbacid. 2005. Mammalian cyclin-dependent kinases. *Trends in biochemical sciences*. 30:630–41. doi:10.1016/j.tibs.2005.09.005.

Malumbres, M., and M. Barbacid. 2009. Cell cycle, CDKs and cancer: a changing paradigm. *Nature reviews. Cancer*. 9:153–66. doi:10.1038/nrc2602.

Margall-Ducos, G., S. Celton-Morizur, D. Couton, O. Brégerie, and C. Desdouets. 2007. Liver tetraploidization is controlled by a new process of incomplete cytokinesis. *Journal of cell science*. 120:3633–9. doi:10.1242/jcs.016907.

Marra, P., L. Salvatore, A. Mironov, A. Di Campli, G. Di Tullio, A. Trucco, G. Beznoussenko, and M.A. De Matteis. 2007. The biogenesis of the Golgi ribbon: the roles of membrane input from the ER and of GM130. *Molecular biology of the cell*. 18:1595–608. doi:10.1091/mbc.E06-10-0886.

Matsumoto, A. 1981. Isolation and electron microscopic observations of intracytoplasmic inclusions containing Chlamydia psittaci. *Journal of bacteriology*. 145:605–12.

Matsumoto, A. 1982. Electron microscopic observations of surface projections on Chlamydia psittaci reticulate bodies. *Journal of bacteriology*. 150:358–64.

Matsumura, F. 2005. Regulation of myosin II during cytokinesis in higher eukaryotes. *Trends Cell Biol*. 15:371–377. doi:S0962-8924(05)00130-3 [pii] 10.1016/j.tcb.2005.05.004.

Matsumura, F., Y. Yamakita, and S. Yamashiro. 2011. Myosin light chain kinases and phosphatase in mitosis and cytokinesis. *Archives of biochemistry and biophysics*. 510:76–82. doi:10.1016/j.abb.2011.03.002.

Maurer, M., O. Komina, and J. Wesierska-Gadek. 2009. Roscovitine differentially affects asynchronously growing and synchronized human MCF-7 breast cancer cells. *Annals of the New York Academy of Sciences*. 1171:250–6. doi:10.1111/j.1749-6632.2009.04717.x.

McClarty, G., and G. Tipples. 1991. In situ studies on incorporation of nucleic acid precursors into Chlamydia trachomatis DNA. *J Bacteriol*. 173:4922–4931.

Mendoza, M., C. Norden, K. Durrer, H. Rauter, F. Uhlmann, and Y. Barral. 2009. A mechanism for chromosome segregation sensing by the NoCut checkpoint. *Nature cell biology*. 11:477–83. doi:10.1038/ncb1855.

Meraldi, P., R. Honda, and E.A. Nigg. 2002. Aurora-A overexpression reveals tetraploidization as a major route to centrosome amplification in p53-/- cells. *The EMBO journal*. 21:483–92.

Miller, A.L., and W.M. Bement. 2009. Regulation of cytokinesis by Rho GTPase flux. *Nature cell biology*. 11:71–7. doi:10.1038/ncb1814.

Mishima, M., S. Kaitna, and M. Glotzer. 2002. Central spindle assembly and cytokinesis require a kinesin-like protein/RhoGAP complex with microtubule bundling activity. *Dev Cell*. 2:41–54. doi:S1534580701001101 [pii].

Mishima, M., V. Pavicic, U. Grüneberg, E.A. Nigg, and M. Glotzer. 2004. Cell cycle regulation of central spindle assembly. *Nature*. 430:908–13. doi:10.1038/nature02767.

Mital, J., and T. Hackstadt. 2011a. Diverse requirements for SRC-family tyrosine kinases distinguish chlamydial species. *mBio*. 2. doi:10.1128/mBio.00031-11.

Mital, J., and T. Hackstadt. 2011b. Role for the SRC family kinase Fyn in sphingolipid acquisition by chlamydiae. *Infection and immunity*. 79:4559–68. doi:10.1128/IAI.05692-11.

Mital, J., N.J. Miller, E.R. Fischer, and T. Hackstadt. 2010. Specific chlamydial inclusion membrane proteins associate with active Src family kinases in microdomains that interact with the host microtubule network. *Cellular microbiology*. 12:1235–49. doi:10.1111/j.1462-5822.2010.01465.x.

Moelleken, K., and J.H. Hegemann. 2008. The Chlamydia outer membrane protein OmcB is required for adhesion and exhibits biovar-specific differences in glycosaminoglycan binding. *Molecular microbiology*. 67:403–19. doi:10.1111/j.1365-2958.2007.06050.x.

Morita, E., V. Sandrin, H.-Y. Chung, S.G. Morham, S.P. Gygi, C.K. Rodesch, and W.I. Sundquist. 2007. Human ESCRT and ALIX proteins interact with proteins of the midbody and function in cytokinesis. *The EMBO journal*. 26:4215–27. doi:10.1038/sj.emboj.7601850.

Morre, S.A., J.M. Lyons, J.I. Ito, and R.P. Morrison. 2000. Murine Models of Chlamydia trachomatis Genital Tract Infection: Use of Mouse Pneumonitis Strain versus Human Strains. *Infection and Immunity*. 68:7209–7211. doi:10.1128/IAI.68.12.7209-7211.2000.

Motegi, F., N. V Velarde, F. Piano, and A. Sugimoto. 2006. Two phases of astral microtubule activity during cytokinesis in C. elegans embryos. *Developmental cell*. 10:509–20. doi:10.1016/j.devcel.2006.03.001.

Moulder, J.W. 1991. Interaction of chlamydiae and host cells in vitro. *Microbiol. Mol. Biol. Rev.* 55:143–190.

Munro, S. 2011. The golgin coiled-coil proteins of the Golgi apparatus. *Cold Spring Harbor perspectives in biology*. 3. doi:10.1101/cshperspect.a005256.

Munsie, L.N., N. Caron, C.R. Desmond, and R. Truant. 2009. Lifeact cannot visualize some forms of stress-induced twisted F-actin. *Nat Methods*. 6:317. doi:nmeth0509-317 [pii] 10.1038/nmeth0509-317.

Murthy, K., and P. Wadsworth. 2008. Dual role for microtubules in regulating cortical contractility during cytokinesis. *Journal of cell science*. 121:2350–9. doi:10.1242/jcs.027052.

Musacchio, A. 2011. Spindle assembly checkpoint: the third decade. *Philosophical transactions of the Royal Society of London. Series B, Biological sciences*. 366:3595–604. doi:10.1098/rstb.2011.0072.

Musacchio, A., and E.D. Salmon. 2007. The spindle-assembly checkpoint in space and time. *Nature reviews. Molecular cell biology*. 8:379–93. doi:10.1038/nrm2163.

Naucler, P., H.C. Chen, K. Persson, S.L. You, C.Y. Hsieh, C.A. Sun, J. Dillner, and C.J. Chen. 2007. Seroprevalence of human papillomaviruses and Chlamydia trachomatis and cervical cancer risk: nested case-control study. *J Gen Virol*. 88:814–822.

Neef, R., U. Gruneberg, R. Kopajtich, X. Li, E.A. Nigg, H. Sillje, and F.A. Barr. 2007. Choice of Plk1 docking partners during mitosis and cytokinesis is controlled by the activation state of Cdk1. *Nat Cell Biol*. 9:436–444. doi:ncb1557 [pii] 10.1038/ncb1557.

Neef, R., C. Preisinger, J. Sutcliffe, R. Kopajtich, E.A. Nigg, T.U. Mayer, and F.A. Barr. 2003. Phosphorylation of mitotic kinesin-like protein 2 by polo-like kinase 1 is required for cytokinesis. *The Journal of cell biology*. 162:863–75. doi:10.1083/jcb.200306009.

Neeper, I.D., D.L. Patton, and C.C. Kuo. 1990. Cinematographic observations of growth cycles of Chlamydia trachomatis in primary cultures of human amniotic cells. *Infect Immun*. 58:2042–2047.

Nguyen, B.D., D. Cunningham, X. Liang, X. Chen, E.J. Toone, C.R.H. Raetz, P. Zhou, and R.H. Valdivia. 2011. Lipooligosaccharide is required for the generation of infectious elementary bodies in Chlamydia trachomatis. *Proceedings of the National Academy of Sciences of the United States of America*. 108:10284–9. doi:10.1073/pnas.1107478108.

Nguyen, B.D., and R.H. Valdivia. 2012. Virulence determinants in the obligate intracellular pathogen Chlamydia trachomatis revealed by forward genetic approaches. *Proceedings of the National Academy of Sciences of the United States of America*. 109:1263–8. doi:10.1073/pnas.1117884109.

Nigg, E.A. 2001. Mitotic kinases as regulators of cell division and its checkpoints. *Nature reviews. Molecular cell biology*. 2:21–32. doi:10.1038/35048096.

Nigg, E.A. 2007. Centrosome duplication: of rules and licenses. *Trends in cell biology*. 17:215–21. doi:10.1016/j.tcb.2007.03.003.

Nishimura, Y., and S. Yonemura. 2006. Centralspindlin regulates ECT2 and RhoA accumulation at the equatorial cortex during cytokinesis. *J Cell Sci*. 119:104–114. doi:jcs.02737 [pii] 10.1242/jcs.02737.

Odell, G.M., and V.E. Foe. 2008. An agent-based model contrasts opposite effects of dynamic and stable microtubules on cleavage furrow positioning. *J Cell Biol*. 183:471–483. doi:jcb.200807129 [pii] 10.1083/jcb.200807129.

Olaharski, A.J., R. Sotelo, G. Solorza-Luna, M.E. Gonsebatt, P. Guzman, A. Mohar, and D.A. Eastmond. 2006. Tetraploidy and chromosomal instability are early events during cervical carcinogenesis. *Carcinogenesis*. 27:337–343. doi:bgi218 [pii] 10.1093/carcin/bgi218.

Ouellette, S.P., F.C. Dorsey, S. Moshiach, J.L. Cleveland, and R.A. Carabeo. 2011. Chlamydia species-dependent differences in the growth requirement for lysosomes. *PloS one*. 6:e16783. doi:10.1371/journal.pone.0016783.

Overholtzer, M., A.A. Mailleux, G. Mouneimne, G. Normand, S.J. Schnitt, R.W. King, E.S. Cibas, and J.S. Brugge. 2007. A nonapoptotic cell death process, entosis, that occurs by cell-in-cell invasion. *Cell*. 131:966–79. doi:10.1016/j.cell.2007.10.040.

Paschen, S.A., J.G. Christian, J. Vier, F. Schmidt, A. Walch, D.M. Ojcius, and G. Häcker. 2008. Cytopathicity of Chlamydia is largely reproduced by expression of a single chlamydial protease. *The Journal of cell biology*. 182:117–27. doi:10.1083/jcb.200804023.

Patton, D.L., M. Askienazy-Elbhar, J. Henry-Suchet, L.A. Campbell, A. Cappuccio, W. Tannous, S.P. Wang, and C.C. Kuo. 1994. Detection of Chlamydia trachomatis in fallopian tube tissue in women with postinfectious tubal infertility. *American journal of obstetrics and gynecology*. 171:95–101.

Pavicic-Kaltenbrunner, V., M. Mishima, and M. Glotzer. 2007. Cooperative assembly of CYK-4/MgcRacGAP and ZEN-4/MKLP1 to form the centralspindlin complex. *Molecular biology of the cell*. 18:4992–5003. doi:10.1091/mbc.E07-05-0468.

Persico, A., R.I. Cervigni, M.L. Barretta, and A. Colanzi. 2009. Mitotic inheritance of the Golgi complex. *FEBS letters*. 583:3857–62. doi:10.1016/j.febslet.2009.10.077.

Peters, J., D.P. Wilson, G. Myers, P. Timms, and P.M. Bavoil. 2007. Type III secretion à la Chlamydia. *Trends in microbiology*. 15:241–51. doi:10.1016/j.tim.2007.04.005.

Petronczki, M., M. Glotzer, N. Kraut, and J.-M. Peters. 2007. Polo-like kinase 1 triggers the initiation of cytokinesis in human cells by promoting recruitment of the RhoGEF Ect2 to the central spindle. *Developmental cell*. 12:713–25. doi:10.1016/j.devcel.2007.03.013.

Piekny, A., M. Werner, and M. Glotzer. 2005. Cytokinesis: welcome to the Rho zone. *Trends Cell Biol*. 15:651–658. doi:S0962-8924(05)00250-3 [pii] 10.1016/j.tcb.2005.10.006.

Piekny, A.J., and M. Glotzer. 2008. Anillin is a scaffold protein that links RhoA, actin, and myosin during cytokinesis. *Current biology : CB*. 18:30–6. doi:10.1016/j.cub.2007.11.068.

Piekny, A.J., and A.S. Maddox. 2010. The myriad roles of Anillin during cytokinesis. *Seminars in cell & developmental biology*. 21:881–91. doi:10.1016/j.semcdb.2010.08.002.

Quintyne, N.J., J.E. Reing, D.R. Hoffelder, S.M. Gollin, and W.S. Saunders. 2005. Spindle multipolarity is prevented by centrosomal clustering. *Science (New York, N.Y.)*. 307:127–9. doi:10.1126/science.1104905.

Rappaport, R. 1961. Experiments concerning the cleavage stimulus in sand dollar eggs. *J Exp Zool*. 148:81–89.

Rappaport, R., and G.W. Conrad. 1963. An Experimental Analysis of Unilateral Cleavage in Invertebrate Eggs. *J Exp Zool*. 153:99–112.

Rappaport, R., and B. Rappaport. 1983. Cytokinesis: Effects of blocks between the mitotic apparatus and the surface on furrow establishment in flattened echinoderm eggs. *Journal of Experimental Zoology*. 227:213–227. doi:10.1002/jez.1402270206.

Raulston, J.E. 1997. Response of Chlamydia trachomatis serovar E to iron restriction in vitro and evidence for iron-regulated chlamydial proteins. *Infection and immunity*. 65:4539–47.

Raulston, J.E., C.H. Davis, T.R. Paul, J. Dave, P.B. Wyrick, and J.D. Hobbs. 2002. Surface Accessibility of the 70-Kilodalton Chlamydia trachomatis Heat Shock Protein following Reduction of Outer Membrane Protein Disulfide Bonds Surface Accessibility of the 70-Kilodalton Chlamydia trachomatis Heat Shock Protein following Reduction of Ou. doi:10.1128/IAI.70.2.535.

Rejman Lipinski, A., J. Heymann, C. Meissner, A. Karlas, V. Brinkmann, T.F. Meyer, and D. Heuer. 2009. Rab6 and Rab11 regulate Chlamydia trachomatis development and golgin-84-dependent Golgi fragmentation. *PLoS pathogens*. 5:e1000615. doi:10.1371/journal.ppat.1000615.

Riedl, J., A.H. Crevenna, K. Kessenbrock, J.H. Yu, D. Neukirchen, M. Bista, F. Bradke, D. Jenne, T.A. Holak, Z. Werb, M. Sixt, and R. Wedlich-Soldner. 2008. Lifeact: a versatile marker to visualize F-actin. *Nat Methods*. 5:605–607.

Ripa, K.T., and P.A. Mårdh. 1977. Cultivation of Chlamydia trachomatis in cycloheximide-treated mccoy cells. *Journal of clinical microbiology*. 6:328–31.

Roshick, C., E.R. Iliffe-Lee, and G. McClarty. 2000. Cloning and characterization of ribonucleotide reductase from Chlamydia trachomatis. *The Journal of biological chemistry*. 275:38111–9. doi:10.1074/jbc.M006367200.

Rosmarin, D.M., J.E. Carette, A.J. Olive, M.N. Starnbach, T.R. Brummelkamp, and H.L. Ploegh. 2012. Attachment of Chlamydia trachomatis L2 to host cells requires sulfation. *Proceedings of the National Academy of Sciences of the United States of America*. 109:10059–64. doi:10.1073/pnas.1120244109.

Russell, P. 1998. Checkpoints on the road to mitosis. *Trends in biochemical sciences*. 23:399–402.

Rzomp, K.A., L.D. Scholtes, B.J. Briggs, G.R. Whittaker, and M.A. Scidmore. 2003. Rab GTPases are recruited to chlamydial inclusions in both a species-dependent and species-independent manner. *Infection and immunity*. 71:5855–70.

Saka, H.A., and R.H. Valdivia. 2010. Acquisition of nutrients by Chlamydiae: unique challenges of living in an intracellular compartment. *Current opinion in microbiology*. 13:4–10. doi:10.1016/j.mib.2009.11.002.

Samoff, E., E.H. Koumans, L.E. Markowitz, M. Sternberg, M.K. Sawyer, D. Swan, J.R. Papp, C.M. Black, and E.R. Unger. 2005. Association of Chlamydia trachomatis with persistence of high-risk types of human papillomavirus in a cohort of female adolescents. *Am J Epidemiol*. 162:668–675. doi:kwi262 [pii] 10.1093/aje/kwi262.

Santamaria, A., R. Neef, U. Eberspächer, K. Eis, M. Husemann, D. Mumberg, S. Prechtl, V. Schulze, G. Siemeister, L. Wortmann, F.A. Barr, and E.A. Nigg. 2007. Use of the novel Plk1 inhibitor ZK-thiazolidinone to elucidate functions of Plk1 in early and late stages of mitosis. *Molecular biology of the cell*. 18:4024–36. doi:10.1091/mbc.E07-05-0517.

Sauer, G., R. Korner, A. Hanisch, A. Ries, E.A. Nigg, and H.H. Sillje. 2005. Proteome analysis of the human mitotic spindle. *Mol Cell Proteomics*. 4:35–43.

Schachter, J., and A.O. Osoba. 1983. Lymphogranuloma venereum. *British medical bulletin*. 39:151–4.

Schiel, J.A., K. Park, M.K. Morphew, E. Reid, A. Hoenger, and R. Prekeris. 2011. Endocytic membrane fusion and buckling-induced microtubule severing mediate cell abscission. *Journal of cell science*. 124:1411–24. doi:10.1242/jcs.081448.

Von Schubert, C., G. Xue, J. Schmuckli-Maurer, K.L. Woods, E.A. Nigg, and D.A.E. Dobbelaere. 2010. The transforming parasite Theileria co-opts host cell mitotic and central spindles to persist in continuously dividing cells. *PLoS biology*. 8:18. doi:10.1371/journal.pbio.1000499.

Scidmore, M.A., E.R. Fischer, and T. Hackstadt. 1996a. Sphingolipids and glycoproteins are differentially trafficked to the Chlamydia trachomatis inclusion. *The Journal of cell biology*. 134:363–74.

Scidmore, M.A., E.R. Fischer, and T. Hackstadt. 2003. Restricted fusion of Chlamydia trachomatis vesicles with endocytic compartments during the initial stages of infection. *Infection and immunity*. 71:973–84.

Scidmore, M.A., D.D. Rockey, E.R. Fischer, R.A. Heinzen, and T. Hackstadt. 1996b. Vesicular interactions of the Chlamydia trachomatis inclusion are determined by chlamydial early protein synthesis rather than route of entry. *Infection and immunity*. 64:5366–72.

Seemann, J., E. Jokitalo, M. Pypaert, and G. Warren. 2000a. Matrix proteins can generate the higher order architecture of the Golgi apparatus. *Nature*. 407:1022–6. doi:10.1038/35039538.

Seemann, J., E.J. Jokitalo, and G. Warren. 2000b. The role of the tethering proteins p115 and GM130 in transport through the Golgi apparatus in vivo. *Molecular biology of the cell*. 11:635–45.

Severson, A.F., D.L. Baillie, and B. Bowerman. 2002. A Formin Homology protein and a profilin are required for cytokinesis and Arp2/3-independent assembly of cortical microfilaments in C. elegans. *Current biology : CB*. 12:2066–75.

Shafikhani, S.H., and J. Engel. 2006. Pseudomonas aeruginosa type III-secreted toxin ExoT inhibits host-cell division by targeting cytokinesis at multiple steps. *Proceedings of the National Academy of Sciences of the United States of America*. 103:15605–10. doi:10.1073/pnas.0605949103.

Shaw, E.I., C.A. Dooley, E.R. Fischer, M.A. Scidmore, K.A. Fields, and T. Hackstadt. 2000. Three temporal classes of gene expression during the Chlamydia trachomatis developmental cycle. *Molecular Microbiology*. 37:913–925. doi:10.1046/j.1365-2958.2000.02057.x.

Sherr, C.J. 2000. The Pezcoller Lecture: Cancer Cell Cycles Revisited. *Cancer Res.* 60:3689–3695.

Shima, D.T., N. Cabrera-Poch, R. Pepperkok, and G. Warren. 1998. An ordered inheritance strategy for the Golgi apparatus: visualization of mitotic disassembly reveals a role for the mitotic spindle. *The Journal of cell biology*. 141:955–66.

Shima, K., G. Kuhlenbäumer, and J. Rupp. 2010. Chlamydia pneumoniae infection and Alzheimer's disease: a connection to remember? *Medical microbiology and immunology*. 199:283–9. doi:10.1007/s00430-010-0162-1.

Shorter, J., and G. Warren. 2002. Golgi architecture and inheritance. *Annual review of cell and developmental biology*. 18:379–420. doi:10.1146/annurev.cellbio.18.030602.133733.

Silins, I., W. Ryd, A. Strand, G. Wadell, S. Törnberg, B.G. Hansson, X. Wang, L. Arnheim, V. Dahl, D. Bremell, K. Persson, J. Dillner, and E. Rylander. 2005. Chlamydia trachomatis infection and persistence of human papillomavirus. *International journal of cancer. Journal international du cancer*. 116:110–5. doi:10.1002/ijc.20970.

Simonetti, A.C., J.H. de L. Melo, P.R.E. de Souza, D. Bruneska, and J.L. de Lima Filho. 2009. Immunological's host profile for HPV and Chlamydia trachomatis, a cervical cancer cofactor. *Microbes and infection / Institut Pasteur*. 11:435–42. doi:10.1016/j.micinf.2009.01.004.

Skop, A.R., H. Liu, J. Yates, B.J. Meyer, and R. Heald. 2004. Dissection of the mammalian midbody proteome reveals conserved cytokinesis mechanisms. *Science (New York, N.Y.)*. 305:61–6. doi:10.1126/science.1097931.

Smith, J.S., C. Bosetti, N. Munoz, R. Herrero, F.X. Bosch, J. Eluf-Neto, C.J. Meijer, A.J. Van Den Brule, S. Franceschi, and R.W. Peeling. 2004. Chlamydia trachomatis and invasive cervical cancer: a pooled analysis of the IARC multicentric case-control study. *Int J Cancer*. 111:431–439. doi:10.1002/ijc.20257.

Somers, W.G., and R. Saint. 2003. A RhoGEF and Rho family GTPase-activating protein complex links the contractile ring to cortical microtubules at the onset of cytokinesis. *Dev Cell*. 4:29–39. doi:S1534580702004021 [pii].

Stary, G., and A. Stary. 2008. Lymphogranuloma venereum outbreak in Europe. *Journal der Deutschen Dermatologischen Gesellschaft = Journal of the German Society of Dermatology : JDDG*. 6:935–40. doi:10.1111/j.1610-0387.2008.06742.x.

Steigemann, P., and D.W. Gerlich. 2009. Cytokinetic abscission: cellular dynamics at the midbody. *Trends in cell biology*. 19:606–16. doi:10.1016/j.tcb.2009.07.008.

Steigemann, P., C. Wurzenberger, M.H.A. Schmitz, M. Held, J. Guizetti, S. Maar, and D.W. Gerlich. 2009. Aurora B-mediated abscission checkpoint protects against tetraploidization. *Cell*. 136:473–84. doi:10.1016/j.cell.2008.12.020.

Stephens, R.S., S. Kalman, C. Lammel, J. Fan, R. Marathe, L. Aravind, W. Mitchell, L. Olinger, R.L. Tatusov, Q. Zhao, E. V Koonin, and R.W. Davis. 1998. Genome sequence of an obligate intracellular pathogen of humans: Chlamydia trachomatis. *Science (New York, N.Y.)*. 282:754–9.

Stirling, P., and S. Richmond. 1977. The developmental cycle of Chlamydia trachomatis in McCoy cells treated with cytochalasin B. *Journal of general microbiology*. 100:31–42.

Storchova, Z., and D. Pellman. 2004. From polyploidy to aneuploidy, genome instability and cancer. *Nat Rev Mol Cell Biol*. 5:45–54. doi:10.1038/nrm1276 nrm1276 [pii].

Strnad, P., and P. Gönczy. 2008. Mechanisms of procentriole formation. *Trends in cell biology*. 18:389–96. doi:10.1016/j.tcb.2008.06.004.

Su, H., G. McClarty, F. Dong, G.M. Hatch, Z.K. Pan, and G. Zhong. 2004. Activation of Raf/MEK/ERK/cPLA2 signaling pathway is essential for chlamydial acquisition of host glycerophospholipids. *The Journal of biological chemistry*. 279:9409–16. doi:10.1074/jbc.M312008200.

Su, H., L. Raymond, D.D. Rockey, E. Fischer, T. Hackstadt, and H.D. Caldwell. 1996. A recombinant Chlamydia trachomatis major outer membrane protein binds to heparan sulfate receptors on epithelial cells. *Proceedings of the National Academy of Sciences of the United States of America*. 93:11143–8.

Su, K.-C., T. Takaki, and M. Petronczki. 2011. Targeting of the RhoGEF Ect2 to the equatorial membrane controls cleavage furrow formation during cytokinesis. *Developmental cell*. 21:1104–15. doi:10.1016/j.devcel.2011.11.003.

Subramanian, R., E.M. Wilson-Kubalek, C.P. Arthur, M.J. Bick, E.A. Campbell, S.A. Darst, R.A. Milligan, and T.M. Kapoor. 2010. Insights into antiparallel microtubule crosslinking by PRC1, a conserved nonmotor microtubule binding protein. *Cell*. 142:433–43. doi:10.1016/j.cell.2010.07.012.

Suchland, R.J., B.M. Jeffrey, M. Xia, A. Bhatia, H.G. Chu, D.D. Rockey, and W.E. Stamm. 2008. Identification of concomitant infection with Chlamydia trachomatis IncA-negative mutant and wild-type strains by genomic, transcriptional, and biological characterizations. *Infection and immunity*. 76:5438–46. doi:10.1128/IAI.00984-08.

Sun, H.S., E.W. Eng, S. Jeganathan, A.T. Sin, P.C. Patel, E. Gracey, R.D. Inman, M.R. Terebiznik, and R.E. Harrison. 2012. Chlamydia trachomatis vacuole maturation in infected macrophages. *J Leukoc Biol*. 92:815–827. doi:10.1189/jlb.0711336 jlb.0711336 [pii].

Sun, H.S., A. Wilde, and R.E. Harrison. 2011. Chlamydia trachomatis inclusions induce asymmetric cleavage furrow formation and ingression failure in host cells. *Mol Cell Biol*. 31:5011–5022. doi:10.1128/MCB.05734-11 MCB.05734-11 [pii].

Tang, D., and Y. Wang. 2013. Cell cycle regulation of Golgi membrane dynamics. *Trends in Cell Biology*. 1–9. doi:10.1016/j.tcb.2013.01.008.

Teixeira, L.K., and S.I. Reed. 2013. Ubiquitin Ligases and Cell Cycle Control. *Annual review of biochemistry*. doi:10.1146/annurev-biochem-060410-105307.

Thomas, S.M., and J.S. Brugge. 1997. Cellular functions regulated by Src family kinases. *Annual review of cell and developmental biology*. 13:513–609. doi:10.1146/annurev.cellbio.13.1.513.

Tipples, G., and G. McClarty. 1993. The obligate intracellular bacterium Chlamydia trachomatis is auxotrophic for three of the four ribonucleoside triphosphates. *Mol Microbiol*. 8:1105–1114.

Tjaden, J., H.H. Winkler, C. Schwöppe, M. Van Der Laan, T. Möhlmann, and H.E. Neuhaus. 1999. Two nucleotide transport proteins in Chlamydia trachomatis, one for net nucleoside triphosphate uptake and the other for transport of energy. *Journal of bacteriology*. 181:1196–202.

Valdivia, R.H. 2008. Chlamydia effector proteins and new insights into chlamydial cellular microbiology. *Curr Opin Microbiol*. 11:53–59. doi:S1369-5274(08)00004-0 [pii] 10.1016/j.mib.2008.01.003.

Vassilev, L.T., C. Tovar, S. Chen, D. Knezevic, X. Zhao, H. Sun, D.C. Heimbrook, and L. Chen. 2006. Selective small-molecule inhibitor reveals critical mitotic functions of human CDK1. *Proceedings of the National Academy of Sciences of the United States of America*. 103:10660–5. doi:10.1073/pnas.0600447103.

Vieira, O. V, R.E. Harrison, C.C. Scott, H. Stenmark, D. Alexander, J. Liu, J. Gruenberg, A.D. Schreiber, and S. Grinstein. 2004. Acquisition of Hrs, an essential component of phagosomal maturation, is impaired by mycobacteria. *Molecular and cellular biology*. 24:4593–604.

Van Vugt, M.A., B.C. van de Weerdt, G. Vader, H. Janssen, J. Calafat, R. Klompmaker, R.M. Wolthuis, and R.H. Medema. 2004. Polo-like kinase-1 is required for bipolar spindle formation but is dispensable for anaphase promoting complex/Cdc20 activation and initiation of cytokinesis. *J Biol Chem*. 279:36841–36854. doi:10.1074/jbc.M313681200 M313681200 [pii].

W.H.O. 2001. Global prevalence and incidence of selected curable sexually transmitted infections: overview and estimates.

Walczak, C.E., S. Cai, and A. Khodjakov. 2010. Mechanisms of chromosome behaviour during mitosis. *Nat Rev Mol Cell Biol*. 11:91–102. doi:nrm2832 [pii] 10.1038/nrm2832.

Wallin, K.L., F. Wiklund, T. Luostarinen, T. Angstrom, T. Anttila, F. Bergman, G. Hallmans, I. Ikaheimo, P. Koskela, M. Lehtinen, U. Stendahl, J. Paavonen, and J. Dillner. 2002. A population-based prospective study of Chlamydia trachomatis infection and cervical carcinoma. *Int J Cancer*. 101:371–374. doi:10.1002/ijc.10639.

Wang, Y., and D.J. Burke. 1995. Checkpoint genes required to delay cell division in response to nocodazole respond to impaired kinetochore function in the yeast Saccharomyces cerevisiae. *Molecular and cellular biology*. 15:6838–44.

Wang, Y., S. Kahane, L.T. Cutcliffe, R.J. Skilton, P.R. Lambden, and I.N. Clarke. 2011. Development of a transformation system for Chlamydia trachomatis: restoration of glycogen biosynthesis by acquisition of a plasmid shuttle vector. *PLoS pathogens*. 7:e1002258. doi:10.1371/journal.ppat.1002258.

Wang, Y., J. Seemann, M. Pypaert, J. Shorter, and G. Warren. 2003. A direct role for GRASP65 as a mitotically regulated Golgi stacking factor. *The EMBO journal*. 22:3279–90. doi:10.1093/emboj/cdg317.

Watanabe, S., Y. Ando, S. Yasuda, H. Hosoya, N. Watanabe, T. Ishizaki, and S. Narumiya. 2008. mDia2 induces the actin scaffold for the contractile ring and stabilizes its position during cytokinesis in NIH 3T3 cells. *Molecular biology of the cell*. 19:2328–38. doi:10.1091/mbc.E07-10-1086.

Wei, J.-H., and J. Seemann. 2009. The mitotic spindle mediates inheritance of the Golgi ribbon structure. *The Journal of cell biology*. 184:391–7. doi:10.1083/jcb.200809090.

Wei, J.-H., and J. Seemann. 2010. Unraveling the Golgi ribbon. *Traffic (Copenhagen, Denmark)*. 11:1391–400. doi:10.1111/j.1600-0854.2010.01114.x.

Werner, M., E. Munro, and M. Glotzer. 2007. Astral signals spatially bias cortical myosin recruitment to break symmetry and promote cytokinesis. *Current biology : CB*. 17:1286–97. doi:10.1016/j.cub.2007.06.070.

Whitfield, M.L., G. Sherlock, A.J. Saldanha, J.I. Murray, C.A. Ball, K.E. Alexander, J.C. Matese, C.M. Perou, M.M. Hurt, P.O. Brown, and D. Botstein. 2002. Identification of genes periodically expressed in the human cell cycle and their expression in tumors. *Mol Biol Cell*. 13:1977–2000. doi:10.1091/mbc.02-02-0030.

Wilson, D.P., P. Timms, D.L.S. McElwain, and P.M. Bavoil. 2006. Type III secretion, contact-dependent model for the intracellular development of chlamydia. *Bulletin of mathematical biology*. 68:161–78. doi:10.1007/s11538-005-9024-1.

Wolfe, B.A., T. Takaki, M. Petronczki, and M. Glotzer. 2009. Polo-like kinase 1 directs assembly of the HsCyk-4 RhoGAP/Ect2 RhoGEF complex to initiate cleavage furrow formation. *PLoS Biol*. 7:e1000110. doi:10.1371/journal.pbio.1000110.

Wurzenberger, C., and D.W. Gerlich. 2011. Phosphatases: providing safe passage through mitotic exit. *Nature reviews. Molecular cell biology*. 12:469–82. doi:10.1038/nrm3149.

Wyrick, P.B., J. Choong, C.H. Davis, S.T. Knight, M.O. Royal, A.S. Maslow, and C.R. Bagnell. 1989. Entry of genital Chlamydia trachomatis into polarized human epithelial cells. *Infection and immunity*. 57:2378–89.

Xia, M., R.J. Suchland, R.E. Bumgarner, T. Peng, D.D. Rockey, and W.E. Stamm. 2005. Chlamydia trachomatis variant with nonfusing inclusions: growth dynamic and host-cell transcriptional response. *The Journal of infectious diseases*. 192:1229–36. doi:10.1086/444394.

Xiang, Y., and Y. Wang. 2010. GRASP55 and GRASP65 play complementary and essential roles in Golgi cisternal stacking. *The Journal of cell biology*. 188:237–51. doi:10.1083/jcb.200907132.

Yang, J., M. Adamian, and T. Li. 2006. Rootletin interacts with C-Nap1 and may function as a physical linker between the pair of centrioles/basal bodies in cells. *Molecular biology of the cell*. 17:1033–40. doi:10.1091/mbc.E05-10-0943.

Ying, S., M. Pettengill, D.M. Ojcius, and G. Häcker. 2007. Host-Cell Survival and Death During Chlamydia Infection. *Current immunology reviews*. 3:31–40. doi:10.2174/157339507779802179.

Yong, E.C., S.J. Klebanoff, and C.C. Kuo. 1982. Toxic effect of human polymorphonuclear leukocytes on Chlamydia trachomatis. *Infection and immunity*. 37:422–6.

Yoshida, S., S. Bartolini, and D. Pellman. 2009. Mechanisms for concentrating Rho1 during cytokinesis. *Genes & development*. 23:810–23. doi:10.1101/gad.1785209.

Yuan, J., R. Yan, A. Krämer, F. Eckerdt, M. Roller, M. Kaufmann, and K. Strebhardt. 2004. Cyclin B1 depletion inhibits proliferation and induces apoptosis in human tumor cells. *Oncogene*. 23:5843–52. doi:10.1038/sj.onc.1207757.

Yuce, O., A. Piekny, and M. Glotzer. 2005. An ECT2-centralspindlin complex regulates the localization and function of RhoA. *J Cell Biol*. 170:571–582. doi:jcb.200501097 [pii] 10.1083/jcb.200501097.

Zhan, P., L. Suo, Q. Qian, X. Shen, L.-X. Qiu, L. Yu, and Y. Song. 2011. Chlamydia pneumoniae infection and lung cancer risk: a meta-analysis. *European journal of cancer (Oxford, England : 1990)*. 47:742–7. doi:10.1016/j.ejca.2010.11.003.

Zhang, J.P., and R.S. Stephens. 1992. Mechanism of C. trachomatis attachment to eukaryotic host cells. *Cell*. 69:861–9.

Zhao, W.M., and G. Fang. 2005a. MgcRacGAP controls the assembly of the contractile ring and the initiation of cytokinesis. *Proc Natl Acad Sci U S A*. 102:13158–13163. doi:0504145102 [pii] 10.1073/pnas.0504145102.

Zhao, W.-M., and G. Fang. 2005b. Anillin is a substrate of anaphase-promoting complex/cyclosome (APC/C) that controls spatial contractility of myosin during late cytokinesis. *The Journal of biological chemistry*. 280:33516–24. doi:10.1074/jbc.M504657200.

Zhong, G. 2009. Killing me softly: chlamydial use of proteolysis for evading host defenses. *Trends in microbiology*. 17:467–74. doi:10.1016/j.tim.2009.07.007.

Zhu, C., and W. Jiang. 2005. Cell cycle-dependent translocation of PRC1 on the spindle by Kif4 is essential for midzone formation and cytokinesis. *Proc Natl Acad Sci U S A*. 102:343–348. doi:0408438102 [pii] 10.1073/pnas.0408438102.

Zhu, C., E. Lau, R. Schwarzenbacher, E. Bossy-Wetzel, and W. Jiang. 2006. Spatiotemporal control of spindle midzone formation by PRC1 in human cells. *Proceedings of the National Academy of Sciences of the United States of America*. 103:6196–201. doi:10.1073/pnas.0506926103.

Appendix I

Chlamydia trachomatis vacuole maturation in infected macrophages.

Epub ahead of print July 17, 2012 - doi:10.1189/jlb.0711336

JLB

Article

Chlamydia trachomatis vacuole maturation in infected macrophages

He Song Sun, Edward W. Y. Eng,* Sujeeve Jeganathan,* Alex T-W. Sin,* Prerna C. Patel,† Eric Gracey,‡ Robert D. Inman,‡ Mauricio R. Terebiznik,* and Rene E. Harrison*,1*

*Departments of Cell and Systems Biology and Biological Sciences, University of Toronto Scarborough, and Departments of †Molecular Genetics and ‡Immunology, University of Toronto, Toronto, Ontario, Canada

RECEIVED JULY 6, 2011; REVISED JUNE 27, 2012; ACCEPTED JUNE 28, 2012. DOI: 10.1189/jlb.0711336

ABSTRACT

Chlamydia trachomatis **is an obligate intracellular bacterium responsible for one of the most common sexually transmitted diseases. In epithelial cells, *C. trachomatis* resides in a modified membrane-bound vacuole known as an inclusion, which is isolated from the endocytic pathway. However, the maturation process of *C. trachomatis* within immune cells, such as macrophages, has not been studied extensively. Here, we demonstrated that RAW macrophages effectively suppressed *C. trachomatis* growth and prevented Golgi stack disruption, a hallmark defect in epithelial cells after *C. trachomatis* infection. Next, we systematically examined association between *C. trachomatis* and various endocytic pathway markers. Spinning disk confocal time-lapse studies revealed significant and rapid association between *C. trachomatis* with Rab7 and LAMP1, markers of late endosomes and lysosomes. Moreover, pretreatment with an inhibitor of lysosome acidification led to significant increases in *C. trachomatis* growth in macrophages. At later stages of infection, *C. trachomatis* associated with the autophagy marker LC3. TEM analysis confirmed that a significant portion of *C. trachomatis* resided within double-membrane-bound compartments, characteristic of autophagosomes. Together, these results suggest that macrophages can suppress *C. trachomatis* growth by targeting it rapidly to lysosomes; moreover, autophagy is activated at later stages of infection and targets significant numbers of the invading bacteria, which may enhance subsequent chlamydial antigen presentation. *J. Leukoc. Biol.* 92: 000–000; 2012.**

Introduction

C. trachomatis is one of the most common causes of sexually transmitted diseases in the world, which can lead to serious complications, such as pelvic inflammatory disease, infertility, and fatal ectopic pregnancy [1]. *C. trachomatis* is a gram-negative, obligate intracellular bacterium that is highly adapted to live inside epithelial cells [1]. The life cycle of *C. trachomatis* involves two phases: the extracellular, infectious yet dormant form known as the EB and the intracellular, noninfectious reproductive form known as the RB [2]. The EB has a diameter of 0.2–0.4 μm and contains electron-dense nuclear material and a rigid cell wall that is well-suited for extracellular survival [3]. The size of a RB ranges from 0.5 to 1.0 μm, and it has less electron-dense nuclear material and a more flexible cell wall than an EB [3]. Upon invasion into epithelial cells, the EB differentiates into the noninfectious RB form and replicates within a vacuolar structure called the inclusion. The RB can differentiate back into the infectious EB form and lyse or extrude from epithelial host cells for dissemination, 2–3 days postinfection [4, 5].

Within the first 30 min of infection in epithelial cells, markers from the host plasma membrane found on the *C. trachomatis* inclusion are removed [6]. Host dynein motors are then recruited to the inclusion to enable its movement toward the microtubule-organizing center [7]. To facilitate their replication process, host cell-derived lipids, including sterols, sphingolipids, glycerophospholipids, sphingomyelin, and cholesterol-rich vesicles from the Golgi, are intercepted by the *C. trachomatis* inclusion [8, 9]. To maintain optimal growth conditions within the host cell, *C. trachomatis* has evolved the ability to disrupt various host cell processes. Recent studies showed that *C. trachomatis* can secret CPAF to cleave host Golgin84 and cause Golgi fragmentation, which significantly enhanced its ability to capture Golgi-derived lipids and bacterial replication [10, 11].

Among the various effector proteins produced by *C. trachomatis*, the Inc protein family has been suggested to act as the

Abbreviations: CIHR=Canadian Institutes of Health Research, CPAF=chlamydial protease-like activity factor, DN=dominant-negative, EB=elementary body, EEA1=early endosome antigen 1, HK=heat-killed, hpi=hours postinfection, Inc=inclusion, LAMP1=lysosome-associated membrane protein 1, LC3=microtubule-associated protein light chain 3, mTOR=mammalian target of rapamycin, RAW macrophage=RAW264.7 macrophage, RB=reticulate body, RFP=red fluorescent protein, SPG=sucrose-phosphate-glutamate, TARP=translocated actin recruiting phosphoprotein

The online version of this paper, found at www.jleukbio.org, includes supplemental information.

1. Correspondence: Dept. of Cell and Systems Biology, University of Toronto Scarborough, Toronto, Ontario, Canada M1C 1A4. E-mail: harrison@utsc.utoronto.ca

central regulators of bacteria–host interactions [12]. IncG can recruit Rab6, Rab11, and Rab14 to the inclusion, which have been suggested to play key roles in intercepting Golgi-derived vesicles [13, 14]. Unlike the recruitment of exocytic Rabs to *Chlamydia* inclusions, endocytic markers, such as EEA1 (early endosomes), Rab5 (early endosomes) and Rab7, and LAMP1 (late endosomes/lysosomes), are absent on the inclusions in epithelial cells [4, 15]. Interestingly, *Parachlamydia acanthamoeba*, a *Chlamydia*-like bacterium, resides in a compartment that acquires EEA1, Rab7, and LAMP1 during its maturation in macrophages [16]. However, in-depth examination of the intracellular trafficking of *C. trachomatis* in immune cells, such as macrophages, has not been performed to date.

Our study, using epifluorescence, spinning disk confocal, and TEM, investigated the maturation process of *C. trachomatis* inclusions in macrophages. We observed that in macrophages, *C. trachomatis* EBs are rapidly targeted to lysosomes. Inhibition of lysosomal acidification or disruption of Rab7 function in macrophages led to a significant increase in *C. trachomatis* replication. During later stages of infection, some *C. trachomatis* compartments were positive for the autophagy marker LC3; moreover, EBs frequently resided in double-membrane-bound vacuoles resembling autophagosomes. Together, our results demonstrate that immune cells, such as macrophages, can combat *C. trachomatis* infection using endocytic and autophagic machineries.

MATERIALS AND METHODS

Cell line and reagents

RAW macrophages and HeLa cells were purchased from American Type Culture Collection. (Manassas, VA, USA). DMEM and FBS were from Wisent (St. Bruno, Quebec, Canada). FuGENE-HD was purchased from Roche Diagnostics (Indianapolis, IN, USA). Rat (ID4B) and mouse (H4A3) anti-LAMP1 antibodies were from Developmental Studies Hybridoma Bank (Iowa City, IA, USA). GM130 antibody was from BD Biosciences (San Jose, CA, USA), Golgin84 antibody was from Abnova (Taipei City, Taiwan), phospho-mTOR (Ser2448) antibody was from Cell Signaling Technology (Danvers, MA, USA), and 4G10 phosphotyrosine antibody was from Millipore (Billerica, MA, USA). TARP and *Chlamydia* antibodies were generous gifts from Dr. David Hackstadt (U.S. National Institutes of Health/National Institute of Allergy and Infectious Diseases, Hamilton, MT, USA). Cy2-, Cy3-, and Cy5-conjugated secondary antibodies were from Jackson ImmunoResearch Laboratories (West Grove, PA, USA). DRAQ5 was from Cell Signaling Technology. LysoSensor Green and BODIPY FL C5-ceramide were purchased from Life Technologies (Burlington, Ontario, Canada). All other reagents were purchased from Sigma-Aldrich (Oakville, Ontario, Canada).

Cell culture, transfection, and *C. trachomatis* infection

HeLa and RAW cells were cultured in DMEM containing 10% heat-inactivated FBS. Primary human macrophages were derived from PBMCs, as described previously [17]. RAW, primary human macrophages, and HeLa cells were grown to 70–80% confluency in DMEM on coverslips at 37°C, supplied with 5% CO_2. For transient expression of constructs, cells were transfected using FuGENE-HD overnight. DNA constructs used were: Rab5-GFP, Rab5 S34N-GFP (DN), Rab5 S34N-mCherry (DN), Rab7-GFP, Rab7 T22N-GFP (DN), and LC3-GFP-RFP. Identity of each construct was confirmed by sequencing.

C. trachomatis serovar L2 was propagated in HeLa cells and purified using a Gastrografin step gradient, as described previously [18]. The purified EBs were stored as small aliquots in SPG buffer at −80°C until use. To generate DRAQ5-labeled EBs, aliquots of purified EBs were pooled together, and DRAQ5 was diluted in SPG buffer and incubated with purified EBs at a final concentration of 1 μM for 10 min at room temperature in the dark. The resulting DRAQ5-labeled EBs were stored in aliquots at −80°C until use. To generate HK EBs, several purified EB aliquots were combined and placed in an 80°C water bath for 50 min. The resulting HK EBs were stored directly in small aliquots at −80°C or labeled with DRAQ5 for 10 min first and then stored at −80°C until use. Efficacy of the HK process was assessed by infecting HeLa cells with HK EBs for 72 h, and no inclusion was observed in the host cells (not shown).

For fixed studies, purified EBs were added to HeLa and RAW cells, and infection was synchronized by centrifugation at 300 *g* for 15 min. Cells were washed with PBS to remove unbound EBs. For live cell imaging experiments, a 35-mm glass-bottom dish (MatTek, Ashland, MA, USA) could not be centrifuged to synchronize infection as a result of the lack of appropriate adaptors. The infection was synchronized by removing culture media from the dish and adding 30 μl fluorescently labeled EBs directly to the cells for 1 min before adding culture media back. As a result of the low volume of liquid present, many EBs attached to the host cells very quickly. In experiments where different cell lines were compared, the same aliquots of EBs were diluted and used to infect the different cell lines.

For overnight inhibition of lysosome acidification, RAW cells were pretreated with 4 nM bafilomycin A1 (Sigma-Aldrich) for 1 h before infection with *C. trachomatis*. Bafilomycin was kept in the culture media at 4 nM throughout the infection until cells were fixed at 24 h.

Immunofluorescence

RAW cells, human macrophages, and HeLa cells were fixed with 4% PFA in PBS for 20 min. Cells were first stained with rabbit anti-EB and Cy5-conjugated anti-rabbit antibodies to label external EBs. Cells were permeabilized using 0.1% Triton X-100/PBS containing 100 mM glycine for 20 min. After permeabilization, cells were washed and blocked with 5% FBS for 1 h. Cells were then incubated with primary antibodies in PBS with 1% FBS for 1 h. Primary antibody dilutions used were: EB (1:200), GM130 (1:200), and LAMP1 antibodies ID4B (1:4) and H4A3 (1:50). All cells were stained with DAPI to visualize the nucleus. Cells were washed and incubated with fluorescent secondary antibodies, prior to mounting and imaging. Slides were imaged with point-scanning confocal microscopy using an LSM 510 META confocal microscope (Carl Zeiss, Thornwood, NY, USA), epifluorescence microscopy using an inverted Axiovert 200 microscope (Carl Zeiss), or a WaveFX-X1 spinning disc confocal (Quorum Technologies, Ontario, Canada).

Western blotting

HeLa and RAW cells were infected with EBs for indicated time-points before cell lysates were collected in RIPA buffer containing 50 mM Tris-HCl (pH 8), 1% Nonidet P-40, 0.15 mM NaCl, 0.9% SDS, phosphatase inhibitor, and protease inhibitor cocktails. Samples were run on SDS polyacrylamide gels before transferred onto nitrocellulose membranes and probed with anti-TARP (1:1,000), anti-4G10 (1:1,000), anti-Golgin84 (1:1,000), or anti-phospho-S2448-mTOR antibody (1:1,000). HRP-conjugated secondary antibody was added for 1 h, and signals were detected with chemiluminescent reagents (Thermo Scientific, Waltham, MA, USA). Blots were imaged using Bio-Rad ChemiDoc XRS and analyzed with ImageJ.

Live cell imaging

Early endosome (Rab5-GFP), late endosome, and lysosome (Rab7-GFP, LAMP1-GFP, or mCherry) and autophagosome (LC3-GFP-RFP) markers were transfected overnight in RAW cells before live cell imaging. LysoSensor Green was added to RAW cells at 1 μM for 1 min to label acidic compartments before the cells were washed twice with fresh media. Rapid time-lapse imaging was carried out using WaveFX-X1 spinning disc confocal with a stage-top incubation system creating a 37°C with 5% CO_2 environment. Images were acquired every 800–900 ms using a Hamamatsu electron-multiplying charge-coupled device camera. For live ceramide trafficking experiments, HeLa and RAW cells were similarly infected with purified EBs for 24 h. BODIPY FL C5-ceramide complexed to BSA was incubated with in-

fected cells at 5 μM concentration for 30 min. Cells were subsequently washed three times to remove excess ceramide and imaged within 30 min. The imaging microscope was controlled by MetaMorph, and movies were edited using Volocity.

TEM analysis of autophagosome–EB interactions

After infecting RAW cells with live or HK EBs for 6 or 9 h, the cells were fixed in 2% gluteraldehyde in 0.1 M Sorenson's phosphate buffer, pH 7.2, for 2 h. Cells were then postfixed in 1% osmium tetroxide, 1.25% potassium ferrocyanide in sodium cacodylate buffer at room temperature for 45 min, stained for 30 min with 1% uranyl acetate in water, and then dehydrated and embedded in Epon resin. Approximately 70–80 nm sections were collected onto copper grids and stained with uranyl acetate and lead citrate. Sections were viewed using a Hitachi H-7500 transmission electron microscope (Hitachi Canada, Mississauga, Ontario, Canada). Subcellular compartments containing electron-dense EBs were quantified as autophagosomes or autolysosomes/lysosomes. The quantification criteria for autophagosomes and autolysosomes/lysosomes were defined previously [19]. Briefly, double-membrane-bound compartments containing undigested cytoplasmic materials were scored as autophagosomes, whereas single-membrane-bound compartments containing cytoplasmic materials were scored as autolysosomes/lysosomes.

C. trachomatis growth assay

RAW and HeLa cells were infected with *C. trachomatis* EBs at a similar MOI as described above. Host cells were scraped at 30 hpi, and lysates were stored at −80°C. The lysates from RAW and HeLa cells were used to reinfect a new culture of HeLa cells that had been grown to equal confluency. Reinfected HeLa cells were fixed at 24 hpi, immunostained, and analyzed by epifluorescence microscopy to quantify the growth of *C. trachomatis* in macrophage and HeLa cells.

Statistical analysis and quantification

All experiments were repeated at least three times, and Student's *t* test was used to determine statistical significance. $P < 0.05$ was used as the significance cut-off. Synchronized movements of overlapping EBs and subcellular compartment markers in time-lapse movies were quantified as positive associations. However, if EBs and fluorescent markers only overlapped in one frame throughout the time lapse, no association was scored. For fluorescent ceramide trafficking quantifications, inclusions containing *C. trachomatis* with visible ceramide decorating membrane of individual bacterium were quantified as positive, whereas inclusions that were devoid of bacteria with visible ceramide incorporation into chlamydial cell membrane were quantified as negative.

RESULTS

Internalization rates of *C. trachomatis* are similar between epithelial cells and macrophages

To first determine if macrophages internalized *C. trachomatis* differently than epithelial cells, we compared the rates of bac-

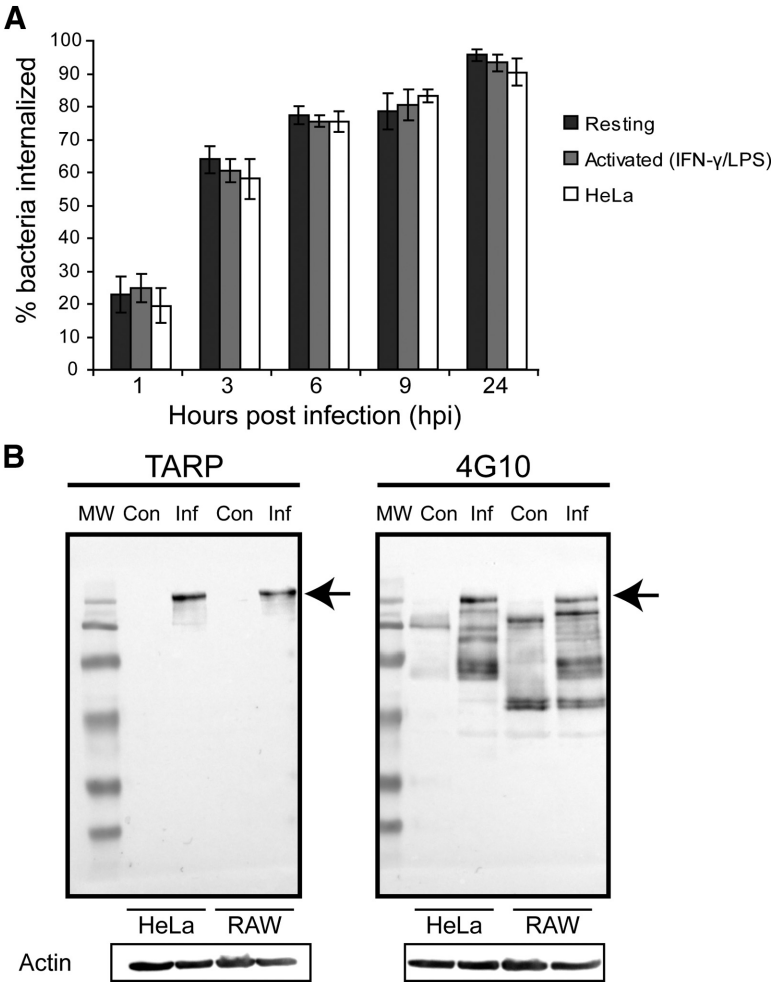

Figure 1. Internalization of *C. trachomatis* EBs is similar among resting, activated RAW macrophages, and HeLa cells. (A) Quantification of the percentage of EBs internalized in resting, activated (IFN-γ- and LPS-stimulated) RAW macrophages, and HeLa cells over time. Cells were fixed and immunostained for external and total EBs before imaging with an epifluorescence microscope. Error bars indicate SEM from three independent experiments ($n>30$/experiment). (B) Phospho-TARP was visualized using total TARP (left) and 4G10 anti-phosphotyrosine antibodies (right) on replicate blots. Actin was used as a loading control. HeLa and RAW cells were infected for 30 min at MOIs of 200 before lysates were taken. TARP was phosphorylated to the same extent in *C. trachomatis*-infected (Inf) HeLa and RAW cells (arrows), compared with uninfected controls (Con), suggesting *Chlamydia* could induce its own uptake into HeLa and RAW cells. At least three independent experiments were performed, and a representative blot is shown.

teria uptake between the two cell types. HeLa (epithelial) and RAW (macrophage) cells were infected with *C. trachomatis* EBs at identical MOIs. Cells were fixed at various time intervals over a 24-h period and immunostained for intracellular and extracellular bacteria. In infected macrophages, many EBs were bound on the surface within the 1st h, with >60% internalized 3 hpi and >75% by 6 hpi (**Fig. 1A**). The rate of internalization of *C. trachomatis* EBs in HeLa cells closely mirrored that of RAW cells (Fig. 1A). Exposure of macrophages to IFN-γ and LPS induces potent, classical activation of macrophages, which up-regulates antimicrobial activities in macrophages, including enhanced binding, phagocytosis, and clearance of microbes [20–25]. Surprisingly, infection of LPS and IFN-γ-activated macrophages also exhibited a similar rate of EB internalization to that of resting macrophages and HeLa cells (Fig. 1A). To confirm that *C. trachomatis* induced its own uptake in HeLa and RAW cells, we measured the levels of phospho-TARP, a key bacterial effector protein involved in EB internalization [26]. TARP becomes activated when it is phosphorylated after being injected into the host cytosol [26–28]. As a result of the lack of phospho-specific TARP antibody, phospho-TARP was detected using duplicate blots of total TARP and 4G10 antiphosphotyrosine antibodies, as carried out by previous studies [26–29]. Similar levels of phospho-TARP were detected in HeLa and RAW cells (Fig. 1B). Together, these results suggested that *C. trachomatis* was internalized into macrophages at a similar rate as in epithelial cells.

Golgi stacks are recruited to *C. trachomatis* inclusions in epithelial cells but not in macrophages

We next investigated the nature of the intracellular *C. trachomatis* compartments in macrophages. In epithelial cells, *Chlamydia* inclusions subvert Golgi-derived vesicles and manipulate the Golgi architecture [8–10]. RAW and HeLa cells were infected with *C. trachomatis* EBs for 24 h and then fixed and immunostained for *Chlamydia* and GM130 to demarcate the

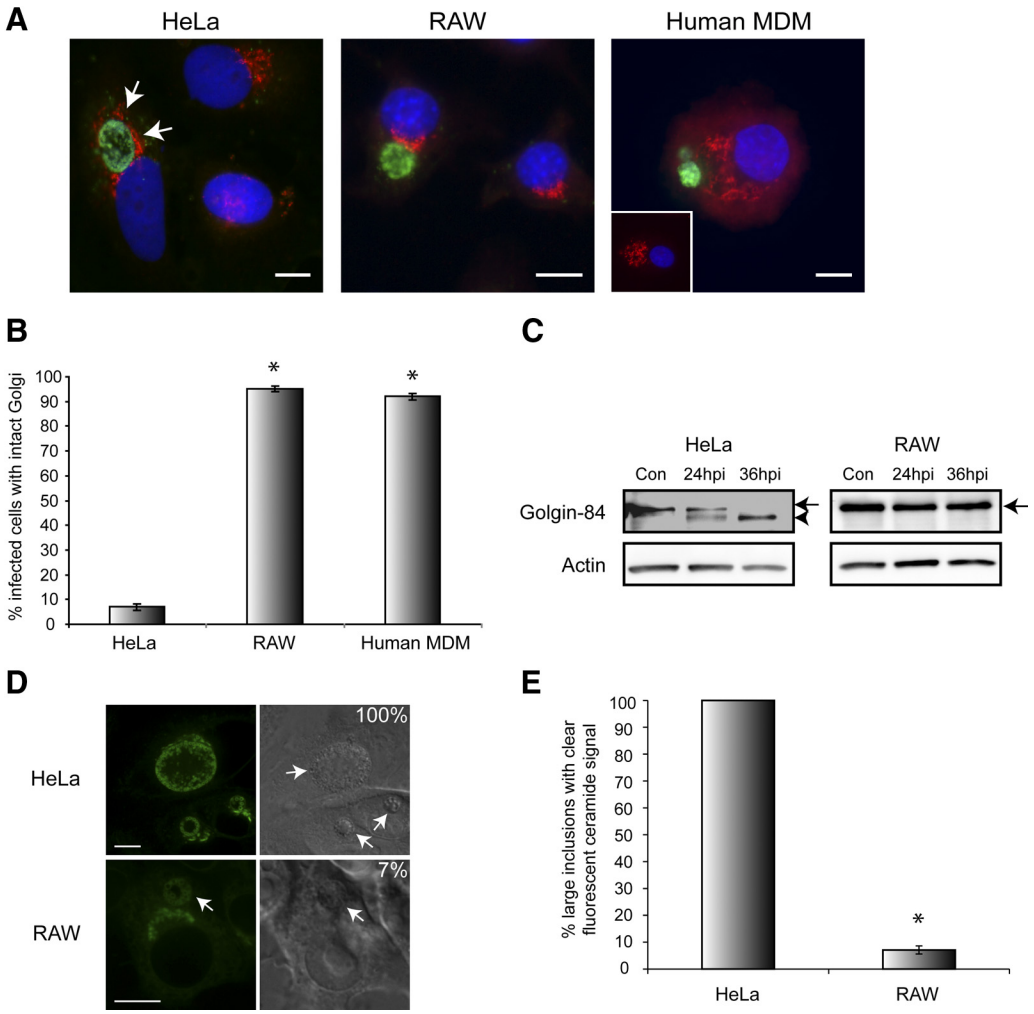

Figure 2. Disruption of host cell Golgi apparatus by *C. trachomatis* occurs in HeLa cells but not in RAW and primary human MDMs. (A) Immunofluorescence images of EBs (green) and the Golgi protein GM130 (red) in *Chlamydia*-infected HeLa, RAW, and human MDMs at 24 hpi. An uninfected human MDM is shown in the inset to demonstrate the naturally dispersed Golgi phenotype in these cells. Arrows indicate the recruitment of Golgi stacks around the inclusion in HeLa cells. (B) Quantification of the percentage of infected cells with normally distributed Golgi in *Chlamydia*-infected HeLa, RAW, and human MDMs at 24 hpi. Error bars represent SEM from three independent experiments (n>30/experiment). (C) HeLa and RAW cells were infected identically for indicated periods. Western blot revealed that Golgin84 was cleaved (arrowhead) in *Chlamydia*-infected HeLa cells but not in RAW cells (arrows). Actin was used as a loading control. At least three independent experiments were performed, and a representative blot is shown. (D) Green BODIPY C5 ceramide was used to assess interception of Golgi-derived vesicles by *C. trachomatis* inclusions (arrows) in HeLa and RAW cells at 24 hpi. *Chlamydia* inclusions could intercept ceramide in HeLa and RAW cells; however, the inclusion ceramide signal was much lower in RAW cells whose Golgi ceramide signal was still pronounced. (E) Only 7% of large inclusions in RAW cells were able to co-opt ceramide to the same extent as inclusions in HeLa cells, whereas 100% of inclusions in HeLa cells obtained bright ceramide signals (n>60/experiment for RAW cells and n>70/experiment for HeLa cells). Error bars represent SEM from three independent experiments. *$P < 0.05$. Original scale bars = 10 μm.

Golgi. In HeLa cells, GM130-positive Golgi stacks closely surrounded the inclusions and were displaced from their normal perinuclear localization. Less than 10% of HeLa cells showed normal, intact Golgi at 24 hpi (**Fig. 2A** and **B**). In contrast, >90% of infected RAW cells had normal, intact perinuclear Golgi staining at 24 hpi, even in the rare cells that contained large inclusions (Fig. 2A and B). Interestingly, Golgi distribution was not altered after *C. trachomatis* infection in human MDMs. Similar to RAW cells, >90% of *Chlamydia*-infected human macrophages showed normal Golgi distribution (Fig. 2A and B). Golgi morphology was intact in all uninfected HeLa, RAW, and MDM cells (data not shown). Consistent with this observation, cleavage of Golgin84, which leads to Golgi stack disruption in epithelial cells [10], occurred in HeLa but not in

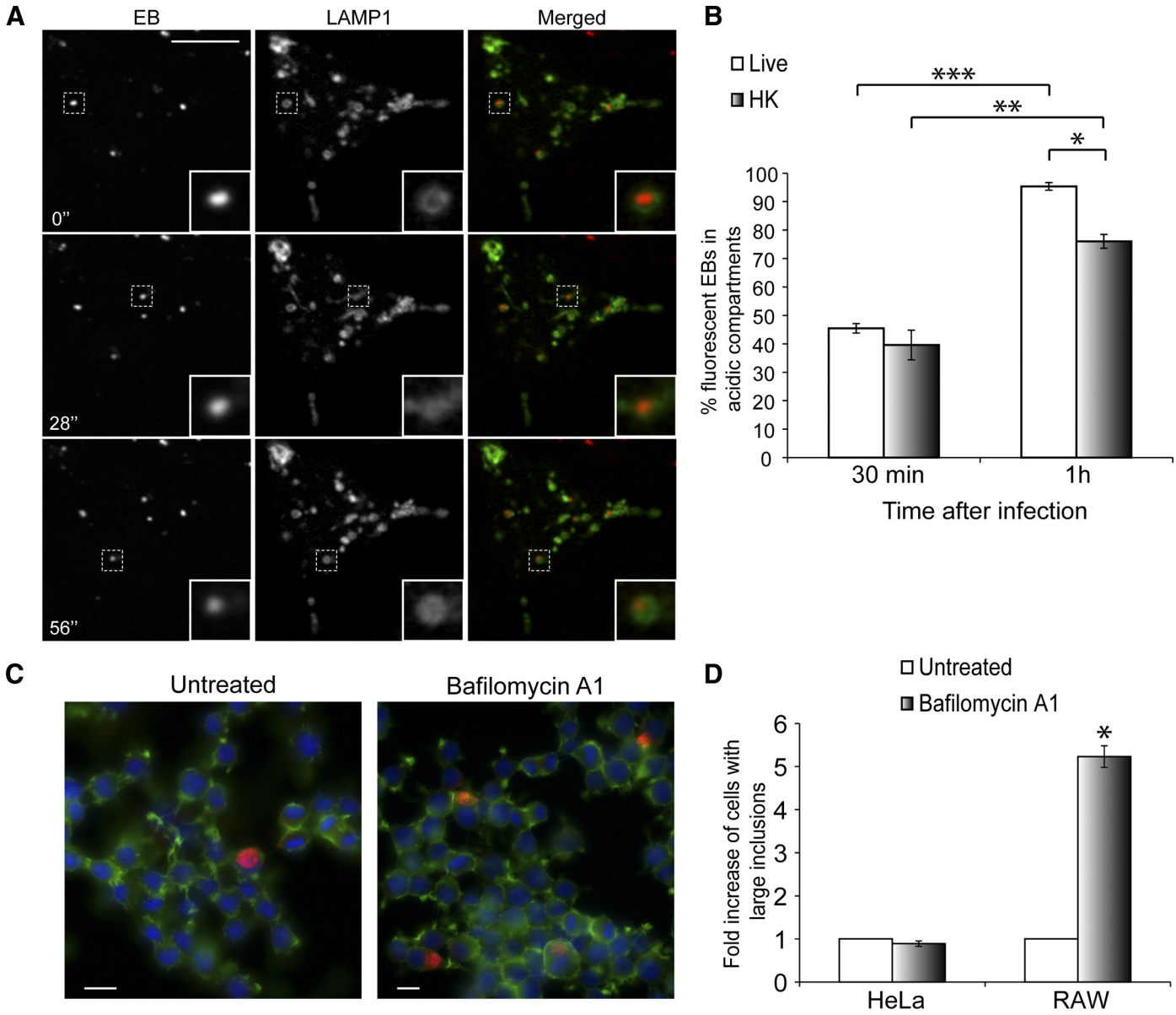

Figure 3. *C. trachomatis* EBs are targeted rapidly to lysosomes in infected RAW macrophages. (A) Purified EBs were labeled with DRAQ5 and added to RAW cells transfected with LAMP1-GFP. Spinning disk confocal time-lapse images were taken within the first 30 min of infection. The majority of EBs associated with LAMP1-positive compartments. Numbers indicate seconds after start of imaging. Insets are magnifications of the dotted regions, which outline various EBs that associate with LAMP1. (B) Acidic compartments in RAW cells were labeled with LysoSensor Green. DRAQ5-labeled live or HK EBs were added to RAW cells, and short time-lapse movies were taken to quantify association between EBs and acidic compartments. $*P < 0.05$, $**P < 0.001$, and $***P < 0.0001$, respectively (n>100/experiment for live and HK EBs). Error bars represent SEM from three independent experiments. (C) Epifluorescence images of RAW cells pretreated with bafilomycin A1 for 1 h prior to infection, which was carried out for 24 h in the presence of bafilomycin A1 before fixation. Cells were stained for actin (green), EBs (red), and nuclei (blue). (D) Quantification of fold increase of cells with large inclusions after bafilomycin treatment. $*P < 0.05$. Error bars represent SEM from three independent experiments (n>1000/experiment). Original scale bars = 10 μm.

RAW cells (Fig. 2C). To directly assess the ability of *C. trachomatis* inclusions to intercept Golgi-derived lipids, the trafficking of fluorescent ceramide to *Chlamydia* inclusions was investigated in infected HeLa and RAW cells. Whereas every *Chlamydia* inclusion was brightly labeled with ceramide in HeLa cells, only a small number of large inclusions in RAW cells obtained substantive ceramide signals (Fig. 2D and E). Together, these results indicate that macrophages could prevent *C. trachomatis*-induced Golgi disruption, which was correlated with decreased Golgi-derived lipid interception.

C. trachomatis is rapidly targeted to lysosomes in macrophages

As *C. trachomatis* was not able to efficiently modify the Golgi in macrophages, we examined the maturation of this compartment to see if it interacted with the endocytic organelles. In epithelial cells, *C. trachomatis* EBs reside in vacuoles that are isolated from the host cell's endocytic machinery to avoid fusion with lysosomes [4, 5, 15]. To investigate whether a similar mechanism exists in macrophages, we generated fluorescently labeled *C. trachomatis* EBs using a DNA-binding dye, DRAQ5. We validated this technique by determining the viability of these bacteria in HeLa cells. First, we confirmed that most of the labeled EBs entered HeLa cells by 3 hpi based on external EB staining (data not shown). In addition, many large *Chlamydia* inclusions formed in HeLa cells infected with these fluorescently labeled EBs at 24 hpi, suggesting the labeled EBs were still viable (data not shown). RAW cells transfected with LAMP1-GFP were infected with DRAQ5-labeled EBs and imaged

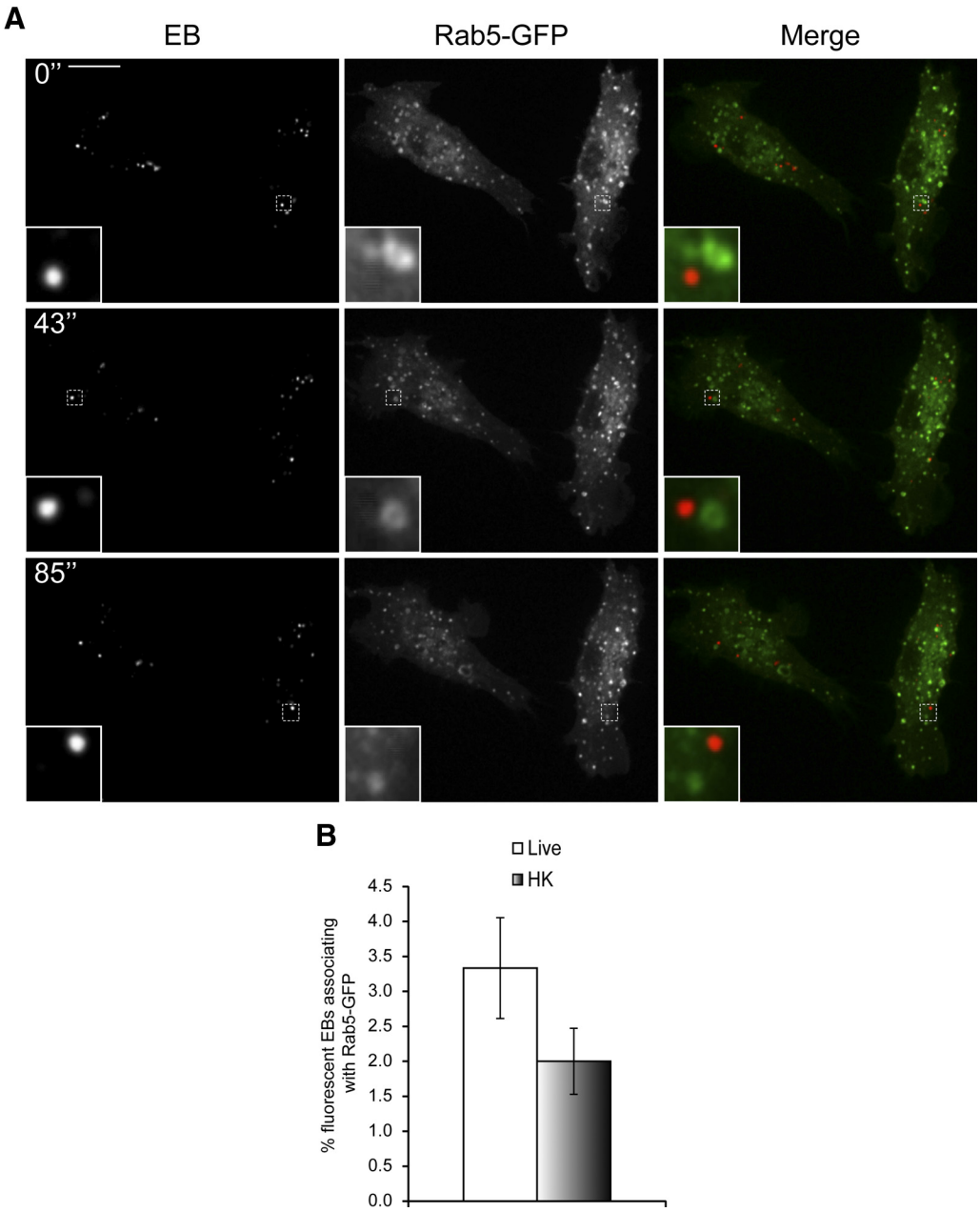

Figure 4. *C. trachomatis* vacuoles rarely associate with Rab5 in RAW macrophages. (A) DRAQ5-labeled EBs were used to infect RAW cells transiently expressing Rab5-GFP, and the cells were imaged live with spinning disk confocal microscopy within the first 30 min of infection. Numbers indicate seconds after start of imaging. Insets are magnifications of the dotted areas, which outline different EBs not associating with Rab5. (B) The percentages of live- or HK-fluorescent EBs associating with Rab5-GFP were quantified. Live and HK EBs rarely associated with Rab5-GFP (n>100/experiment for live and HK EBs). Error bars represent SEM from three independent experiments. Original scale bar = 10 μm.

within 30 min of infection. Surprisingly, many of the fluorescent EBs associated and moved synchronously with LAMP1-GFP compartments (**Fig. 3A** and Supplemental Movie 1) within the first 30 min of infection. To confirm this result, we labeled acidic compartments in RAW cells with LysoSensor Green and infected these cells with DRAQ5-labled live or HK EBs. Quantification of rapidly acquired time-lapse images revealed that ~45% of live and ~40% of HK EBs associated with acidic compartments within the first 30 min of infection. After 1 h of infection, ~95% of live and ~76% of HK EBs associated with acidic compartments (Fig. 3B). Consistent with these results, when

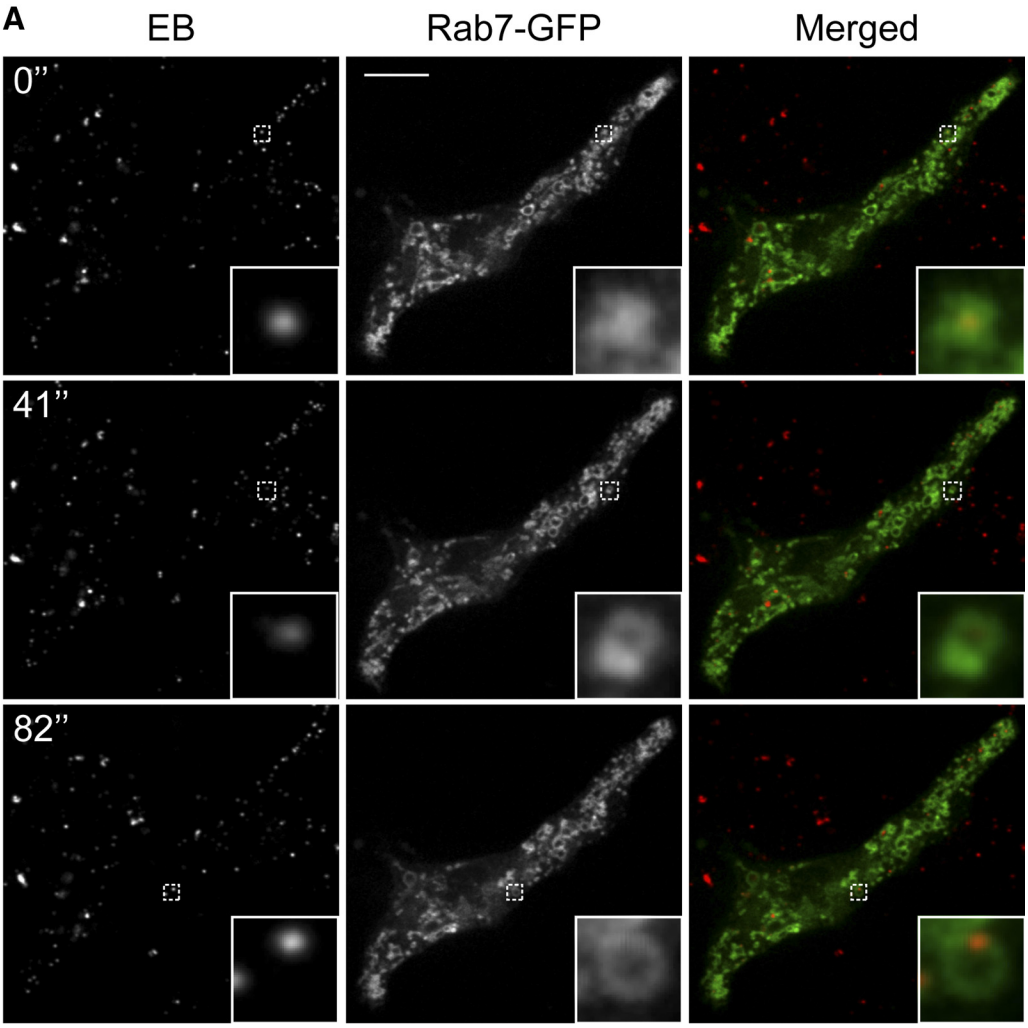

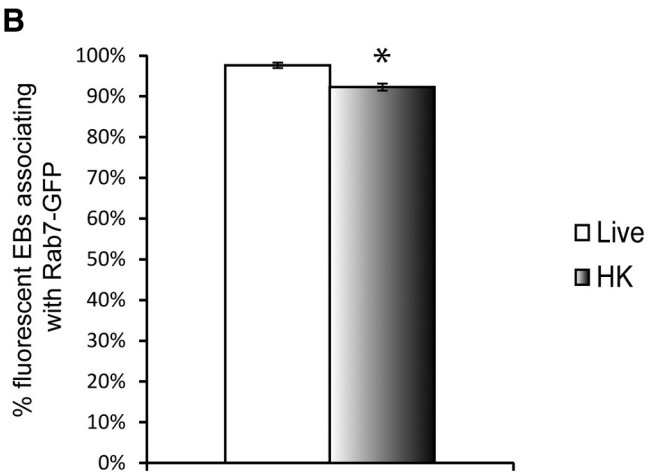

Figure 5. *C. trachomatis* vacuoles frequently associate with Rab7-GFP in macrophages. (A) DRAQ5-labeled EBs were used to infect RAW cells expressing Rab7-GFP, and the cells were imaged live with spinning disk confocal microscopy within 30 min of infection. Numbers indicate seconds after start of imaging. Insets are magnifications of the dotted areas, which outline different EBs that associate with Rab7. (B) The percentages of live- or HK-fluorescent EBs associating with Rab7-GFP were quantified. Live and HK EBs frequently associated with Rab7-GFP. $*P < 0.05$ (n>100/experiment for live and HK EBs). Error bars represent SEM from three independent experiments. Original scale bar = 10 μm.

we inhibited lysosome acidification with bafilomycin, there was a fivefold increase in the number of large *Chlamydia* inclusions in RAW cells (Fig. 3C and D). These findings suggested that *C. trachomatis* EBs were rapidly transported to lysosomes, and their growth was suppressed significantly by lysosomal acidification.

C. trachomatis compartments frequently associate with Rab7 but not Rab5 in macrophages

As we observed a rapid targeting of fluorescent EBs to lysosomes, we next determined which of the Rab-GTPases were involved in this process. Rab5 directs compartments toward fusion with early endosomes [30, 31], whereas Rab7 is critical for late endosome/lysosome recruitment [30, 32]. Rab5-GFP appeared as distinct vesicles in macrophages, as described previously [33] (**Fig. 4A**). Surprisingly, only <5% of live- or HK-fluorescent EBs associated with Rab5-GFP, even within the first 30 min of infection (Fig. 4A and B and Supplemental Movie 2). In contrast, 98% of live and 93% of HK DRAQ5-labeled EBs associated with Rab7-GFP compartments in RAW macrophages within 30 min of infection (**Fig. 5A** and **B** and Supplemental Movie 3).

To confirm that Rab5 did not play an important role in targeting EBs to late endosomes and lysosomes, we cotransfected RAW cells with Rab5-DN-mCherry [34, 35] and Rab7-GFP and carried out infections with DRAQ5-labeled EBs. Time-lapse imaging of these cells demonstrated that even after Rab5-DN expression, >99% of live- and HK-fluorescent EBs still localized to Rab7-GFP compartments within the first 30 min of infection (**Fig. 6A** and **B**). Consistent with these findings, Rab5-DN-mCherry expression did not lead to significant changes in the number of macrophages containing large *C. trachomatis* inclusions at 24 hpi. To assess the functional role of Rab7 in *C. trachomatis* trafficking in macrophages, Rab7-DN-GFP [36] was transfected into RAW macrophages. Cells were fixed and immunostained for EBs at 24 hpi. Expression of DN-Rab7 sig-

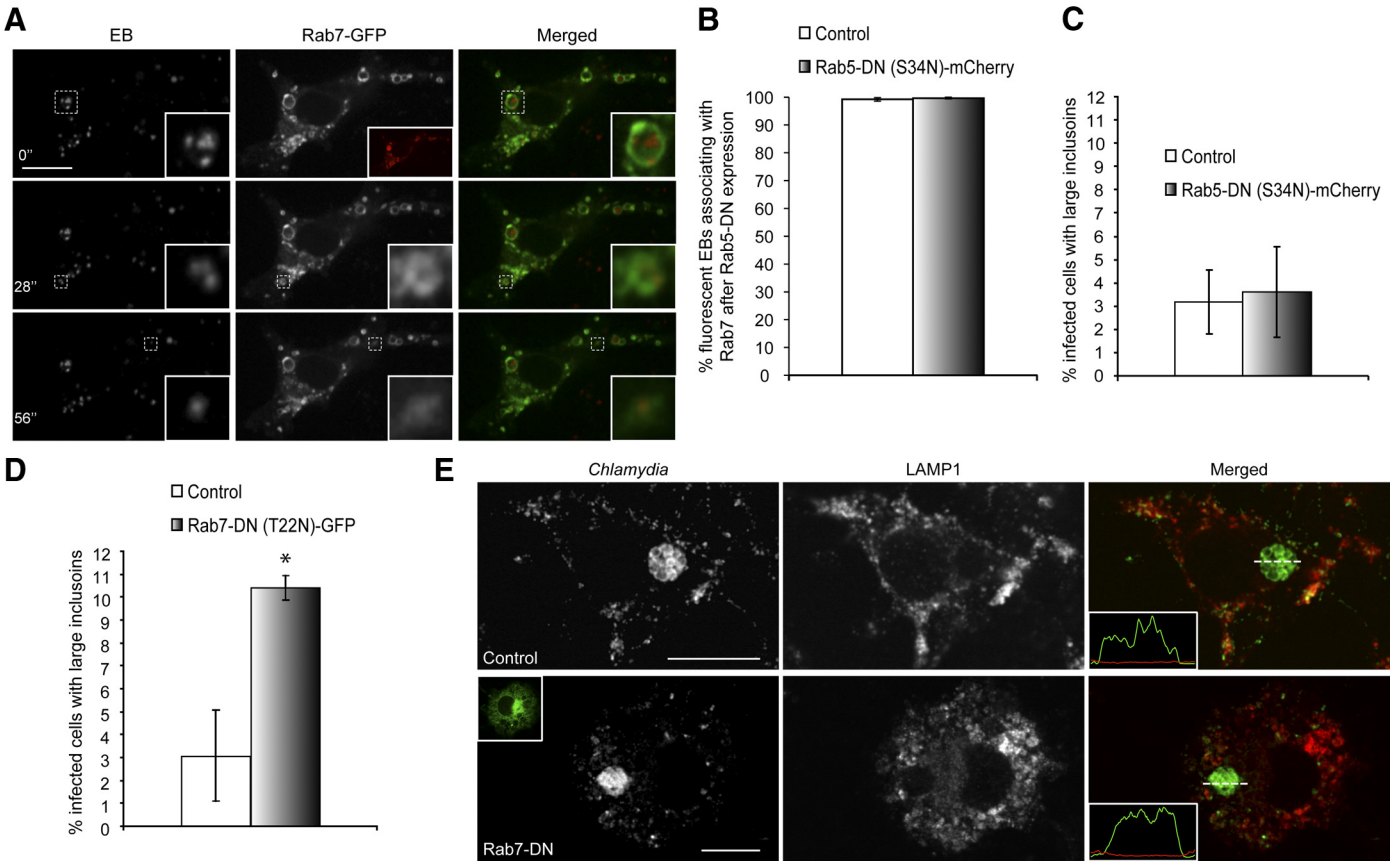

Figure 6. Expression of DN Rab7, but not Rab5, leads to increased *C. trachomatis* replication in macrophages. (A) DRAQ5-labeled EBs were used to infect RAW cells cotransfected with Rab5-DN-mCherry (inset, red) and Rab7-GFP. Cells were imaged live with spinning disk confocal microscopy within 30 min of infection. Numbers indicate seconds after start of imaging. Insets are magnifications of the dotted areas, which outline different EBs that associate with Rab7. (B) The percentages of live- or HK-fluorescent EBs associating with Rab7-GFP were quantified. Live and HK EBs associated very frequently with Rab7-GFP in cells expressing Rab5-DN-mCherry (n>100/experiment for live and HK EBs). Error bars represent SEM from three independent experiments. (C) Quantification of the percentage of infected RAW cells with large inclusions after transfection with Rab5-DN-mCherry. Error bars represent SEM from three independent experiments (n>30/experiment). (D) Expression of Rab7-DN-GFP caused a slight yet significant increase in the percentages of RAW cells with large inclusions. *$P < 0.05$. (E) Spinning disk confocal images of immunostained cells demonstrated that large *C. trachomatis* inclusions in control and cells expressing Rab7-DN-GFP (inset, green) did not associate with LAMP1. Original scale bars = 10 μm.

nificantly increased the number of RAW cells containing large inclusions compared with nontransfected cells (Fig. 6D); moreover, spinning disk confocal and line-intensity profile analysis revealed that large inclusions in untransfected and cells expressing Rab7-DN-GFP did not colocalize with LAMP1 (Fig. 6E). These results suggested that the recruitment of late endosomes/lysosomes to *C. trachomatis* inclusions was critical for limiting the growth of *C. trachomatis* in macrophages.

C. trachomatis associates with the autophagy marker LC3 in macrophages

Autophagy is an intracellular process that enables the host cell to recycle intracellular components and can provide protection against pathogens [37, 38]. LC3 is the most commonly used marker for autophagosomes in microscopy studies [39]. To determine whether autophagy plays a role in *C. trachomatis* vacuole trafficking in macrophages, we transfected RAW cells with LC3-GFP, followed by infection with DRAQ5-labeled EBs. Cells were imaged live with spinning disk confocal at various times after infection. We observed a small fraction of live-fluorescent EBs that associated with LC3-GFP in macrophages, and this fraction of EBs increased significantly by 8 hpi (**Fig. 7A** and **B** and Supplemental Movie 4). As autophagosomes fuse with lysosomes, LC3-GFP signal is destroyed as a result of degradation [40, 41]. Consistent with these results, when we blocked acidification of lysosomes with bafilomycin for 3 h to protect LC3-GFP signal from degradation, the percentage of live-fluorescent EBs associating with LC3-GFP increased significantly to almost 50% (Fig. 7C).

To confirm the LC3-GFP association results at a higher resolution, the same experiments were performed, and the samples were examined using TEM. *C. trachomatis* EBs were identified by TEM using previously established ultrastructural characteristics of the bacteria [42]. In macrophages, live and HK EBs were observed routinely in large, double-membrane-bound, multivesicle-containing compartments (**Fig. 8A**), indica-

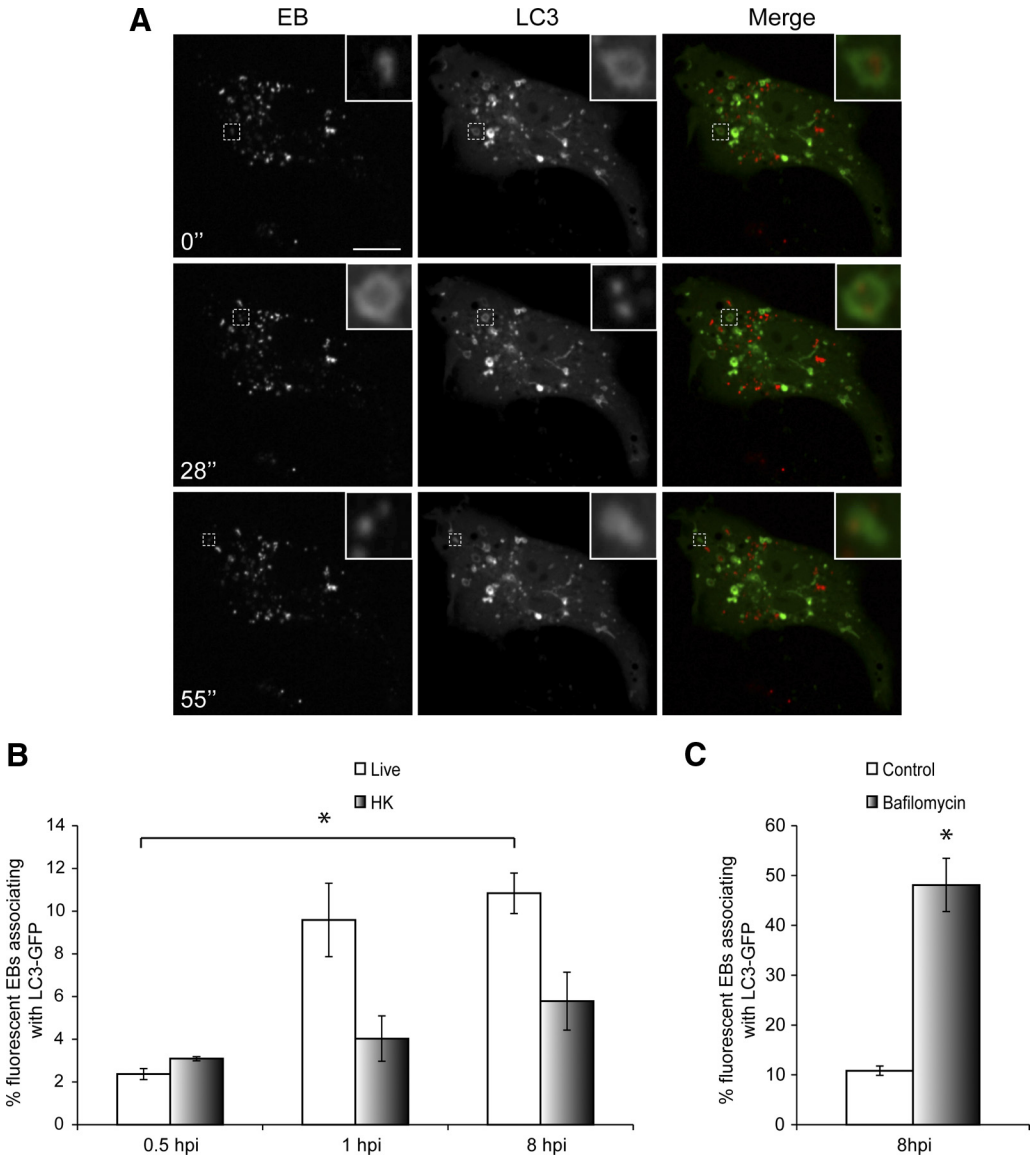

Figure 7. *C. trachomatis* compartments associate with autophagy marker LC3 in macrophages. (A) RAW cells transfected with LC3-GFP were infected with DRAQ5-labeled EBs, and spinning disk confocal time-lapse images were taken 8 hpi. Numbers indicate seconds after start of imaging. Insets are magnifications of the dotted areas. (B) The numbers of live- or HK-fluorescent EBs associating with LC3-GFP at various times after infection were quantified (n>90/experiment for live and HK EBs). (C) Bafilomycin was added to infected RAW cells at 5 hpi and incubated with the cells for 3 h at the concentration of 400 nM. Spinning disk confocal time-lapse images were taken at 8 hpi, and the percentage of fluorescent EBs associating with LC3-GFP was quantified (n>40/experiment). Error bars represent SEM from three independent experiments. *$P < 0.05$. Original scale bar = 10 μm.

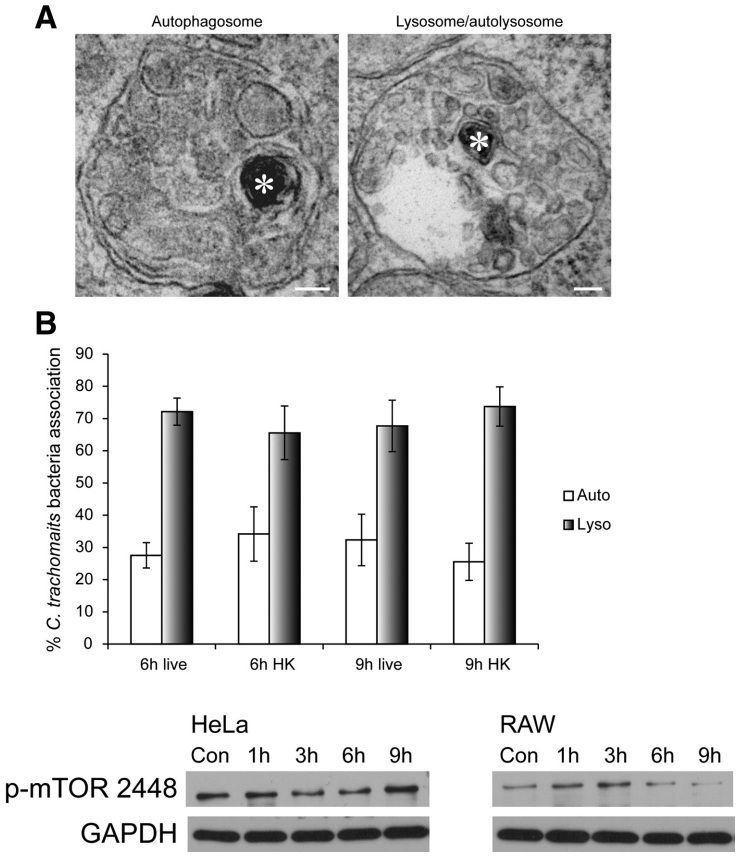

Figure 8. Interaction between autophagosomes and lysosomes with *C. trachomatis* EBs in RAW macrophages. (A) TEM images of EB (asterisks) inside an autophagosome (left panel) or a lysosome/autolysosome (right panel) in RAW macrophages. Original scale bars = 100 nm. (B) The numbers of live or HK EBs in autophagosomes or lysosomes at 6 and 9 hpi were quantified using TEM images. (C) Western blot of HeLa and RAW cell lysates infected with *C. trachomatis* over a 9-h period showed that phospho-S2448 mTOR levels decreased in RAW but not in HeLa cells. GAPDH was used as the loading control. Three independent experiments were carried out, and representative blots are shown.

tive of autophagosomes [43]. In addition, >97% of live and HK EBs were found in autophagosomes or autolysosome/lysosomes at 6 and 9 hpi (Fig. 8B). To determine how autophagy is regulated in response to *C. trachomatis* infection in macrophages, we examined the levels of phospho-mTOR (S2448), an endogenous negative regulator of autophagy [44]. The levels of phospho-mTOR (S2448) did not decrease significantly over time in HeLa cells following *C. trachomatis* infection (Fig. 8C), whereas this repressor of autophagy started to decrease 6 hpi in macrophages (Fig. 8C). These results suggested that autophagy was turned on in macrophages but not in epithelial cells following *C. trachomatis* infection through down-regulation of active mTOR.

The replication rate of *C. trachomatis* in macrophages is slower than that in epithelial cells

As we observed a very frequent association between *Chlamydia* and lysosomes and autophagosomes, we examined whether this cellular trafficking affected *C. trachomatis* replication in macrophages. Throughout our analyses, we consistently observed reduced formation of large inclusions in infected RAW cells, compared with HeLa cells (**Fig. 9A** and **B**). To further validate this notion, the number of infectious *C. trachomatis* progenies in RAW macrophages was compared with that in HeLa cells using a reinfection assay. The number of large inclusions generated after reinfection of new HeLa cells was used as a measure of *C. trachomatis* growth. The lysate from infected HeLa cells led to the formation of large inclusions in ~35% of the new HeLa culture, whereas only 2–3% of the new HeLa culture formed large inclusions when infected with the RAW lysate (Fig. 9B and C). Together, these results indicated that macrophages could significantly restrict *C. trachomatis* replication by targeting these bacteria to degradative organelles.

DISCUSSION

Extensive research has demonstrated that *C. trachomatis* manipulates epithelial cells to evade the endocytic pathway, which may promote its replication [4, 15]. We focused our study on the less-known trafficking pathway of *C. trachomatis* in macrophages. Our results demonstrated that *Chlamydia* replication was hindered significantly in macrophages compared with epithelial cells. We observed very similar rates of internalization of *Chlamydia* in both cell types, and the internalization rate is independent of the activation state of the macrophages. Moreover, based on comparable internalization kinetics and phospho-TARP levels, it is likely that *C. trachomatis* could induce its own uptake into macrophages similar to epithelial cells [45, 46].

Once inside the macrophage, *C. trachomatis* inclusions showed several notable differences from inclusions in epithelial cells. Unlike the striking redistribution of Golgi stacks in HeLa cells [8, 9], this organelle remained intact after *C. trachomatis* infection in murine and primary human macrophages. Recent studies have demonstrated that *C. trachomatis* can se-

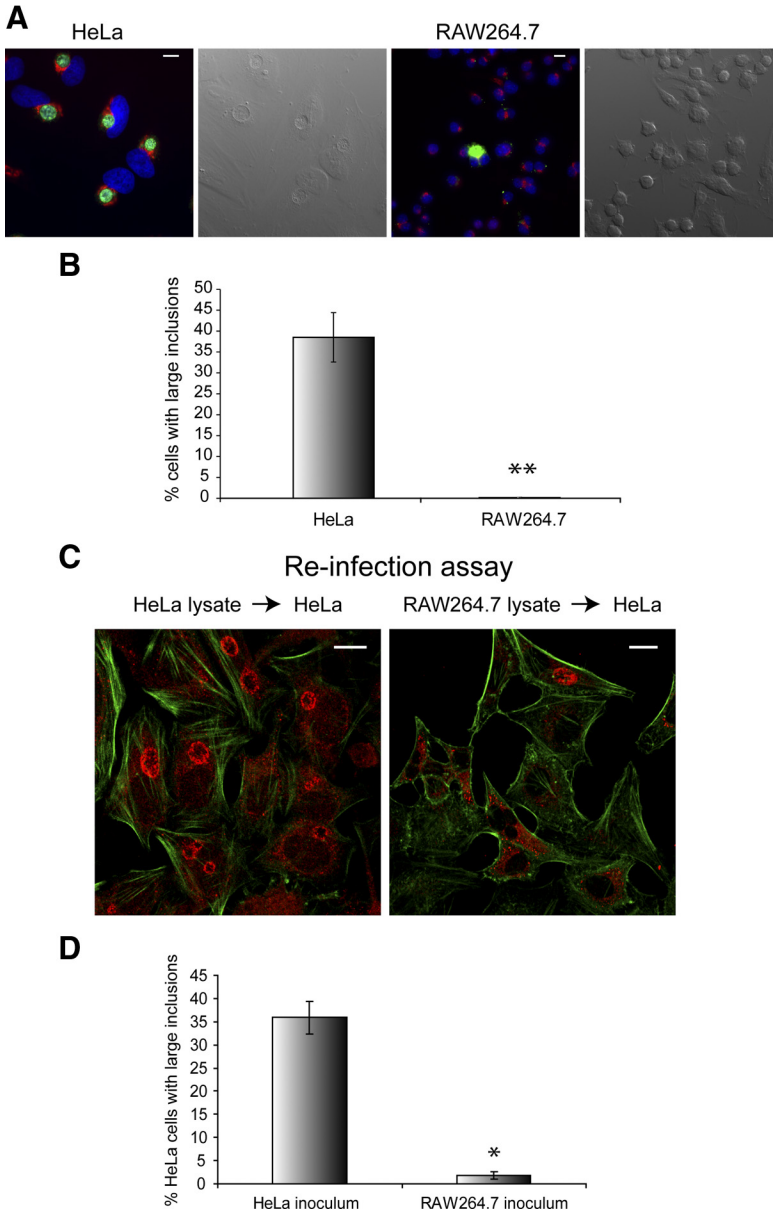

Figure 9. Development of *C. trachomatis* inclusions are suppressed significantly in RAW macrophages compared with HeLa cells. (A) Large inclusions often formed in *Chlamydia*-infected HeLa but not RAW cells at 24 hpi. Cells were immunostained for Golgi (red), EB (green), and nuclei (blue) and imaged using an epifluorescent microscope. (B) The percentages of HeLa and RAW cells with large inclusions at 24 hpi were quantified. (C) Confocal images of HeLa cells infected with *C. trachomatis*-infected HeLa or RAW lysates. Cells were immunostained for actin (green) and inclusions (red). (D) Quantification of the reinfection assay demonstrated that HeLa lysates contained much more infectious *Chlamydia* than RAW lysates at 30 hpi. $*P < 0.05$; $**P < 0.01$. Error bars represent SEM from three independent experiments ($n>100$/experiment). Original scale bars = 10 μm.

crete CPAF and cause the cleavage of Golgin84 to disrupt Golgi stacks in epithelial cells [10, 11]. This Golgi disruption does not occur to a significant degree in macrophages, as there was no detectable level of Golgin84 cleavage products in these cells. Moreover, the efficiency of *C. trachomatis* inclusions to capture Golgi-derived lipids, as measured by fluorescent ceramide trafficking, is reduced significantly in macrophages, consistent with the notion that Golgi fragmentation is important for efficient interception of lipids from the Golgi [10, 11].

We used the readily transfectable RAW cells to characterize the trafficking of *C. trachomatis* in macrophages. Whereas *C. trachomatis* inclusions in epithelial cells are devoid of known endocytic markers, such as EEA1, Rab7, and LAMP1 [4, 5, 15], we observed >98% association between lysosome markers LAMP1 and *C. trachomatis* EBs within the first 30 min of infection using spinning disk confocal live cell imaging. Close to 97% of fluorescent EBs associated with acidic compartments labeled by LysoSensor Green. Moreover, bafilomycin treatment increased the formation of large inclusions in RAW cells by more than fivefold, suggesting the acidification of lysosomes is important for limiting the *C. trachomatis* growth. These results are consistent with the notion that RAW cells can rapidly detect and target invading *C. trachomatis* EBs to lysosomes, which would suppress the bacterial growth through acidification. As >95% of *C. trachomatis* EBs were trafficked into the lysosomes where their development was compromised severely, they likely do not survive long enough to activate bacterial effectors required for Golgin84 cleavage. Thus, lysosome targeting and bacterial destruction appear to block the pathway of Golgi targeting and ceramide interception in macrophages.

We also observed association of *C. trachomatis* EBs with Rab7 but not with Rab5 in macrophages using live cell imaging.

This is very unique compared with the canonical trafficking of internalized particles in macrophages [47]. Despite using very rapid spinning disk confocal imaging, we still could not capture significant association between Rab5-GFP and *C. trachomatis* EBs. Whereas it is possible that Rab5 associates with *C. trachomatis* so transiently or at such low levels that our live cell imaging was not sensitive enough to capture this event, it is also possible that Rab5 is not involved in the trafficking of *C. trachomatis* EBs in macrophages. Unlike our Rab7-DN-GFP findings, DN Rab5 failed to enhance the growth rate and formation of large inclusions in macrophages. Moreover, >99% of fluorescent EBs were still trafficked into Rab7-GFP compartments, even after the expression of Rab5-DN-mCherry. These results suggest that Rab5 is not essential in the trafficking of *C. trachomatis* to lysosomes in macrophages. HK *C. trachomatis* EBs also showed negligible Rab5 recruitment and strong Rab7/lysosome recruitment, although at lower levels compared with live bacteria, which is possibly attributed to a slower internalization rate.

As autophagy has been demonstrated to play an important role in controlling microbial infection [37, 48], we next examined whether *C. trachomatis* EBs associated with autophagic structures at later stages of infection. With the use of live cell imaging, we observed a significant increase in LC3-GFP association for fluorescently labeled EBs at 8 hpi. Moreover, this association was enhanced dramatically when acidification of lysosomes was inhibited with bafilomycin to protect the GFP signal. Consistent with the fluorescent imaging results, we observed that ~30% of *C. trachomatis* EBs resided within double-membrane-bound, multivesicular body-containing compartments characteristic of autophagosomes using TEM at 6 and 9 hpi [43]. Accordingly, we observed a decreased activation level of the repressor of autophagy, mTOR, at these later stages of *C. trachomatis* infection. Together, these results indicate that macrophages not only rapidly target invading *C. trachomatis* EBs into lysosomes during early infection but also elevate their autophagy levels at later stages of the infection through down-regulation of mTOR activity. More than 95% of EBs were targeted into lysosomes and almost 50% of *C. trachomatis* associated with LC3-GFP after 3 h of bafilomycin treatment at 8 hpi. These numbers suggest that a significant portion of EBs trafficked into lysosomes is targeted again by autophagy. As *C. trachomatis* EBs were already within acidic lysosomes in the 1st h of infection, it is unlikely that a later, second round of lysosomal targeting through autophagy could further enhance bacterial degradation. As the level of the autophagy repressor, phospho-mTOR S2448, only decreased 6 hpi, it is very likely that instead of being involved in the early trafficking of *C. trachomatis* EBs, autophagy plays a role in the subsequent processing of this bacterium. Numerous studies have demonstrated that autophagy can enhance pathogen antigen presentation by macrophages (reviewed in ref. [49]). A recent study showed that the efficacy of *Mycobacterium tuberculosis* vaccine is enhanced by elevated autophagy levels [50]; therefore, it will be interesting to explore whether autophagy can similarly improve vaccines against *C. trachomatis*.

AUTHORSHIP

H.S.S., E.W.Y.E., S.J., A.T-W.S., and P.P. carried out the experiments in this study. E.W.Y.E. and H.S.S. wrote the manuscript. E.G., M.R.T., R.D.I., and R.E.H. assisted in experimental design and editing of the manuscript.

ACKNOWLEDGMENTS

This project is funded by a MOP-68992 grant from the CIHR to R.E.H. M.R.T. was supported by a National Sciences and Engineering Research Council grant. R.E.H. is a recipient of a CIHR New Investigator Award and an Ontario Early Researcher Award. We thank Dr. Sergio Grinstein (The Hospital for Sick Children, Toronto, ON, Canada) for the Rab5-GFP, Rab5 S34N-GFP, Rab7-GFP, and Rab7 T22N-GFP constructs and Dr. Nicola Jones (The Hospital for Sick Children) for the LC3-GFP construct. We thank Dr. David Hackstadt (U.S. National Institutes of Health/National Institute of Allergy and Infectious Diseases, Hamilton, MT, USA) for the generous gifts of *Chlamydia* EB and TARP antibodies. We thank Bob Temkin for his generous help with TEM.

REFERENCES

1. Valdivia, R. H. (2008) *Chlamydia* effector proteins and new insights into chlamydial cellular microbiology. *Curr. Opin. Microbiol.* **11,** 53–59.
2. Beatty, W. L., Morrison, R. P., Byrne, G. I. (1994) Persistent chlamydiae: from cell culture to a paradigm for chlamydial pathogenesis. *Microbiol. Rev.* **58,** 686–699.
3. Hatch, T. P., Allan, I., Pearce, J. H. (1984) Structural and polypeptide differences between envelopes of infective and reproductive life cycle forms of *Chlamydia* spp. *J. Bacteriol.* **157,** 13–20.
4. Heinzen, R. A., Scidmore, M. A., Rockey, D. D., Hackstadt, T. (1996) Differential interaction with endocytic and exocytic pathways distinguish parasitophorous vacuoles of *Coxiella burnetii* and *Chlamydia trachomatis*. *Infect. Immun.* **64,** 796–809.
5. Dautry-Varsat, A., Balana, M. E., Wyplosz, B. (2004) *Chlamydia*-host cell interactions: recent advances on bacterial entry and intracellular development. *Traffic* **5,** 561–570.
6. Scidmore, M. A., Fischer, E. R., Hackstadt, T. (2003) Restricted fusion of *Chlamydia trachomatis* vesicles with endocytic compartments during the initial stages of infection. *Infect. Immun.* **71,** 973–984.
7. Grieshaber, S. S., Grieshaber, N. A., Hackstadt, T. (2003) *Chlamydia trachomatis* uses host cell dynein to traffic to the microtubule-organizing center in a p50 dynamitin-independent process. *J. Cell Sci.* **116,** 3793–3802.
8. Hackstadt, T., Rockey, D. D., Heinzen, R. A., Scidmore, M. A. (1996) *Chlamydia trachomatis* interrupts an exocytic pathway to acquire endogenously synthesized sphingomyelin in transit from the Golgi apparatus to the plasma membrane. *EMBO J.* **15,** 964–977.
9. Carabeo, R. A., Mead, D. J., Hackstadt, T. (2003) Golgi-dependent transport of cholesterol to the *Chlamydia trachomatis* inclusion. *Proc. Natl. Acad. Sci. USA* **100,** 6771–6776.
10. Heuer, D., Lipinski, A. R., Machuy, N., Karlas, A., Wehrens, A., Siedler, F., Brinkmann, V., Meyer, T. F. (2009) *Chlamydia* causes fragmentation of the Golgi compartment to ensure reproduction. *Nature* **457,** 731–735.
11. Christian, J. G., Heymann, J., Paschen, S. A., Vier, J., Schauenburg, L., Rupp, J., Meyer, T. F., Hacker, G., Heuer, D. (2011) Targeting of a chlamydial protease impedes intracellular bacterial growth. *PLoS Pathog.* **7,** e1002283.
12. Rockey, D. D., Scidmore, M. A., Bannantine, J. P., Brown, W. J. (2002) Proteins in the chlamydial inclusion membrane. *Microbes Infect.* **4,** 333–340.
13. Capmany, A., Damiani, M. T. (2010) *Chlamydia trachomatis* intercepts Golgi-derived sphingolipids through a Rab14-mediated transport required for bacterial development and replication. *PLoS One* **5,** e14084.
14. Rejman Lipinski, A., Heymann, J., Meissner, C., Karlas, A., Brinkmann, V., Meyer, T. F., Heuer, D. (2009) Rab6 and Rab11 regulate *Chlamydia trachomatis* development and Golgin-84-dependent Golgi fragmentation. *PLoS Pathog.* **5,** e1000615.
15. Rzomp, K. A., Scholtes, L. D., Briggs, B. J., Whittaker, G. R., Scidmore, M. A. (2003) Rab GTPases are recruited to chlamydial inclusions in

both a species-dependent and species-independent manner. *Infect. Immun.* **71,** 5855–5870.
16. Greub, G., Mege, J. L., Gorvel, J. P., Raoult, D., Meresse, S. (2005) Intracellular trafficking of *Parachlamydia acanthamoebae*. *Cell. Microbiol.* **7,** 581–589.
17. Patel, P. C., Harrison, R. E. (2008) Membrane ruffles capture C3bi-opsonized particles in activated macrophages. *Mol. Biol. Cell* **19,** 4628–4639.
18. Caldwell, H. D., Kromhout, J., Schachter, J. (1981) Purification and partial characterization of the major outer membrane protein of *Chlamydia trachomatis*. *Infect. Immun.* **31,** 1161–1176.
19. Mager, D. L. (2006) Bacteria and cancer: cause, coincidence or cure? A review. *J. Transl. Med.* **4,** 14.
20. Wirth, J. J., Kierszenbaum, F., Sonnenfeld, G., Zlotnik, A. (1985) Enhancing effects of γ interferon on phagocytic cell association with and killing of *Trypanosoma cruzi*. *Infect. Immun.* **49,** 61–66.
21. Goerdt, S., Politz, O., Schledzewski, K., Birk, R., Gratchev, A., Guillot, P., Hakiy, N., Klemke, C. D., Dippel, E., Kodelja, V., Orfanos, C. E. (1999) Alternative versus classical activation of macrophages. *Pathobiology* **67,** 222–226.
22. Spinelle-Jaegle, S., Devillier, P., Doucet, S., Millet, S., Banissi, C., Diu-Hercend, A., Ruuth, E. (2001) Inflammatory cytokine production in interferon-γ-primed mice, challenged with lipopolysaccharide. Inhibition by SK&F 86002 and interleukin-1 β-converting enzyme inhibitor. *Eur. Cytokine Netw.* **12,** 280–289.
23. Nacife, V. P., Soeiro Mde, N., Gomes, R. N., D'Avila, H., Castro-Faria Neto, H. C., Meirelles Mde, N. (2004) Morphological and biochemical characterization of macrophages activated by carrageenan and lipopolysaccharide in vivo. *Cell Struct. Funct.* **29,** 27–34.
24. Gordon, M. A., Jack, D. L., Dockrell, D. H., Lee, M. E., Read, R. C. (2005) γ Interferon enhances internalization and early nonoxidative killing of *Salmonella enterica serovar Typhimurium* by human macrophages and modifies cytokine responses. *Infect. Immun.* **73,** 3445–3452.
25. Schroder, K., Hertzog, P. J., Ravasi, T., Hume, D. A. (2004) Interferon-γ: an overview of signals, mechanisms and functions. *J. Leukoc. Biol.* **75,** 163–189.
26. Clifton, D. R., Fields, K. A., Grieshaber, S. S., Dooley, C. A., Fischer, E. R., Mead, D. J., Carabeo, R. A., Hackstadt, T. (2004) A chlamydial type III translocated protein is tyrosine-phosphorylated at the site of entry and associated with recruitment of actin. *Proc. Natl. Acad. Sci. USA* **101,** 10166–10171.
27. Jewett, T. J., Dooley, C. A., Mead, D. J., Hackstadt, T. (2008) *Chlamydia trachomatis* tarp is phosphorylated by src family tyrosine kinases. *Biochem. Biophys. Res. Commun.* **371,** 339–344.
28. Clifton, D. R., Dooley, C. A., Grieshaber, S. S., Carabeo, R. A., Fields, K. A., Hackstadt, T. (2005) Tyrosine phosphorylation of the chlamydial effector protein Tarp is species specific and not required for recruitment of actin. *Infect. Immun.* **73,** 3860–3868.
29. Mehlitz, A., Banhart, S., Hess, S., Selbach, M., Meyer, T. F. (2008) Complex kinase requirements for *Chlamydia trachomatis* Tarp phosphorylation. *FEMS Microbiol. Lett.* **289,** 233–240.
30. Chavrier, P., Parton, R. G., Hauri, H. P., Simons, K., Zerial, M. (1990) Localization of low molecular weight GTP binding proteins to exocytic and endocytic compartments. *Cell* **62,** 317–329.
31. Bucci, C., Parton, R. G., Mather, I. H., Stunnenberg, H., Simons, K., Hoflack, B., Zerial, M. (1992) The small GTPase rab5 functions as a regulatory factor in the early endocytic pathway. *Cell* **70,** 715–728.
32. Feng, Y., Press, B., Wandinger-Ness, A. (1995) Rab 7: an important regulator of late endocytic membrane traffic. *J. Cell Biol.* **131,** 1435–1452.
33. Roberts, R. L., Barbieri, M. A., Ullrich, J., Stahl, P. D. (2000) Dynamics of rab5 activation in endocytosis and phagocytosis. *J. Leukoc. Biol.* **68,** 627–632.
34. Vieira, O. V., Bucci, C., Harrison, R. E., Trimble, W. S., Lanzetti, L., Gruenberg, J., Schreiber, A. D., Stahl, P. D., Grinstein, S. (2003) Modulation of Rab5 and Rab7 recruitment to phagosomes by phosphatidylinositol 3-kinase. *Mol. Cell. Biol.* **23,** 2501–2514.
35. Sarantis, H., Balkin, D. M., De Camilli, P., Isberg, R. R., Brumell, J. H., Grinstein, S. (2012) *Yersinia* entry into host cells requires Rab5-dependent dephosphorylation of PI(4,5)P(2) and membrane scission. *Cell Host Microbe* **11,** 117–128.
36. Harrison, R. E., Bucci, C., Vieira, O. V., Schroer, T. A., Grinstein, S. (2003) Phagosomes fuse with late endosomes and/or lysosomes by extension of membrane protrusions along microtubules: role of Rab7 and RILP. *Mol. Cell. Biol.* **23,** 6494–6506.
37. Huang, J., Brumell, J. H. (2009) Autophagy in immunity against intracellular bacteria. *Curr. Top. Microbiol. Immunol.* **335,** 189–215.
38. Moreau, K., Luo, S., Rubinsztein, D. C. (2010) Cytoprotective roles for autophagy. *Curr. Opin. Cell Biol.* **22,** 206–211.
39. Tanida, I., Ueno, T., Kominami, E. (2008) LC3 and autophagy. *Methods Mol. Biol.* **445,** 77–88.
40. Barth, S., Glick, D., Macleod, K. F. (2010) Autophagy: assays and artifacts. *J. Pathol.* **221,** 117–124.
41. Klionsky, D., Abeliovich, J., Agostinis, H., Agrawal, P., Aliev, D. K., Askew, G., Baba, D. S., Baehrecke, M., Bahr, E. H., Ballabio, B. A.. (2008) Guidelines for the use and interpretation of assays for monitoring autophagy in higher eukaryotes. *Autophagy* **4,** 151–175.
42. Manor, E., Sarov, I. (1986) Fate of *Chlamydia trachomatis* in human monocytes and monocyte-derived macrophages. *Infect. Immun.* **54,** 90–95.
43. Yla-Anttila, P., Vihinen, H., Jokitalo, E., Eskelinen, E. L. (2009) Monitoring autophagy by electron microscopy in mammalian cells. *Methods Enzymol.* **452,** 143–164.
44. Tanida, I., Minematsu-Ikeguchi, N., Ueno, T., Kominami, E. (2005) Lysosomal turnover, but not a cellular level, of endogenous LC3 is a marker for autophagy. *Autophagy* **1,** 84–91.
45. Boleti, H., Benmerah, A., Ojcius, D. M., Cerf-Bensussan, N., Dautry-Varsat, A. (1999) *Chlamydia* infection of epithelial cells expressing dynamin and Eps15 mutants: clathrin-independent entry into cells and dynamin-dependent productive growth. *J. Cell Sci.* **112,** 1487–1496.
46. Hybiske, K., Stephens, R. S. (2007) Mechanisms of *Chlamydia trachomatis* entry into nonphagocytic cells. *Infect. Immun.* **75,** 3925–3934.
47. Flannagan, R. S., Jaumouille, V., Grinstein, S. (2012) The cell biology of phagocytosis. *Annu. Rev. Pathol.* **7,** 61–98.
48. Levine, B., Mizushima, N., Virgin, H. W. (2011) Autophagy in immunity and inflammation. *Nature* **469,** 323–335.
49. Crotzer, V. L., Blum, J. S. (2009) Autophagy and its role in MHC-mediated antigen presentation. *J. Immunol.* **182,** 3335–3341.
50. Jagannath, C., Lindsey, D. R., Dhandayuthapani, S., Xu, Y., Hunter R. L., Jr., Eissa, N. T. (2009) Autophagy enhances the efficacy of BCG vaccine by increasing peptide presentation in mouse dendritic cells. *Nat. Med.* **15,** 267–276.

KEY WORDS:
lysosome · autophagy · RAW cell · elementary body · reticulate body · fluorescent chlamydia · live imaging · spinning disk confocal

Copyright Acknowledgements

Statement of Publications

The research presented in this thesis has appeared or has been submitted as a series of original publications in refereed journals.

Chapter 3

Sun HS, Wilde A, Harrison RE (2012) *Chlamydia trachomatis* inclusions induce asymmetric cleavage furrow formation and ingression failure in host cells. *Molecular and Cellular Biology* **31(24)**:5011-22

http://mcb.asm.org/content/31/24/5011.long

Chapter 4

Sun HS, Harrison RE (Submitted) Chlamydia inclusions actively localize to the host cell centre during mitosis to co-opt replicated Golgi in multinuclear cells

Appendix I

Sun HS, Eng EW, Jeganathan S, Sin AT, Patel PC, Gracey E, Inman RD, Terebiznik MR, Harrison RE (2013) *Chlamydia trachomatis* vacuole maturation in infected macrophages. *Journal of Leukocyte Biology* **92(4)**:815-27.

http://www.jleukbio.org/content/92/4/815.long